Studies on metal-oxo cluster and bipyridine derivatives

**A thesis submitted for the degree of
Doctor of Philosophy**

by

Tanmay Chatterjee

**School of Chemistry
University of Hyderabad
Hyderabad - 500 046
India**

November, 2010

<u>Certificate</u>

Certified that the work contained in the thesis entitled "**Studies on metal–oxo cluster and bipyridine derivatives**" has been carried out by Mr. Tanmay Chatterjee under my supervision and the same has not been submitted elsewhere for a degree.

<div align="right">

Prof. Samar K. Das
(Supervisor)

</div>

Dean
School of Chemistry

<div align="right">

Hyderabad
November, 2010

</div>

This thesis is dedicated to

My parents, My late grandmother,
Prof. Samar K. Das (my supervisor),
My brothers (fuchi and piku) and
Monima

<u>Statement</u>

I hereby declare that, the matter embodied in this thesis is the result of investigations carried out by me in the School of Chemistry, University of Hyderabad, Hyderabad, India, under the supervision of Prof. Samar K. Das.

In keeping with the general practice of reporting scientific observations, due acknowledgements have been made wherever the work described is based on the findings of other investigators. Any omission, which might have occurred by oversight or error, is regretted.

Tanmay Chatterjee

Hyderabad
November, 2010

Acknowledgements

Index

Introduction and motivation of the present work: A general overview on metal–oxo clusters and 2,2'–bipyridine derivatives

1

Abstract:– The present thesis deals with two different systems *viz*. metal–oxo cluster anions or polyoxometalates (POMs) and 2,2'–bipyridines. Both the systems are well known in diverse areas of the chemical research and are completely different in terms of their molecular structures. POMs are inorganic metal–oxide based framework type solids and the bipyridines are nitrogen containing heterobiaryl compounds. POMs are mainly known in the nano sciences and catalysis. Transition metal complexes of the 2,2'–bipyridines are good candidate in optoelectronics, non-linear optics and photovoltaics. This chapter gives a general overview on these two systems and is divided into five sections *viz*., preface, polyoxometalates, 2,2'–bipyridines, motivation of the work and references. Accounts on these two systems include structural features, synthesis followed by their applications in the materials chemistry, each in brief.

1.1. Preface

The fundamental sequence of the experimental research is synthesis, characterization of the bench–top synthesized compounds, comprehending the importance of the obtained compounds and subsequent publication of the results. Synthesis of the desired compounds might be one–pot or multiple–pot depending upon the molecular systems. Experimental chemists are interested in obtaining multifunctional materials with potential applications in the materials chemistry. The research in experimental chemistry can be classified in two broad categories *viz*., (i) establishing new and more effective methodologies in obtaining known or new materials and (ii) designing and synthesizing new materials with widespread applications adopting / modifying the established standard methodologies. Advancement of science and technology has made it simplistic to assemble sophisticated instruments for easier characterization of the experimentally obtained compounds and examination of their diverse physical and chemical properties. Rontgens's invention of X–ray, Braggs' discovery of X–ray scattering ability by crystalline solids, brought a revolution in science which is explored by the manufacture of X–ray diffractometers for the ultimate structural determination of crystalline solids.

However, the major and worse drawback of the single crystal X–ray crystallography is that it needs a crystal for obtaining data and subsequent structural characterization. While considerable difficulties lie in growth of crystalline solids of some compounds, technology and computation have been improved in solving structures even from powdery (microcrystalline) solids by X–ray diffraction technique. Unfortunately, X–ray diffraction technique is in deep silence to the amorphous solids, liquid and gaseous materials. At this point, it is worth mentioning that, although the registered number of crystal structures in the Cambridge Structural Database (CSD) is in the order of millions, the number of synthesized compounds till date is probably in the order of billions. In other words, it can be said that, researchers do not like to be dependent only upon the X–ray crystallography. Chemical research started long before the first systematic studies and publications about X–rays by Rontgen (1875), the Braggs' (father and son) discovery on Thomson scattering of X–rays by crystals (1913) and determination of the first crystal structure of table salt in 1914. The X–ray diffractometer was first introduced sometimes in the late 20th century. Spectroscopy is another superior technique for the characterization of the synthesized compounds. Till date several spectroscopic techniques, for example, Infra–red (IR) spectroscopy, Nuclear Magnetic Resonance (NMR) spectroscopy, one photon and multi photon absorption (UV–visible) spectroscopy, emission spectroscopy, Mössbauer spectroscopy, mass spectroscopy, Electron Spin Resonance (ESR) spectroscopy etc. have been developed that can determine the chemical structure of the synthesized compounds to whom X–ray diffraction do not respond positively.

The present thesis includes both these above mentioned techniques for analyzing the synthesized compounds. The first two chapters are basically concentrated on the crystallographic analysis of some solids comprising of metal–oxo cluster counter anions, although detailed spectroscopic characterizations of the concerned solids have been included. The third chapter is rather dominated by the physical organic chemistry and incorporates synthesis of some fluorescent π–conjugated–2,2'–bipyridines, their spectroscopic characterizations and examination of their photo–physical properties through absorption and emission spectroscopy. As the thesis involves two different molecular systems i.e. metal–oxide cluster anions and 2,2'–bipyridines, a general

introduction on these two systems is obligatory before entering into the main content of the present work.

1.2. Polyoxometalates

1.2.1. General features and synthesis

Polyoxometalates (POMs) are transition metal–oxide clusters comprising metal centers (usually group 5 or group 6 transition metals) linked by shared oxygen atoms.[1] These inorganic clusters posses close three dimensional framework structures and are mostly anionic in nature and include external cations for their successful isolation. The metal atoms that build the framework are called as *addenda atoms* which are usually in their higher / highest oxidation states. In this state, their electronic configuration is d^0 or d^1. Typical and most common examples of some addenda atoms are molybdenum (VI), tungsten (VI), vanadium (V) etc. Molybdenum and tungsten show excellences as polyoxoanion formers because both of them have favorable combination with oxygen as far as their ionic radius and charge are concerned along with availability of empty d– orbitals for metal–oxygen π–bonding. Other transition metals, like niobium (V), tantalum (V), hexavalent Tc, Re, Ru, Os; pentavalent Cr, Mo, W, Tc, Re, tetravalent Ti, V, Cr, Mo, W etc. are also useful ingredients for cluster formation. When more than one *addendum* is present, the cluster is called a *mixed addenda* cluster. These clusters contain highly symmetrical core assemblies of MO_n units and often adopt quasi–spherical structures. The majority of the polyoxometalate clusters incorporate bridging of the metal centers by oxide ions, but other elements, such as S and Br may also substitute some of the oxide ions. A sulfur–substituted POM is called a *polyoxothiometalate*.

Berzelius (1826) noted the formation of a yellow precipitate while mixing ammonium molybdate with phosphoric acid. The structural characterization of the concerned solid by X–ray diffraction analysis revealed that it was a polyoxoanion and now it is known as ammonium 12–molybdophosphate formulated as $(NH_4)_3(PMo_{12}O_{40})$. Based on the composition of these solids, they can be broadly classified into two categories:

(i) Heteropolyanions: these are metal oxide clusters that include hetero element along with the *addenda* atoms. These represent by far the most explored subset of POM clusters with over 5000 papers being reported on these compounds during the last four years

alone. These cluster anions are formulated as $[X_xM_mO_y]^{q-}$ (x $\leq$ m) where M is the *addenda* atom and X is the heteroelement. Many different elements can act as hetero atoms, with various coordination numbers. Examples include (a) 4–coordinate (tetrahedral e. g., PO_4, SiO_4, AsO_4 etc.) in Keggin, Dawson and Lindqvist structures; (b) 6–coordinate (octahedral e. g., $Al(OH)_6$, TeO_6 etc.)) in Anderson structure; (c) 8–coordinate (square antiprism) in $((CeO_8)W_{10}O_{28})^{8-}$; (d) 12–coordinate (icosahedral) in $(UO_{12})Mo_{12}O_{30}{}^{8-}$. The hetero atom may be located in the centre of the anion, such as in the Keggin structure, or in the center of a structural fragment, such as the two phosphorus atoms in the Dawson ion, which are central to its two symmetric fragments.

(ii) Isopolyanions: these are composed of a metal–oxide framework consisting of only *addenda* atoms and oxygen without any hetero atom. As a result, they are often much more unstable than their heteropolyanion counterparts. However they also have interesting physical properties, such as, high charges and strongly basic oxygen surfaces, meaning that they are attractive building blocks for materials formation. These clusters are formulated as $[M_mO_y]^{p-}$.

Polyoxometalates with addenda atoms, excluding Group 5 and 6 transition metals, are also known *e.g.*, the dodecatitanates $Ti_{12}O_{16}(OPr^i)_{16}$ (where OPr^i stands for an isopropyloxy group) and the iron oxoalkoxometalates. These POMs are known as *polyoxoalkoxometalates* due to the presence of the alkoxy groups.

The structures of the polyoxoanions are administered by the well–known electrostatic and radius ratio principles observed for extended ionic lattices. The concerned structures are conveniently described in terms of assemblages of metal–centered MO_n polyhedra through corner, edge and (rarely) face sharing. However, all the polyoxoanion structures do not include metal atoms lying at the centre of the polyhedron of oxide ions; rather they are strongly displaced towards a vertex or edge of its own polyhedron. Attention has been made to the analogy between MO_6 octahedra in polyanions and the mononuclear oxo complexes MOL_5 and MO_2L_4. POM anions can also be classified into three other sets based on the number of unshared oxygen atoms attached to the metal centers in their structures (see Scheme 1.1). They are (i) Type–I: these structures comprise the M atom in an approximately tetragonal (C_{4v}) site with a single shared oxygen atom. (ii) Type–II: in these structures, each M atom is connected with two mutually *cis*– unshared oxygen

atoms (MO_2L_4 type species). (iii) Type III: these anions posses both sorts of M atom sites (see Scheme 1.1). Some of the common examples of these categories have been included in Scheme 1.1.

Polyoxoanions

Based on composition ‖ *Based on unshared oxygen*

Isopolyanions | Heteropolyanions | Type –I | Type–II | Type–III
$[Mo_6O_{19}]^{2-}$ | $[XM_{12}O_{40}]^{n-}$ | (MOL_5) | (MO_2L_4) | $(MOL_5$ and
$[W_6O_{19}]^{2-}$ etc. | $[X_2M_{18}O_{40}]^{n-}$ etc. | $[XMo_{12}O_{40}]^{n-}$ | $[XM_6O_{24}]^{n-}$ | $MO_2L_4)$
| | $[X_2M_{18}O_{62}]^{n-}$ | $[X_2Mo_5O_{23}]^{n-}$ | $[XM_9O_{34}]^{n-}$
| | $[M_6O_{19}]^{n-}$ | $[XM_9O_{32}]^{n-}$ | $[H_2W_{12}O_{42}]^{4-}$
| | $[Mo_7O_{24}]^{6-}$ | $[XM_{12}O_{42}]^{n-}$
| | | $[Co_2Mo_{10}O_{38}H_4]^{6-}$
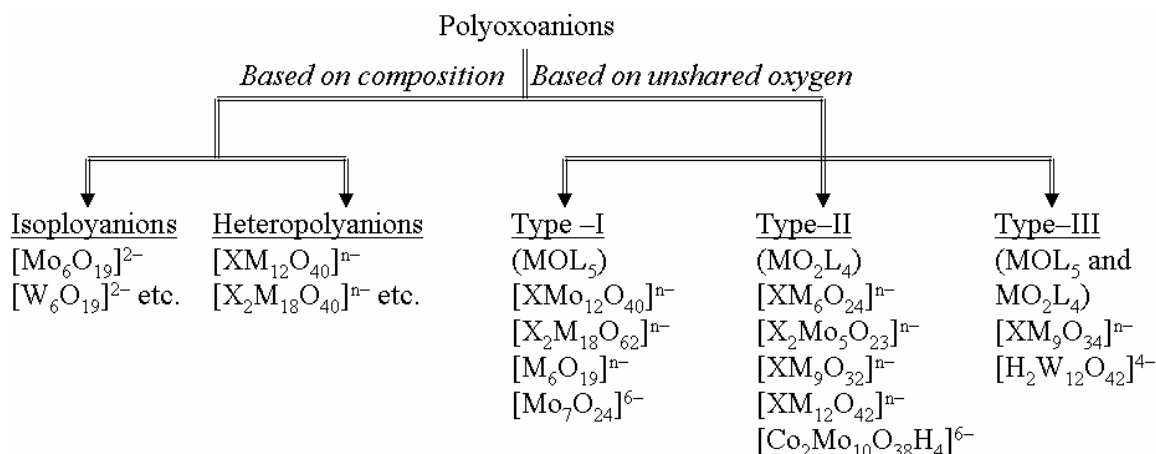
Scheme 1.1 Classification of the polyoxoanions.

The polyoxoanions can be isolated from both aqueous and non–aqueous solutions. There is no rule of thumb that can explain the systematic and designed rational synthesis of polyoxometalates. Synthesis and isolation of these cluster anions are well controlled by many factors, under confined conditions. Some of themes have been discussed below.

Acidification of aqueous solutions containing dissolved oxoanions results in the formation of large number of isopolyanions or heteropolyaions (if necessary heteroatoms are added). For example,

$8H^+ + 7[WO_4]^{2-} \rightarrow [W_7O_{24}]^{6-} + 4H_2O$

$8H+ + 7[MoO_4]^{2-} \rightarrow [Mo_7O_{24}]^{6-} + 4H_2O$

$23H^+ + [HPO_4]^{2-} + 12[MoO_4]^{2-} \rightarrow [PMo_{12}O_{40}]^{3-} + 12H_2O$

$6H^+ + [Cr(H_2O)_6]^{3+} + 6[MoO_4]^{2-} \rightarrow [Cr(OH)_6Mo_6O_{18}]^{3-} + 6H_2O$
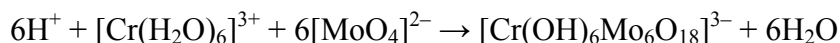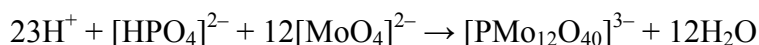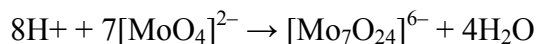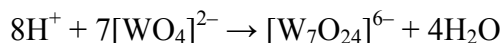
In many cases, the equilibrium constants and rates of formation are so large that the polyanions can be crystallized as salts from stoichiometrically acidified mixtures of the components at room temperature. The formation of heteropolyanions can be chosen according to the heteroatom used in the reaction mixture. The synthesis of these inorganic cluster anions is also dependent on various other factors like temperature and pH. For example,

$H^+ + [WO_4]^{2-} + H_3PO_4$ (excess) $\rightarrow [P_2W_{18}O_{62}]^{6-}$ (isomers) + other tungstophosphates (hot condition)

$H^+ + [WO_4]^{2-} + [SiO_3]^{2-} \rightarrow \beta–[SiW_9O_{34}]^{10-}$ (cold condition)

$H^+ + [WO_4]^{2-} + [SiO_3]^{2-} \rightarrow \alpha–[SiW_9O_{34}]^{10-}$ (hot condition)

Formation and isolation of the polyoxometalates also depend upon the sequence of adding reagents. For example,

$[SiO_3]^{2-} + [WO_4]^{2-} + H^+ \rightarrow \alpha–[SiW_{12}O_{49}]^{4-}$

$[WO_4]^{2-} + H^+ + [SiO_3]^{2-} + H^+ \rightarrow \beta–[SiW_{12}O_{49}]^{4-}$

Acidifications are commonly performed by addition of well known mineral acids, but if the involvement of other anions is to be avoided, homogeneous acidification by electrolytic oxidation of the solvent or addition of the appropriate anhydride might be useful. The isolation of these cluster anions is mostly achieved by addition of suitable counter cations, commonly alkali metals, ammonium or tetraalkyl–ammonium. The lithium and the sodium salts have enhanced solubility in water than those of the larger cations. Salts of the larger alkyl–ammonium and similar cations, tetrabutylammonium, tetraphenyl phosphonium or tetraphenyl arsonium etc. are usually insoluble in water, but recrystallizable from solvents such as acetone, acetinitrile, nitromethane etc.

The POM anions also act as precursors for the synthesis of even larger POM anions. Removal of the addenda atoms from the parent clusters at higher pH by controlled addition of an alkali results in the formation of another important class of defected polyanions (named as 'Lacunary polyanions') containing vacant sites. These vacant sites can be occupied by the other suitable heteroatom at proper reaction conditions.

Polyoxoanions can also be obtained from organic solutions. For example, hydrolysis of the metal esters by organic bases leads to the isolation of the polyoxometalate cluster anions containing an organic counter cation.

$WO(OEt)_4 + NR_4OH + H_2O \rightarrow (NR_4)_2[W_6O_{19}]$

$VO(OBu^t)_2 + Bu_4NOH + EtOH \rightarrow (BuN)_3H_3[V_{10}O_{28}]$

Other techniques in this area incorporate the dissolution of metal oxides in organic bases and the precipitation from non–aqueous solution of salts and mixtures subsequently recrystallizable from organic solvents.

$V_2O_5 + Bu_4NOH \rightarrow (Bu_4N)_3HV_4O_{12}$

$[MoO4]^{2-}$ + H^+ + Bu_4N^+ (pH 1.5) → mixture of insoluble Bu_4N^+ salts → $(Bu_4N)_2$ $[Mo_6O_{19}]$ (after recrystallization from acetone)

Structural representation of some common polyoxometalates have been shown below

| (a) | (b) | (c) | (d) |
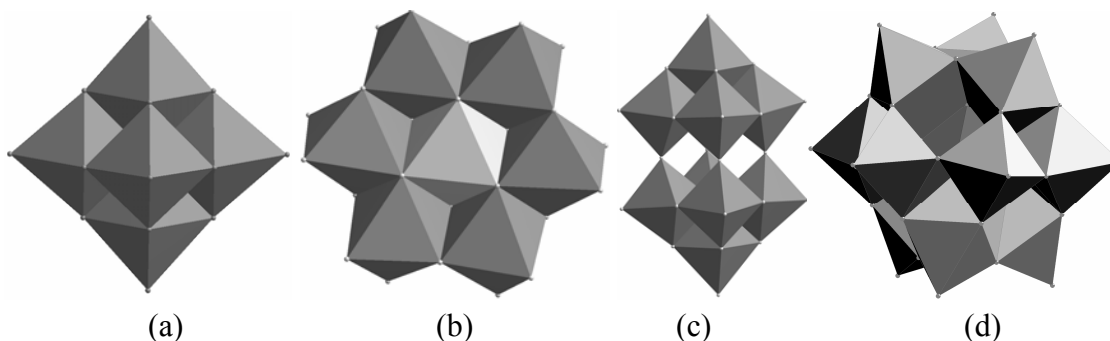
Figure 1.1 Structures of some common polyoxometalate clusters (a) $[Mo_6O_{19}]^{2-}$, (b) $[XMo_6O_{24}]^{3-}$, (c) $[W_{10}O_{32}]^{4-}$ and (d) $[XM_{12}O_{40}]^{n-}$.

1.2.2. Functionalization of the POM surface

The surface modification of POMs with organic species has attracted considerable attention in recent years, because it affords a convenient and effective way to generate novel organic–inorganic hybrid materials. The terminal oxygen atom(s) of the POM clusters can be substituted by external ligands resulting in the formation of functionalized polyoxometalate clusters. In the case of the hexamolybdate ion, $[Mo_6O_{19}]^{2-}$, varieties of derivatives of the type $[Mo_6O_{18}(L)]^{n-}$ have been reported in which an exogenous ligand L replaces a terminal oxo ligand within the parent structure. Structurally characterized examples of such systems include the nitrosyl $[Mo_6O_{18}(NO)]^{3-}$,[2] diazenido species $[Mo_6O_{18}(N=NAr)]^{3-}$,[3] a hydrazido derivative $[Mo_6O_{18}(N=NMePh)]^{2-}$,[4] the organometallic $[Mo_6O_{18}(\eta^5–C_5Me_5)]^-$,[5] and the diazoalkane complex anion $[Mo_6O_{18}(N=NC(Me)Ar)]^{2-}$.[6] Among the many organic derivatives of $[Mo_6O_{18}(L)]^{n-}$ species, organoimido derivatives have attracted particular interest because the organic π–electrons may extend their conjugation to the inorganic framework, thus resulting in strong d–π interactions. Moreover, organoimido derivatives of POMs with a remote organic functional group can be utilized as building blocks to construct more complicated POM–organic hybrids. Majority of the work in this direction has been focused on the hexamolybdate ion, $[Mo_6O_{19}]^{2-}$. Three different methodologies have been developed to obtain the imido

derivatives of hexmolybdates. The reactions, shown below, demonstrate the reactions of hexamolybdate cluster with phosphinimines, isocyanates and aromatic amines.

$$[Mo_6O_{19}]^{2-} + Ph_3P=NAr \xrightarrow[85\ ^\circ C,\ 48\ h]{pyridine} [Mo_6O_{18}(NAr)]^{2-} + Ph_3P=O$$

$$[Mo_6O_{19}]^{2-} + ArNCO \xrightarrow[110\ ^\circ C,\ 2\text{-}13\ d]{pyridine} [Mo_6O_{19-x}(NAr)_x]^{2-} + CO_2$$

$$[Mo_6O_{19}]^{2-} + ArNH_2 \xrightarrow[150\ ^\circ C]{PhCN,\ Et_3N} [Mo_6O_{18}(NAr)]^{2-} + H_2O$$
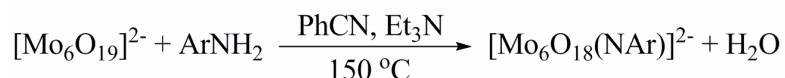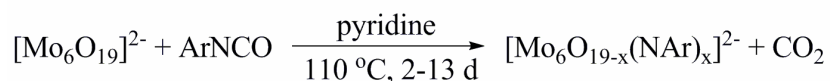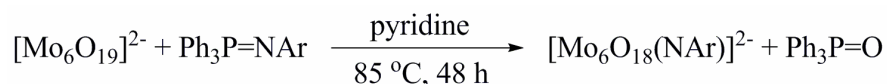
The first reaction was reported by Maatta and coworkers in 1992.[7a] Although the phosphinimine, used in the reaction, is not–easily accessible reactant, it nevertheless demonstrates that direct functionalization can be carried out on parent clusters in a clear–cut manner. The second reaction was first reported by Errington and coworkers,[8] who paved the way to obtain both the alkyl and aryl imido derivatives of hexamolybdates by using organoisocyanates. Maatta and co–workers reported a modified version of the second reaction i.e. the third one (anhydrous pyridine was used as the solvent instead of acetonitrile or benzonitrile, which was initially used by Errington) and used organi–amines instead of the isocyanates to prepare a number of organoimido derivatives.[7f–h, 8] It should be noted that the reaction needs to be carried out in strictly anhydrous conditions (to avoid the hydrolysis) at high temperature for a prolonged time.

However, the above mentioned reactions have some drawbacks, for example, phosphinimines and isocyanates are not easily accessible; their reactions with $[Mo_6O_{19}]^{2-}$ need to be carried out under strictly anhydrous conditions for a prolonged time (several days), the reaction conditions of $[Mo_6O_{19}]^{2-}$ with aromatic amines are even harsher (benzonitrile as the solvent and a reaction temperature of 150 °C), and only moderate yields can be obtained. Peng and coworkers found that dicyclohexylcarbodiimide (DCC) or other diimides can dramatically facilitate the reaction of $[Mo_6O_{19}]^{2-}$ with aromatic amines.[9] The relevant report demonstrates that, in the presence of 1 equiv of DCC, $[Mo_6O_{19}]^{2-}$ reacts smoothly with a variety of aromatic amines under refluxing acetonitrile. The reaction is usually completed in less than 12 h and offers the products in usually higher yields. This reaction protocol proved to be very effective and since its discovery, many organoimido derivatives of hexamolybdate cluster have been reported

using this methodology.[10] Few representative well characterized systems have been presented in Figure 1.2.
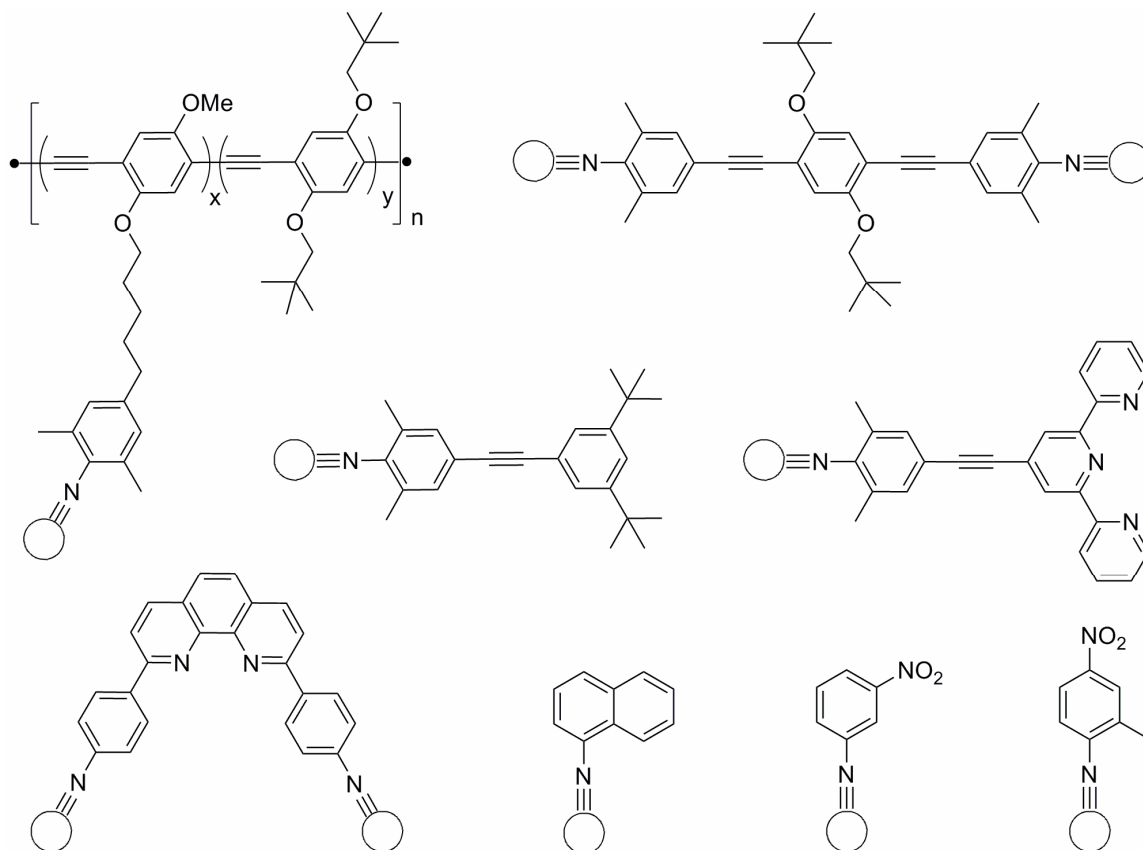
Figure 1.2 Molecular structures of some of the organoimido functionalized hexamolybdates. ◯ = {Mo_6}$^{2-}$ cluster.

1.2.3. Polyoxometalates in supramolecular chemistry

The construction of supramolecular assemblies from oxide–based molecular building blocks has been attracting extensive interest in the recent years. One of the important targets in the preparation of supramolecular ensembles is to establish the appropriate connections between the different molecular fragments on the basis of various intermolecular interactions in the crystal. In this molecular assembling process, hydrogen bonding of conventional O–H···O and N–H···O motifs has been most commonly used as supramolecular cement, yet weaker forces such as C–H···O, C–H···N have also been used. It is worth mentioning that, mixed–valence electronic and diverse spin structures have been realized using the transition metal oxide cluster–based building blocks

(polyoxometalates). These cluster anions can serve two types of roles in their crystals: (i) can act as counter anion and hydrogen bonding acceptor through the surface oxygen atoms and (ii) can act a ligand in making dative linkages to the external metal centers through the bridging or terminal oxygen atoms. The design of the cationic units could be a highly effective strategy to control the cluster arrangements from the perspective of designing one–dimensional (1D), two dimensional (2D), or three–dimensional (3D) network structures. In this section, some representative phenomena have been discussed where the POM clusters have been used as a counter anion, a supramolecular building block, a ligand or to obtain discrete to complicated molecular frameworks.

(a)   (b)

(c)   (d)
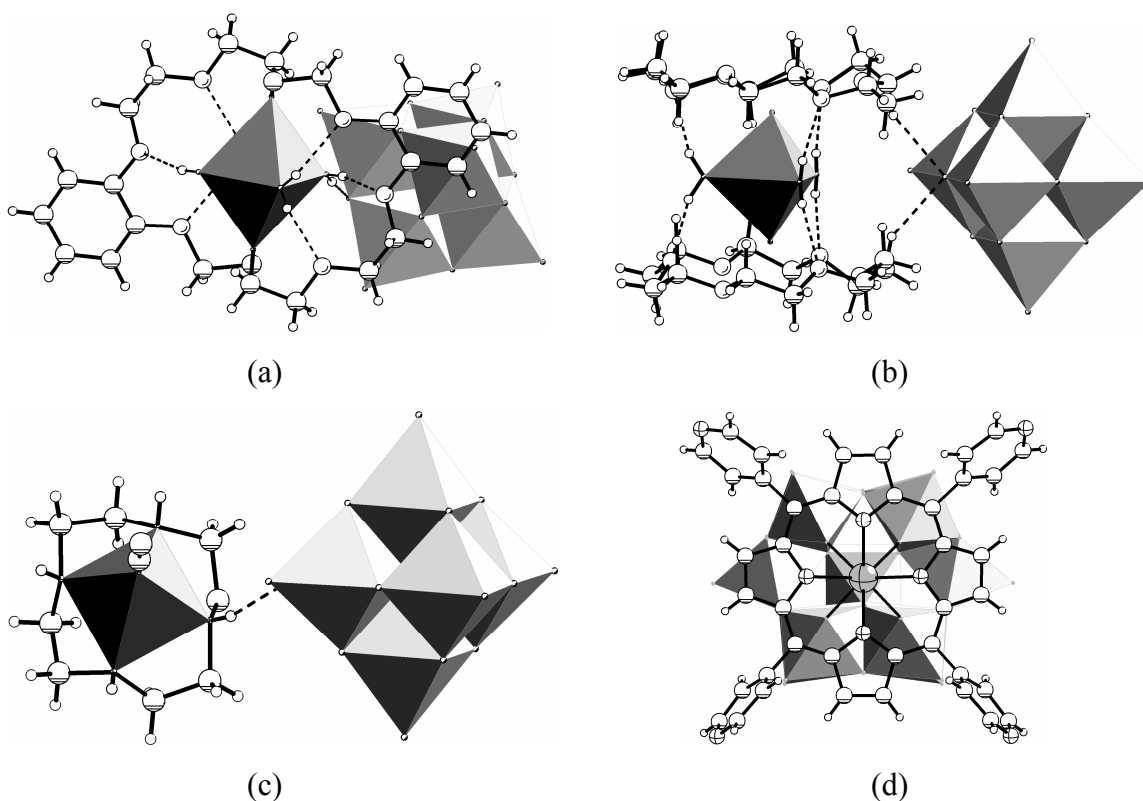
Figure 1.3 Picture displaying representative examples of transition metal coordination complexes of macrocyclic systems in association with polyoxoanions: (a) $[Cu(H_2O)_5$ (dibenzo–24–crown–8)]$[Mo_6O_{19}]$,[11i] (b) $[Cu(H_2O)_5(18–crown–6)_2][Mo_6O_{19}]$,[11k] (c) [Cu (cyclen)(MeCN)]$[W_6O_{19}]$,[11l] (d) $[(tpyp)Hf(PW_{11}O_{39})]^{5–}$ (tpyp = tetrapyrido porphyrin).[11m]

Crown ethers are useful building blocks in the supramolecular chemistry / crystal engineering. The combination of highly anisotropic cationic units with the almost spherical shaped POMs has been reported which include supramolecular cations formed

by complexation of a metal ion (M^{n+}) within a crown ether–host.[11] In these salts, the alkali and/or transition metal ions are included into the cavity of crown ethers, and the size of overall cation structure can be controlled by changing the crown ether ring–size. The modification of crown ethers affects the electrostatic interactions between the supramolecular cations and POM in the crystals. From the size compatibility between the supramolecular cation and POM clusters, relatively large crown ethers such as dibenzo–18–crown–6 and dibenzo–24–crown–8 have been employed for the counter cations of $[Mo_6O_{19}]^{2-}$ and $[PMo_{12}O_{40}]^{3-}$ clusters.[11g,i] For example, Shivaiah et al. reported a solid in which, hydrated $[Cu(H_2O)_4]^{2+}$ was included into the cavity of dibenzo–24–crown–8, forming the supramolecular cation of $[Cu(H_2O)_4(dibenzo–24–crown–8)]^{2+}$ that yields the 1D alternate arrangements of cations and $[Mo_6O_{19}]^{2-}$ through hydrogen bonded interactions (Figure 1.3).[11i] Another solid reported by the same authors demonstrated a penta aqua $[Cu(H_2O)_5]^{2+}$ species sandwiched between two 18–crown–6 macrocycles resulting in the formation of the effective cation $[Cu(H_2O)_5(18–crown–6)_2]^{2+}$ which associates with the hexamolybdate cluster anions through hydrogen bonding forces in a 2D fashion (Figure 1.3).[11k] The hydrated $[Na(H_2O)_{1.5}(dibenzo–24–crown–8)]^+$ also regulated the $[Mo_6O_{19}]^{2-}$ clusters as the 1D structure.[11g] Although the effective intermolecular interactions between the cation and $[Mo_6O_{19}]^{2-}$ were not observed in $[Na_2(H_2O)_3(dibenzo–24–crown–8)_2][Mo_6O_{19}]$ salt, the 1D array of $[Mo_6O_{19}]^{2-}$ was obtained. By changing the size of POM from $[Mo_6O_{19}]^{2-}$ to $[PMo_{12}O_{40}]^{3-}$, the supramolecular cation of $[Na(H_2O)_2(dibenzo–24–crown–8)]^+$ changed the cluster arrangement from a 1D chain to a 2D layer of $[PMo_{12}O_{40}]^{3-}$.[11g] The hydrogen bonding $[Na(H_2O)_2(dibenzo–24–crown–8)]^{3+}_3$ trimer units were assembled to each other forming a 3D honeycomb porous network. The compatible diameter of $[PMo_{12}O_{40}]^{3-}$ cluster to the size of honeycomb pore organizes each $[PMo_{12}O_{40}]^{3-}$ cluster to the 2D supramolecular cationic assembly. The construction of 2D honeycomb pore structures, where the size of pore is necessary to fit the diameter of POM, is one useful method to array the POM clusters as the 2D layer. Transition metal complexes of the nitrogen containing macrocycles, for example, aza–crown ethers / macrocycles,[11l] porphyrines[11m] etc. have also been introduced in order to crystallize with the POM cluster anions and in obtaining multi–dimensional supramolecular arrays. For example, a recent report by M. Sarma et

al. demonstrates a solid [Cu(cyclen)(MeCN)][W_6O_{19}] where the penta–coordinated Cu–cyclen complexes associate with the [W_6O_{19}]$^{2-}$ clusters in forming an intricate 3D supramolecular architecture (Figure 1.3).[111] Similarly, Drain and coworkers reported Zr (IV) and Hf (IV) complexes of tetrapyrido porphyrin covalently attached to the surface of a lacunary polyoxometalate, [$PW_{11}O_{39}$]$^{7-}$ (Figure 1.3).[11m] 2D arrangement of the resulting complexes through supramolecular weak interactions have been observed in the relevant crystal. Apart from engineering with the transition metal complexes of the macrocyclic systems in polyoxometalate association, interests have been made on the same with the hydrogen bonded complexes of the crown poly ethers. For example, supramolecular chemistry of the crown ether hydrogen bonding complexes of protonated 1,3– and 1,4–phynelenediamines, associated with Keggin type polyoxometalates, have been described in recent literature.[11n,o]

1.2.4. Applications

The POM clusters are unique class of inorganic solid–state materials that have made a mark on disciplines as diverse as medicine, catalysis, magnetic material science, geochemistry, nuclear waste processing and applications involving photochemical or electrochemical response. The majority of the applications of the POMs are found in the area of catalysis. About 80 – 85% of the patents and applied literature are associated with catalysis. The remaining 15 – 20% of the applications can be put in several areas. A brief description of applications of the POM anions in various fields is presented in the following sections.

1.2.4.1. Polyoxometalates in medicine

Several features of the POMs make them attractive for applications in the medicinal sciences. The principal advantageous feature of POMs is that nearly every molecular property that impacts the recognition and reactivity of POMs with target biological macromolecules can be altered. These include polarity, redox potentials, surface charge distribution, shape, and acidity. Another attractive feature is that rational and reproducible synthetic methods are available for the replacement of one or more of the skeletal early transition metal cations in POMs with d– or p–block ions and also for the covalent attachment of organic groups to POMs via linkages that are compatible with

physiological conditions (long half–lives in H_2O or buffers at pH ≈ 7). The major disadvantage of POMs in the area of medicinal science is that they are not organic species. Low molecular weight organic species dominate the pharmaceutical industry (drug discovery, synthesis, and development). However, as the POM based pharmaceuticals are not cost effective, interests have been grown on using the POMs as biologically active substrate. Two general types of POM activity, antiviral and antitumoral, have dominated the medicinal chemistry of these compounds. One example include polyoxotungstate mediated enhancement of the antibiotic effectiveness against otherwise resistant strains of bacteria when used in combination with β–lactam antibiotics. Research has also focused on the antiviral properties of POMs because they are generally nontoxic to normal cells.

Table 1.1 *In vitro* antiviral activities of some poloxometalates.

POM	virus[a]	cell line[b]	antiviral activity EC_{50}, µM	toxicity IC_{50}, µM	ref
$K_7[A–α–SiNb_3W_9O_{40}]$	RSV	Ma 104	0.5	>100	13a
$K_{17}[Eu(P_2W_{17}O_{61})_2]$	HIV–1$_{IIIB}$	MT–4	11.6	42.0	13b
$K_{10}[H_2W_{12}O_{42}]$	HIV–1$_{LAI}$	PBMC	2.5	>100	13c
$H_6[ZnW_{12}O_{40}]$	HIV–1$_{LAI}$	PBMC	0.90	12.0	13d
$K_8[MnP_2W_{17}O_{61})_2]$	FluV–A	MDCK	3.8	50.0	13e
$[(NH_4)_{17}Na][NaSb_9W_{21}O_{86}]$	FluV–A	MDCK	1.8	50.0	13e
$Na_9[SiW_9O_{39}H]$	HIB–1$_{IIIB}$	MT–4	28	120	13f
$(Me_3NH)_8[Si_2Nb_6W_{18}O_{77}]$	RSV	Ma 104	0.8	>100	13a
$K_5[SiAlW_{11}O_{39}(H_2O)]$	HIV–1$_{IIIB}$	MT–4	4.0	140	13f
$K_5[Si(TiCp)W_{11}O_{39}]$	HIV–1$_{IIIB}$	MT–4	0.6	>80	13g

Abbreviations: [a] RSV, respiratory syncytial virus; HIV, human immunodeficiency virus; FluV–"x", FluV virus. [b] Ma 104, embryonic African green monkey kidney cells; MT–4, human T–cell leukemia isolated from patients with adult T–cell leukemia, PBMC, peripheral blood mononuclear cells; MDCK, Madin–Darby canine kidney cells.

The degree of cellular penetration and localization of a drug directly impacts its mechanism of viral inhibition and other biological attributes. Several lines of evidence using different techniques and types of experiments indicate that POMs do, in fact, cross cell membranes and they have been reported to be active at both the cell surface and in

the cytoplasm. The antiviral activity of POMs was reported as early as 1971. Raynaud *et al.* noted that polytungstosilicate heteropoly compounds inhibited murine leukemia sarcoma virus *in vitro*.[12a] Much of the early work focused on these polytungstosilicates and $(NH_4)_{17}Na[NaSb_9W_{21}O_{86}]$ which is commonly known as HPA–23. Prior to 1990, *in vitro* studies, conducted by various groups, showed the efficacy of these POMs against several viruses: murine leukemia sarcoma (MLSV), vesicular stomatitis (VSV), polio, rubella, rauscher leukemia (RLV), rabies (RV), rhabdovirus, and epstein–barr (EBV).[12b–j]

Table 1.2 In vivo activities of some poloxometalates.

POM	virus / tumor type[a]	animal	efficiency[b]	Ref
	Antiviral activity			
$(NH_4)_{17}Na[KSb_9W_{21}O_{86}]$	FLV	OF$_1$ mice, male	++	14a
$(NH_4)_{17}Na[NaSb_9W_{21}O_{86}]$	RV$_{CVS}$	Swiss OF$_1$ mice, female	++	14b
$(NH_4)_4[Sb_2W_5O_{20}]$	FLV	DBA/2 mice, both sexes	+/++	14c
$K_6[BVW_{11}O_{40}]$	FLV induced splenomegaly	mice, type x	+	14d
$(NH_4)_{17}[SrSb_9W_{11}O_{86}]$	RV	OF$_1$ mice, male	+/++	14a
	Antitumoral activity			
$[NH_3Pr^i]_6[Mo_7O_{24}]$	MX–1 human breast cancer	Balb/c mice	+	14e
$[NH_4]_6[Mo_7O_{23}(OH)]$	CO–4 human colon cancer	ICR mice, female	—	14f
$[NH_3Pr^i]_6[H_xMo_7O_{24}]$ x = 1 or 2	Meth A sarcoma	Balb/c mice, female	+/++	14g
$Na_5[IMo_6O_{24}]$	CO–4 human colon cancer	ICR mice, female	++	14f

Abbreviations: [a] FLV, friend leukemia virus; RV, rabies virus. [b] +, somewhat effective, ++ effective.

Polytungstosilicate heteropoly compounds showed significant promise against VSV, MLSV, rubella, RLV, and polioviruses. Most of these POMs showed good inhibitory activity with low cytotoxicity, in a variety of cell lines. HPA–23 was shown to be an effective antiviral agent against MLSV, RV, rhabdo virus, and EBV at doses nontoxic to cells. Because HPA–23 exhibited sufficiently promising results *in vitro*, it was reasoned that it might be effective against human immunodeficiency virus, HIV, the causative

agent of AIDS. Unfortunately, the results of the clinical trials were less than promising. Few examples of the pharmaceutical *in vitro* and *in vivo* activities of various POMs have been presented in the Tables 1.1–1.2.

Table 1.3 Homogeneous catalysis by the heteropoly acids in organic media.
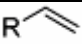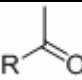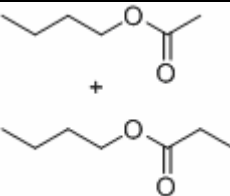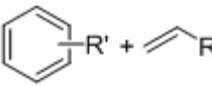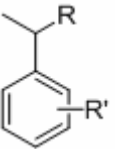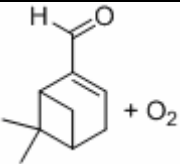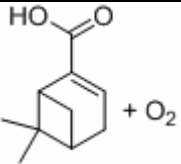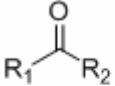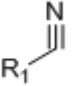
Reaction	rate ratio	T (°C)	Ref
hydration of phenylacetylene	100	60	16a
$PhC(CH_3)_2OOH \rightarrow PhOH + CH_3COCH_3$	1000	25	16b
olefin + HOAc → ester	90	110	16b
ester → olefin + carboxylic acid	100	128	16c
$THF + Ac_2O \rightarrow AcO(CH_2CH_2CH_2CH_2O)_nAc$	>1000	50	16a

1.2.4.2. Polyoxometalates in catalysis

Among numerous applications of the polyoxometalates, catalysis is by far the most important. Systematic investigations on catalysis of POMs began in the early 1970s when the great potential of these compounds for catalytic applications became apparent. These compounds are vastly advantageous in catalysis, the most important being their multifunctionality and structural elasticity. The heteropolyoxometalates are stronger Brønsted acid, they are efficient oxidants, exhibiting fast reversible multielectron redox transformations under mild conditions. Their acid–base and redox properties can be altered over a large range by varying their chemical composition. Again these compounds are usually highly soluble in many polar solvents and fairly thermally stable in the solid state. Because of their unique properties, heteropoly compounds are promising acid-, redox- and bifunction (acid and redox)-catalysts. The catalytic reactions can be performed in homogeneous as well as heterogeneous systems. A final and crucial consideration for a catalyst is that it must be cost effective. The cost of production of POMs varies greatly. Simple tungstophosphate POMs can readily be synthesized on a large scale from cheap salts. However, POMs, that contain rare metals, are of course much more expensive. The goal and assumption of attempting to produce POM catalysts are that, since the POM catalysts are generally degraded at a very slow rate, the overall process is cheaper than if stoichiometric amounts of reagents are used. In the 1970–80s, several new industrial chemical processes utilizing polyoxometalate catalysts were

developed and commercialized in Japan. The first commercial process was the liquid–phase hydration of propene to 2–propanol launched in 1972. It followed by the vapor phase oxidation of methacrolein to methacrylic acid (1982), the liquid phase hydration of

Table 1.4 Representative examples of polyoxometalate catalysis.

Catalyst	Substrate	Product	Ref
$[(C_6H_{13})_4N]_5[Ru(H_2O)SiW_{11}O_{39}]$ (photo–reduction with tertiary amines)	CO_2	CO	17a
$H_5PV_2Mo_{10}O_{40}$ Pd/Al_2O_3 as cocatalyst	CO	CO_2	17b
$Pd(15–crown–5–phen)Cl_2–$ $H_5PV_2Mo_{10}O_{40}$ (NO as oxidant in Wacker type oxidation)	R	R O	17c
$H_5PV_2Mo_{10}O_{40}$ (C−C bond cleavage instead of C–H bond activation)	OH		17d
$[NO\{C(NH_2)_3\}_2][PW_{12}O_{40}]$ (alkene activation in arene alkylation and dimerization)	—R' + R	R —R'	17e
$[Mo_{12}^{V}O_{39}(\mu_2–OH)_{10}H_2\{X^{II}(H_2O)_3\}_4]$ (X = Ni, Co, Mn and Cu)	+ O_2	+ O_2	17f
$Na_{12}[WZn_3(H_2O)_2[ZnW_9O_{34})_2]$ (oximation of ketones and aldehydes with aqueous ammonia and hydrogen peroxide)	R_1 = alkyl, benzyl R_2 = alkyl, H		17g

isobutene for its separation from the butane–butene fraction (1984), the biphasic polymerization of tetrahydrofuran to polymeric diol (1985), the hydration of n–butenes to 2–butanol (1989) and many others successes. Thus, the topic became a broad subject area for research and till date several authors have reported variety of organic transformations effectively catalyzed by the POMs. Due to the dearth of space, only very few examples of the polyoxometalate catalyzed reactions have been accounted and some reactions have

been presented in Tables 1.3 and 1.4. The heteropoly acids (HPAs) for example, $H_3PW_{12}O_{40}$, $H_4PW_{11}VO_{40}$, $H_4SiW_{12}O_{40}$, $H_3PMo_{12}O_{40}$, $H_4SiMo_{12}O_{40}$ etc. catalyze a wide variety of reactions in homogeneous liquid phase offering strong options for more efficient and cleaner processing compared to conventional mineral acids. Being stronger acids, HPAs will have significantly higher catalytic activity than mineral acids.[15] In particular, in organic media, the molar catalytic activity of HPA is often 100–1000 times higher than that of H_2SO_4. This makes it possible to carry out the catalytic process at a lower catalyst concentration and/or at a lower temperature. Moreover, HPA catalysis lacks side reactions such as sulfonation, chlorination, nitration, etc., which occur with mineral acids. As stable, relatively nontoxic crystalline substances, HPAs are also preferable with regard to safety and ease of handling.

Kozhevnikov *et al.* have shown that HPA is an efficient catalyst for condensations in the syntheses of vitamins E, K1 and C.[16d] Thus, phosphotungstate and silicotungstate Keggins catalyze the condensation of isophytol with 2,3,5– trimethylhydroquinone (TMHQ) to R–tocopherol, which is the active form of vitamin E. The reaction is performed in a homogeneous phase (e.g., in butyl acetate or acetic acid) or in a heterogeneous system (e.g., in toluene) with ~ 1% wt of HPA based on TMHQ. With HPA, practically the same yield and quality of vitamin E is obtained as with $ZnCl_2$ which is a good commercial catalyst. However, $ZnCl_2$ is used in a stoichiometric amount, resulting in a large amount of waste. In contrast to $ZnCl_2$, HPA can be recovered after the reaction and reused.

1.2.4.3. Other applications

The POMs have potential applications in several other areas. Some of the examples have been presented in Table 1.5. Lomakina and co–workers have investigated corrosion inhibition by the use of POMs for aluminum and its alloys under high temperature in aqueous conditions. These alloys are generally considered for their uses as construction materials in atomic industries, and thus a corrosion inhibitor must exhibit high radiation stability. The wood pulp can be brightening by degradation or removal of organic chromophores. POMs can be used for this purpose as reversible oxidants; POMs offer a safe alternative to chlorine. For example, Weinstock *et al.* reported the use of

$H_5PMo_{10}V_2O_{40}$ for the bleaching the pulp in paper industry. POMs can also be used for the precipitation / isolation of proteins.

Table 1.5 Illustrative examples for the applications of POMs in diverse areas other than medicine and catalysis.[18]

POM	Application
$H_4PMo_{11}VO_{40}$	modification of carbon electrodes, capacitors
$H_3PMo_{12}O_{40}$, $H_3PW_{12}O_{40}$	electrolytic capacitors
$[C_{16}H_{33}N(CH_3)_3]_x$	
$H_{4-x}SiMo_{12}O_{40}$	corrosion resistant coatings, primers
$Na_5H_2PV_6Mo_6O_{42}$	corrosion inhibitor for steel St3 (mild steel)
$(NH_4)_{10}H_2W_{12}O_{42}$	corrosion inhibitors of Al alloys
$H_4SiW_{12}O_{40}$	colorants for pigmenting paints, printing inks and plastics, treatment of cathode electrodes (vitreous C and graphite) dopant of polyaniline and polypyrrole
$H_9P_2V_3W_{15}O_{62}$, $Na_6V_{10}O_{28}$	wood pulp bleaching
$H_3PW_{12}O_{40}$	electrochromic–ion conducting gels, films, xerogels photochromic coatings for copiers, dopant of poly(N–methylpyrrole) 244
$H_6P_2W_{18}O_{62}$	dopant in poly(1–naphthol)
$[(C_4H_9)_4N]_4[PW_{11}O_{39}Fe(OH_2)]$	dopant in polypyrrole
$H_3PMo_6W_6O_{40}$	as porous support for the purification of vent air
$H_5PV_2Mo_{10}O_{40}$	decontamination of mustard (HD) analogues
$(NH_3)_6[H_2W_{12}O_{40}]$, $H_3PW_{12}O_{40}$	flame retardant for aramid fibers

1.3. 2,2'–Bipyridines

1.3.1. General features

Bipyridines (also known as bipyridyls, dipyridyls and dipyridines) are nitrogen containing hetero–biaryl compounds, that are extensively known in the area of coordination chemistry.[19] Based on the position of the C–C bond between two pyridine rings, these aromatic heterocycles contain six possible regioisomers–2,2', 2,3', 2,4', 3,3', 3,4' and 4,4' (Figure 1.4); most common of which is the 2,2'–bipyridine, which is famous as a bidentate chelating ligand for metal coordination. These ligands interact with the metal ions via σ–donating nitrogen atoms as well as π–accepting molecular orbitals.[3] Both the N atoms of 2,2'–bipyridines are in their sp^2 hybridized state and comprises one

lone pair on each of the atoms. Due to *lone pair–lone pair* repulsive interaction, the uncoordinated bipyridine ligands prefer to attain a coplanar structure with the nitrogen atoms in *trans*–conformation. These molecules readily coordinate to transition metal ions and the resulting coordination complexes that are formed are highly stable owing to the formation of a five membered chelate ring.
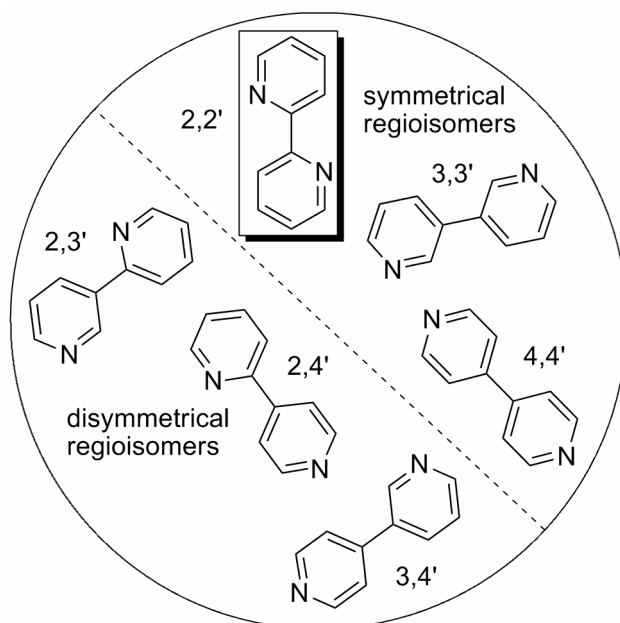
Figure 1.4 Regioisomers of bipyridine heterocycles.

1.3.2. Synthesis

2,2'–Bipyridine (bpy) and the symmetrically substituted derivatives have traditionally been synthesized by a number of different synthetic methodologies, including the Ullmann reaction, which involves homocoupling of a halopyridine in the presence of M^0 where M = copper or nickel. This process, most often used for a large scale industrial manufacturing of bpy, is Raney nickel coupling of simple pyridine. While this Ni^0 catalyst can also be used with methyl pyridines (picolines) to form dimethyl substituted bipyridines; this process is limited to simple, symmetric derivatives. More complex unsymmetrical derivatives have been generated by reaction of pyridinium salts with α,β–unsaturated ketones followed by treatment with ammonium acetate to effect cyclization of the second ring. This preparation, known as Kröhnke method, is still commonly used to prepare bipyridine derivatives. More recent synthetic methods involve cross coupling

of halopyridines with organometallic pyridines and transition metal mediated homocoupling of halopyridines. These methods allow the construction of the bipyridine ligands in higher yields and permit the incorporation of a number of functional groups. A few well known synthetic routs in obtaining the different bipyridines have been discussed bellow.

Equation 1.1

Equation 1.2

X = Cl, Br, I, OTf

Y = SnR$_3$; Stille ZnX; Negishi BOR$_2$; Suzuki

E = Me$_3$Si, PhCH(OH), PhCMe(OH)

Equation 1.3
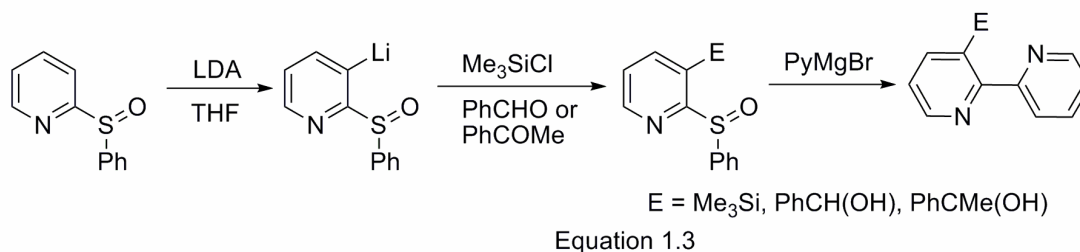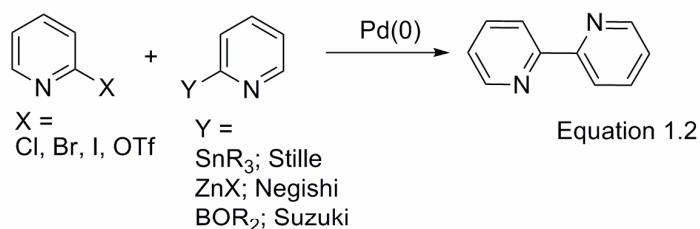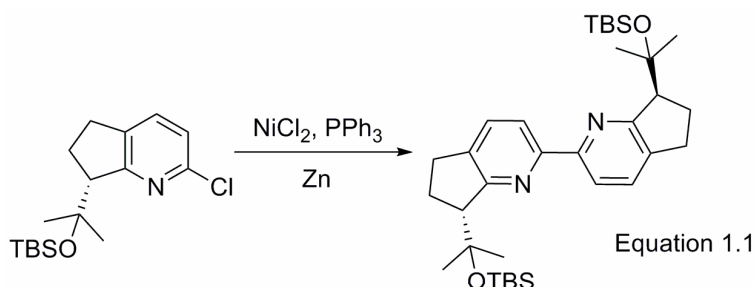
The most useful transition metal mediated halopyridine homocoupling makes use of a Ni^0 catalyst, most often generated *in situ* through reduction of a Ni^{II} complex.[20a] This method provides products in such higher yield than the classic Ulmann reaction and is compatible with many functional groups. One example of this reaction has been presented by Equation 1.1.[20b] Reactions, which employ other catalytic systems for halopyridine homocouplings such as Pd/C[20c] and Cu[20d], typically afford products in lower yields. In order to synthesize unsymmetrical as well as symmetrical bipyridines, methods involving cross coupling of a halopyridine with an organometallic pyridine have been developed. Typically, halopyridines / pyridyl triflates couple with either pyridylborates

(Suzuki–Miyaura), pyridylstannanes (Stille) or pyridyl zinc reagents (Negishi) in a Pd(0) catalytic system resulting in the bipyridines, where the two pyridines may or may not have the same structure to give the symmetrical (homo coupling) or unsymmetrical (cross coupling) biaryls respectively (Equation 1.2). One valuable feature of the Suzuki coupling reaction is that it is compatible with the stannanes. A pyridyl diethyl borane has been coupled to a tributyl tin functionalized pyridyl bromide.[20e] This compatibility is useful for olypyridine synthesis because subsequent Stille coupling of the bipyridyl stannane is possible. Another synthetic strategy that produces substituted bipyridines in moderate to higher yields involves coupling of pyridyl sulfoxides with pyridyl Grignard reagents as shown in Equation 1.3.[20f,g]

Bipyridines may be oxidized to picolinic acids in hot permanganate[21a,b] and reduced to 2,2'–bipiperidine with sodium metal in refluxing alcohols[21c] or via hydrogenation.[21d] Reaction of bipyridine ligands with peroxides or peracids generates either 1– or 1,1'–N–oxides (or a mixture of the two) which serve as valuable intermediates in many synthetic schemes, because one or more nitrogen atoms is protected. Removal of the oxide is effected by reagents, such as, phosphorus trichloride or hydrogen iodide.[21b,e] Electrophilic substitution reactions primarily occur at *meta*– to the nitrogen atoms, while more common nucleophilic substitutions typically take place at positions *ortho*– and *para*– to nitrogen. Halogen substituted bipyridines are very useful precursors in synthesizing oligopyridine derivatives as well building block of many other derivatizations.

Halomethyl bipyridines are another important class of reagents that can be derivatived for use in many different contexts. Classical preparation includes reaction of dimethyl bipyridine with *N*–bromosuccinimide or *N*–chlorosuccinimide. However, these reactions often render multiply halogenated products which make the isolation of the desired products difficult. An alternate highly efficient method, described by Fraser and coworkers, incorporates lithiation of the methyl bipyridines followed by coupling of the reactive carbanions with various electrophiles. Conversion of the carbanion to a trimethylsilyl group prior to the addition of an electrophile has proven useful in many cases for high yield transformations of the methyl to halomethyl bipyridines.[22] Before accounting the applications of the bipyridine ligands and their transition metal complexes, a few representative 2,2'–bipyridines have been presented in Table 1.6 and

Chart 1.1.

Table 1.6
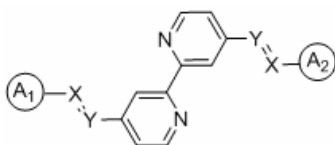
#	X	Y	A₁	A₂	Ref
1a	C	C	(4–dibutylamino)phenyl	(4–dibutylamino)phenyl	23a
1b	C	C	(4–octyloxy)phenyl	(4–octyloxy)phenyl	23a
1c	C	C	(4–octylsulfonyl)phenyl	(4–octylsulfonyl)phenyl	23a
1d	C	C	(4–nitro)phenyl	(4–nitro)phenyl	23a
1e	C	C	(5–dibutylamino)–2–theanyl	(5–dibutylamino)–2–theanyl	23a
1f	N	N	(4–dibutylamino)phenyl	(4–dibutylamino)phenyl	23a
1g	N	C	(4–diethylamino)phenyl	(4–diethylamino)phenyl	23a
1h	C	C	(4–dibutylaminostyryl)phenyl	(4–dibutylaminostyryl)phenyl	23b
1i	C	C	(4–(3–methoxystyryl))phenyl	(4–(3–methoxystyryl))phenyl	23c
1j	C	C	(4–(2,4–dimethoxystyryl))phenyl	(4–(2,4–dimethoxystyryl))phenyl	23c
1k	C	C	(4–(2,5–dimethoxystyryl))phenyl	(4–(2,5–dimethoxystyryl))phenyl	23c
1l	C	C	(2,5–dimethoxy)phenyl	(2,5–dimethoxy)phenyl	23d
1m	C	C	benzo–15–crown–5	benzo–15–crown–5	23e
1n	C	C	benzo–18–crown–6	benzo–18–crown–6	23e
1o	C	C	benzo–15–crown–5	benzo–18–crown–6	23e
1p	C	C	benzo–15–crown–5	1–ferrocene	23e
1q	C	C	1–ferrocene	1–ferrocene	23e

1.3.3. Complexation and applications

The electronic blending of 2,2'–bipyridine with suitable donor groups attached to the 4– or 4,4'– positions through π–linker (transmitter), results in the construction of 4– or 4,4'–π–conjugated–2,2'–bipyridines, where the electron drifting nature of the pyridine rings makes them archetypal examples of the 'push–pull' or EDA molecules. These molecules are synthetically flexible and offer easy optical tuning (absorption, emission etc.) through variation / simple modification of their π–backbones. Metal ions are excellent three–dimensional templates for macroscopic assemblies of the 2,2'–bipyridine based coordinating ligands. Based on the coordinating nature of the concerned transition metal ion, the amount of reactants (metal ion and ligands) and reaction conditions, coordination complexes of different geometries / coordination numbers (for example, oc-

Chart 1.1

2a[24a]

2b[24b]

2c[24c]

2d[24d]

2e[24e]

2f[24f]

2g[24g]

2h[24e]

2i[24h]

2j[24i]
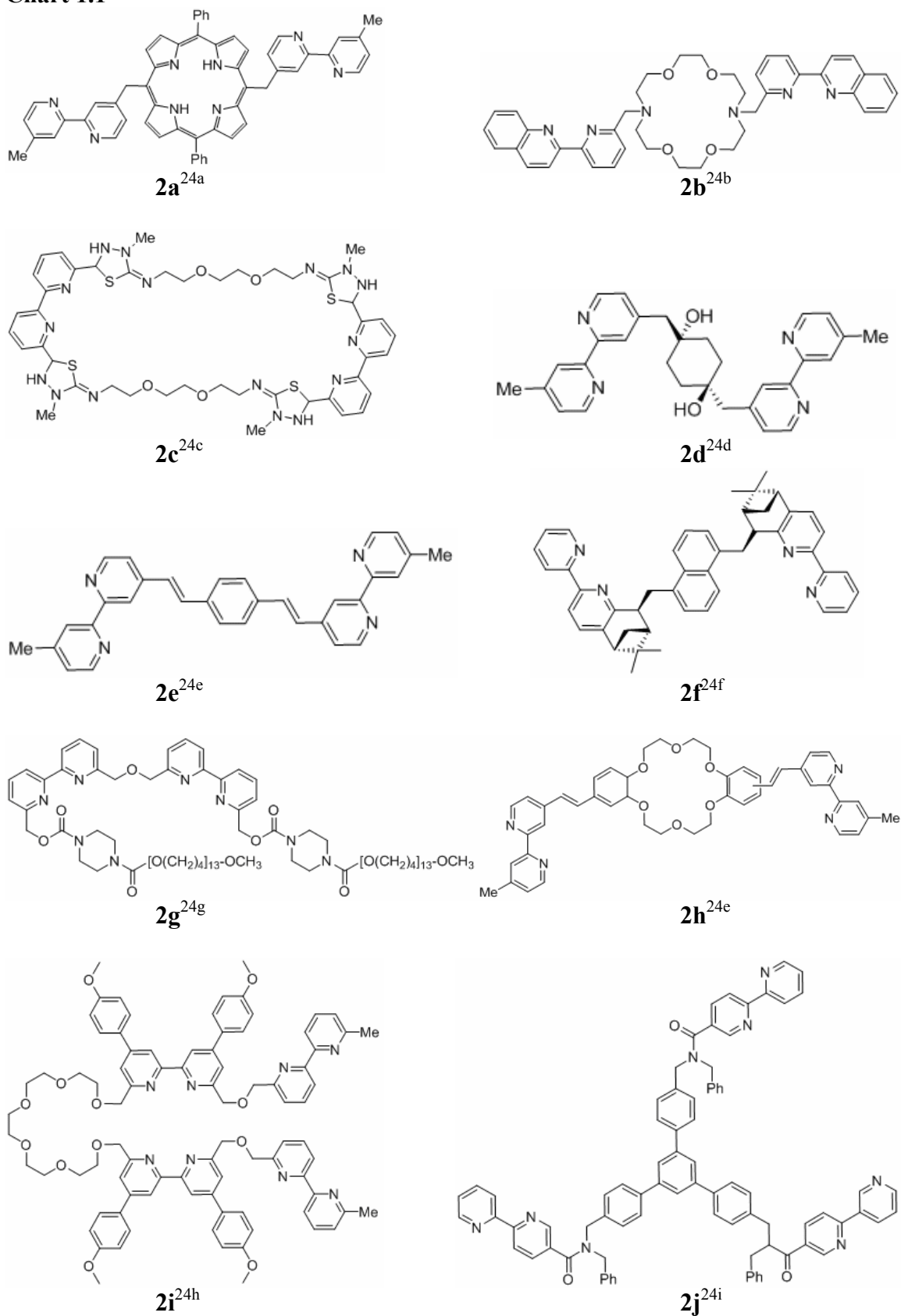
-tahedral, tetrahedral, square planar etc.) can controllably be isolated. The *tris*–bipyridine octahedral complexes of transition metals exist as two enantiomers *viz.* Δ and Λ isomers as shown in Scheme 1.2. Electronic properties of the coordination complexes of the 2,2'–bipyridines, bearing suitable donor groups attached to the pyridine rings through π–linkers, depend strongly upon the nature of the central metal ion and the donor groups present at the π–backbone of the coordinating ligands. In the resulting coordination complexes, the metal ion plays some crucial roles such as: (i) metal ions act as powerful templates to assemble the bipyridine ligands in octupolar arrangements; (ii) it can encourage a low–energy $d_\pi(M) \rightarrow \pi^*(L)$ i.e. metal to ligand charge transfer (MLCT) transition and (iii) Lewis acidity of the metal ions lowers the energy of the intra–ligand charge transfer (ICT) transition inside the 'push–pull' chromophores.

Δ–isomer   Λ–isomer
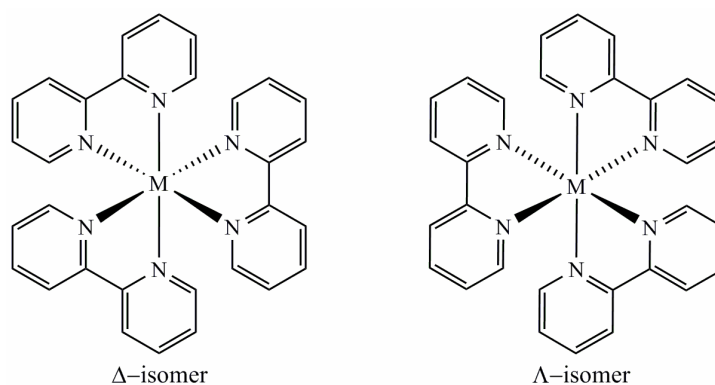
Scheme 1.2 Enantiomers of tris–bipyridine coordination complexes.

Transition metal coordination complexes of the functionalized bipyridines have been found to have potentiality as NLO–phores. In a general consideration, NLO–phores are dipolar 'push–pull' chromophores in which, the inversion symmetry of the concerned dipole is lost due to thermally assisted electrical polling. Apart from the dipolar concept, approach toward octupolar nonlinearity have been developed in early 1990 on the basis of group theoretical and quantum mechanical calculations.[25] The octupolar structure can best be described as a cubic structure with alternating donor and acceptor groups at the edges of the cube. Pure octupolar symmetries can now be derived from this cubic structure either by projection along the 3–fold rotational axis of the cube, resulting in D_3 or D_{3h} symmetry, or by fusion of one type of charge at the barycentre of the cube leading to D_{3h}, D_3, T_d or D_{2d} symmetry (see Figure 1.5). Apart from excellent octupolar non–

linearities based on purely organic molecules, coordination chemistry can also be a useful tool in building octupolar e.g. octahedral or pseudo–tetrahedral systems simply by gathering the coordinating ligands in a pre–designed fashion.
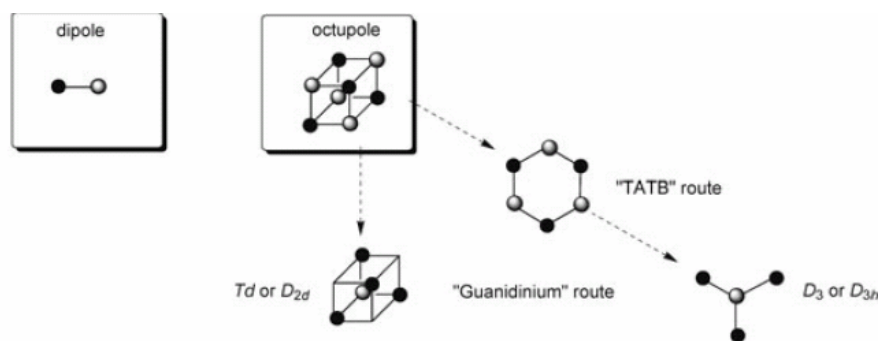
Figure 1.5 Prototype of the second–order NLO–active structures.

Zyss and coworkers first demonstrated octupolar non–linearity for coordination complexes on $[Ru(bpy)_3]^{2+}$ (bpy = 2,2'–bipyridine) which has D_3 symmetry. This concept triggered a new field of research which is illustrated by literature documentation of a large number of NLO–active transition metal complexes of functionalized 2,2'–bipyridine systems from many research laboratories, especially from the research group of Bozec.[26] At this point, it is worth mentioning that, the highest NLO–active compound, reported so far, is constructed from Zn(II) templated octupolar assembly (D_3) of an OPV functionalized 2,2'–bipyridine.[26d]

Ruthenium complexes of π–conjugated–2,2'–bipyridines show outstanding performance as sensitizers in harvesting solar energy i.e. in construction of photovoltaics. The operational method of photovoltaic devices is based on the concept of charge separation at an interface of two materials of different conduction mechanism. To date, this field has been dominated by solid–state p–n junction devices, usually made up of silicon. Dye–sensitized solar cells (DSSCs) have been introduced by Michael Grätzel and Brian O'Regan about two decades ago, as lower cost alternatives of silicon–based semiconductor solar cells (photovoltaics) and belong to the group of thin film solar cells. These photo–electrochemical devices (DSSCs) consist of a semiconductor, which is formed by a photosensitized anode and an electrolyte. These extremely promising cells can be fabricated even with less pure materials, thereby reducing manufacturing cost

compared to silicon based solid–state p–n junction semiconductor devices (which play both the roles of light absorption and charge carrier transport). The highest reported photovoltaic efficiency by DSSCs (~11%) is significantly lower than that by traditional silicon cells (photovoltaic efficiency ~24%). Although, many research groups are at present involved in improving photovoltaic efficiency of DSSCs to make them more competitive to Si–based photovoltaics, and also to contribute appreciably to world energy
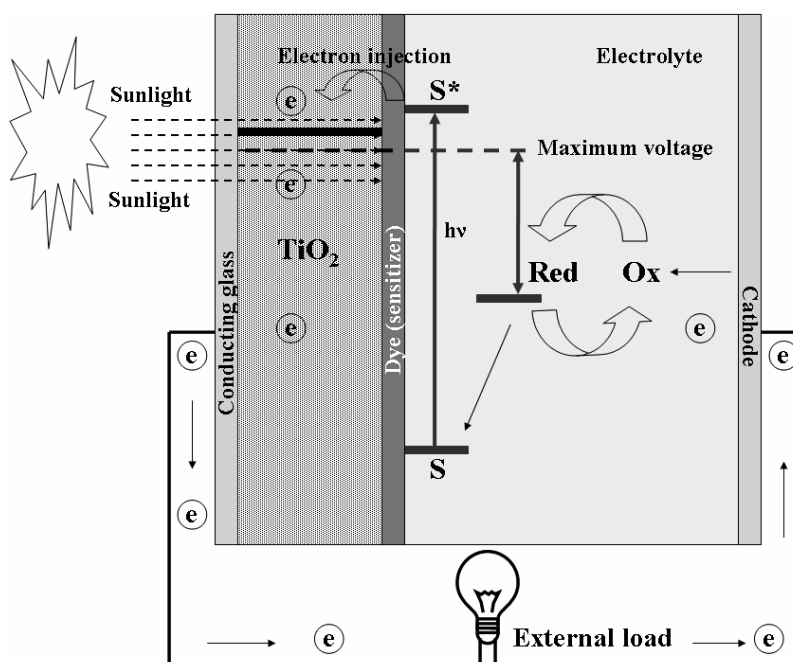
Figure 1.6 Schematic representation of the functioning methodology of a dye sensitized solar cell. Photo–excitation of the sensitizer (S) results in electron injection into conduction band of the mesoporous TiO$_2$ semiconductor. Original state of the dye molecule is restored by the red–ox system which itself is regenerated at the counter electrode by electrons passed through the external load.

needs. These cells are fabricated using a transparent mesoporous oxide layer (which serves as electron conductor) composed of nanosized TiO$_2$ particles (anatase), covered with a molecular charge–transfer dye (e.g. ruthenium complex of a 2,2'–bipyridine derivative) which is competent to absorb sunlight. A liquid electrolyte containing a red–ox couple such as, iodide / triiodide couple (I^-/I_3^-) in an organic solvent is then introduced. The TiO$_2$ layer is commonly supported on a transparent conductive contact, usually fluorine–doped tin oxide (FTO) on glass, so that light can be introduced from the

"TiO$_2$" side of the device. The device is completed by placing another FTO glass "counter electrode" facing the TiO$_2$–coated electrode with a ~20 μm gap between the two

Chart 1.2
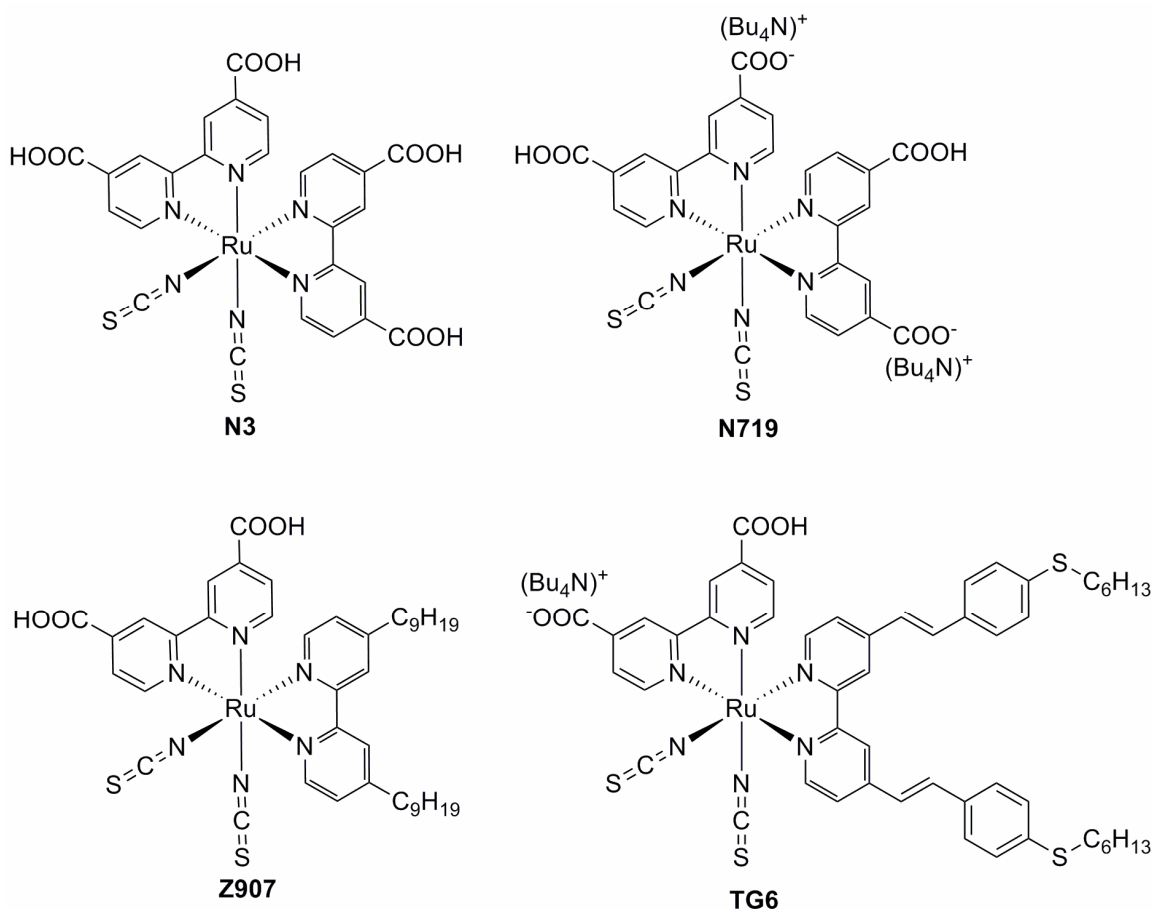
electrodes. The edges are sealed in order to prevent evaporation or contamination of the electrolyte. A schematic representation of a dye–sensitized solar cell has been shown in Figure 1.6. Thus, in a fabricated dye sensitized solar cell, light absorption occurs in the monolayer of the dye at the interface between the transparent oxide electron conductor and the transparent electrolyte. Sunlight enters into the dye layer, where on photo–excitation, the excited state of the dye molecule is relaxed by injecting an electron into conduction band of the oxide (TiO$_2$). The electrons flow toward the transparent electrode, where they are collected for powering an external load. After flowing through the external circuit, they are re–introduced into the cell on a metal electrode on the back, flowing into the electrolyte. The electrolyte then transports the electrons back to the

oxidized dye molecules restoring the original state of the dye. The iodide is regenerated, in turn, by the reduction of triiodide at the counter electrode. Some of the classical ruthenium–bipyridine based dyes have been represented in Chart 1.2. Since past two decades, ruthenium complexes bearing thiocyanate ligands have shown outstanding performance among thousands of dyes that have been synthesized and tested. The revolutionary studies on this field started with *cis*–dithiocyanato–*bis*–(4,4′–dicarboxylic acid–2,2′–bipyridine) Ruthenium(II), (commonly known as N3 dye, see Chart 1.2). The *bis*–tetrabutylammonium salt of this dye (commonly known as N719 dye, Chart 1.2) that showed ~11% photovoltaic conversion efficiency, became a paradigm in this field. Since then, several research groups have been involved in reporting higher efficient dyes by applying different strategies such as, extending the conjugation in the ancillary ligand,[27] modifying the ancillary ligand with electron–donating groups,[28] the use of multi–chromophoric dyes or both[29] etc. However, none of them has displaced N719 for use in record cells. After a long period of 17 years, TG6 dye has been reported to have photovoltaic conversion efficiency close to N719. Although this record of accomplishment might seem dispiriting, it must be kept in mind that the number of possible dyes is nearly infinite and the number of reported dyes is still close to only 1000.

1.4. Motivation of the present work

Braggs' revolutionary invention of the X–ray scattering ability by the atoms in a crystal (more specifically electron density) and latter manufacturing of the single crystal X–ray diffractometer made a radical activation in the structural chemistry. Similarly, fabrication / marketing of many sophisticated instruments have made science easier than the past. During the last few years, the field of polyoxometalate (POM) chemistry has undergone a revolution fuelled by the availability of extremely fast single crystal data collection strategies. This has allowed the characterization of ultra–large clusters that have nuclearities as high as 368 metal atoms in a single cluster molecule. Of course, such discoveries have only been possible because of advances of the instrumentation used to collect the diffraction data coupled with the advent of cheap and powerful computing power for structure solution and refinement. As already mentioned, the POM cluster anions posses a negatively charged surface with two types of oxygen atoms viz. bridging

and terminal. The metal centers of these anions are (usually) in their higher / highest oxidation states and depending upon the electronic nature of these atoms, they can be partially reduced. Again, oxygen atom, due to its higher electronegativity, is a well known hydrogen bonding acceptor in the supramolecular chemistry. Thus, a POM cluster anion can be utilized both as a counter anion as well as a supramolecular synthon in crystal engineering. In the recent years, interests have been grown in incorporating POM cluster anions with the supramolecular complexes of crown ethers. The crown ethers can encapsulate a cation *via* two possible ways: (i) in case of the metal ions they form dative linkages with the formers and (ii) the hydrogen containing cations (e.g. $R–NH_3^+$, H_3O^+ etc.) get encapsulated by D–H⋯O hydrogen bonding interactions (D = donor) with the oxygen atoms of the crown ethers. The basic difference between the metal ions and the ammonium (NH_4^+) / organic ammonium ions $R/Ar–NH_3^+$) is that, the former are spherical in nature whereas, the latter have tetrahedral geometry. Thousands of crystallographic data deposited in the Cambridge Structural Database (CSD) use the POM clusters either as a counterion or as a ligand, but few of them utilize them as a building block in crystal engineering. This concept has motivated us to investigate / analyze the supramolecular weak interactions in the crystals built up of the ammonium–crown ether inclusion complexes in polyoxometalate association. The relevant crystallographic examinations have been described in the Chapter–1. Kochi and coworkers reported a series of crystals that incorporated anthracene or pyrene based cations crystallized with POM counteranions.[30] Structural analysis of the relevant crystals depict charge transfer interactions between the aromatic ring and the POM surfaces. In a continuation of this work a series of anthracene–imidazolidazolium or anthracene–benzimidazolium cations have been attempted to crystallize with the hexametalate cluster anions and the pertinent solids have been reported in the Chapter–2. Advancement of several spectroscopic tools, interesting optical properties of the bipyridines and / or applications of these compounds in optoelectronic devices have prompted to synthesize a series of π–conjugated–2,2'–bipyridines and to examine their optical behaviors. The relevant results have been reported in the Chapter–3.

1.5. References

1. M. T. Pope, *Heteropoly and Isopoly Oxometalates*; Springer–Verlag:Berlin,1983.

2. (a) P. Gouzerh, Y. Jeannin, A. Proust, F. Robert, *Angew. Chem., Int. Ed.*, **1989**, *28*, 1363. (b) A. Proust, R. Thouvenot, F. Robert, P. *Gouzerh, Inorg. Chem.*, **1993**, *32*, 5299.

3. (a) T.–C. Hsieh, J. A. Zubieta, *Polyhedron*, **1986**, *5*, 1655. (b) S. Bank, S. Liu, S. N. Shaikh, X. Sun, J. Zubieta, P. D. Ellis, *Inorg. Chem.*, **1988**, *27*, 3535.

4. H. Kang, J. Zubieta, *J. Chem. Soc., Chem. Commun.*, **1988**, 1192.

5. (a) F. Bottomley, J. Chen, *Organometallics*, **1992**, *11*, 3404. (b) A. Proust, R. Thouvenot, P. Herson, *J. Chem. Soc., Dalton Trans.*, **1999**, 51.

6. H. Kwen, V. G. Young, E. A. Maatta, *Angew. Chem. Int. Ed.* **1999**, *38*, 1145–1146.

7. (a) Y. Du, A. L. Rheingold, E. A. Maatta, *J. Am. Chem. Soc.*, **1992**, *114*, 345. (b) J. B. Strong, R. Ostrander, A. L. Rheingold, E. A. Maatta, *J. Am.Chem. Soc.*, **1994**, *116*, 3601. (c) A. Proust, R. Thouvenot, M. Chaussade, F. Robert, P. Gouzerh, *Inorg. Chim. Acta*, **1994**, *224*, 81. (d) W. Clegg, R. J. Errington, K. Fraser, S. A. Holmes, A. Schäfer, *J. Chem. Soc., Chem. Commun.*, **1995**, 455. (f) J. L. Stark, A. L. Rheingold, E. A. Maatta, *J. Chem. Soc., Chem.Commun.*, **1995**, 1165. (g) J. L. Stark, V. G. Young, E. A. Maatta, *Angew. Chem., Int.Ed.*, **1995**, *34*, 2547. (h) J. B. Strong, B. S. Haggerty, A. L. Rheingold, E. A. Maatta, *J. Chem. Soc., Chem. Commun.*, **1997**, 1137. (i) J. B. Strong, G. P. A. Yap, R. Ostrander, L. M. Liable–Sands, A. L. Rheingold, R. Thouvenot, P. Gouzerh, E. A. Maatta, *J. Am.Chem. Soc.*, **2000**, *122*, 639.

8. W. Clegg, R. J. Errington, K. A. Fraser, C. Lax, D. G. Richards, *Polyoxometalates: From Platonic Solids to Anti–Retroviral Activity* (Eds.: M. T. Pope, A. Müller), Kluwer Academic Publishers, Dordrecht, The Netherlands, 1994, p. 113.

9. Y. Wei, B. Xu, C. L. Barnes, Z. Peng, *J. Am. Chem. Soc.*, **2001**, *123*, 4083.

10. J. Hao, L. Ruhlmann, Y. Zhu, Q. Li, Y. Wei *Inorg. Chem.*, **2007**, *46*, 4960. (b) Y. Zhu, Z. Xiao, N. Ge, N. Wang, Y. Wei, Y. Wang, *Cryst. Growth Des.* **2006**, *6*, 1620. (c) S. Xue, A. Chai, Y. Wei, C. Xiang, W. Bian, J. Shen, *J. Mol. Struct.*,

2008, *888*, 300. (d) S. Xue, A. Chai, Z. Cai, Y. Wei, C. Xiang, W. Biana, J.Shena, *Dalton Trans*., **2008**, 4770. (e) S. Xue, C. Xiang, Y. Wei, Z. Tao,A. Chai, W. Bian, Z. Xu, *Cryst. Growth. Des.*, **2008**, *8*, 2437. (f) Z. Peng., *Angew. Chem. Int. Ed.* **2004**, *43*, 930 and the references therein.

11. (a) O. Nagao, Y. Sasaki, *Acta. Cryst.*, **1979**, *B 35*, 2387. (b) R. Neier, C. Trojanowski, R. Mattes, *J. Chem. Soc., Dalton Trans.*, **1995**, 2521. (c) A. Drljaca, M. J. Hardie, C. L. Raston, *J. Chem. Soc., Dalton Trans.*, **1999**, 3629. (d)W. S. You, E. B.Wang, Y. Xu, Y. Li, L. Xu, *Inorg. Chem.*, **2001**, *40*, 5648. (e) W. You, E .Wang, Q. He, L. Xu, Y. Xing, H. Jia, *J. Mol. Struct.*, **2000**, *524*, 133. (f) W. You, E. Wang, L. Xu, Z. Zhu, Y. Gu, *J. Mol. Struct.*, **2002**, *605*, 41. (g) Y. Li, N. Hao, E. Wang, M. Yuan, C. Hu, N. Hu, H. Jia, *Inorg. Chem.*, **2003**, *42*, 2792. (h) X. Lu, B. Liu, S. Wang, C. Ye, *Polyhedron*, **2005**, *24*, 2889. (i) V. Shivaiah, S. K. Das, *Inorg. Chem.*, **2005**, *44*, 7313. (j) V. Shivaiah, *Inorg. Chem. Commun.*, **2006**, *6*, 1191. (k) V. Shivaiah, S. K. Das, *Angew. Chem., Int. Ed.*, **2006**, *45*, 245. (l) M. Sarma, T. Chatterjee, S. K. Das, *Inorg. Chem. Commun.*, **2010**, *13*, 1114 and the references therein. (m) A. Falber, B. P. Burton–Pye, I. Radivojevic, L. Todaro, R. Saleh, L. C. Francesconi, C. M. Drain, *Eur. J. Inorg. Chem.*, **2009**, 2459 and the references therein. (n) T. Akutagawa, D. Endo, F. Kudo, S. I. Noro, S. Takeda, L. Cronin, T. Nakamura, *Cryst. Growth Des.*, **2008**, *8*, 812. (o) T. Akutagawa, D. Endo, H. Imai, S. I. Noro, L. Cronin, T. Nakamura, *Inorg. Chem.*, **2006**, *45*, 8628.

12. (a) M. Raynaud, J. C. Chermann, F. Plata, C. Jasmin, G. C. R. Mathe´, *Acad. Sci., Ser. D*, **1971**, *272*, 347. (b) M. Raynaud, J. C. Chermann, F. Plata, C. Jasmin, G. Mathe´, F. Sinoussi, *Prog. Immunobiol. Stand.*, **1972**, *5*, 285. (c) N. Raybaud, C. Jasmin, J. Huppert, J. C. Chermann, G. Mathe´, M. Raynaud, *Rev. Eur. Etud. Clin. Biol.* **1972**, *17*, 295. (d) C. Bonissol, P. Kona, J. C. Chermann, C. Jasmin, M. C. R. Raynaud, *Acad. Sci., Ser. D.* **1972**, *274*, 3030. (e) C. Jasmin, N. Raybaud, J. C. Chermann, D. Haapala, F. Sinoussi, C. B. Loustau, C. Bonissol, P. Kona, M. Raynaud, *Biomedicine*, **1973**, *18*, 319. (f) J. C. Chermann, F. C. Sinoussi, C. Jasmin, *Biochem. Biophys. Res. Commun.*, **1975**, *65*, 1229. (g) H. Tsiang, P. Atanasiu, J. C. Chermann, C. J. Jasmin, *Gen. Virol.*, **1978**, *40*, 665. (h)

F. Bussereau, J. C. Chermann, E. De Clercq, C. Hannoun, *Ann. Virol.*, **1983**, *134E*, 127. (i) F. Bussereau, A. Ermine, *Ann. Virol. (Inst. Pasteur)*, **1983**, *134E*, 487. (j) M. Souyri–Caporale, G. Tovey, K. Ono, C. Jasmin, J. C. Chermann, *Gen. Virol.*, **1984**, *65*, 831.

13. (a) D. L. Barnard, C. L. Hill, T. Gage, J. E. Matheson, J. H. Huffman, R. W. Sidwell, M. I. Otto, R. F. Schinazi, *Antiviral Res.*, **1997**, *34*, 27. (b) Y. Inouye, Y. Fujimoto, M. Sugiyama, T. Yoshida, T. Yamase, *Biol. Pharm. Bull.*, **1995**, *18*, 996. (c) C. L. Hill, M. Hartnup, M. Faraj, M. Weeks, C. M. Prosser–McCartha, R. B. Brown, M. Kadkhodayan, J. –P. Sommadossi, R. F. Schinazi, *In Advances in Chemotherapy of AIDS*; Diasio, R. B., Sommadossi, J.–P., Eds.; Pergamon Press, Inc.: New York, 1990. (d) C. L. Hill, M. S. Weeks, R. F. Schinazi, *J. Med. Chem.*, **1990**, *33*, 2767. (e) S. Shigeta, S. Mori, J. Watanabe, M. Baba, A. M. Khenkin, C. L. Hill, R. F. Schinazi, *Antiviral Chem. Chemother.*, **1995**, *6*, 114. (f) Y. Inouye, Y. Tokutake, J. Kunihara, T. Yoshida, Y. Yamase, A. Nakata, S. Nakamura, *Chem. Pharm. Bull.*, **1992**, *40*, 805. (g) N. Yamamoto, D. Schols, E. De Clercq, Z. Debyser, R. Pauwels, J. Balzarini, H. Nakashima, M. Baba, M. Hosoya, R. Snoeck, J. Neyts, G. Andrei, B. A. Murrer, B. Theobald, G. Bossard, G. Henson, M. Abrams, D. Picker, *Mol. Pharmacol.*, **1992**, *42*, 1109.

14. (a) F. Bussereau, M. Picard, C. Malick, A. Teze, J. Blancou, *Ann. Inst. Pasteur/Virol.*, **1986**, *137E*, 391. (b) R. H. Kimberlin, C. A. Walker, *Antimicrob. Agents Chemother.*, **1986**, *30*, 409. (c) C, Jasmin, J. C. Chermann, G. Herve´, A. Teze, P. Souchay, C. Boy–Loustau, N. Raybaud, F. Sinoussi, M. Raynaud, *J. Natl. Cancer Inst.*, **1974**, *53*, 469. (d) L. Ni, F. D. Boudinot, *Eur. J. Drug Metab. Pharmacokinet.*, **1995**, *20*, 209. (e) H. Fujita, T. Fujita, T. Sakurai, T. Yamase, Y. Seto, *Tohoku J. Exp. Med.*, **1992**, *168*, 421. (f) T. Yamase, *Mol. Eng.*, **1993**, *3*, 241. (g) T. Yamase, H. Fujita, K. Fukushima, *Inorg. Chim. Acta*, **1988**, *151*, 15.

15. For exaple, pK values of some common HPAs and mineral acids have been outlined here. Values in the perenthesis indicate pK_1, pK_2 and pK_3 in order. $H_3PW_{12}O_{40}$ (1.6, 3.0 and 4.0); $H_4PW_{11}VO_{40}$ (1.8, 3.2 and 4.4); $H_4SiW_{12}O_{40}$ (2.0, 3.6 and 5.3); $H_3PMo_{12}O_{40}$ (2.0, 3.6 and 5.3); $H_4SiMo_{12}O_{40}$ (2.1, 3.9 and 5.9); H_2SO_4 (6.6); HCl (4.3); HNO_3 (9.4).

16.   (a) Y. Izumi, K. Urabe, M. Onaka, *Zeolite, Clay and HeteropolyAcid in Organic Reactions*; Kodansha/VCH: Tokyo, 1992; p 99. (b) I. V. Kozhevnikov, K. I. Matveev, *Appl. Catal.*, **1983**, *5*, 135. (c) C. Hu, M. Hashimoto, T. Okuhara, M. Misono, *J. Catal.*, **1993**, *143*, 437. (d) I. V. Kozhevnikov, S. M. Kulikov, N. G. Chukaeva, A. T. Kirsanov, A. B. Letunova, V. I. Blinova, *React. Kinet. Catal. Lett.*, **1992**, *47*, 59.

17.   (a) A. M. Khenkin, I. Efremenko, L. Weiner, J. M. L. Martin, R. Neumann, *Chem. Eur. J.*, **2010**, *16*, 1356. (b) H. Goldberg, I. Kaminker, D. Goldfarb, R. Neumann, *Inorg. Chem.*, **2009**, 48, 7947. (c) J. Ettedgui, R. Neumann, *J. Am. Chem. Soc.*, **2009**, 131, 4. (d) A. M. Khenkin, R. Neumann, *J. Am. Chem. Soc.*, **2008**, *130*, 14474. (e) A. M. Khenkin, R. Neumann, *J. Am. Chem. Soc.*, **2008**, *130*, 11886. (f) D. Sloboda–Rozner, K. Neimann, R. Neumann, *J. Mol. Cat. A.*, **2007**, *262*, 109. (g) D. Sloboda–Rozner, R. Neumann, *Green Chem.*, **2006**, *8*, 679.

18.   D. E. Katsoulis, *Chem. Rev.*, **1998**, *98*, 359 and the references therein.

19.   (a) C. Kaes, A. Katz, M. W. Hosseini, *Chem. Rev.* **2000**, *100*, 3553–3590 and the references therein. (b) U. S. Schubert, C. Eschbaumer, *Angew. Chem. Int. Ed.* **2002**, *41*, 2892–2926 and the references therein.

20.   (a) E. C. Riesgo, X. Jin, R. P. Thummel, *J. Org. Chem.*, **1996**, *61*, 3017. (b) C.–Y. Hung, T.–L. Wang, Z. Shi, R. P. Thummel, *Tetrahedron*, **1994**, *50*, 10685. (c) S. Gladiali, G. Chelucci, F. Soccolini, G. Delogu, G. Chessa, *J. Organomet. Chem.*, **1989**, *370*, 285. (d) F. Wu, R. P. Thummel, *Inorg. Chim. Acta.*, **2002**, *327*, 26. (e) S. Krishnan, D. G. Kuhn, G. A. Hamilton, *J. Am. Chem. Soc.*, **1977**, *99*, 8121. (f) C. J. Moody, C. W. Rees, R. Thomas, *Tetrahedron*, **1992**, *48*, 3589. (g) Y. Shen, B. P. Sulivan, *Inorg. Chem.*, **1995**, *34*, 6235.

21.   (a) D. Tzalis, Y. Tor, Chem. Commun., 1996, 1043. (b) D. Tzalis, Y. Tor, J. Am. Chem. Soc., 1997, 119, 852. (c) W. Guo, E. Galoppini, G. Rydja, G. Pardi, *Tetrahedron Lett.*, **2000**, *41*, 7419. (d) M. Schmittel, C. Michel, A. Wiegrefe, V. Kalasani, *Synthesis,* **2001**, 1561. (e) C. –X. liu, C. Michel, *Org. Lett.*, **2000**, *2*, 3959.

22.   (a) Smith, A. P.; Lamba, J. J. S.; Fraser, C. L. *Org. Syn.* **2004**, *10*, 107 – 112; (b) Fraser, C. L.; Anastasi, N. R.; Lamba, J. J. S. *J. Org. Chem.* **1997,** *62*, 9314–9317.

23.   (a) O. Maury, J.–P. Guégan, T. Renouard, A. Hilton, P. Dupau, N. Sandon, L. Toupet, H. Le Bozec, *New J. Chem.* **2001**, *25*, 1553. (b) L. Viau, O. Maury, H. Le Bozec, *Tetrahedron Lett.* **2004**, *45*, 125. (c) T. Chatterjee, M. Sarma, S. K. Das, *Tetrahedron Lett.* **2010**, *51*, 1985–1988. (d) D. Berner, C. Klein, M. K. Nazeeruddin, F. De Angelis, M. Castellani, Ph. Bugnon, R. Scopelliti, L. Zuppirolid, M. Graetzel, *J. Mater. Chem.* **2006**, *16*, 4468. (e) O. Kocian, R. J. Mortimer, P. D. Beer, *J. Chem. Soc., Perkin Trans. 1* **1990**, 3203.

24.   (a) S. G. DiMagno, V. S. –Y. Lin, M. J. Therien, *J. Org. Chem.*, **1993**, *58*, 5983 (b) H. Tsukube, J. Uenishi, H. Higaki, K. Kikkawa, T. Tanaka, S, Wakabayashi, S. Oae, *J. Org. Chem.*, **1993**, *58*, 4389. (c) P. Molina, A. Tarraga, C. Gaspar, A. Espinosa, *J. Org. Chem.*, **1994**, *59*, 3665. (d) C. K. Ryu, R. Wang, R. H. Schmehl, S. Ferrere, M. Ludwikow, J. W. Merkert, C. E. L. Headford, C. M. Elliott, *J. Am. Chem. Soc.*, **1992**, *114*, 430. (e) O. Kocian, R. J. Mortimer, P. D. Beer, *Tetrahedron Lett.*, **1990**, *31*, 5069. (f) O. Mamula, A. von Zelewsky, T. Bark, G. Bernardinelli, *Angew. Chem., Int. Ed.*, **1998**, *37*, 290. (g) C. D. Eisenbach, U. S. Schubert, G. R. Baker, G. R. Newkome, *J. Chem. Soc., Chem. Commun.*, **1995**, 69. (h) T. Nabeshima, T. Inaba, N. Furukawa, T. Hosoya, Y. Yano, *Inorg. Chem.*, **1993**, *32*, 1407. (i) P. Belser, A. von Zelewsky, M. Frank, C. Seel, F. Vogtle, L. De Cola, F. Barigelletti, V. Balzani, *J. Am. Chem. Soc.*, **1993**, *115*, 4076.

25.   Topical issue on NLO: D. M. Burland, Ed. *Chem. Rev.* **1994**, *94*, 1–278 and the references therein.

26.   H. Le Bozec, T. Renouard, *Eur. J. Inorg. Chem.* **2000**, 229–239. (b) K. Sénéchal, O. Maury, H. Le Bozec, I. Ledoux, J. Zyss, *J. Am. Chem.. Soc.* **2002**, *124*, 4560–4561. (c) O. Maury, H. Le Bozec, *Acc. Chem. Res.* **2005**, *38*, 691–704. (d) O. Maury, L. Viau, K. Sénéchal, B. Corre, J.–P. Guégan, T. Renouard, I. Ledoux, J. Zyss, H. Le Bozec, *Chem. Eur. J.* **2004**, *10*, 4454 – 4466. (e) V. Aubert, V. Guerchais, E. Ishow, K. Hoang–Thi, I. Ledoux, K. Nakatani, H. Le Bozec, *Angew. Chem. Int. Ed.* **2008**, *47*, 577–580.

27.   (a) K. J. Jiang, N. Masaki, J. B. Xia, S. Noda, S. Yanagida, *Chem. Commun.* **2006**, 2460–2462. (b) C. Klein, M. K. Nazeeruddin, P. Liska, D. Di Censo, N. Hirata, E. Palomares, J. R. Durrant, M. Grätzel, *Inorg. Chem.* **2005**, *44*, 178–180.

(c) P. Wang, C. Klein, R. Humphry–Baker, S. M. Zakeeruddin, M. Grätzel, *J. Am. Chem. Soc.* **2005**, *127*, 808–809. (d) D. Kuang, C. Klein, S. Ito, J. E. Moser, R. Humphry–Baker, N. Evans, F. Duriaux, C. Grätzel, S. M. Zakeeruddin, M. Grätzel, *Adv. Mater.* **2007**, *19*, 1133–1137. (e) M. K. Nazeeruddin, T. Bessho, L. Ceveya, S. Ito, C. Klein, F. De Angelis, S. Fantacci, P. Comtea, P. Liska, H. Imai, M. Grätzel, *J. Photochem. Photobiol. A* **2007**, *185*, 331–337.

28.   (a) C. Y. Chen, S. J. Wu, C. G. Wu, J. G. Chen, K. C. Ho, *Angew. Chem., Int. Ed.* **2006**, *45*, 5822–5825. (b) N. Hirata, J. J. Lagref, E. J. Palomares, J. R. Durrant, M. K. Nazeeruddin, M. Grätzel, D. Di Censo, *Chem. Eur. J.* **2004**, *10*, 595–602.

29.   (a) B. O'Regan, M. Grätzel, *Nature* **1991**, *353*, 737–740. (b) W. M. Campbell, A. K. Burrell, D. L. Officer, K. W. Jolley, *Coord. Chem. Rev.* **2004**, *248*, 1363–1379. (c) R. Amadelli, R. Argazzi, C. A. Bignozzi, F. Scandola, *J. Am. Chem. Soc.* **1990**, *112*, 7099–7103. (d) S. R. Jang, R. Vittal, J. H. Lee, N. Jeong K. J. Kim, *Chem. Commun.* **2006**, 103–105.

30.   P. Le Magueres, S. M. Hubig, S. V. Lindeman, P. Veya, J. K. Kochi**, *J. Am. Chem. Soc.*, **2000,** *122,* 10073.

Supramolecular architectures from ammonium–crown ether inclusion complexes in polyoxometalate association

2

Abstract:– Supramolecular association between crown–ether inclusion complexes of simple ammonium ion (NH_4^+) or organic ammonium ion ($Ar–NH_3^+$) and a polyoxometalate cluster anion has been demonstrated in six ion–pair salts formulated as, $[NH_4(B18C6)][Bu_4N][Mo_6O_{19}]$ (**1**), $[NH_4(B18C6)]_4[SiW_{12}O_{40}].2CH_3CN$ (**2**), $[NH_4(DB18C6)]_2[Mo_6O_{19}].4H_2O$ (**3**), $[NH_4(DC18C6)]_2[Mo_6O_{19}]$ (**4**), $[NH_4(DB30C10)]_2 [Mo_6O_{19}].CH_3COOH$ (**5**) and $[Bu_4N][OPDAH(18C6)][Mo_6O_{19}]$ (**6**) where, B18C6 = benzo–18–crown–6, DB18C6 = dibenzo–18–crown–6, DC18C6 = dicyclohexyl–18–crown–6, DB30C10 = dibenzo–30–crown–10, 18C6 = 18–crown–6 and OPDAH = mono-protonated o–phynelenediamine. This chapter describes detailed spectroscopic characterizations (IR, ^1H NMR, and UV–visible) of these solids along with unambiguous structural determinations by single crystal X–ray crystallography.

2.1. Preface

Since Pedersen's serendipitous discovery of dibenzo–18–crown–6,[1] the macrocyclic crown poly–ethers have been extensively used in the areas of supramolecular chemistry and/or crystal engineering as a host for variety of cationic species.[2] Numerous crown ether related structural entries in the Cambridge Structural Database (CSD) is the illustration of the matter. These structurally flexible macrocycles encapsulate small guest molecular cations of the type DH_n^{m+}, for example, oxonium ion (H_3O^+), ammonium ion (NH_4^+) etc. through supramolecular D–H⋯O hydrogen–bonding interactions (D = donor) and thus, act as good stabilizing ligands for these guests. The structure of the resulting supramolecular cationic species is controlled by the cavity size of the crown ether hosts. Larger and structurally more elastic crown poly–ethers bind smaller cations (cation size considerably smaller than the crown ether cavity) either by wrapping around the ion or by intriguing more than one ion in their cavities. A recent perspective "crown ethers as stabilizing ligands for oxonium ions" covers most of the issues where oxonium ions (H_3O^+, $H_5O_2^+$, $H_7O_3^+$ etc.) have been integrated with the crown ether hosts.[3] There are some reports, where simple ammonium ion (NH_4^+) has been shown to be included in the

crown ether cavity.[4] Simple oxonium ion (H_3O^+) is an almost planar guest cation and is incorporated with the macrocycles through three O^+–H···O hydrogen bonding interactions. Whereas, ammonium ion (NH_4^+) is a tetrahedral guest cation, that is generally included in the smaller crown ethers (e.g. 18–crown–6) *via* three N^+–H···O supramolecular interactions and the fourth N–H bond is projected outward from the crown ether cavity and can be involved in N^+–H···A hydrogen bonding interaction (A = acceptor) with an acceptor atom suitably placed in the crystal lattice (Scheme 2.1). Structurally flexible larger crown ethers might result in alteration of the theme by wrapping around the ion thereby making it inert toward the aforesaid acceptor atom (in terms of supramolecular interactions).

A = acceptor   interaction through terminal oxygen atom   interaction through bridging oxygen atom
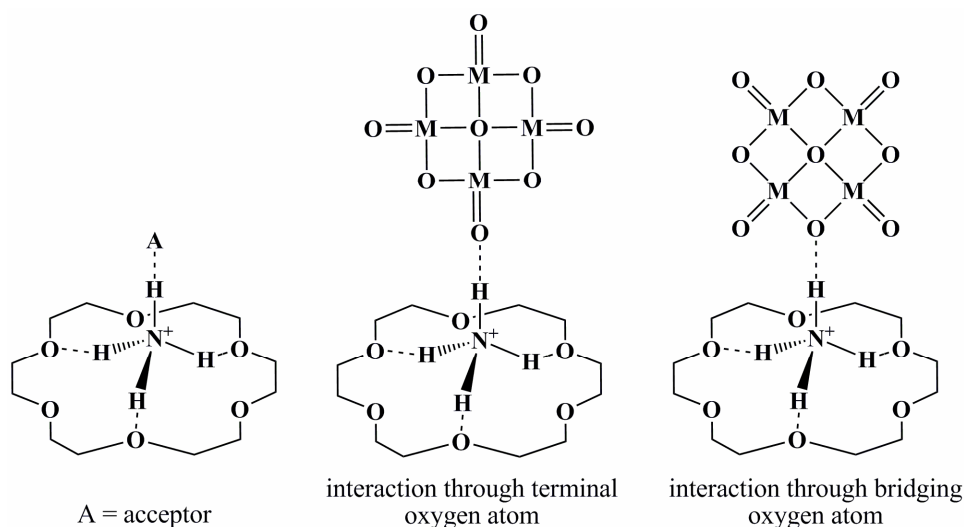
Scheme 2.1 A schematic representation showing diverse interactions between the ammonium crown–ether cation and segment of a POM anion as hydrogen bonding acceptor.

Polyoxometalates (POMs) or metal–oxide based cluster anions encompassing electronic and structural diversites,[5] comprise negatively charged oxygen atoms on their surfaces that can participate in hydrogen bonding interactions with a donor atom. As a result, an ammonium–crown ether supramolecular complex cation can be associated with a POM anion both by coulombic as well as supramolecular N^+–H···O hydrogen bonding interactions after placing the latter at suitable acceptor site in the crystal as mentioned above. A little ambiguity might be there for structural prediction, because the POM anion

can use either terminal or bridging O atom as the H–bond accepting site (Scheme 2.1). However, these cluster anions are symmetrical and upon operation of the symmetry elements on these supramolecular interactions, a supramolecular network is expected to generate. Moreover, the C–H···O interactions between the crown ether and the POM anion would also play an important role toward the crystal packing. Both the simple ammonium ion (NH_4^+) and organic ammonium ions ($R–NH_3^+$ or $Ar–NH_3^+$) have tetrahedral geometry. The only structural difference between them is that, the latter one has hydrophobic alkyl or aryl group. Again compared to alkyl groups, the phenyl ring of the aromatic amines might undergo π–stacking interactions in the lattice with the generation of a totally different type of crystal packing than that in crown ether inclusion complexes of the simple ammonium or alkyl ammonium cations. Therefore, an attempt to perform engineering with the POM anions associated with ammonium–crown ether supramolecular counter cations would be an interesting task. At this point, it is worth to mention that several multidimensional assemblies formed by the POM macro–anions as supramolecular bricks and molecular interactions (covalent or weak) as supramolecular cement, have been well–documented in literature.[6–8]

Several research groups have earlier described the supramolecular chemistry of POM associated crown ether inclusion complexes.[9–11] Supramolecular chemistry of the crown ether hydrogen bonding complexes of protonated 1,3– and 1,4–phynelenediamines, associated with Keggin type polyoxometalates, have been described in recent literature.[11a–c] However, the hydrogen bonding situation in a crystal, built from the supramolecular adduct (1,2–phynelenediamine–associated–crown ether) and the POM cluster anion, would be different from the crystal, composed of the POM anion and the similar adduct containing any one of the other two positional isomers of phynelenediamines as shown in Scheme 2.2.

Based on the position of the amino groups, phynelenediamines have different bite angles for hydrogen bonding interactions (Scheme 2.2). 1,3– and 1,4–phynelenediamines have the amino groups at 120º and 180º angular separation respectively; thus, in protonated or non–protonated form they can meet two crown ethers (smaller cavity size) *via* N–H···O hydrogen bonding interaction with the macrocycle (direction of the supramolecular interactions are marked by arrows in Scheme 2.2). On the other hand,

1,2–phenylenediamine (*o*–phynelenediamine, OPDA) has only 60º angular separation of the amino groups. Therefore, this diamine (or its protonated analogue) can interact with only one crown ether. Again, as the cavity size of 18–crown–6 fits for encapsulation of only one ammonium cation, complete encapsulation of the concerned diamine (OPDA or
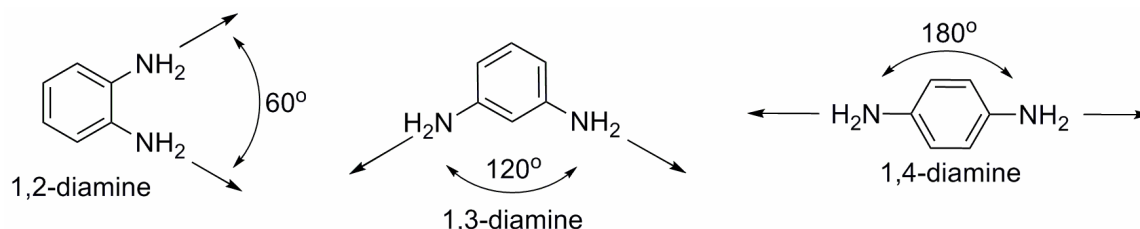
Scheme 2.2 Angular spans for the hydrogen bonding interactions in various phynelene diamines. The straight arrows indicate direction of the hydrogen bonding vectors (D→A, D = donor, A = acceptor)

protonated–OPDA) by the crown ether (18–crown–6) cavity is not possible. Consequently, only one $-NH_2$ / $-NH_3^+$ group would be encapsulated in the concerned crown ether cavity and the other group would project at an angle of 60º to this group. This free amino / ammonium group of the protonated OPDA might interact with a POM anion through N–H···O hydrogen bonding interactions if possible and it is interesting to investigate this situation. For this purpose, a simple POM anion i.e. $[Mo_6O_{19}]^{2-}$ isopolyanion have been chosen.

Here, in this chapter, six POM associated ammonium ion and/or organic–ammonium ion $\subset$ (crown ether) supramolecular complexes (compounds **1–6**) have been demonstrated using five different crown ethers namely, 18–crown–6 (18C6), benzo–18–crown–6 (B18C6), dibenzo–18–crown–6 (DB18C6), dicyclohexyl–18–crown–6 (DC18C6) and dibenzo–30–crown–10 (DB30C10) and two different POM cluster anions ($[Mo_6O_{19}]^{2-}$ and $[SiW_{12}O_{40}]^{4-}$).[12] All these macrocyclic poly–ethers (crown ethers) are distinct from each other in terms of their symmetry as well as their cavity size. For example, dibenzo–30–crown–10 has a large cavity and is the most flexible crown–ether among all the five used.

The hexamolybdate anion $[Mo_6O_{19}]^{2-}$ is an octahedral symmetrical (O_h) iso–polyanion and the silicotungstate anion $[SiW_{12}O_{40}]^{4-}$ is a tetrahedral symmetrical (T_d) hetero–polyanion. The central oxygen atom in $[Mo_6O_{19}]^{2-}$ anion and the Si heteroatom in

$[SiW_{12}O_{40}]^{4-}$ anion occupy the O_h and T_d symmetrical sites respectively, the first one being centrosymmetric with respect to the central oxygen atom. Out of six structures described in this chapter, five of them (**1**, **3–6**) are constituted with the hexamolybdate anion which is a very popular POM anion due to the simplicity in its structure. The anion is known to crystallize with a variety of counter cations for example, alkylammoniums,[13] phenylphosphonium and/or arsonium,[14] dithiolenes,[15] planar aromatic cations,[16] transition metal complexes,[17] even with crown ether complexes[9–11] rendering simple to complicated dimensionalities in molecular packing in the resulting crystalline solids. However, in the present chapter, the anion has been introduced not only as a counter anion but also as a supramolecular building block in comprehending the intermolecular weak interactions between ammonium ion, crown ether and a POM anion.

2.2. Results and Discussion

2.2.1. Synthesis

Single crystals for the title compounds **1–6** have been grown from acidified organic (compounds **1**, **2**, **5** and **6**) or acidified aqueous–organic medium (compounds **3–4**) using two different synthetic routes. For compounds **1**, **2** and **5**, the ready–made POM cluster precursors $[Bu_4N]_2[Mo_6O_{19}]$ (compounds **1**, **5**) and $H_4SiW_{12}O_{40}$ (compound **2**) have been used with crown ether and NH_4SCN (as the NH_4^+ ion source). The POM anions are reasonably stable in the reaction condition and crystallize after their association with the $[NH_4^+ \subset (crown\ ether)]$ cations (a supramolecular cationic species). On the other hand, for compounds **3** and **4**, ammonium heptamolybdate has been utilized to serve for both the NH_4^+ ion source as well as to generate the isopolyanion $[Mo_6O_{19}]^{2-}$ in situ from acidified MeCN–H_2O medium. Although various POM anions can be assembled in this reaction condition, the probable reason for the selectivity of the macro–cyclic cation toward hexamolybdate anion is not so clear. It is notable that, single crystals for compounds **3** and **4** could not be isolated using the reaction condition described for compounds **1**, **2** and **5** and vice versa. The compound **6** was obtained as greenish–yellow plates from acidified acetonitrile solution at room temperature. In the present reaction co-ndition OPDA got monoprotonated and the resulting mono–cation (OPDAH$^+$) was found to form the supramolecular complex cation $[OPDAH(18C6)]^+$ after incorporation with

the crown ether, 18C6. This cation, [OPDAH(18C6)]$^+$, in turn, replaced one [Bu$_4$N]$^+$ cation from the [Bu$_4$N]$_2$[Mo$_6$O$_{19}$] POM cluster resulting in formation of the compound **6**. All the attempts for complete replacement of the tetrabutylammonium cations by using excess of OPDA, crown ether or acid were failed. Similarly, the expected compounds would be formulated as [OPDAH(18C6)]$_2$[Mo$_6$O$_{19}$] (monoprotonated OPDA) or [OPDAH$_2$(18C6)][Mo$_6$O$_{19}$] (diprotonated OPDA) and all the repeating trials in isolation of these solids by variation of the reactant amounts have ended with the isolation of [Bu$_4$N][OPDAH(18C6)][Mo$_6$O$_{19}$] i.e. compound **6** only.

2.2.2. UV–visible spectroscopy

Compounds **1** and **2** consist of same crown ether i.e. B18C6, but different POM anions, i.e. [Mo$_6$O$_{19}$]$^{2-}$ and [SiW$_{12}$O$_{40}$]$^{4-}$ for compound **1** and **2** respectively whereas, compound **3** contains DB18C6 macrocycle and [Mo$_6$O$_{19}$]$^{2-}$ POM anion. To check the outcome of varying crown ether or POM anion on the absorption properties of the relevant compounds, UV–visible spectra of compounds **1–3** have been recorded in DMSO (concentration: ~ 10^{-4}M) at 298K. The corresponding spectra have been presented in Figure 2.1. Crystals of the compounds **1** and **3** are orange–red in colour while that of the compound **2** are yellow. But in the relevant spectra no band in the visible region of the spectra is observed. Instead, a structureless broad band is observed in the ultraviolet region of the spectra (compounds **1** and **3**) centred at ca. 320 nm. For the compound **2**, a broad shoulder originating from 360 nm is observed (Figure 2.1). Thus, changing the crown ether from B18C6 to DB18C6 has not altered the absorption property of the corresponding compounds in solution state, whereas, a significant change has been noticed when the POM anion is changed from [Mo$_6$O$_{19}$]$^{2-}$ (in compound **1**) to [SiW$_{12}$O$_{40}$]$^{4-}$ (in compound **2**).

2.2.3. Infra–red spectroscopy

Infrared spectroscopy is a useful tool for the detection of particular functional groups. Free ammonium ion (NH$_4^+$) has T_d symmetry, which usually displays a strong and broad absorption in the region of 3300–3030 cm^{-1} because of N–H stretching vibrations. Another strong band near 1400 cm^{-1} is normally observed due to the N–H bending motions.[18] These bands move to higher and lower wavelengths respectively when the

relevant ion is involved in H–bonding. Thus, in compounds **1–5**, inclusion phenomenon of NH_4^+ ion in the crown ether cavity is easily realized by means of IR spectroscopy, as
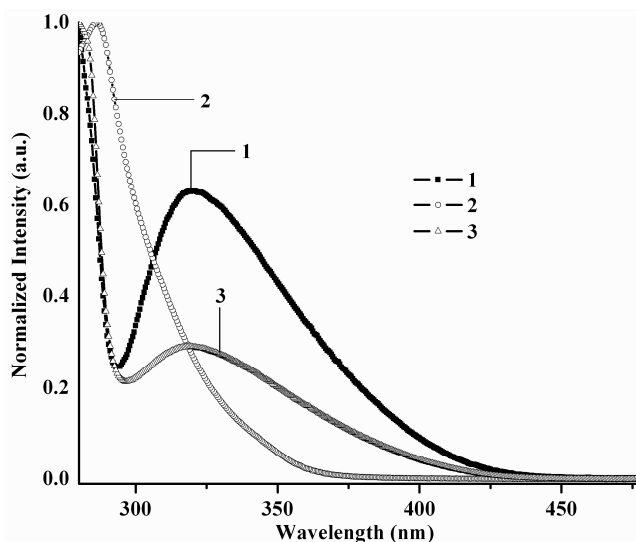
Figure 2.1 Normalized UV–visible spectra of the compounds **1–3** in DMSO recorded at 298K.

the ion is assimilated within the crown ether cavity through supramolecular hydrogen bonding interactions. Appearance of a broad vibrational band centred at 3530 cm^{-1} in the IR spectrum of the compound **3** suggests the presence of solvent / H–bonded water molecule in the compound. Strong and broad bands at 3175, 3209, 3254, 3182, 3238 cm^{-1} (Figure 2.2) for compounds **1–5** respectively are assigned to the N–H stretching vibrations of the NH_4^+ ion; the variation in band positions is possibly due to difference in H–bonding environment around the ion. The IR bands at 1458, 1454, 1454, 1456, 1456 cm^{-1} for compounds **1–5** respectively are attributed to N–H$_{def}$ vibrations of the NH_4^+ ion. In the case of compound **6**, two medium intensity sharp bands at 3420 and 3352 cm^{-1} are observed that are attributed to the asymmetrical and symmetrical N–H stretching vibrations respectively of aromatic –NH_2 or –NH_3^+ group, whereas the band at 1633 cm^{-1} with a shoulder might be due to overlapping of the N–H$_{def}$ vibrations with others (e.g. aromatic C=C). Multiple bands in the region of 3075–2950 cm^{-1} are due to various C(Ar)–H, C(sp^3)–H along with combined N–H stretching vibrations in compounds **1–6**. A weak intensity band at 2251 cm^{-1} in the spectrum of compound **2** resembles –C≡N stretching of aliphatic nitrile. A sharp IR band of medium intensity at 1712 cm^{-1}, in the

spectrum of compound **5**, is attributed to the >C=O stretching of saturated aliphatic acid dimer (that is observed indeed in the relevant crystal structure) but the associated O–H st-
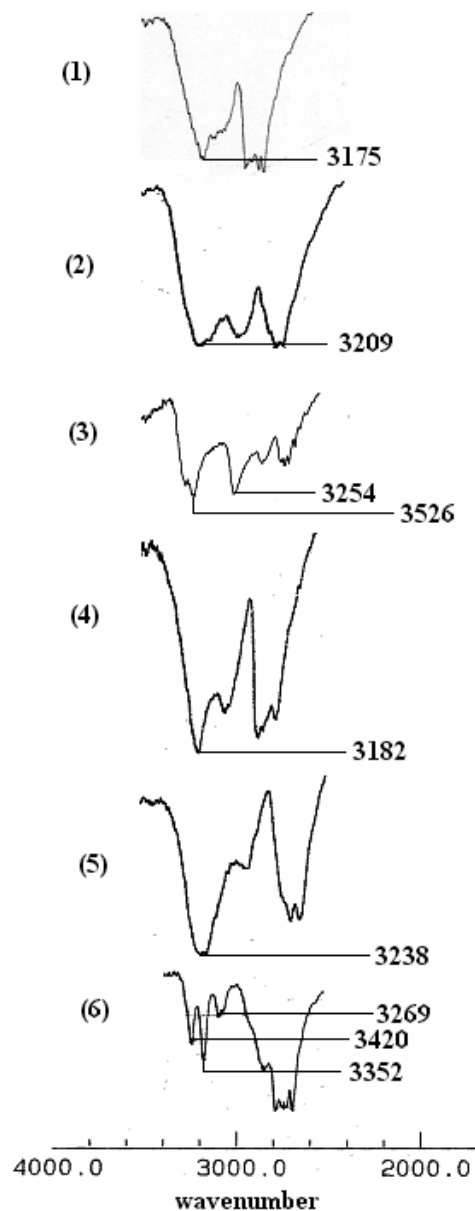
Figure 2.2 IR spectra of the compounds **1–6** in high frequency region (solid state, KBr pellets). Number in the parenthesis at left side of each spectrum keeps up a correspondence with the relevant compound.

-retching (which generally appears at $\approx$2800–3400 cm^{-1} as a broad band) is not distinctly observed in the spectrum, probably due to its merging with other vibrations. Aromatic C=C bond stretching vibrations of the phenyl ring of crown ethers appear as two strong

sharp bands at 1595–1590 and 1506–1504 cm^{-1} respectively for **1**, **2**, **3** and **5**. These bands are not observed in the spectrum of compound **4**, as it does not contain any aromatic moiety. Sharp IR bands in the region of 1255–1240 cm^{-1} in the relevant spectra of compound **1–6** suggest the presence of the crown ethers (C–O–C stretching). The out–of–plane C–H bending vibrational band for the *o*–substituted aromatic ring at 744 cm^{-1} is detected in the IR spectra of **3** and **5** (crown ethers DB18C6 and DB30C10 respectively), whereas mixture of this vibrational band with υ(M–O–M) (M = Mo, W) vibration results in strong and broad absorptions in the range of 800–790 cm^{-1} for compounds **1**, **2**, **4** and **6**. Strong sharp bands in the region 950–970 cm^{-1} in the IR spectra of compounds **1–6** are attributed to M=O stretching vibration of the $[Mo_6O_{19}]^{2-}$ or $[SiW_{12}O_{40}]^{4-}$ anions. IR spectra of compound **1–6** in the high frequency region have been presented in Figure 2.2.

2.2.4. ^{1}H NMR Spectroscopy

^{1}H NMR spectra of compounds **1–6** have been recorded in DMSO–d$_6$ at room temperature. For comparison purpose, the same for NH$_4$Cl have also been recorded in the same solvent. Selected region of the spectra of the relevant compounds have been presented in Figure 2.3. NH$_4$Cl shows a sharp singlet at δ 7.49 in DMSO, whereas, there is profound variation in the nature of NH$_4^+$ ion resonances in the spectra of compounds **1–4** (Figure 2.3a). Intramolecular interactions between the NH$_4^+$ ion and the crown ethers inside the relevant hydrogen bonded complexes are visually observed in the solid state through X–ray diffraction technique. There is certain possibility of retention of these interactions in the solution state too, because of their invariance (unlike intermolecular interactions) with the molecular concentration in solution. Thus, the relevant matter should be realized through ^{1}H NMR spectral studies with respect to chemical shift of the NH$_4^+$ ion in an aprotic solvent. Although it is known that high polar solvents like DMF or DMSO have the chance to break ionic assemblies, we were constrained to record the spectra of the relevant compounds in DMSO only because of the poorer solubility of these compounds in MeCN etc. Hence, a firm conclusion about the effect of the POM anion on the chemical shift/signal splitting of the NH$_4^+$ ion in the relevant spectra should not be drawn. However, a clear distinction of the corresponding resonances with respect to NH$_4$Cl proves the retention of the intramolecular interactions inside the

[NH$_4^+$⊂(crown ether)] supramolecular complexes in solution, the variation of chemical shift being due to difference in the electronic environment around the ion. In all the cases,
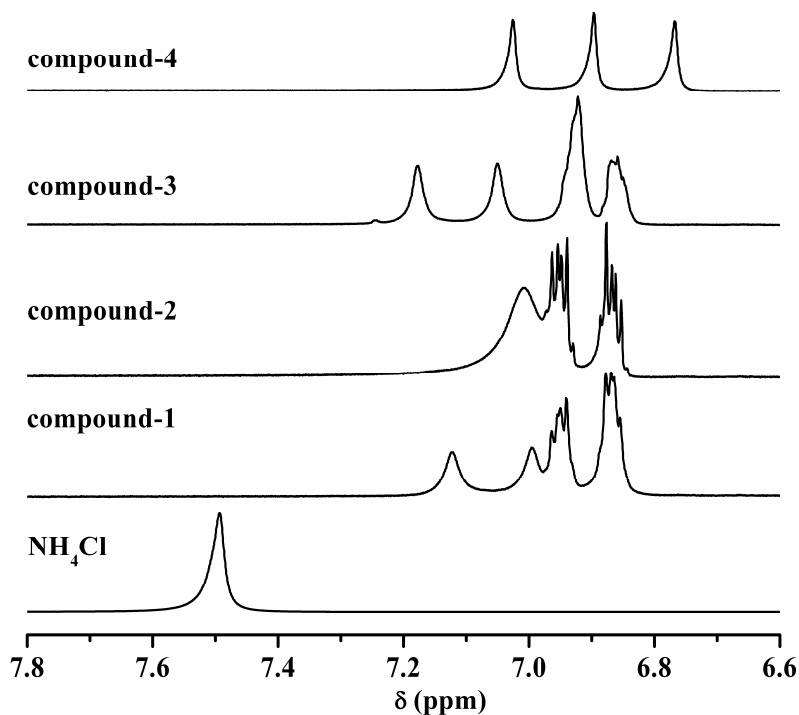
(a)
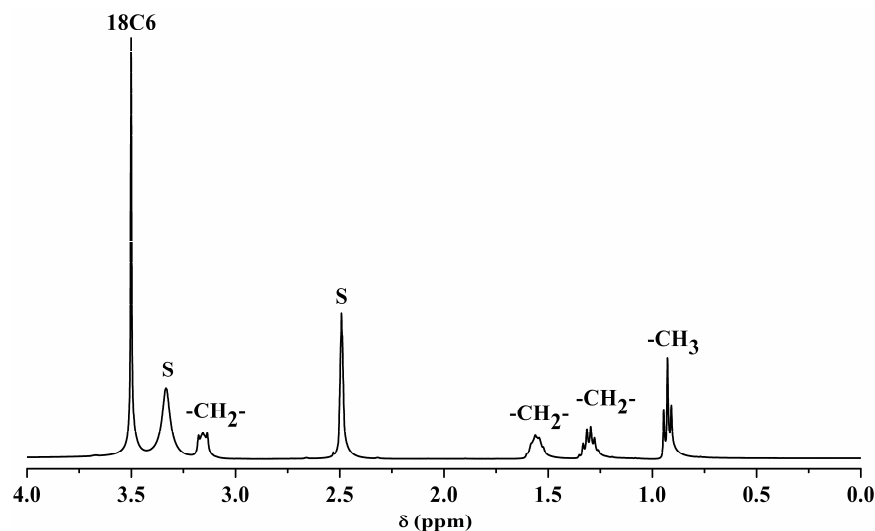
(b)

Figure 2.3 (a) ^{1}H NMR spectra of the compounds **1–4** (DMSO–d$_6$) showing shift and/or splitting of the NH$_4^+$ signals with respect to NH$_4$Cl. (b) ^{1}H NMR spectrum (aliphatic region) of the compound **6** in DMSO–d$_6$ recorded at 298K. The resonances labeled as S correspond to the solvent (DMSO) signals.

resonance due to the concerned ion has occurred at higher fields with respect to NH_4Cl (Figure 2.3a). The probable reason for this up–field shifting of the signals might be due to shielded environment around the ion inside the crown ether cavity (due to lone pair on O atoms etc.). As shown in Figure 2.3a, (in case of compounds **1** and **3**), the resonance has occurred twice with (approximately) 1:1 relative intensity (δ 7.12, 7.10 for compound **1** and δ 7.12, 7.05 for compound **2** respectively) of the signals, whereas, for compound **4** it has appeared thrice (δ 7.03, 6.90, 6.77) with *ca*. 1:1:1 relative intensity ratio. For compound **2**, a broad signal at δ 7.01 has been observed. Tetrahedrally symmetrical NH_4^+ ion should resonate once, while the multiple resonances due to the NH_4^+ ion correspond to the breakage of its symmetry due to the presence of H–bonding interactions with the crown ethers in solution. ^1H NMR spectral investigation on the compound **6** has also been performed in DMSO–d_6 at ambient temperature (compound **6** is not soluble in other organic solvents). Selected region of the relevant spectrum has been displayed in the Figure 2.3b. The spectrum almost determines stochiometry of the solid (compound **6**). Presence of some strong signals in the aliphatic region of the spectrum clearly indicates existence of the tetrabutylammonium cation in the compound **6**. A broad signal at δ 7.02 is due to resonance of the N–H proton (6H) of the amine. Again, two multiplets at δ 6.85–6.83 (2H) and δ 6.75–6.72 (2H) are attributable to the C(Ar)–H resonances of the amine. A strong and sharp singlet at δ 3.50 (24H) is due to the crown ether (–CH_2–). The other resonances at δ 3.16 (t, 8H, N^+–CH_2–), δ 1.56 (p, 8H, –CH_2–), δ 1.30 (p, 8H, –CH_2) and δ 0.93 (t, 12H, –CH_3) illustrates the feature of the tetrabutylammonium cation present in the compound **6** (see crystallographic section).

Thus, the overall features of the IR and ^1H NMR spectral investigations on compound **6** reveals the following points considering the charge balance of the cations and anion: (i) one tetrabutylammonium cation is present in the solid, (ii) OPDA should be mono–protonated for the replacement of one of the tetrabutylammonium cations from $[Bu_4N]_2[Mo_6O_{19}]$ precursor, used in the synthesis of compound **6**, (iii) the crown ether 18C6 is in attendance in the crystalline solid, and (iv) $[Mo_6O_{19}]^{2-}$ POM cluster anion is existed in the compound **6**. From these spectral evidences, the ion–pair solid can be formulated as $[Bu_4N][OPDAH(18C6)][Mo_6O_{19}]$.

2.2.5. Ammonium ion or hydroxonium ion?

18–crown–6 and its derivatives are known to be good stabilizing ligands for hydroxonium ion (H_3O^+).[3] Hydrogen atoms for the ammonium cations in compounds **2** and **3** were not located from the difference Fourier map (see crystal structure description section, *vide infra*). Thus, an ambiguity might appear about the cation: whether it is ammonium ion (NH_4^+) or hydroxonium ion (H_3O^+)? In this context, it should be mentioned that, a clearer distinction between a free O atom and a N atom cannot be firmly established with the help of crystallography (in presence of heavy scatterers e.g. heavy metal atoms) unless the relevant H atoms are located in their crystal structures. Both the atoms (N and O) have almost identical X–ray scattering abilities. As such, a wrong assignment of the electron density in the difference Fourier map does not alter the structural refinement minimisation parameters (R_1, wR_2, shift/esd etc.) to a considerable extent. Wang and co–workers reported the isolation of $[H_3O^+ \subset 18C6]$[10d] and $[H_3O^+ \subset DB18C6]$[10f] supramolecular crown ether adducts in the $PMo_{12}O_{40}{}^{3-}$ POM matrix from a mixture of crown ether and $H_3PMo_{12}O_{40}$ in MeCN or MeOH–MeCN mixture. Hydroxonium ion in its crown ether complexes generally shows a broad IR absorption at $\approx$2950 cm^{-1} (overlapped with C–H stretching) characteristic for the O–H stretching vibration.[10d,10f,19a] Another typical band appears at $\approx$1098cm^{-1} that corresponds to the C–O–C stretching of the crown ether coupled with the O–H bending motion of the hydroxonium ion.[19b] The characteristic broad absorption for hydroxonium ion (that generally appears around 2950 cm^{-1}), as mentioned above, is clearly missing in compounds **2** and **3** (Figure 2.2). This indicates that NH_4^+ ion (not H_3O^+) is encapsulated in the crown ether cavity of compounds **2** and **3** as the cation. Moreover, the characteristic IR absorption band for the NH_4^+ ion appears at 3300–3030 cm^{-1} (N–H stretching) and $\approx$1400 cm^{-1} (N–H bending). Thus, the bands at 3209 and 3254 cm^{-1} in the IR spectra of compounds **2** and **3** respectively strongly suggest the presence of ammonium ions (N–H stretching) in the crystalline material. The matter is further supported by the appearance of bands at 1454 cm^{-1} (N–H bending) for both the compounds. Thus, any possibility to include H_3O^+ cation instead of the NH_4^+ cation in the crown ether cavity is ruled out.

Table 2.1 Crystal data and structure refinement parameters for compounds **1**–**3**

	1	2	3
formula	$C_{32}H_{64}Mo_6N_2O_{25}$	$C_{68}H_{118}N_6O_{66}SiW_{12}$	$C_{40}H_{52}Mo_6N_2O_{35}$
fw	1451.49	4309.80	1691.44
T (K), λ (Å)	298 (2), 0.71073	298 (2), 0.71073	298 (2), 0.71073
crystal system, sp. gr.	triclinic, $P-1$	triclinic, $P-1$	monoclinic, $C2/c$
a (Å)	11.453(3)	13.4862(18)	21.4502(14)
b (Å)	11.792(3)	15.132(2)	11.7332(7)
c (Å)	19.729(5)	15.324(2)	22.0464(14)
α (°)	73.125(4)	66.302(2)	90.00
β (°)	73.409(4)	70.832(2)	90.8450(10)
γ (°)	85.848(4)	74.559(2)	90.00
V (Å^3)	2443.5(10)	2671.9(6)	5806.7(6)
Z, $d_{calcd.}$ (mg m^{-3})	2, 1.974	1, 1.688	4, 1.936
μ (mm^{-1}), F(000)	1.576, 1444	11.975, 1998	1.355, 3336
GooF on F^2	1.017	1.399	1.097
R_1/wR_2[I>2$\sigma(I)$]	0.0330/0.0721	0.0597/0.1374	0.0599/0.1211
R_1/wR_2 (all data)	0.0480/0.0778	0.0635/0.1388	0.0817/0.1312
largest diff. peak/hole (e.Å^{-3})	0.590/–0.651	1.288/–1.247	1.141/–0.488

Table 2.2 Crystal data and structure refinement parameters for compounds **4**–**6**

	4	5	6
formula	$C_{40}H_{80}Mo_6N_2O_{31}$	$C_{60}H_{96}Mo_6N_2O_{43}$	$C_{34}H_{69}Mo_6N_3O_{25}$
fw	1660.70	2109.03	1495.56
T (K), λ (Å)	100 (2), 0.71073	100 (2), 0.71073	298 (2), 0.71073
crystal system, sp. gr.	monoclinic, $P2_1/n$	monoclinic, $C2/m$	monoclinic, $C2/c$
a (Å)	11.3773(6)	16.4726(11)	17.5055 (10)
b (Å)	11.1057(6)	23.9302(16)	16.2661 (9)
c (Å)	20.1711(9)	11.1349(8)	37.006(2)
α (°)	90.00	90.00	90.00
β (°)	104.5980 (10)	123.6100(10)	94.8510 (10)
γ (°)	90.00	90.0	90.00
V (Å^3)	2924.8(2)	3983.8(5)	10499.7(10)
Z, d_{calcd}(mg m^{-3})	2, 1.886	2, 1.757	8, 1.892
μ (mm^{-1}), F(000)	1.337, 1668	1.013, 2128	1.471, 5968
GooF on F^2	1.110	1.167	1.121
R_1/wR_2 [I>2$\sigma(I)$]	0.0218/0.0513	0.0378/0.0944	0.0571/0.1214
R_1/wR_2 (all data)	0.0234/0.0521	0.0403/0.0956	0.0678/0.1270
largest diff. peak/hole(e.Å^{-3})	0.395/–0.329	0.646/–0.915	1.347/ –0.570

2.2.6. Description of Crystal Structure

Compound [NH$_4$(B18C6)][Bu$_4$N][Mo$_6$O$_{19}$] (1)

Compound [NH$_4$(B18C6)][Bu$_4$N][Mo$_6$O$_{19}$] (1) crystallizes in *P–1* space symmetry (triclinic, $Z' = 1$) from the MeCN–CH$_3$COOH solution. The structure consists of two different cations *viz.* [NH$_4$(B18C6)]$^+$ and [Bu$_4$N]$^+$ along with the [Mo$_6$O$_{19}$]$^{2-}$ isopolyanion in its asymmetric unit. Attempts for complete replacement of the tetrabutylammonium cation using excess of ammonium thiocyanate have remained unsuccessful. Thus, there is an unwanted perturbation from the tetrabutylammonium cation with the molecular and/or crystal symmetry of compound 1. Anticipated structure would contain two ammonium–crown ether supramolecular cations along with the [Mo$_6$O$_{19}$]$^{2-}$ anion for electro neutrality. Accordingly, the expected structure of the molecule might be a centrosymmetric one with the centre of inversion being the central oxygen atom of the hexamolybdate anion. However, this did not happen. Crystal structure of compound 1 has been shown in Figure 2.4a. The [Mo$_6$O$_{19}$]$^{2-}$ isopolyanion (also known as Lindqvist type polyoxometalate anion) is a symmetrical, almost spherical polyoxometalate, with all the Mo atoms at +VI oxidation states. Each Mo atom attains a distorted octahedral geometry coordinating to one central (O$_c$), one terminal (O$_t$), and four bridging (O$_b$) oxygen atoms and the polyoxoanion is formed by six edge shared {MoO$_6$} octahedra. The Mo–O bond lengths can be grouped into three sets: Mo–O$_t$ 1.674–1.680Å, Mo–O$_b$ 1.876–1.932Å, and Mo–O$_c$ 1.299–1.328Å. The bond angles of Mo–O$_b$–Mo are observed in the range of 116.0–117.18º, while that of Mo–O$_c$–Mo are 89.44–90.60º and 179.5–179.78º in the relevant crystal structure. On the other hand, B18C6 is a macrocyclic polyether consisting of six O atoms that falls into two categories: (a) catechol oxygen atoms i.e. O atoms attached to the phenyl ring and (b) glycolic oxygen atoms i.e. atoms attached to the ethylene chains. In the crystal structure of compound 1, the various bond distances for the crown ether B18C6 have been observed as follows: C(aryl)–O(aryl) 1.360–1.373Å, C(alkyl)–O(aryl) 1.412–1.434Å, C(alkyl)–O(alkyl) 1.321–1.420Å, C(aryl)–C(aryl) 1.352–1.389Å and C(alkyl)–C(alkyl) 1.243–1.481Å (see Table 2.5). 1:1 inclusion complexation between the ammonium ion and the crown ether B18C6 has been observed in the crystal structure of compound 1 and the macrocycle is found to be slightly bent outwards from the cation (see Figure 2.4). The

NH_4^+ guest cation has been included in the crown ether cavity through six bifurcating N^+–H⋯O hydrogen bonding interactions with the crown ether oxygen atoms O(1) to O(6)

(a)   (b)

(c)
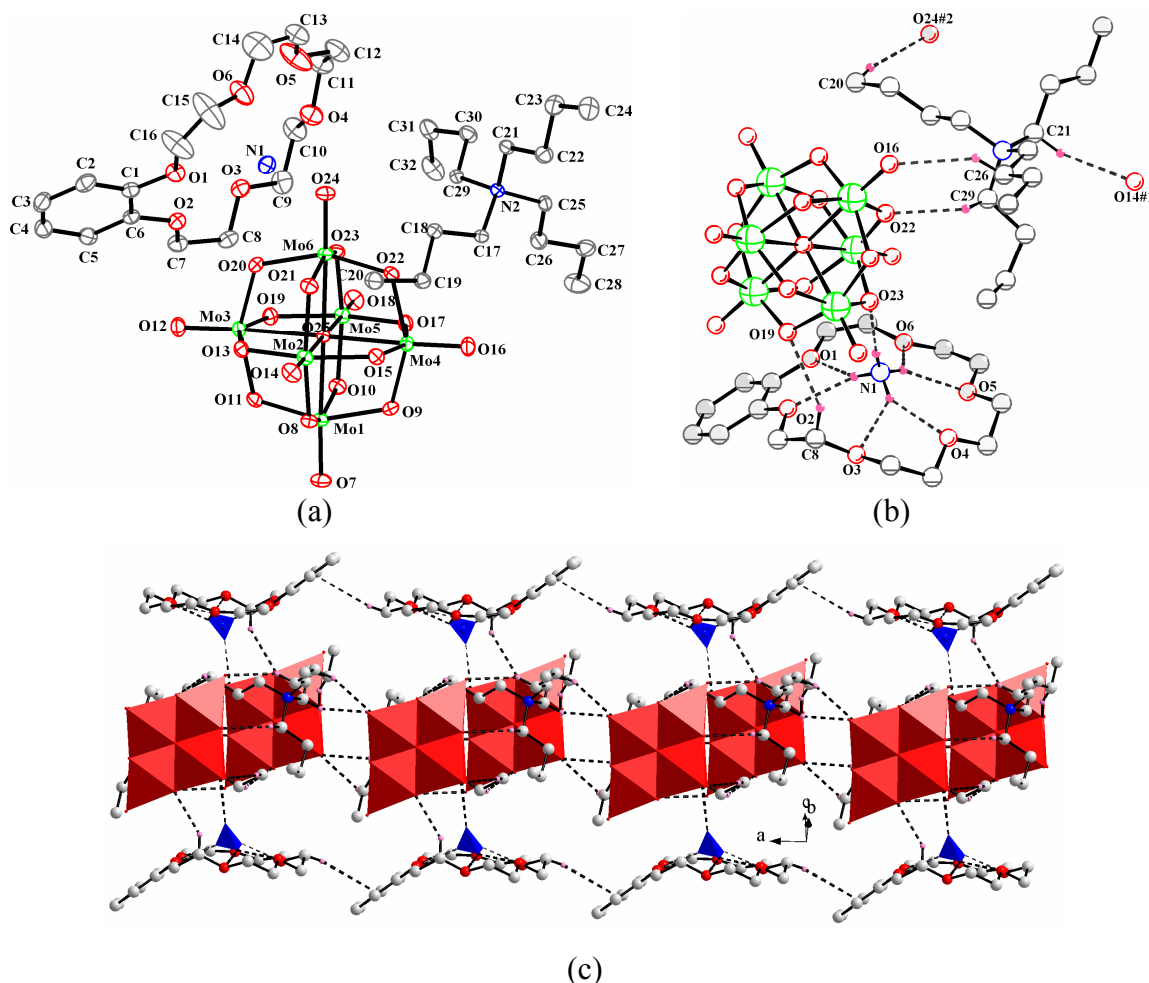
Figure 2.4 (a) Thermal ellipsoidal plot of the compound **1** in 20% probability distribution; (b) Hydrogen bonding environment in the crystal structure; (c) Supramolecular chain–like assembly of compound **1** viewed parallel to the crystallographic [101] plane. C–H⋯π interactions between the crown ethers are visualized in the picture. H–atoms are omitted for clarity.

using three N–H bonds. The fourth N–H proton is projected outward from the crown ether cavity and is involved in hydrogen bonding interaction with the O(23), bridging oxygen atom of the associated $[Mo_6O_{19}]^{2-}$ isopolyanion. This type of interaction between the ammonium–crown ether supramolecular complex and the POM anion has already been proposed in Scheme 2.1. C–H⋯O interaction between the crown ether and the POM cluster anion [C(8)–H(8A)⋯O(19)] has also been demonstrated in the crystal structure

(Figure 2.4b). In–a–word, the POM cluster anion holds both the crown ether (C–H⋯O interaction) and the NH_4^+ ion (N^+–H⋯O interaction) in suitable positions through supramolecular interactions. The tetrabutylammonium cation is involved in C–H⋯O inte-
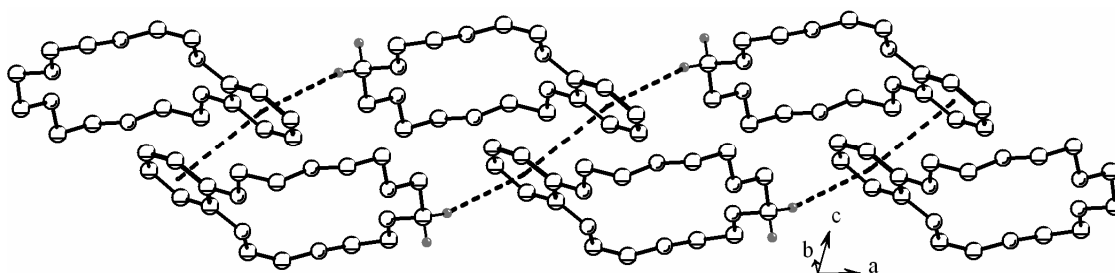
Figure 2.5 C–H⋯π and π⋯π stacking interactions between the crown ethers parallel to the crystallographic [100] axis in the crystal structure of the compound **1**. Geometrical parameters for these interactions are as follows: for C–H⋯π interaction, d(H12B⋯Cg) = 3.134(4), d(C12⋯Cg) = 4.068 (9)Å, <(C12–H12B⋯Cg) = 162.01(17)° (symmetry: 1+x, y, z); for π⋯π interaction, d(Cg–Cg) = 3.632(3)Å, α = 0.02 (symmetry: 2–x,1–y,–z), where Cg refers to the centroid of the concerned phenyl ring.

-ractions with three POM anions using C(20), C(21), C(26) and C(29) atoms of the cation (see Figure 2.4b). H–bonding parameters for **1** have been summarized in Table 2.3. Figure 2.4c clearly illustrates how the nature of these supramolecular interactions paves the way towards supramolecular assembly of a chain–like arrangement. Two inversion symmetry related molecules of compound **1** forms a hydrogen bonded dimer through C–H⋯O interactions between the tetrabutylammonium cation and the POM cluster anion thus, builds the basic supramolecular hydrogen bonded unit (ammonium–crown ether)$^+$–POM–2[Bu$_4$N]$^+$–POM–(ammonium–crown ether)$^+$ (not shown in picture). These dimmers are, in turn, connected through C(21)–H(21A)⋯O(14) hydrogen bond and its symmetry complement (inversion) along the crystallographic *a*–axis resulting in the formation of a supramolecular chain like topology in the relevant crystal structure (see Figure 2.4c). Packing of the molecules in the crystal lattice of **1** can be further characterized by the abundance of C–H⋯π and π⋯π interactions among the crown ethers. The combination of C–H⋯π interaction between C(12)–H(12B) of one crown ether and the π–ring of its translation equivalent with π⋯π interactions between the phenyl rings of two inversion symmetry related crown ethers results in stacking of the macrocyles parallel to the crystallographic *a*–axis as shown in Figure 2.5. Tetrabutylammonium

cations and the POM anions fill up the space between two such translation related crown ether only chains resulting in the complicated three dimensional crystal packing of compound **1** (not shown in picture).

Table 2.3 Geometrical parameters for the H–Bonding interactions in compound **1**.

D–H⋯A	d(D–H)	d(H⋯A)	d(D⋯A)	<(DHA)
C(8)–H(8A)⋯O(19)	0.97	1.46	3.328(5)	148.4
C(20)–H(20A)⋯O(24)#2	0.96	1.53	3.452(6)	160.5
C(21)–H(21A)⋯O(14)#1	0.97	1.46	3.361(5)	155.2
C(26)–H(26A)⋯O(16)	0.97	1.59	3.448(5)	147.1
C(29)–H(29A)⋯O(22)	0.97	1.40	3.215(5)	141.2
N(1)–H(2N)⋯O(23)	0.85(6)	1.24(7)	3.085(6)	172(6)
N(1)–H(4N)⋯O(1)	0.73(5)	1.32(5)	1.923(6)	141(5)
N(1)–H(4N)⋯O(2)	0.73(5)	1.28(5)	1.932(6)	150(5)
N(1)–H(3N)⋯O(3)	0.94(8)	1.16(8)	1.913(6)	136(6)
N(1)–H(3N)⋯O(4)	0.94(8)	1.16(8)	1.947(6)	140(7)
N(1)–H(1N)⋯O(5)	0.97(7)	1.12(7)	1.997(7)	150(6)
N(1)–H(1N)⋯O(6)	0.97(7)	1.18(7)	1.905(6)	131(5)

Symmetry transformations used to generate equivalent atoms: #1 x–1,y, z; #2 –x+1,–y+1,–z+1

Compound NH$_4$(B18C6)]$_4$[SiW$_{12}$O$_{40}$]·2CH$_3$CN (2)

The crystal structure of compound [NH$_4$(B18C6)]$_4$[SiW$_{12}$O$_{40}$]·2CH$_3$CN (**2**) consists of [SiW$_{12}$O$_{40}$]$^{4-}$ as the counter–anion, which is known as α–Keggin type heteropolyanion. The compound **2** crystallizes as an acetonitrile solvate and its crystal structure is characterized by four ammonium–crown ether supramolecular complex cations associated with one [SiW$_{12}$O$_{40}$]$^{4-}$ anion (Z′ = ½) (see Figure 2.6a). Si(1) atom of the POM cluster anion is located at the centre of crystallographic *ac* plane (xyz = 0.5,0,0.5) with half occupancy and is the inversion centre of the molecule. The crystallographically observed [SiW$_{12}$O$_{40}$]$^{4-}$ POM anion in the crystal structure of compound **2** is best described as symmetrically distorted α–Keggin type structure.[10a,20] All the W atoms of [SiW$_{12}$O$_{40}$]$^{4-}$ anion reside in distorted octahedral geometry {WO$_6$} coordinating to two terminal (O$_t$), four bridging (O$_b$) and two central (O$_c$) oxygen atoms (see Table 2.5 for experimentally observed various bond lengths). In the crystal structure of the compound

2, the POM anion accepts four ammonium–crown ether supramolecular cations at its surface both by coulombic as well as supramolecular H–bonding interactions (see Table 2.4 for the related H–bonding parameters and Figure 2.6b for pictorial representation). Although the directional nature of H–bonding interactions between the ammonium ion

(a)   (b)

(c)
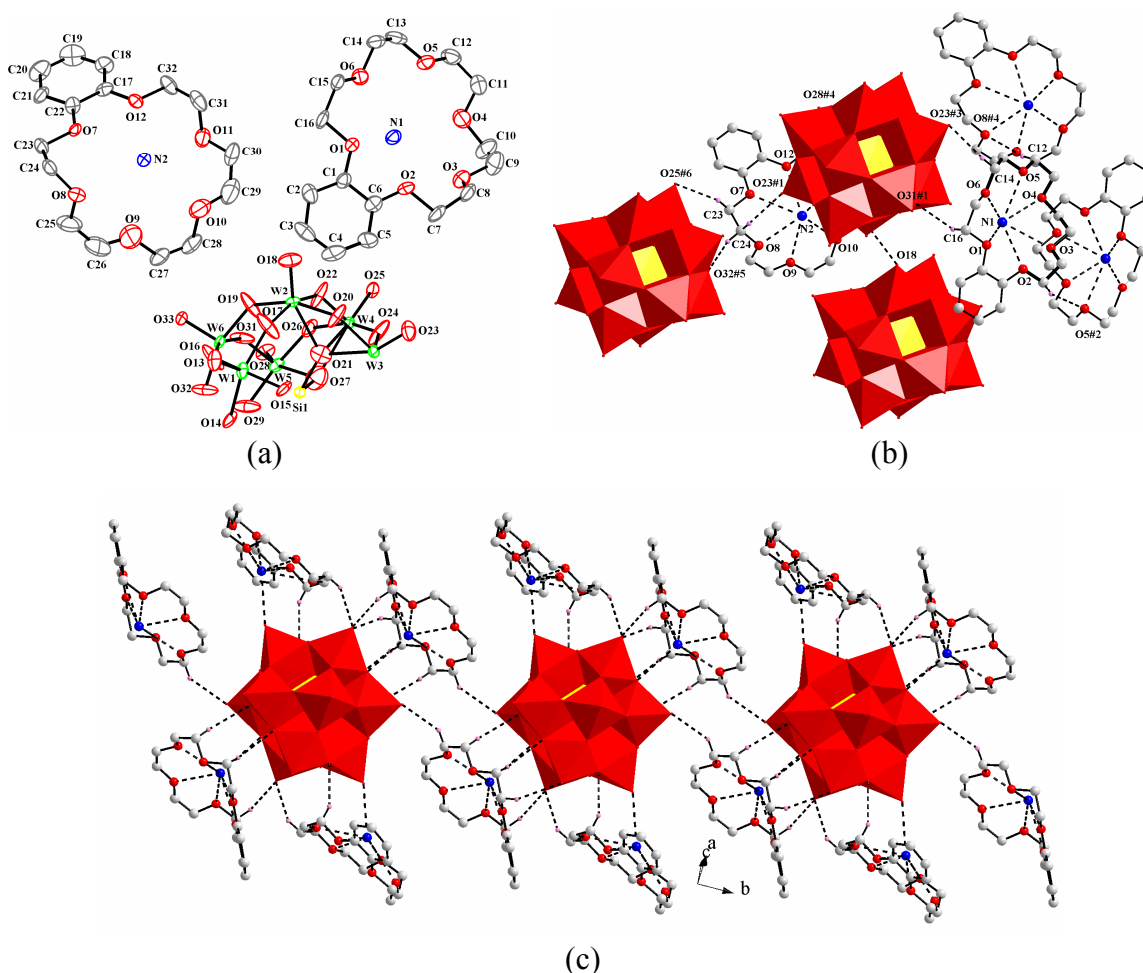
Figure 2.6 (a) Crystal structure of compound **2** with atom labelling scheme in 40% thermal probability distribution. Only the asymmetric unit has been displayed. Hydrogen atoms and the solvent MeCN molecule are omitted for a clearer view. (b) Hydrogen bonding environment in the crystal lattice of compound **2**. Symmetry codes are in correspondence with Table 2.4. (c) Formation of supramolecular chain as a result of supramolecular interactions between the crown ethers and the POM anions viewed down the crystallographic [001] axis.

and the POM remains undetermined (H atoms of the cation are not located), short N···O contact N(2)···O(20) [3.033(10)Å, symmetry 1–x,1–y,1–z] suggests the supramolecular interaction between them. Inside the ammonium–crown ether adducts, the N–O distances

are found to be in the range of 1.798(8)–3.01(2)Å (see Table 2.5). In contrast to compound **1**, compound **2** consists of two different types of crown ether adducts as far as

Table 2.4 Geometrical parameters for the H–Bonding interactions in the compound **2**.

D–H⋯A	d(D–H)	d(H⋯A)	d(D⋯A)	<(DHA)
C(7)–H(7A)⋯O(5)#2	0.97	1.64	3.54(3)	153.4
C(12)–H(12B)⋯O(8)#4	0.97	1.67	3.60(3)	161.1
C(14)–H(14B)⋯O(23)#3	0.97	1.55	3.37(3)	141.5
C(16)–H(16B)⋯O(31)#1	0.97	1.67	3.54(3)	149.5
C(23)–H(23B)⋯O(25)#6	0.97	1.54	3.44(2)	153.8
C(24)–H(24A)⋯O(23)#1	0.97	1.53	3.39(2)	146.9
C(24)–H(24B)⋯O(32)#5	0.97	1.67	3.54(2)	149.6
C(29)–H(29A)⋯O(18)	0.97	1.56	3.38(3)	141.9
C(30)–H(30B)⋯O(17)#1	0.97	1.67	3.59(4)	158.8
C(32)–H(32A)⋯O(28)#3	0.97	1.69	3.55(3)	148.0
C(34)–H(34B)⋯O(12)#1	0.96	1.62	3.54(4)	161.2

Symmetry transformations used to generate equivalent atoms: #1 –x+1,–y+1,–z+1; #2 –x+2,–y+1,–z+2; #3 x,y+1,z; #4 x+1,y,z; #5 –x,–y+1,–z+1; #6 x–1,y+1,z

puckering of the macrocycle is concerned. In one ammonium–crown supramolecular cation (consisting of O(7) to O(12)) the crown ether is twisted outward from the ammonium ion and in the other one (consisting of O(1) to O(6)), the macrocycle is curved inward to the ammonium cation as shown in Figure 2.6b. In the crystal structure, the basic supramolecular units, $4(NH_4–crown)^+–SiW_{12}O_{40}^{4-}$ are further connected by C(29)–H(29A)⋯O(18) interaction and their symmetry equivalent partners, resulting in the formation of a supramolecular chain that propagates parallel to the crystallographic *b*–axis (Figure 2.6c). Each of such chains are again connected by means of supramolecular C(23)–H(23B)⋯O(25) hydrogen bonding interaction along with their symmetry equivalents parallel to crystallographic *c*–axis. However, no C–H⋯π or π⋯π interactions are observed among the crown ethers in the crystal lattice of compound **2**, possibly owing to the fact that the larger surface area of the POM anion inpeds the crown ethers from getting involved into such type of stacking interactions due to dearth of space.

Table 2.5 Selected bond lengths for the crystal structure of the compounds **1**–**3**.

Compound–**1**

C(1)–C(2)	1.380(6)	C(2)–C(3)	1.381(7)	C(3)–C(4)	1.352(7)
C(4)–C(5)	1.379(7)	C(5)–C(6)	1.371(6)	C(1)–C(6)	1.389(6)
C(7)–C(8)	1.481(6)	C(9)–C(10)	1.476(7)	C(11)–C(12)	1.477(7)
C(13)–C(14)	1.409(9)	C(15)–C(16)	1.243(8)	C(1)–O(1)	1.361(5)
C(6)–O(2)	1.374(5)	C(7)–O(2)	1.434(5)	C(8)–O(3)	1.419(5)
C(9)–O(3)	1.410(5)	C(10)–O(4)	1.407(6)	C(11)–O(4)	1.411(6)
C(12)–O(5)	1.414(7)	C(13)–O(5)	1.321(7)	C(14)–O(6)	1.321(8)
C(15)–O(6)	1.332(7)	C(16)–O(1)	1.412(6)		

Compound–**2**

C(1)–C(2)	1.35(3)	C(2)–C(3)	1.42(3)	C(3)–C(4)	1.32(3)
C(4)–C(5)	1.37(3)	C(5)–C(6)	1.36(3)	C(1)–C(6)	1.40(3)
C(7)–C(8)	1.45(3)	C(9)–C(10)	1.41(4)	C(11)–C(12)	1.45(3)
C(13)–C(14)	1.46(3)	C(15)–C(16)	1.48(3)	C(1)–O(1)	1.39(2)
C(6)–O(2)	1.36(2)	C(7)–O(2)	1.48(2)	C(8)–O(3)	1.42(3)
C(9)–O(3)	1.47(3)	C(10)–O(4)	1.45(3)	C(11)–O(4)	1.42(3)
C(12)–O(5)	1.45(3)	C(13)–O(5)	1.42(3)	C(14)–O(6)	1.42(2)
C(15)–O(6)	1.39(2)	C(16)–O(1)	1.44(2)	C(17)–C(18)	1.34(3)
C(18)–C(19)	1.37(4)	C(19)–C(20)	1.39(4)	C(20)–C(21)	1.39(3)
C(21)–C(22)	1.35(3)	C(17)–C(22)	1.39(3)	C(17)–O(12)	1.40(2)
C(22)–O(7)	1.38(2)	C(23)–O(7)	1.45(2)	C(23)–C(24)	1.47(3)
C(24)–O(8)	1.42(2)	C(25)–C(26)	1.36(4)	C(25)–O(8)	1.38(3)
C(26)–O(9)	1.28(4)	C(27)–C(28)	1.28(4)	C(27)–O(9)	1.32(3)
C(28)–O(10)	1.41(4)	C(29)–C(30)	1.39(4)	C(29)–O(10)	1.45(4)
C(30)–O(11)	1.40(3)	C(31)–O(11)	1.41(3)	C(31)–C(32)	1.46(3)
C(32)–O(12)	1.41(2)				

N1⋯O1	3.00(2)	N1⋯O2	3.10(2)	N1⋯O3	3.01(2)
N1⋯O4	1.94(2)	N1⋯O5	3.00(2)	N1⋯O6	1.90(2)
N1⋯O17	1.798(8)	N2⋯O7	3.009(18)	N2⋯O8	1.82(2)
N2⋯O9	3.00(3)	N2⋯O10	1.85(2)	N2⋯O11	3.01(2)
N2⋯O12	1.93(2)				

Compound–**3**

C(2)–C(3)	1.384(9)	C(3)–C(4)	1.369(11)	C(4)–C(5)	1.361(11)
C(5)–C(6)	1.387(10)	C(6)–C(7)	1.380(10)	C(2)–C(7)	1.383(9)
C(1)–O(11)	1.439(8)	C(2)–O(11)	1.378(8)	C(7)–O(12)	1.378(8)
C(8)–O(12)	1.425(8)	C(8)–C(9)	1.483(10)	C(9)–O(13)	1.413(8)
C(10)–O(13)	1.438(8)	C(11)–C(12)	1.368(15)	C(12)–C(13)	1.372(16)
C(13)–C(14)	1.390(13)	C(14)–C(15)	1.347(12)	C(16)–C(17)	1.467(13)
C(18)–C(19)	1.495(13)	C(15)–O(14)	1.391(10)	C(16)–O(14)	1.436(9)
C(17)–O(15)	1.438(11)	C(18)–O(15)	1.421(11)	C(19)–O(16)	1.418(9)
C(20)–O(16)	1.368(11)				
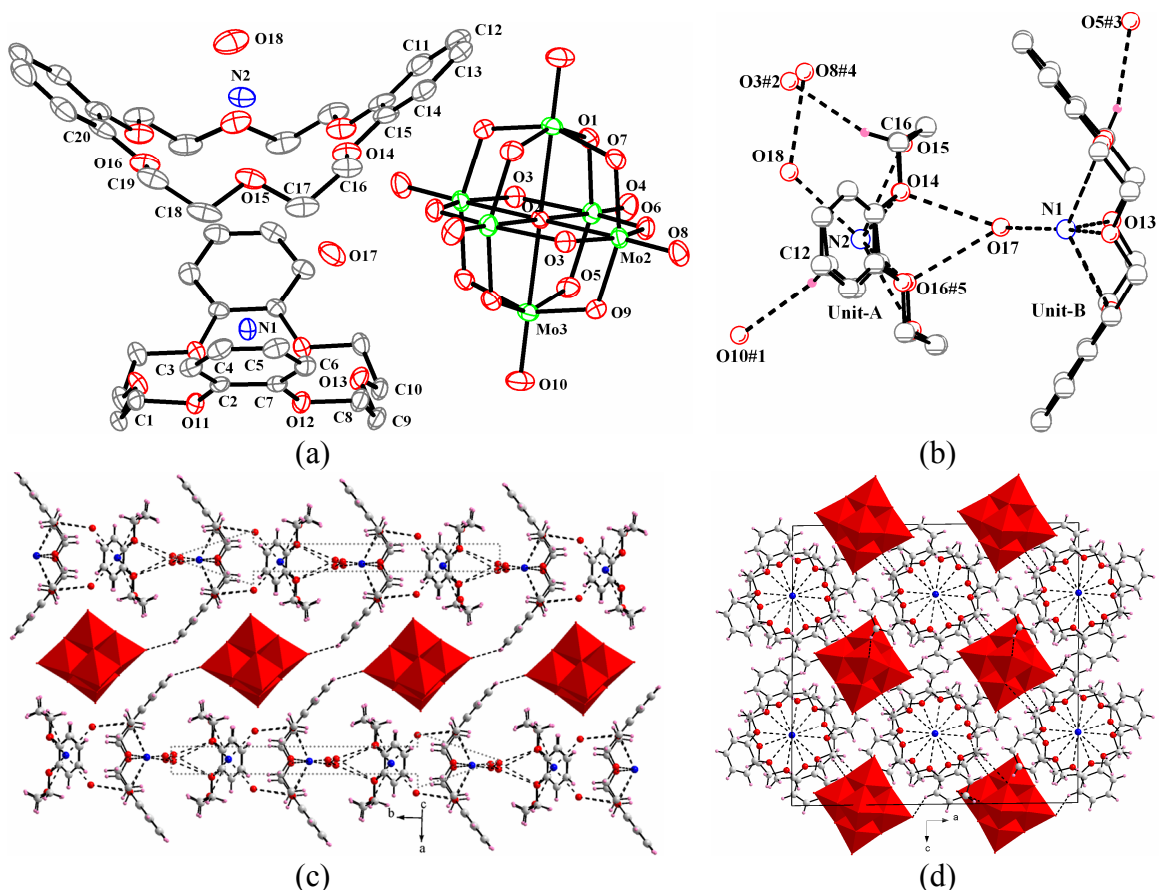
Figure 2.7 (a) Thermal ellipsoidal plot of the compound **3** in 20% confidence level. (b) Hydrogen bonding environment in the crystal structure of compound **3**. Atoms labeled with additional symmetry operations are in accord with Table 2.6. (c) Interconnection between two oppositely directed supramolecular chains through polyoxometalate bridge. These chains are related to each other by the inversion symmetry. (d) Packing of the molecules in the crystal lattice of compound **3** viewed down the crystallographic [010] axis.

Compound [NH$_4$(DB18C6)]$_2$[Mo$_6$O$_{19}$]·4H$_2$O (3)

Replacing the less symmetrical crown ether B18C6 with a more symmetrical one DB18C6 has resulted in a different mode of crystal packing in compound **3** compared to the last two crystal structures (compounds **1** and **2**). The compound [NH$_4$(DB18C6)]$_2$ [Mo$_6$O$_{19}$]·4H$_2$O (**3**) crystallizes as a hydrate in rather higher symmetrical space group (*C2/c*) than compounds **1** and **2** (both crystallized in *P–1* space symmetry). The asymmetric unit in the crystal structure of compound **3** is characterized by two symmetry independent half ammonium–crown ether supramolecular complex cations, half of the [Mo$_6$O$_{19}$]$^{2-}$ anion and two solvent water molecules (Z′ = ½). Both the N(1) and N(2)

atoms of the ammonium cations are found at the concave sides of the crown ethers (Figure 2.7a) and they reside along the two–fold symmetry axis of a monoclinic unit cell with half occupancies. Similarly the central oxygen atom of the POM anion O(2) is positioned at the inversion centre (xyz = 0.25, 0.25, 0.50) of the crystal. Figure 2.7a depicts the crystal structure of compound **3**. In the relevant crystal structure, the bond len-

Table 2.6 Hydrogen bonding parameters for the compound **3**.

D–H⋯A	d(D–H)	d(H⋯A)	d(D⋯A)	<(DHA)
C(8)–H(8A)⋯O(5)#3	0.97	1.66	3.607(9)	166.2
C(12)–H(12)⋯O(10)#1	0.93	1.68	3.525(13)	151.5
C(16)–H(16A)⋯O(3)#2	0.97	1.60	3.515(10)	156.6
N1⋯O11			3.013(6)	
N1⋯O12			1.996(6)	
N1⋯O13			1.978(5)	
N2⋯O14			1.986(7)	
N2⋯O15			1.977(6)	
N2⋯O16			3.043(7)	
N1⋯O17			1.798(8)	
N2⋯O18			1.790(9)	
O(17)⋯O(14)			3.059(8)	
O(18)⋯O(8)#4			1.889(11)	
O(17)⋯O(16)#5			3.118(9)	

Symmetry transformations used to generate equivalent atoms: #1 x,y+1,z; #2 x,–y+1,z+1/2; #3 x,–y,z+1/2; #4 –x+1/2,y+1/2,–z+1.5; #5 –x, y, –z+1.5

-gths of the crown ether (DB18C6) are observed as follows: C(aryl)–C(aryl) 1.347–1.392 Å, C(alkyl)–C(alkyl) 1.467–1.495 Å., C(aryl)–O(aryl) 1.378–1.391 Å, C(aryl)–O(alkyl) 1.427–1.429 Å and C(alkyl)–O(alkyl) 1.413–1.439 Å (see Table 2.5). As the H–atoms of both the ammonium ions as well as the solvent water molecules are not located in the relevant crystal structure, the direction / nature of the supramolecular interactions between the NH_4^+–crown ether complex cations, solvent water molecules and POM anions are not so clear. But a qualitative idea can be drawn from the concerned short N⋯O and O⋯O distances (see Table 2.6). Inside the NH_4^+–DB18C6 supramolecular adducts, six short N⋯O distances are observed in the range of 1.977–3.043 Å that represent strong interactions between the ammonium cations and the crown ethers. In the
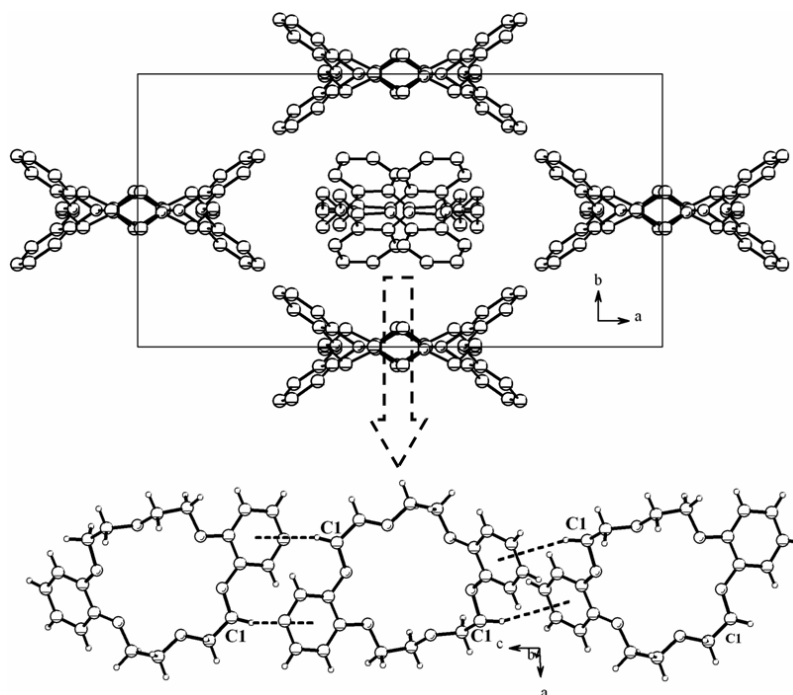
Figure 2.8 Arrangement of crown ethers in the crystal lattice of compound **3**. Two distinct arrangements for the crown ethers are clearly visible. Parameters for C–H···π interactions. d(H1B···Cg) = 3.20(10)Å, d(C1···Cg) = 4.137(7), <(C1–H1···Cg) = 161.90(19)°. Symmetry: 0.5–x, 0.5–y, 1–z.

between the ammonium cation and the POM anion has been observed. Possibly the bowl shape of the crown ether DB18C6 has made this difference. The lattice water molecule O(17) is located in between two orthogonally arranged supramolecular crown ether cationic complexes and joins them through N(1)···O(17) [1.798(8)Å], O(17)···O(14) [3.059(8)Å] and O(17)···O(16) [3.118(9)Å] supramolecular weak interactions (see Figure 2.7b). Translation of these interactions results in a chain like topology for the arrangement of the crown ether complexes parallel to the crystallographic *b*–axis (see Figure 2.7c). Two such oppositely directed chains (which are related by the inversion symmetry) are bridged by the POM anion through C(12)–H(12)···O(10) [3.607(9)Å] supramolecular inetraction as shown in Figure 2.7c (see Table 2.6 for the parameters for these interactions). It has already been described that, the crystal structure of compound **3** consists of two differently oriented symmetry independent crown ethers (see Figure 2.7a). Thus, two dissimilar types of packing of the crown ethers are expected in the relevant crystal lattice. Reflection symmetry related crown ethers parallel to the crystallographic *c*–axis along with their symmetry equivalents (rotation and translation)

pack in a channel like arrangement (Figure 2.8). Another chain of C–H⋯π stacked crown ethers runs accross this channel, i.e. perpendicular to the crystallographic *ab*–plane (see
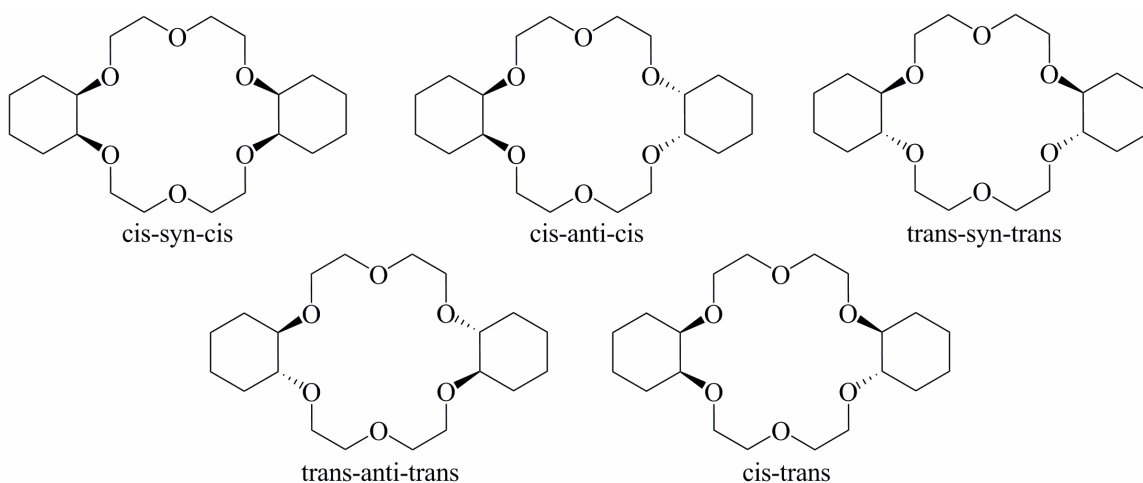
Scheme 2.3 Stereoisomers of dicyclohexyl–18–crown–6.

Figure 2.8). The resultant packing of the molecules in the crystal structure of compound **3** is beautiful and symmetrical as shown in Figure 2.7d. The packing nature of compound **3** is found to be almost identical with the crystal structure of bis–(tetrachlorodibenzo–18–crown–6) tetrachloro–aurate(III) oxonium tetrahydrate (CCDC depository code QUQPEX) described by Steed and coworkers.[21a] Space group of the same was incorrectly assigned to *Cc*, which was further correctly assigned to *C2/c* by R. E. Marsh.[21b]

Compound [NH$_4$(DC18C6)]$_2$[Mo$_6$O$_{19}$] (4)

Dicyclohexyl–18–crown–6 (DC18C6) is the saturated analogue of dibenzo–18–crown–6 (DB18C6). Based on the fusion of the cyclohexane rings (*cis* or *trans*) and the relationship between the two (*syn* or *anti*), this crown ether exists as five stereoisomers [22,23] as shown in Scheme 2.3. The crown ether DC18C6 contains two cyclohexyl rings which are non–planer, non–aromatic in contrast to the planer and aromatic phenyl rings of its aromatic analogue DB18C6. Depending upon the nature of stereoisomerization of the crown ether, the two oxygen atoms on the same cyclohexane ring can either be both in axially or equatorially positioned or might be one is in axial position and another in equatorial position (or vice versa). Whereas, the catechol oxygen atoms of the macrocycle DB18C6 are in plane with the phenyl rings. As the crown ether DC18C6

does not contain any π–ring, no π–stacking interactions would be present in the crystal lattice of compound $[NH_4(DC18C6)]_2[Mo_6O_{19}]$ (**4**) and thus, the packing mode of the molecules would obviously deviate from that of the compounds **1** and **3**. The molecules of compound $[NH_4(DC18C6)]_2[Mo_6O_{19}]$ (**4**) assemble in $P2_1/n$ space symmetry with one

(a)   (b)

(c)
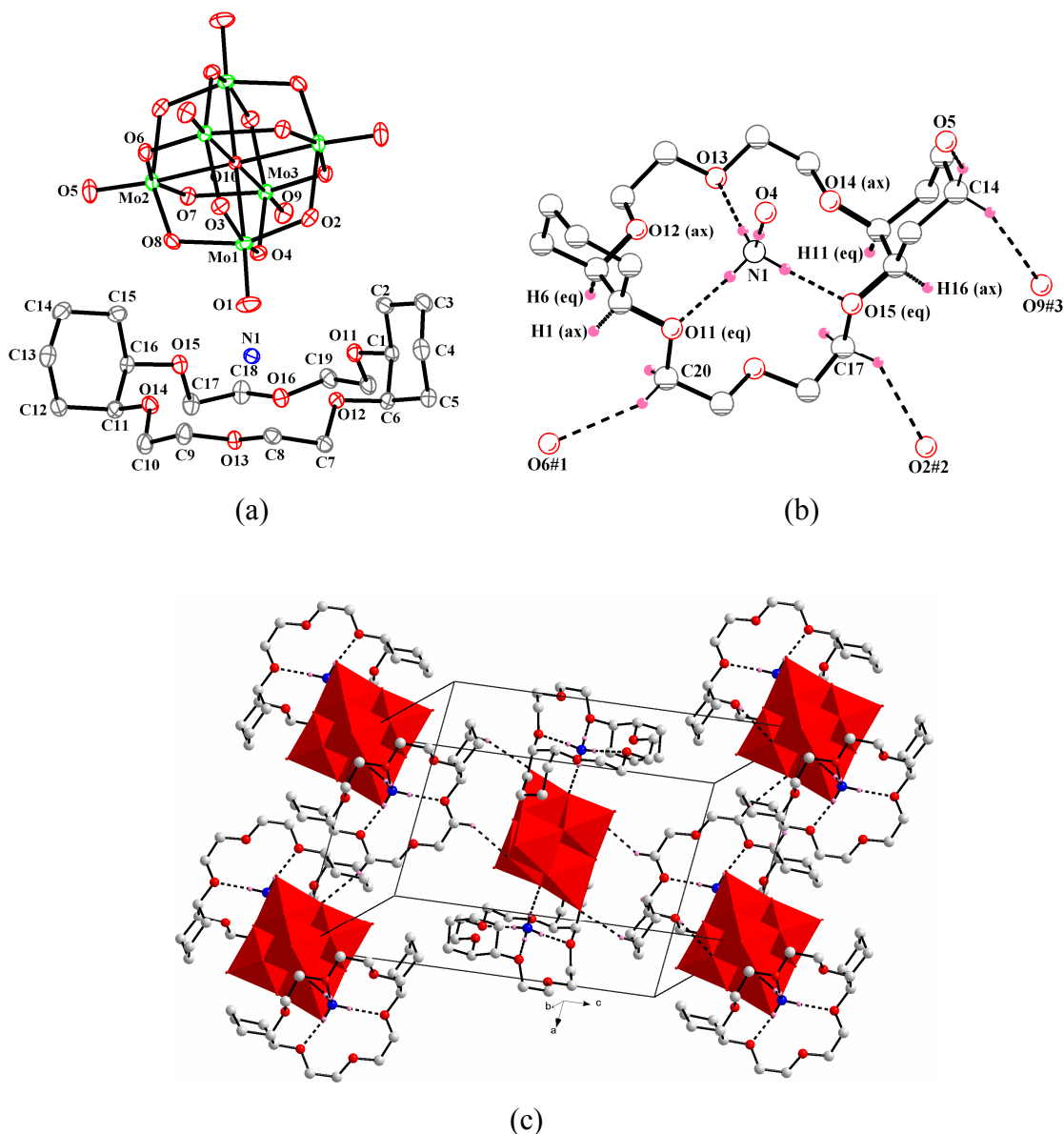
Figure 2.9 (a) ORTEP diagram of the compound **4** in 50% probability distribution. Only one crown ether cation has been displayed for a clearer view; (b) H–bonding interactions in the title compound displaying the geometry of the crown ether, bonds in bold = atoms upward, dashed bond = atoms downward, ax = axial and eq = equatorial; (c) Ribbon like arrangement of the supramolecular sandwiches through C–H···O interactions.

ammonium–crown ether supramolecular complex cation and half of the $[Mo_6O_{19}]^{2-}$ anion in its asymmetric unit (Z′ = ½). An attempt to refine the structure in the standard symmetry $P2_1/c$ has resulted in unusually poor data convergence (with high shift/esd), so

Table 2.7 Selected bond lengths for the crystal structure of the compounds **4–6**.

		Compound–**4**			
C(1)–C(2)	1.519(3)	C(2)–C(3)	1.526(4)	C(3)–C(4)	1.527(4)
C(4)–C(5)	1.525(4)	C(5)–C(6)	1.529(3)	C(1)–C(6)	1.523(3)
C(7)–C(8)	1.495(3)	C(9)–C(10)	1.502(4)	C(11)–C(12)	1.533(3)
C(12)–C(13)	1.525(4)	C(13)–C(14)	1.525(4)	C(14)–C(15)	1.532(4)
C(15)–C(16)	1.515(3)	C(11)–C(16)	1.520(3)	C(17)–C(18)	1.499(3)
C(19)–C(20)	1.496(3)	C(1)–O(11)	1.438(3)	C(6)–O(12)	1.434(3)
C(7)–O(12)	1.426(3)	C(8)–O(13)	1.429(3)	C(9)–O(13)	1.429(3)
C(10)–O(14)	1.422(3)	C(11)–O(14)	1.437(3)	C(16)–O(15)	1.441(3)
C(17)–O(15)	1.425(3)	C(18)–O(16)	1.424(3)	C(19)–O(16)	1.423(3)
C(20)–O(11)	1.431(3)				
		Compound–**5**			
C(1)–C(2)	1.395(7)	C(2)–C(3)	1.379(10)	C(3)–C(4)	1.353(10)
C(4)–C(5)	1.401(7)	C(5)–C(6)	1.373(7)	C(1)–C(6)	1.398(7)
C(7)–C(8)	1.506(6)	C(9)–C(10)	1.474(10)	C(11)–C(12)	1.431(9)
C(13)–C(14)	1.488(10)	C(1)–O(9)	1.357(6)	C(6)–O(10)	1.386(5)
C(7)–O(10)	1.432(5)	C(8)–O(11)	1.412(6)	C(9)–O(11)	1.415(7)
C(10)–O(12)	1.390(7)	C(12)–O(13)	1.402(8)	C(13)–O(13)	1.403(8)
C(14)–O(9)	1.441(6)	C(15)–C(16)	1.64(3)	C(16)–O(14)	1.259(13)
		Compound–**6**			
C(17)–C(18)	1.442(15)	C(19)–C(20)	1.626(18)	C(21)–C(22)	1.470(18)
C(23)–C(24)	1.489(16)	C(25)–C(26)	1.525(16)	C(27)–C(28)	1.517(14)
C(18)–O(25)	1.255(12)	C(19)–O(25)	1.450(13)	C(20)–O(24)	1.357(12)
C(21)–O(24)	1.430(13)	C(22)–O(23)	1.306(15)	C(23)–O(23)	1.406(12)
C(24)–O(22)	1.358(12)	C(25)–O(22)	1.450(12)	C(26)–O(21)	1.335(10)
C(27)–O(21)	1.407(11)	C(17)–O(20)	1.429(11)	C(28)–O(20)	1.339(12)

the space group of the relevant crystal has been assigned to $P2_1/n$ only. The crystal structure of the compound **4** has been displayed in Figure 2.9a. The POM anion is situated at the corner of the crystallographic *ac* plane, the central oxygen atom of the POM i.e. O(10) being the inversion centre (xyz = 1.0, 0.0, 1.0) of the molecule. Oxygen atoms attached to the cyclohexane rings of the crown ether are found to face upwards and the rings also project to the same direction thereby making the crown ether look like an umbrella with *cis–syn–cis* conformation. In this context, it should be mentioned that the

commercially procured DC18C6 (Sigma–Aldrich) was a mixture of the isomers, while in the resulting crystal structure only one stereoisomer of the crown ether is found (see PXRD discussions). The reason for this selectivity is not clear to us. As seen in Figure 2.9a, the crown ether is highly puckered and the ammonium ion is located at a distance of 1.0231(2)Å from the mean macrocycle {O6} plane. O(12) and O(14) atoms of the crown ether are in axial positions while O(11) and O(15) are in the equatorial positions with respect to the two cyclohexane rings (see Figure 2.9b), the rings being in chair conformations. In the crystal structure of compound **4**, the bond lengths of the crown ether are observed as follows: C(cyclohexyl)–C(cyclohexyl) 1.515–1.534Å which are longer than the C(alkyl)–C(alkyl) bonds 1.495–1.502Å; C(cyclohexyl)–O(axial) 1.433–1.437Å which are shorter than the C(cyclohexyl)–O(equatorial) bonds 1.438–1.441Å and the C(alkyl)–O bonds in the range of 1.422–1.432Å (see Table 2.7). The guest cation (ammonium) is incorporated into the crown ether cavity through three strong N^+–H···O hydrogen bonding interactions with O(11), O(13) and O(15) of the macrocycle, and interacts with the POM anion through N(1)–H(1N)···O(4) hydrogen bond donation (see Scheme 2.1). N^+–H···O interaction between N(1)···O(4) followed by the inversion symmetry with respect to O(10) generates the full molecule where the POM anion is sandwiched between two supramolecular ammonium–crown ether adducts (see Figure 2.9c). These supramolecular sandwiches are further supported by the C–H···O interaction

Table 2.8 Hydrogen bonding parameters for the compound **4**.

D–H···A	d(D–H)	d(H···A)	d(D···A)	<(DHA)
C(14)–H(14A)···O(5)	0.97	1.61	3.498 (3)	151.6
C(14)–H(14B)···O(9)#3	0.97	1.59	3.459(3)	149.0
C(17)–H(17A)···O(2)#2	0.97	1.51	3.352(3)	145.6
C(20)–H(20B)···O(6)#1	0.97	1.50	3.386(3)	151.6
N(1)–H(3N)···O(15)	0.92(4)	1.90(4)	1.814(3)	176(3)
N(1)–H(4N)···O(13)	0.83(3)	1.11(4)	1.942(3)	178(3)
N(1)–H(2N)···O(11)	0.86(4)	2.01(4)	1.848(3)	166(3)
N(1)–H(1N)···O(4)	0.86(3)	2.03(3)	1.870(3)	166(3)

Symmetry transformations used to generate equivalent atoms: #1 x–1,y,z; #2 x–1/2,–y+1/2,z–1/2; #3 –x+3/2,y+1/2,–z+3/2

between C(14) of the crown ether and O(5) of the POM anion. H–bonding parameters in the crystal structure of compound **4** have been tabulated in Table 2.8. Each of such supramolecular sandwiches are again connected to molecules of the same kind to form a zig–zag ribbon–like arrangement *via* C(20)–H(20B)···O(6) [3.386(3) Å], C(17)–H(17A)···O(2) [3.352(3) Å] and C(14)–H(14B)···O(9) [3.459(3) Å] hydrogen bonding interactions as shown in Figure 2.9c.

(a)

(b)
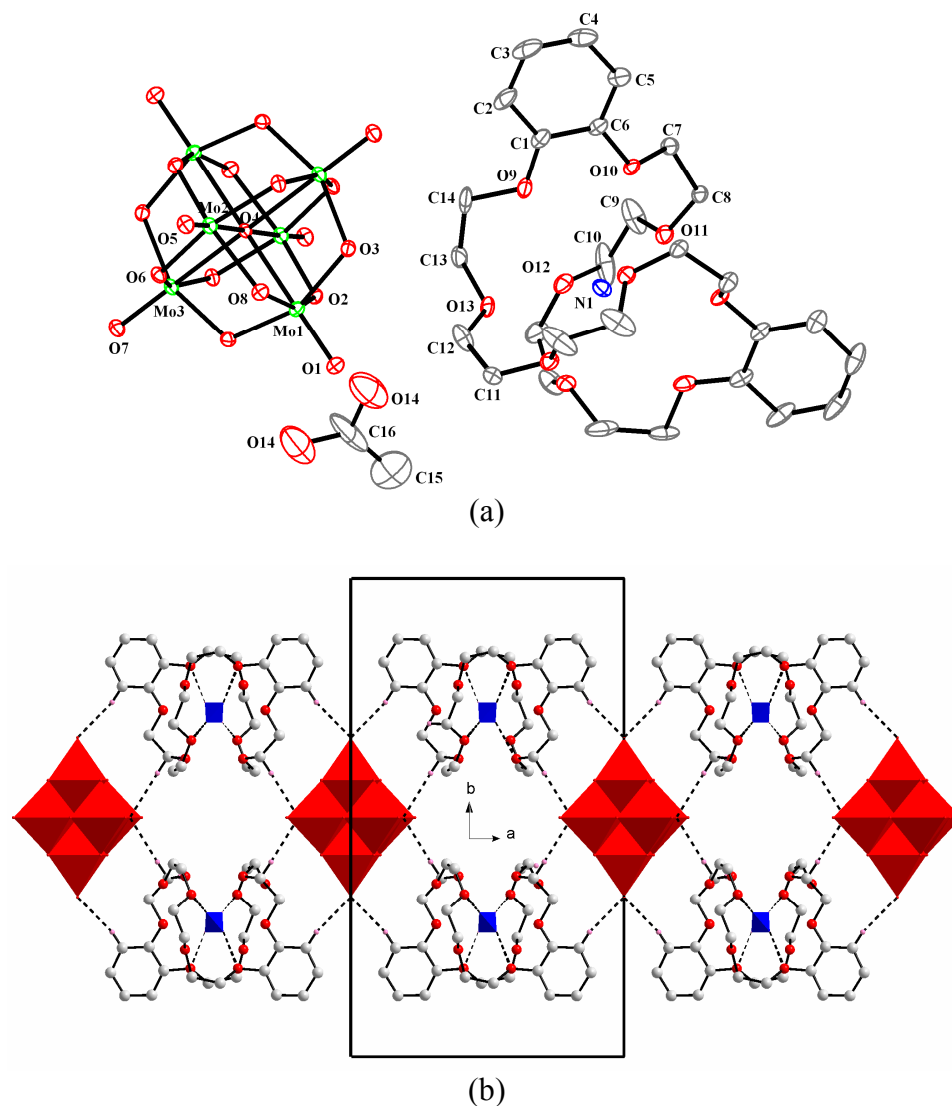
Figure 2.10 (a) Crystal structure of the compound **5** in 30% thermal distributions. Only one inclusion complex has been shown for clarity. (b) One dimensional chain–like topology of the supramolecular ensemble through C–H···O interactions viewed down the crystallographic [001] axis. H atoms and the acetic acid dimers have been excluded for clarity.

Compound [NH$_4$(DB30C10)]$_2$[Mo$_6$O$_{19}$].CH$_3$COOH (5)

Unlike compounds **1–4**, compound **5** comprises the larger crown ether dibenzo–30–crown–10 (DB30C10) that contains sixteen sp^3 hybridized C atoms, and so, it is structurally the most flexible one among all the crown ethers used in the present case. This larger macrocycle (DB30C10) can swallow a cation either by wrapping around it or by occupying more than one cation in its cavity.[24] Single crystal structure of the crown ether, DB30C10 shows a chair–like conformation of the crown ether which can best be described as a quasi–planar form.[24g] However, after interacting with a cation, the crown ether takes up different conformations depending on the nature of binding. Encapsulation of metal cations or hydroxonium ions,[24a–h] even substituted ammonium ions[24i,j] in the cavity of DB30C10 has been discussed in literature. Here, in the case of compound [NH$_4$(DB30C10)]$_2$[Mo$_6$O$_{19}$].CH$_3$COOH (**5**), effect of the N$^+$–H⋯O hydrogen bonding interaction for binding a single NH$_4^+$ ion in the big cavity of DB30C10 has been demonstrated. The title compound **5** crystallizes in monoclinic crystal system, *C2/m* space group with one acetic acid molecule per formula unit (Z′ = ½) (see Figure 2.10a). The POM anion is positioned at the centre of the crystallographic *b*–axis. O(4)–Mo(3)–O(7) axis of the [Mo$_6$O$_{19}$]$^{2-}$ cluster anion lies parallel to the 2–fold rotational axis of the monoclinic unit cell. The central atom of the POM anion i.e. O(4) is located at inversion

Table 2.9 Geometrical parameters for the H–bonding interactions in compound **5**.

D–H⋯A	d(D–H)	d(H⋯A)	d(D⋯A)	<(DHA)
C(2)–H(2)⋯O(7)#1	0.95	1.60	3.490(6)	155.2
C(10)–H(10B)⋯O(11)#2	0.99	1.56	3.463(8)	151.3
C(13)–H(13A)⋯O(2)	0.99	1.62	3.608(7)	176.6
N(1)–H(1N)⋯O(10)	0.80(6)	1.23(6)	3.000(6)	162(6)
N(1)–H(2N)⋯O(12)	0.83(6)	1.26(6)	3.043(5)	158(6)

Symmetry transformations used to generate equivalent atoms: #1 –x+2,–y+1,–z+2; #2 –x+1/2,–y+3/2,–z+1

centre (xyz = 1.0, 0.5, 1.0) and so it sits in a four–fold symmetrical site with quarter occupancy in the asymmetric unit. The Mo atoms of the POM are also found at two– fold symmetrical sites with half occupancies. NH$_4^+$ tetrahedron, too, has occupied a two–fold

symmetrical site with respect to the rotational axis. Thus, in the crystal structure of compound **5**, there are more number of special position constraints compared to the last four crystal structures (compounds **1–4**). Except C(7) and C(8) all other aliphatic carbon atoms of the crown ether DB30C10 experience higher thermal vibrations even at lowered temperature (data has been collected at 100K), which is very common for crystal structures associated with the structurally flexible crown ethers. In the crystal structure of compound **5**, various bond lengths of the concerned crown ether are observed as follows: C(aryl)–C(aryl) 1.353–1.401Å, C(aryl)–O(aryl) 1.357–1.386Å, C(alkyl)–O(aryl) 1.431–1.441Å, C(alkyl)–O(alkyl) 1.391–1.416Å, C(alkyl)–C(alkyl) 1.430–1.506Å (see Table 2.7). Interestingly, 1:1 inclusion complexation between the ammonium ion and the crown ether has been observed in the crystal structure of the compound **5** where, the guest cation is encapsulated in the crown ether cavity through four N^+–H···O hydrogen–bonding interactions and the giant macrocycle wraps around the cation. In the last four crystal structures it has been observed that, the NH_4^+ cation has interacted with the crown ethers using three N–H bonds (N^+–H···O hydrogen bonding interaction), while the fourth N–H bond has been donated to an acceptor atom (bridging O atom of POM in case of **1**, **2**, **4** and solvent water molecule in case of **3**). But, in the present case, as the cation has used all the four N–H bonds to sit inside the crown ether cavity, N^+–H···O interactions between the cation and the POM anion has been restricted. This kind of host–guest interaction is possible only if the host (here crown ether DB30C10) is highly structurally flexible. The C–H···O interactions between the crown ether and the POM anion play a significant role towards formation of one dimensional supramolecular chain like topology in the crystal lattice of compound **5** (see Figure 2.10b). The 2–fold rotational symmetry equivalence of the chain with respect to the crystallographic *b*–axis is clearly visible in the relevant picture. Alternately arranged crown ethers in between two POM anions are related to each other by the reflection and inversion symmetries. Apart from these intermolecular interactions between the crown ethers and the POM anions, the macrocycles are again stacked with each other by means of C–H···O or C–H···π interactions in the crystal lattice, giving rise to a complicated crystal packing. C(10)–H(10B)···O(11) [3.463(8) Å] interaction between two reflection equivalent crown ethers results in the formation of another one–dimensional chain propagating perpendicular to

the crystallographic [011] plane (see Table 2.9 for the H–bonding parameters for compound **5**). Crown ethers in this chain further interact with each other via C–H⋯π interactions as shown in Figure 2.11.
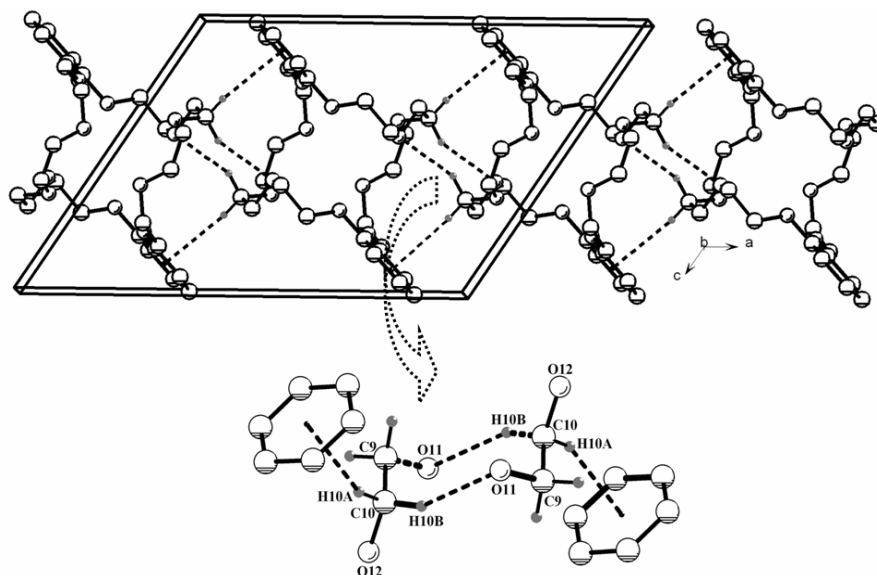
Figure 2.11 Intermolecular C–H⋯O and C–H⋯π interactions between the crown ethers in crystal lattice of the compound **5**. Parameters for C–H⋯π interactions: d(C10–H10A) 0.99Å, d(H10A⋯Cg) 1.82(1)Å, d(C10⋯Cg) 3.756(13)Å, <(C10–H10A⋯Cg) 157.49(19)º (symmetry: 0.5–x, 1.5–y, 1–z) where Cg refers to the centroid of the concerned phenyl ring.

Compound [Bu$_4$N][OPDAH(18C6)][Mo$_6$O$_{19}$] (6)

Single crystal X–ray structural analysis on a greenish–yellow plate unambiguously has determined the structure of the compound [Bu$_4$N][OPDAH(18C6)] [Mo$_6$O$_{19}$] (**6**) that is in full concurrence with the spectroscopic analyses as describe above. The concerned crystal structure is characterized by a [OPDAH–18C6]$^+$ supramolecular complex cation, a tetrabutylammonium cation and a hexamolybdate POM cluster anion in its asymmetric unit or molecular structure (Z′ = 1) (see Figure 2.12a). 1:1 supramolecular association between the protonated amine and the crown ether has been noticed in the relevant crystal structure. Molecules in the relevant crystal pack in a controsymmetric space group (*C2/c*) with an elongated *c*–axis (37.006(2) Å). The diamine (OPDA) is found to be mono–protonated in the crystal structure of compound **6** and the resulting cation, OPDAH$^+$ is embedded with the crown ether cavity through supramolecular interactions that involve

both the –NH$_2$ and –NH$_3^+$ groups and the crown ether. Crown ethers have more affinity toward aminium / anilinium cations (Ar–NH$_3^+$) compared to amino groups (–NH$_2$). In another words, it can be said that, the –NH$_3^+$ group is more prone towards encapsulation in the crown ether cavity in comparison with the –NH$_2$ group. The cavity size of the crown ether 18C6 and its derivatives fits for inclusion of only one amino or ammonium group. Thus, in the crystal structure of compound **6**, it is observed that the OPDAH$^+$ cation has a tilted orientation (Figure 2.12) after interacting with the crown ether through

(a)

(b)

(c)
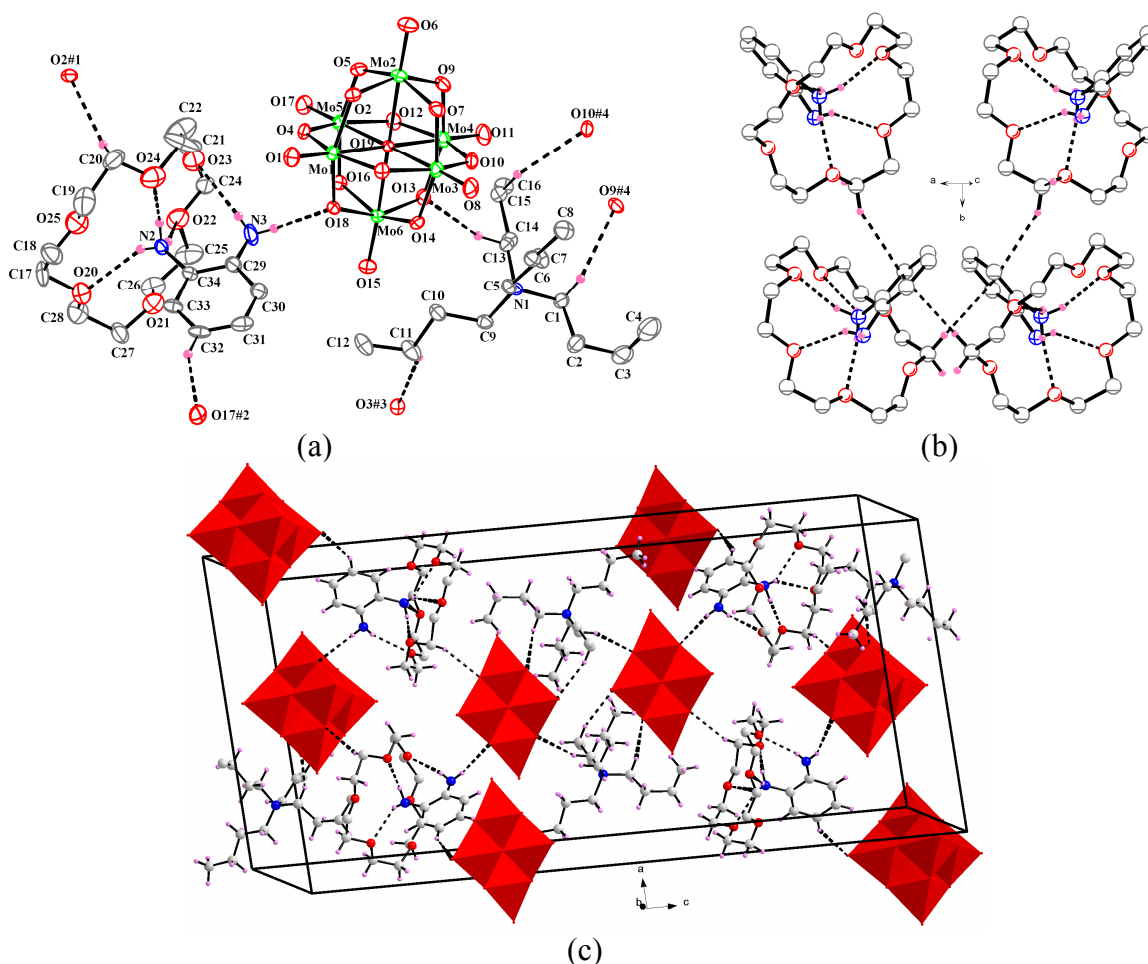
Figure 2.12 (a) Thermal ellipsoidal plot of compound **6** in 20% confidence labels with the H–bonding interactions in the crystal structure. H–atoms have been omitted for clarity. Atoms labeled with additional symmetry codes are in accord with that of Table 2.10. (b) C–H⋯π interactions between the crown ethers and OPDAH observed in the crystal packing of the compound **6**. (c) A portion of packing of the molecules in the crystal lattice of compound **6** showing an aassembly of the [OPDAH–18C6]$^+$ and [Bu$_4$N]$^+$ cations with the POM anions through intermolecular hydrogen bonding interactions.

supramolecular interactions. Four strong N^+–H⋯O hydrogen bonding interactions between the Ar–NH_3^+ group of the $OPDAH^+$ cation and the crown ether (see Table 2.10 for the H–bonding parameters) have resulted in inclusion of the Ar–NH_3^+ group in the macrocycle cavity. Aromatic amino group at the *ortho–* position with respect to the Ar–NH_3^+ group has further stabilized the inclusion by means of N–H⋯O supramolecular interaction with the crown ether [N(3)–H(3NA)⋯O(23) d = 3.002(13)Å] and the POM cluster anion [N(3)–H(3NB)⋯O(18) d = 3.162(12)Å]. In the crystal structure of the compound **6**, various bond lengths for the different molecular fragments are observed as

Table 2.10 Geometrical parameters for the hydrogen bonding interactions in the crystal structure of the compound **6**.

D–H⋯A	d(D–H)	d(H⋯A)	d(D⋯A)	<(DHA)
C(1)–H(1B)⋯O(9)#4	0.97	1.70	3.482(8)	138.5
C(11)–H(11A)⋯O(3)#3	0.97	1.61	3.427(9)	141.3
C(13)–H(13A)⋯O(13)	0.97	1.60	3.499(8)	153.7
C(15)–H(15B)⋯O(10)#4	0.97	1.61	3.511(9)	153.8
C(20)–H(20A)⋯O(2)#1	0.97	1.47	3.292(13)	141.3
C(32)–H(32)⋯O(17)#2	0.93	1.50	3.336(8)	149.9
N(2)–H(2NA)⋯O(24)	0.88(10)	2.05(10)	1.896(11)	163(8)
N(2)–H(2NB)⋯O(20)	0.65(11)	1.36(12)	1.912(10)	144(13)
N(2)–H(2NB)⋯O(25)	0.65(11)	1.43(12)	1.984(12)	145(13)
N(2)–H(2NC)⋯O(22)	0.81(8)	1.13(8)	1.930(10)	170(7)
N(3)–H(3NB)⋯O(18)	0.76(13)	1.45(13)	3.162(12)	157(13)
N(3)–H(3NA)⋯O(23)	0.70(6)	1.38(7)	3.002(13)	148(8)

Symmetry transformations used to generate equivalent atoms: #1 –x+1, y, –z+1/2 #2 x–1/2, y+1/2, z   #3 x–1/2, y–1/2, z #4 –x+1, –y+1, –z+1

follows: (i) for the $OPDAH^+$ cation: C–C 1.351(13)–1.392(12)Å, C–N 1.365(17)–1.455(10)Å; (ii) for the crown ether: C–C 1.441(18)–1.626(19)Å, C–O 1.256(15)–1.450(15) and (iii) for the POM cluster anion: Mo–O_t 1.679(5)–1.692(5), Mo–O_b 1.899(4)–1.960(4), Mo–O_c 1.311(4)–1.327(3) (see Table 2.7 for the selected observed bond lengths). As shown in Figure 2.12a, the POM cluster anion bridges the $[OPDAH(18C6)]^+$ and the $[Bu_4N]^+$ cations through hydrogen bonding interactions. The tetrabutylammonium cation is also found to be involved in supramolecular interactions

with three POM anions (C–H···O interactions). Thus, although there is an unwanted perturbation by the tetrabutylammonium cation with the molecular symmetry, this cation plays an important role in crystal packing through hydrogen bonding interactions. Extensive C–H···π stacking interactions between the crown ether and the phenyl ring of the OPDAH$^+$ cation are also observed in the crystal lattice of compound **6** (see Figure 2.12b). Two–fold rotational equivalence of the [OPDAH(18C6)]$^+$ supramolecular complex cations in a monoclinic crystal system is clearly visible from the relevant picture (Figure 2.12b). The resulting crystal packing of the compound **6** is an intricate one. Thus, a portion of packing of the molecules in the crystal structure of compound **6** has been shown in Figure 2.12c.
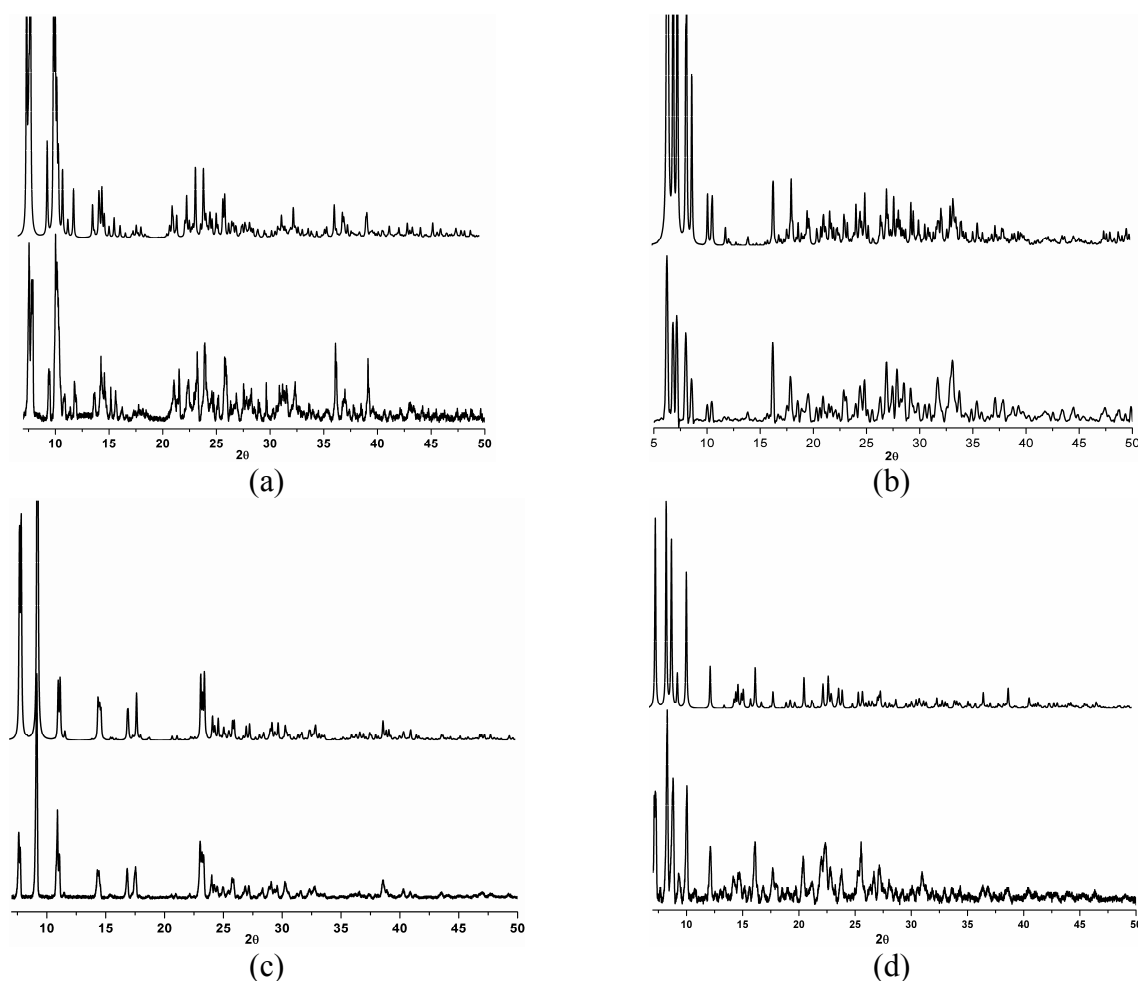
Figure 2.13 Observed (bottom) *vs* simulated (top) X–ray powder diffraction patterns for the compounds (a) **1**, (b) **2**, (c) **3** and (d) **4**.

2.2.7 Powder X–ray Diffraction Study

X–ray powder diffraction data for the grinded crystals of the compounds **1**–**4** have been recorded. Insufficient amount of sample has restricted us in doing so with the compounds **5** and **6**. Similar diffraction patterns for the simulated data (calculated from the single crystal X–ray data) and observed data prove the bulk homogeneity of the samples (see Figure 2.13).

2.3. Conclusion

As such, crown–ether–cavity encapsulated ammonium complexes were long known; however, the same was not known with polyoxometalate association. We have described six ammonium–crown ether supamolecular complexes associated with polyoxometalate counter–anions in compounds **1**–**6**. We have shown the diversity in supramolecular interactions between the molecular fragments, as we analyze the supramolecular structures from compound **1** through compound **6**. Changing the POM anion hasn't shown any disparity in the hydrogen bonding interactions between the ammonium ion and the POM anions as described in the crystal structures of compounds **1** and **2**. But alteration of the crown ethers from less symmetrical to higher symmetrical or from smaller to larger has shown diversity in crystal symmetry of the compounds **1**–**5**. All the crystal structures depict 1:1 supramolecular adduct formation between the hosts (crown ethers) and the guest (ammonium ion). In the crystal structures of compounds **1**, **2** and **4,** it has been observed that, the ammonium cation interacts with the POM anions through the bridging O atom of the latter in all the cases. Possibly usage of the bridging O atom of the POM anion makes the latter in slightly tilted orientation (see Scheme 2.1) thereby bringing the terminal O atoms closer to the crown ethers to accept the C–H bond donation. This type of interaction might result in more close packing of the molecules in the crystal compared to the other mode of interaction i.e. interaction with the ammonium ion using the terminal O atom. In this mode of interaction, the bridging O atoms of the POM anion are apart from the crown ethers to accept the C–H bond donation from the latter (see Scheme 2.1). We also have performed detailed spectroscopic studies (UV–visible, IR and NMR) to support the supramolecular structures in compounds **1**–**6**, that are established by crystallography and purity of the solids have been checked by PXRD

analysis. We have also shown, how spectroscopy has helped us to elucidate the cationic motifs in some of these compounds, that were not confirmed from their respective crystal structures.

2.4. Experimental Section

2.4.1. Materials and Methods

All the crown ethers (18–crown–6, benzo–18–crown–6, dibenzo–18–crown–6, dicyclohexyl–18–crown–6, dibenzo–30–crown–10) have been purchased from Sigma–Aldrich and used as received. Acetonitrile solvent, sodium molybdate, ammonium heptamolybdate have been received from Merck. Tungstosilisic acid was supplied by Alfa–Acer. $[Bu_4N]_2[Mo_6O_{19}]$ has been prepared using a literature procedure.[25] FLASH EA series 1112 CHNS analyzer performed elemental analyses. Infrared spectra were recorded as KBr pellets on a JASCO–5300 FT–IR spectrophotometer at 298K. A Cary 100 Bio UV–visible spectrophotometer was used to record the electronic absorption spectra. ^{1}H NMR spectra were recorded in Bruker AV 400 MHz spectrometer. The chemical shifts (δ) are reported in ppm. Powder X–ray diffraction patterns on the grinded crystals of the compounds **1–4** were recorded on a Bruker diffractometer using Cu Kα_1 (1.5406Å) and Kα_2 (1.54439Å) radiation.

2.4.2. Synthesis

[NH$_4$ (B18C6)][Bu$_4$N][Mo$_6$O$_{19}$] (1): To a stirred solution of benzo–18–crown–6 (0.04g, 0.13 mmol) in 50 ml acetonitrile, was added $[Bu_4N]_2[Mo_6O_{19}]$ (0.13g, 0.09 mmol). After all the materials dissolved, 0.06 g ammonium thiocyanate (0.79 mmol) was added, followed by the addition of 10ml glacial acetic acid (100%). The resulting orange colored solution was stirred at room temperature for 17 h, filtered and allowed to evaporate slowly. Orange colored crystalline blocks appeared after 10 days. They were isolated from the mother liquor by filtration. Yield: 0.025g (26% based on crown–ether used). Anal. calcd. for $C_{32}H_{64}Mo_6N_2O_{25}$: C, 26.46; H, 4.44; N, 1.93. Found: C, 26.30; H, 4.48; N, 2.01. IR (KBr, cm^{-1}): 3175, 2964, 2872, 1915, 1682, 1591, 1506, 1458, 1417, 1249, 1201, 1120, 952, 798, 592.

[NH$_4$(B18C6)]$_4$[SiW$_{12}$O$_{40}$].2CH$_3$CN (2): 0.08 g of H$_4$SiW$_{12}$O$_{40}$.4H$_2$O (0.027 mmol) was dissolved in 50 ml acetonitrile to which 10ml glacial acetic acid was added. To this mixture, was added 0.03g benzo–18–Crown–6 (0.096 mmol), followed by the addition of 0.1g ammonium thiocyanate (1.31 mmol). The resulting pink colored solution was stirred at room temperature for 15 h, filtered and allowed to evaporate slowly. Deep yellow block shaped crystals were isolated after 10 days. Yield: 0.04g(39% based on crown–ether used). Anal. calcd. for C$_{68}$H$_{118}$N$_6$O$_{66}$SiW$_{12}$: C, 18.95; H, 1.76; N, 1.95. Found: C, 19.2; H, 1.61; N, 1.1. IR (KBr, cm^{-1}): 3209, 3047, 2903, 2251, 1722, 1593, 1504, 1454, 1321, 1249, 1209, 1122, 970, 920, 792, 530.

[NH$_4$(DB18C6)]$_2$[Mo$_6$O$_{19}$].4H$_2$O (3): 0.035 g dibenzo–18–Crown–6 (0.097 mmol) was dissolved in a mixture of 50 ml acetonitrile and 10 ml glacial acetic acid (100%). To this solution, 5 ml aqueous solution containing 0.05g ammonium heptamolybdate (0.04 mmol) was added. The resulting pale yellow colored reaction mixture was then stirred on a magnetic stirrer for 10 minutes, heated slowly in a mantle to concentrate the volume to almost 40 ml. The deep yellow colored reaction mixture was filtered and kept for crystallization without further disturbances. Orange crystalline blocks appeared after 8 days, which were isolated by filtration. Yield: 0.06g (73% based on crown–ether used). Anal. calcd. for C$_{40}$H$_{52}$Mo$_6$N$_2$O$_{35}$: C, 28.38; H, 1.85; N, 1.65. Found: C, 28.44; H, 1.81; N, 1.73. IR (KBr, cm^{-1}): 3526, 3254, 3057, 2901, 1624, 1595, 1504, 1454, 1358, 1325, 1248, 1209s, 1124, 1060, 952, 798, 744, 599.

[NH$_4$(DC18C6)]$_2$[Mo$_6$O$_{19}$] (4): This compound was synthesized using the same procedure as **3**. 0.03 g of dicyclohexyl–18–crown–6 (0.08 mmol) dissolved in 50 ml of acetonitrile, was mixed with 10 ml of acetic acid (100%). To this solution, an aqueous solution (5 ml) containing 0.05g of ammonium heptamolybdate (0.06 mmol) was added. It was subsequently stirred for 10 minutes at room temperature and then concentrated to ≈40 ml by slow heating on a heating mantle. It was then filtered and kept for crystallization at room temperature. Yellow plate shaped crystals appeared after two days which was then filteres and dried under vacuum. Yield: 0.025g (38% based on crown–ether used). Anal. calcd. for C$_{40}$H$_{80}$Mo$_6$N$_2$O$_{31}$: C, 28.93; H, 4.85; N, 1.68. Found: C,

29.86; H, 4.83; N, 1.86. IR (KBr, cm^{-1}): 3182, 2937, 1456, 1423, 1356, 1288, 1244, 1205, 1084, 991, 956.

[NH$_4$(DB30C10)]$_2$[Mo$_6$O$_{19}$].CH$_3$COOH (5): 0.03 g dibenzo–30–crown–10 (0.056 mmol) was dissolved in 50 ml acetonitrile. To this, were added ammonium thiocyanate (0.14 g, 1.84 mmol) and 0.05 g [Bu$_4$N]$_2$[Mo$_6$O$_{19}$] (0.04 mmol) and finally 20 ml of acetic acid (100%). The reaction mixture was stirred at room temperature for 18h and filtered to remove the precipitated white material. The orange colored filtrate, thus obtained, was kept for crystallization at open condition. Orange–colored crystals were collected by filtration after 15 days. Yield: 0.015 g (25% based on crown–ether used). Anal. calcd. for. C$_{60}$H$_{96}$Mo$_6$N$_2$O$_{43}$: C, 34.16; H, 4.59, N, 1.33. Found: C, 33.91; H, 4.53; N, 1.38. IR (KBr, cm^{-1}): 3237.77, 3067.09, 2908.92, 1915.49, 1711.94, 1593.35, 1501.68, 1456.39, 1350.29, 1255.77, 1209.48, 1118.81, 1047.44, 956.78, 798.60, 744.59, 601.84, 421.45.

[Bu$_4$N][OPDAH(18C6)][Mo$_6$O$_{19}$] (6): 0.05 g of [Bu$_4$N]$_2$[Mo$_6$O$_{19}$] (0.36 mmol) was dissolved in 15 ml of acetonitrile followed by addition of 0.05 g of *o*–phenelene diamine (0.49 mmol), 10 ml acetic acid and finally 5 ml acetonitrile solution containing 0.05 g of 18–crown–6 (0.19 mmol). The resulting reaction mixture was stirred at room temperature for 16 h. It was then filtered to remove any precipitated material and allowed to evaporate slowly at room temperature. Greenish–brown colored crystals of compound **1** were isolated after two weeks. Yield = 0.025g (9% based on crown–ether used). IR (KBr, cm^{-1}) 3420, 3352, 3026, 2962, 1633, 1504, 1459, 1350, 1296, 1248, 1099, 956, 796. Anal. calcd. for (C$_{34}$H$_{69}$Mo$_6$N$_3$O$_{25}$): C, 27.31; H, 4.65; N, 1.81 . Found: C, 27.41; H, 4.60; N, 1.84.

2.4.3. X–ray Data Collection and Structure Determination

Single crystals suitable for structural determination of all the compounds (**1**–**5**), were mounted on a three circle Bruker SMART APEX CCD area detector system under Mo–Kα (λ = 0.71073 Å) graphite monochromatic X–ray beam, crystal to detector distance 60mm and a collimator of 0.5mm. The scans were recorded with an ω scan width of 0.3º. Data reduction performed by SAINTPLUS,[26a] empirical absorption corrections using equivalent reflections performed program SADABS,[26b] structure solution using

SHELXS–97[26c] and full–matrix least square refinement using SHELXL–97[26d] for above compounds. All the non–hydrogen atoms were refined anisotropically. Hydrogen atoms on the C atoms of the crown ethers were introduced on calculated positions and were included in the refinement riding on their respective parent atoms. Attempts to locate the hydrogen atoms for the ammonium cations in the crystal structure of compounds **2** and **3** and the same for the solvent water molecules in the crystal structure of compound **3** failed. However, no attempts were made to fix these atoms on their parents. Crystal data and structure refinement parameters for all the compounds (**1**–**6**) have been presented in Tables 2.1 and 2.2.

2.5 References

1. Pedersen, C. J. *J. Am. Chem. Soc*. **1967**, *89*, 7017–7036. (b) Pedersen, C. J. *J. Am. Chem. Soc*. **1970**, *92*, 391. (c) Pedersen, C. J. *J. Am. Chem. Soc*. **1970**, *92*, 386–391. (d) Pedersen, C. J. *Science* **1988**, *241*, 536. (e) Pedersen, C. J. *J. Inclusion Phenom. Mol. Recognit. Chem*. **1992**, *12*, 7.

2. (a) Robson, R.; Abrahams, B. F.; Batten, S. R.; Gable, R. W.; Hoskins, B. F.; Liu, J. In *Supramolecular Architecture*; American Chemical Society: Washington, DC, 1992. (b) Atwood, J. L.; Steed, J. W. In *Encyclopaedia of Supramolecular Chemistry*; Taylor & Francis, 2004. (c) Lehn, J. M. In *Comprehensive Supramolecular Chemistry*; Elsevier, 1996. (d) Dietrich, B.; Viout, P.; Lehn, J.–M. In *Macrocyclic Chemistry: Aspects of Organic and Inorganic Supramolecular Chemistry*; VCH, 1993. (e) Lehn, J.–M. In *Nobel Lectures in Chemistry (1981–1990)*; World Scientific Publishing Co. Pte. Ltd., 1992, 444.

3. Junk, P. C. *New. J. Chem*. **2008**, *32*, 762–773 and the references therein.

4. (a) Braga, D.; Gandolfi, M.; Lusi, M.; Paolucci, D.; Polito, M.; Rubini, K.; Grepioni, F. *Chem. Eur. J*. **2007**, *13*, 5249–5255. (b) Bhogala, B. R.; Nangia, A. *Cryst. Growth. Des*., **1996**, *6*, 32–35. (c) Gibson, H. W.; Wang, H.; Slebodnick, C.; Merola, J.; Kassel, W. S.; Rheingold, A. L. *J. Org. Chem*. **2007**, *72*, 3381–3393. (d) Shephard, D. S.; Johnson, B. F. G.; Matters, J.; Parsons, S. *J. Chem. Soc., Dalton Trans*. **1998**, 2289–2292. (e) Dapporto, P.; Paoli, P.; Matijasic, I.; Tusek–Bozic, L. *Inorg. Chim. Acta*. **1996**, *252*, 383–389. (f) Simonov, Y. A.;

Fonari, M. S.; Lipkowski, J.; Yavolovskii, A. A.; Ganin, E. V. *J. Inclusion Phenom. Macrocyclic Chem.* **2003**, *46*, 27–36.

5.   (a) Pope, M. T. In *Heteropoly and Isopoly Oxometalates*; Springer–Verlag: Berlin, 1983. (b) Pope, M. T.; Müller A. In *Polyoxometalate Chemistry*; Eds.; Kluwer: Dordrecht, 2001. (c) Topical issue on polyoxometalates: Hill, C. L., Guest Ed. *Chem. Rev.* **1998**, *98*, 1–389 and the references therein.

6.   (a) Müller, A.; Peters, F.; Pope, M. T.; Gatteschi, D. *Chem. Rev.* **1998**, *98*, 239–272 and the references therein. (b) Klemperer, W. G.; Wakk, C. G. *Chem. Rev.* **1998**, *98*, 297–306 and the references therein. (c) Pope, M. T.; Müller, A. *Angew. Chem., Int. Ed*. **1991**, *30*, 34–48 and the references therein. (d) Jeanin, Y. P. *Chem. Rev*. **1998**, *98*, 51–76 and the references therein.

7.   (a) Pavani, K.; Lofland, S. E.; Ramanujachary, K.V.; Ramanan, A. *Eur. J. Inorg. Chem.* 2007, 568–578. (b) Pavani, K.; Ramanan, A. *Eur. J. Inorg. Chem.* **2005**, 3080–3087. (c) Chakrabarti, S.; Natarajan, S. *Crystal Growth & Design* **2002**, *2*, 333–335. (d) Thomas, J.; Ramanan, A. *Cryst. Growth. Des.* **2008**, *8*, 3390–3400.

8.   (a) Armatas, N. G.; Allis, D. G.; Prosvirin, A.; Carnutu, G.; O'Connor, C. J.; Dunbar, K.; Zubieta, J. *Inorg. Chem.* **2008**, *47*, 832–854. (b) Hagrman, D.; Hagrman, P. J.; Zubieta, J. *Angew. Chem., Int. Ed. Engl.* **1999,** *38,* 3165–3168. (c) Hagrman, P. J.; Zubieta, J. *Inorg. Chem.* **2000**, *39,* 3252–3260. (d) Hagrman, P. J.; Hagrman, D.; Zubieta, J. *Angew. Chem., Int. Ed. Engl.* **1999,** *38*, 2638–2684 and the references therein. (e) Khan, M. I. *J. Solid State Chem.* **2000**, *152***,** 105–112. (f) Khan, M. I.; Yohannes, E.; Powell, D. *Chem. Commun.* **1999,** 23–24. (g) Khan, M. I.;Yohannes, E.; Dödens, D. *Angew. Chem., Int. Ed. Engl.* **1999,** *38***,** 1292–1294. (h) Khan, M. I.; Yohannes, E.; Dödens, R. J.; Tabussum, S.; Cevik, S.; Manno, L.; Powell, D. *Cryst. Eng.* **1999,** *2*, 171–179.

9.   (a) Shivaiah, V.; Das, S. K. *Angew. Chem. Int. Ed.* **2006**, *45*, 245–248. (b) Shivaiah, V.; Das, S. K. *Inorg. Chem*. **2005**, *44*, 7313–7315.

10.   (a) Li, Y.; Hao, N.; Wang, E.; Yuan, M.; Hu, C.; Hu, N.; H. Jia, *Inorganic Chemistry* **2003**, *42*, 2729–2735. (b) You, W.; Wang, E.; Xu, Y.; Li, Y.; Xu, L.; Hu, C. *Inorg. Chem.* **2001,** *40,* 5468–547. (c) You, W. S.; Wang, E.; Zhang, H.; Xu, L.; Wang, Y. B. *J. Mol. Struct.* **2000**, *554*, 141–147. (d) You, W. S.; Wang,

E.; Xu, L.; Zhu, Z. M.; Gu, Y. P. *J. Mol. Struct.* **2002**, *605*, 41–49. (e) You, W. S.; Wang, E.; He, Q. L.; Xu, L.; Xing, Y.; Jia, H. Q. *J. Mol. Struct.* **2000**, *524*, 133–139. (f) Li, Y. G.; Wang, E.; Wang, S. T.; Lu, Y.; Hu, C. W.; Hu, N. H.; Jia, H. Q. *J. Mol. Struct.* **2001**, *607*, 133–141.

11.   (a) Akutagawa, T.; Endo, D.; Kudo, F.; Noro, S.–I.; Takeda, S.; Cronin, L.; Nakamura, T. *Cryst. Growth Des.* **2008**, *8*, 812–816. (b) Akutagawa, T.; Endo, D.; Imai, H.; Noro, S.–I.; Cronin, L.; Nakamura, T. *Inorg. Chem.* **2006**, *45*, 8628–8637. (c) Akutagawa, T.; Endo, D.; Noro, S.–I.; Cronin, L.; Nakamura, T. *Coord. Chem. Rev.* 2007, 251, 2541–2561. (d) Soares–Santos, P. C. R.; Silva, L. C.; Sousa, F. L.; Nogueira, H. I. S. *J. Mol. Str.* **2008**, *888*, 99–106. (e) Streb, C.; McGlone, T.; Brücher, O.; Long, D.–L.; Cronin, L. *Chem. Eur. J.* 2008, 14, 8861–8868. (f) Zhao, Y.; Shi, Z.; Ding, S.; Bai, N.; Liu, W.; Zou, Y.; Zhu, G.; Zhang, P.; Mai, Z.; Pang, W. *Chem. Mater.* **2000**, *12*, 2550–2556.

12.   (a) Chatterjee, T.; Sarma, M.; Das, S. K. *Cryst. Growth Des.* **2010**, *10*, 3149–3163. (b) Chatterjee, T.; Sarma, M.; Das, S. K. *J. Mol. Struct.* **2010**, *91*, 34-39.

13.   (a) Wu, D.; Wang, S.; Lin, X.; Lu, C.; Zhuang, H. *Acta Crystallogr.* **2000**, *C56*, e55. (b) Rheingold, A. L.; White, C. B.; Haggerty, B. S.; Maatta, E. A. *Acta Crystallogr.* **1993**, *C49*, 756. (c) Ito, T.; Sawada, K.; Yamase, T. *Chem. Lett.* **2003**, *32*, 938.

14.   (a) Clegg, W.; Sheldrick, G. M.; Garner, C. D.; Walton, I. B. *Acta Crystallogr.* **1982**, *B38*, 2906. (b) Alyea, E. C.; Craig, D.; Dance, I.; Fisher, K.; Willett, G.; Scudder, M. *CrystEngComm* **2005**, *7*, 491.

15.   (a) Avarvari, N.; Fourmigue, M. *Chem. Commun.* **2004**, 2794. (b) Kuduva, S. S.; Avarvari, N.; Fourmigue, M. *J. Chem. Soc., Dalton Trans.* **2002**, 3686. (c) Avarvari, N.; Fourmigue, M. *Chem. Commun.* **2004**, 1300. (d) Dolbecq, A.; Guirauden, A.; Fourmigue, M.; Boubekeur, K.; Batail, P.; Rohmer, M.–M.; Benard, M.; Coulon, C.; Salle, M.; Blanchard, P. *J. Chem. Soc., Dalton Trans.* **1999**, 1241. (e) Triki, S.; Ouahab, L.; Fabre, J. M. *Acta Crystallogr.* **1994**, *C50*, 219. (f) Coronado, E.; Galan–Mascaros, J. R.; Gimenez–Saiz, C.; Gomez–Garcia, C. J.; Rovira, C.; Tarres, J.; Triki, S.; Veciana. J. *J. Mater. Chem.* **1998**, *8*, 313. (g) Minelli, M.; Hoang, My Le; Kraus, M.; Kucera, G.; Loertscher, J.; Reynolds,

M.; Timm, N.; Chiang, M. Y.; Powell, D. *Inorg. Chem.* **2002**, *41*, 5954. (h) Triki, S.; Ouahab, L.; Grandjean, D.; Fabre, J. M. *Acta Crystallogr.* **1991**, *C47*, 645

16. (a) Clemente–Leon, M.; Coronado, E.; Gimenez–Saiz, C.; Gomez–Garcia, C. J.; Martinez–Ferrero, E.; Almeida, M.; Lopes, E. B. *J. Mater. Chem.* **2001**, *11*, 2176. (b) Modec, B.; Brencic, J. V.; Zubieta, J. *J. Chem. Soc., Dalton Trans.* **2002**, 1500. (c) Maguere`s, P. Le; Hubig, S. M.; Lindeman, S. V.; Veya, P.; Kochi, J. K. *J. Am. Chem. Soc.* **2000**, *122*, 10073–10082.

17. (a) Burkholder, E.; Zubieta, J. *Inorg. Chim. Acta* **2004**, *357*, 279. (b) Wang, W.; Xu, L.; Wei, Y.; Li, F.; Gao, G.; Wang, E. *J. Solid State Chem.* **2005**, *178*, 608. (c) Wang, X.; Guo, Y.; Wang, E.; Duan, L.; Xu, X.; Hu, C. *J. Mol. Struct.* **2004**, *691*, 171. (d) Pedrosa, M. R.; Aguado, R.; Diez, V.; Escribano, J.; Sanz, R.; Arnaiz, F. J. *Eur. J. Inorg. Chem.* **2007**, 3952. (e) Guo, Y.; Wang, X.; Li, Y.; Wang, E.; Xu, L.; Hu, C. *J. Coord. Chem.* **2004**, *57*, 445. (f) Wang, X.; Guo, Y.; Li, Y.; Wang, E.; Hu, C.; Hu, N. *Inorg. Chem.* **2003**, *42*, 4135.

18. (a) Silverstein, R. M.; Webstar F. X. In *Spectrometric Identification of Organic Compounds*; John Wiley and Sons, 6th Ed. (b) Pa*via*, D. L.; Lampman, G. M.; Kriz G. S. In *Introduction to* Spectroscopy, Thomson Learning Inc., 2001. (c) Likhacheva, A. Yu.; Paukshtis, E. A.; Seryotkin, Yu. V.; Shulgenko, S. G. *Phys. Chem. Minerals.* **2002**, *29*, 617–623.

19. (a) Chênevert, R.; Rodrigue, A.; Beauchesne, P.; Savoie, R. *Can. J. Chem.* **1984**, *62*, 2293–2298. (b) Kříž, J.; Dybal, J.; Makrlík, E.; Budka, J. *J. Phys. Chem. A* **2008**, *112*, 10236–10243.

20. (a) Neier, R.; Trojanowski, C.; Mattes, R. *J. Chem. Soc., Dalton Trans.* **1995**, 2521–2528. (b) Evans, H. T.; Popev, M. T. *Inorg. Chem.* **1984**, *23*, 501–504. (c) Attanasio, D.; Bonamico, M.; Fares, V.; Imperatori, P.; Suber, L. *J. Chem. Soc., Dalton Trans.* **1990**, 3221–3228. (d) Maguere`s, P. L.; Quahab, L.; Golhen, S.; Grandjean, D.; Pena, O.; Jegaden, J. C.; Gomez–Garecia, C. J.; Delhae`s, P. *Inorg. Chem.* **1994**, *33*, 5180–5187. (e) Fender, N. S.; Kahwa, I. A.; White, N. J. P.; Williams, D. J. *J. Chem. Soc., Dalton Trans.* **1998**, 1729–1730.

21. (a) Calleja, M.; Johnson, K.; Belcher, W. J.; Steed, J. W. *Inorg. Chem.* **2001**, *40*, 4978–4985. (b) Marsh, R. E. *Acta Crystallogr.* **2004**, *B60*, 252–253.

22. Yamato, K.; Bartsch, R. A.; Dietz, M. L.; Rogers, R. D. *Tetrahedron Letters* **2002**, *43*, 2153–2156 and the references therein.

23. CCDC depositions for crystal structures of the isomers of DC18C6. Former one is the deposition number and the latter one refers to the assigned space group. (a) *cis–syn–cis*: DCHXCR01, *P2₁2₁2₁*. (b) *cis–anti–cis*: DCHXCS01, *P2₁/n*. (c) *trans–syn–trans*: DCHXCT & DCHXCT01, *P–1*. (d) *trans–anti–trans*: XOVKOI, *P2₁2₁2₁*. (e) *cis–trans*: DCHXCS02, *Pccn*.

24. (a) Agnihotri, P.; Suresh, E.; Ganguly, B.; Paul, P.; Ghosh, P. K. *Polyhedron* **2005**, *24***,** 1023–1032. (b) Hasek, J.; Hlavata, D.; Huml, K. *Acta Crystallogr.* **1980**, *B36*, 1782–1785. (c) Willey, G. R.; Meehan, P. R.; Rudd, M. D.; Drew, M. G. B. *J. Chem. Soc., Dalton Trans.* **1995**, 811–817. (d) Lu, T.; Gan, X.; Tan, M.; Yu, K. *J. Coord. Chem.* **1993**, *29*, 215–224. (e) Shiping, Y.; Zonghui, J.; Diazheng, L.; Genglin, W.; Ruji, W.; Honggen, W.; Xinkan, Y. *J. Inclusion Phenom. Macrocyclic Chem.* **1993**, *15*, 159–165. (f) Steed, J. W.; Johnson, K.; Legido, C.; Junk, P. C. *Polyhedron* **2003**, *22*,769–774. (g) Bush, M. A.; Truter, M. R. *J. Chem. Soc., Perkin Trans. 2* **1972**, 345–350. (h) Owen, J. D.; Truter, M. R. *J. Chem. Soc., Dalton Trans.* **1979**, 1831–1835. (i) Colquhoun, H. M.; Stoddart, J. F.; Williams, D. J.; Wolstenholme, J. B.; Zarzycki, R. *Angew. Chem. Int. Ed.* **2003**, *20*, 1051–1053 and the references therein. (j) Allwood, B. L.; Colquhoun, H. M.; Doughty, S. M.; Kohnke, F. H.; Slawin, A. M. Z.; Stoddart, J. F.; Williams, Zarzycki, D. J.; R. *Chem. Commun.* **1987**, 1054–1058.

25. Che, M.; Fournier, M.; Launay, J. P. *J. Chem. Phys.* **1979**, *71*, 1954–1960.

26. (a) SAINT: *Software for the CCD Detector System*; Bruker Analytical X–ray Systems, Inc.: Madison, WI, 1998. (b) SADABS: *Program for absorption correction*; Sheldrick, G. M. University of Göttingen: Göttingen, Germany, 1997. (c) SHELXS–97: *Program for structure solution*; Sheldrick, G. M. University of Göttingen: Göttingen, Germany, 1997. (d) SHELXL–97: *Program for Crystal Structure Analysis*; Sheldrick, G. M. University of Göttingen: Göttingen, Germany, 1997.

Crystallization of hexametalate cluster anions with anthracene based counter cations: Salts or coulombic co-crystals?

3

Abstract:– A series of ion–pair complexes, comprising of Lindqvist type isopolyanions *viz.*, $[Mo_6O_{19}]^{2-}$ and $[W_6O_{19}]^{2-}$ as the counter anions and anthracene–imidazolium / anthracene benzimidazolium as counter cations, have been demonstrated. Structures of the isolated stoichiometric solids have been unambiguously determined by single crystal X–ray diffraction analysis. In spite of the structural incompatibility between anthracene (planer) and the polyoxoanions (spherical), coulombic and several intermolecular weak interactions e.g. C–H···O, C–H···π, π–π etc. compensate the destabilization energy raised due to presence of the structurally mismatched components in the same crystal lattice. Single-crystal as well as PXRD analyses reveal isostructurility between the hexamolybdates and hexatungstates. Conformational variation has been observed in the crystal structures containing benzyl benzimidazolium counter cations.

3.1. Preface

The term 'cocrystal', in a broader sense, denotes crystalline solids made from more than one component held together by non–covalent intermolecular interactions. To–date, many authors have defined the term in diverse ways although an accurate and universally accepted definition of 'cocrystal' is not yet available. Even there is contradiction with the term, whereas some authors believe the term should be 'cocrystal',[1a] many others have shown their preferences toward using 'co–crystal',[1b] 'molecular complex'[1c] or 'multi component molecular crystal',[1d] etc. However, throughout the present work, the term 'cocrystal' has only been used for no apparent reasons. Another characteristic feature of the cocrystals is that they exhibit distinct physical properties (for example, solubility, thermal stability, melting point etc.) than those of the cocrystal formers. Thus, after the intermolecular association of more than one molecular component (not necessarily to be both solids), a crystalline solid (necessarily to be solid) is formed where the uniqueness / identity of the constituents vanish and a modulation of their physico–chemical properties (in solution state there might be a retention of their individuality) is observed. Hydrates, solvates *etc.* are also considered as multi component cocrystals where one component is

water (hydrate) or any organic solvent (solvate) that occupies the interstitial space / void created by the packing arrangement of the another component (crystallizing substance) in the relevant crystal lattice. The crystallizing substance is commonly named as the 'host' and the molecules (generally solvents) incorporated into the void spaces are called as the 'guests'. Out of the several views published by several authors, some representative definitions of the term 'cocrystal' are summarized bellow:

Kitaigorodsky (1986) –"…crystals composed of different molecules and also to solids that are a mixture of crystals with different structures."[2a]

Aakeröy (2005) – "compounds constructed from discrete neutral molecular species...all solids containing ions, including complex transition–metal ions, are excluded". "made from reactants that are solids at ambient conditions". "structurally homogeneous crystalline material that contains two or more neutral building blocks that are present in definite stoichiometric amounts"[2b]

Zaworotko (2006) – "are formed between a molecular or ionic API and a co–crystal former that is a solid under ambient conditions"[2c]

Jones (2006) – "a crystalline complex of two or more neutral molecular constituents bound together in the crystal lattice through noncovalent interactions, often including hydrogen bonding"[2d]

Stahly (2007) – "a molecular complex that contains two or more different molecules in the same crystal lattice"[1a]

Childs (2007) – "crystalline material made up of two or more components, usually in a stoichiometric ratio, each component being an atom, ionic compound, or molecule"[2e]

Bond (2007) – "synonym for multi–component molecular crystal"[2f]

Nangia (2008) – "multi–component solid–state assemblies of two or more compounds held together by any type or combination of intermolecular interactions"[2g]

The definition by Aakeröy has been contradicted in several publications that involve one component of cocrystals as ions or transition metal coordination complexes etc. Very often in the case of cocrystals, a central molecule is focused which is cocrystallized with various other secondary components (called as coformers[3]). At this point it should be remembered that, cocrystals do not involve only organic molecules, but also ionic compounds, inorganic compounds / complexes as coformers. The first cocrystal (all

organic) was discovered by Wohler (1844) in the *era* before the invention of X–ray by Rontgen (1895).[4] The nature of the intermolecular interactions inside the new material obtained by mixing quinone and hydroquinone remained unknown until the determination of its crystal structure in 1930s and 1940s. X–ray structural analyses of the newly obtained beautiful green colored solid revealed coexistence of discrete quinone and hydroquinone moieties and confirmed Wohler's view of 1:1 stoichiometry of the two components in the relevant solid.[5] Since then, cocrystals turned out to be a subject of immense interest and at present majority of the cocrystals reported in literature incorporate active pharmaceutical ingredients (APIs) as one component in achieving bioactive materials.[6] Some representative solid state aggregation of the molecular components have been shown in Figure 3.1.
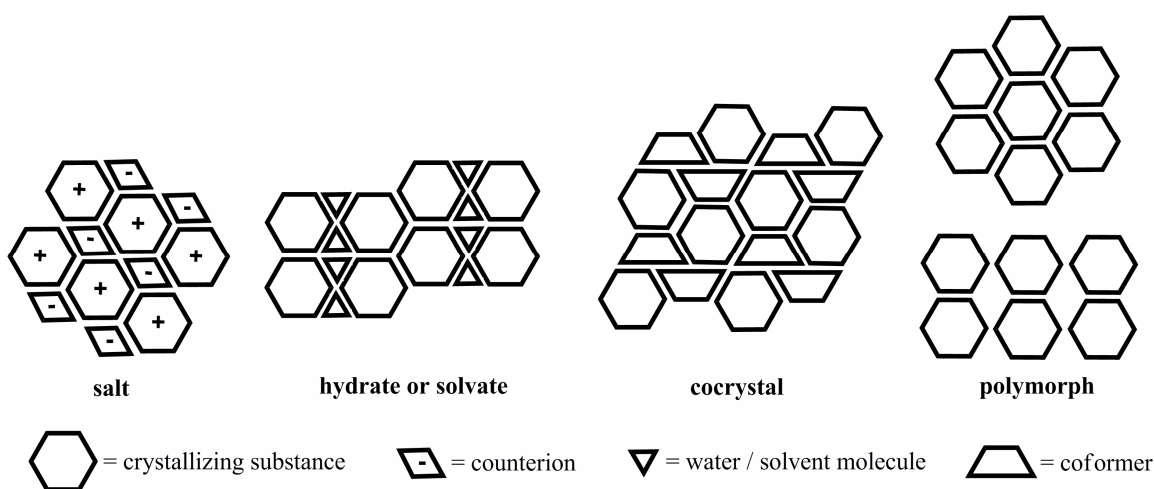
Figure 3.1 Illustration of different molecular aggregations in solid–state.

Apart from cocrystals obtained from only neutral hosts or guests, ionic compounds are also found to form cocrystals with definite stoichiometry. Few representative examples include cocrystals containing both carboxylic acid and acid salt, phenolic acid and acid salt or organic : inorganic cocrystals.[3] It is worth mentioning that, majority of the commercial drugs are marketed as their salts (usually hydrochloride), formation of which needs presence of particular acidic or basic functional groups in the drug moiety. However, the physico–chemical properties (water solubility, stability toward moisture etc.) of the APIs are easily tuned through cocrystallization with a coformer. Some of the

representative cocrystals (that can best be described as salts) containing ionic APIs have been displayed in Figure 3.2.
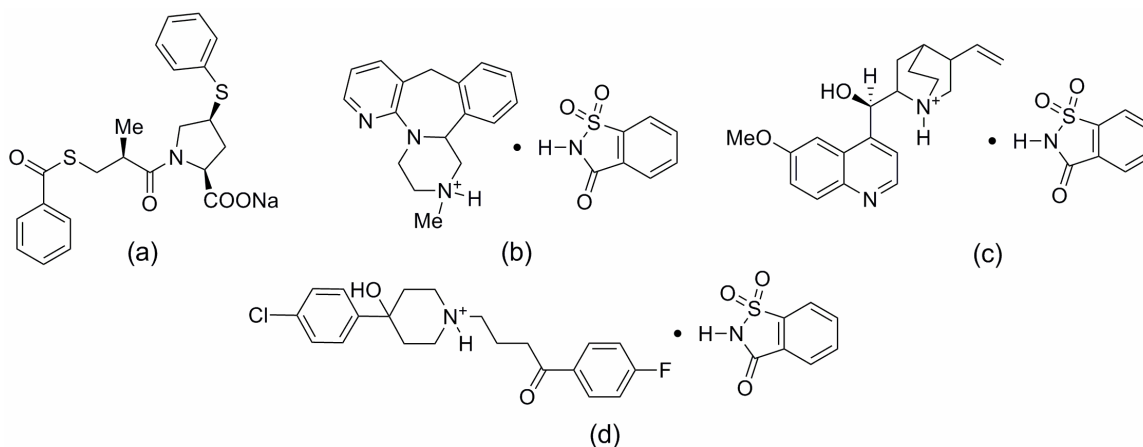
Figure 3.2 (a) Zofenopril sodium salt,[7] (b) Mirtazapine saccharinate salt,[8] (c) Quinine saccharinate salt[8] and (d) Haloperidol saccharinate salt.[8]

Several intermolecular forces, for example, hydrogen bonding, van der Walls, electrostatic, π–stacking etc. govern molecular packing of the crystallizing substances in a crystal lattice. The central aim of the supramolecular chemistry is to gain organized arrangement / packing of the molecules in a crystal using these intermolecular interactions.[9] Apart from the cocrystals built from simple organic : organic or organic : inorganic molecular components, interests have been grown to incorporate complex molecular systems such as, molecules with curved and flat external surfaces in the crystal lattice. Obtaining multidimensional and/or larger supramolecular ensembles using the fullerenes as the crystallizing substances became a subject of extensive research to the structural chemists / crystallographers since the last two decades. The ubiquitous three–dimensional and higher symmetrical shape of the fullerenes (for example C_{60} has Icosahedral (*I* or *I*h) symmetry, see Figure 3.3) along with their exciting physical and chemical properties (e.g., their facile electron accepting abilities) have drawn significant attention to the structural chemists for choosing them as good candidates to build complex supramolecular architectures. Initially it was proposed that fullerenes, as they posses curved / convex external surfaces, could cocrystallize only with molecules containing curved / concave surfaces for shape complementarity in optimizing the lattice energy. Thus, several approaches were made in obtaining curved surfaces that could

encircle the spherically shaped fullerenes in the crystal lattice. At this point it is worth mentioning that, Balch and coworkers isolated a black crystalline solid of formula $C_{60}[Ag(NO_3)]_5$ from the solution of silver nitrate and the fullerene, C_{60} where the subsequent structural analysis revealed encapsulation of the fullerene by a curved infinite

| C_{60} (I_h) | {Mo}$_{132}$ cluster (I_h) | $[M_6O_{19}]^{2-}$ (O_h) |

| M–porphyrin complex (flat) | Anthracene and pyrene (flat) | Ni–OMTAA complex (curved) |
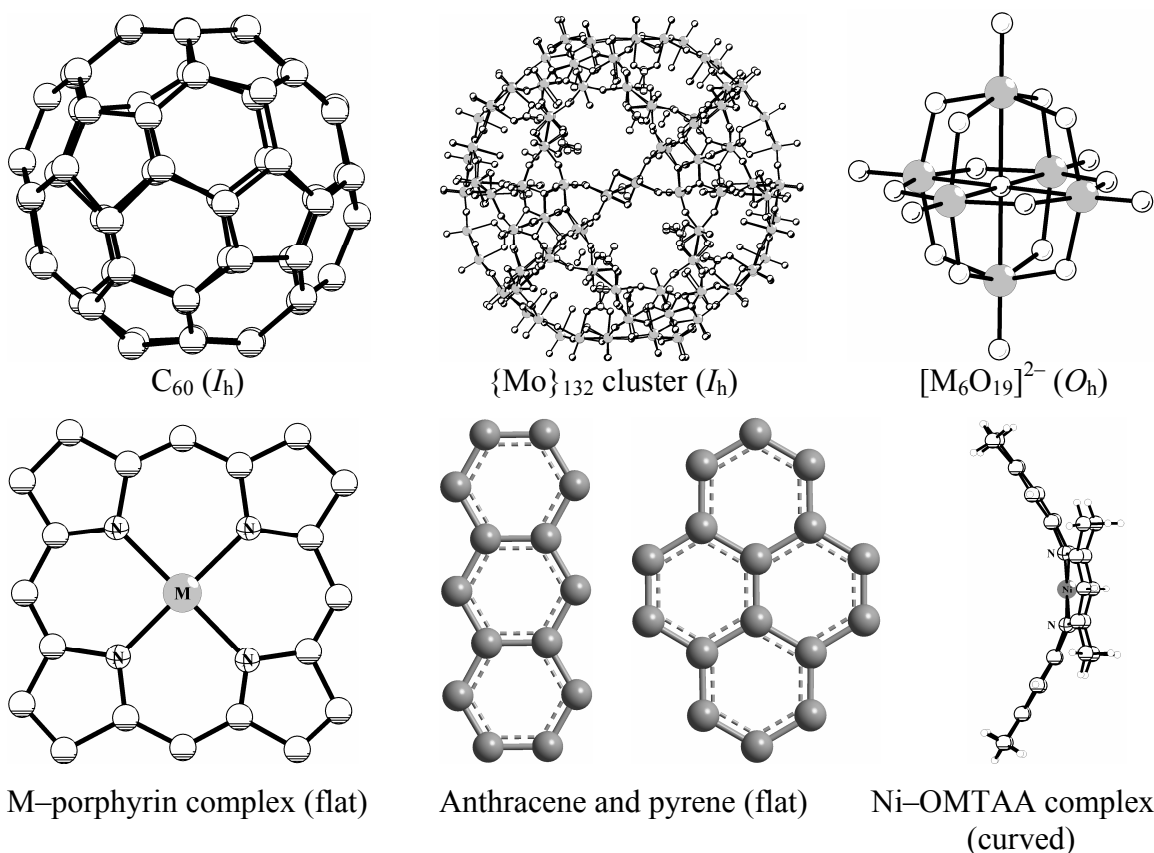
Figure 3.3 Picture representing some compounds having spherical, flat and curved external surfaces. OMTAA = 5,14–dihydro–2,3,6,8,11,12,15,17–octamethyldibenzo–[*b,i*][1,4,8,11]tetraazacyclotetradecinate.

silver nitrate network.[10] Several fullerene based cocrystals, reported at the end of 1990s by Atwood, Raston and other research groups, mainly documented concave / bowel shaped coformers for example, calixarenes,[11] cyclodextrins,[12] cyclotriveratrylene,[13] saddle shaped Ni(II) macrocyclic complexes[14] (see Figure 3.3) etc. After various reports of cocrystals encompassing all curved components (fullerene based), hunting began to obtain fullerene based cocrystals incorporating coformers of flat molecular surfaces despite the size–mismatch (convex : flat) between the constituents. The investigation started with transition metal complexes of porphyrins based on the idea that, planer π

surface of porphyrin would supramolecularly interact with the π cloud of fullerene through stacking interactions (non–covalent). However, crystallographic analyses on the related synthesized compounds explored covalent attachments between porphyrin and fullerene[15] thus, failed to fulfill the basic requirements of cocrystals that need non–covalent interaction between the components. Olmstead and Balch have first reported the cocrystal formation between fullerenes and molecules with flat surfaces in 1999.[16a] The relevant publication demonstrated cocrystallization of C_{60}, $C_{60}O$, C_{70}, and $C_{120}O$ fullerenes with Co, Zn and Fe complexes of octaethyl–porphyrin, both the components being in close contact with each other without any covalent linkages between them and thus, violated the convex–concave size matching assumption. In a separate publication, Boyd and Reed described unique cocrystallities of C_{60} and C_{70} fullerenes with tetraphenyl–porphyrins.[16b] Another similar publication by Ishii et al (2000) documented C_{60} fullerene based cocrystals with *anti*–formed metal complexes of octaethyl–porphyrins.[16c]

Polyoxometalates (POMs), on the other hand, are transition metal–oxide based cluster anions comprising metal ions bridged by oxygen atoms.[17] This area has received an extensive attention by the contemporary chemists because of their diverse physical and chemical properties e.g., diversity in their shape, size, electrochemistry, acid–base chemistry, charge distribution *etc*.[18] These macroanions are readily generated in aqueous solutions by hydrolysis of their precursor salts (e.g. molybdates, tungstates, *etc*.). Various POM cluster anions with simple to complex molecular compositions are easily obtained by changing pH of the solutions or by adding other suitable components to the solution.[19] Depending upon the electrochemical nature, the metal centers of the POM anions can be partially reduced by addition of controlled amount of a reducing agent which generate highly colored mixed-valent cluster anions, where inter-valence charge transfer (IVCT) causes the intense color of the relevant anions (heteropoly blues[17]). Even Icosahedral (I_h) symmetrical POM anions, for example, the $\{Mo\}_{132}$ cluster (see Figure 3.3) are obtained in simple one–pot synthesis using controlled amount of a reducing agent to an aqueous solution of sodium molybdate at suitable pH.[20] The surface of these macro–anions bearing oxygen atoms, are of particular interest. Functionalization of the POM surfaces by an organic moiety, e.g. imido functionalization, generates an important

class of hybrid materials with charge transfer interactions between the organic moiety and the POM.[21] Interestingly, some features of the POM anions resemble that of the fullerenes e.g. (i) their electron accepting nature[22] (the metal centers are in their higher oxidation states and thus can be partially reduced by a secondary substance), (ii) highly symmetrical shape etc. Therefore, they can be introduced in supramolecular chemistry as the low–cost alternative to the fullerenes despite the fact that, the POM anions have profound chances to form dative linkages to the external metal centers (thus act as ligands) via the terminal oxygen atoms.[23] Crystallization of the POM anions with supramolecular complexes of the macrocyclic systems[24–25] or other counter cations[26] have
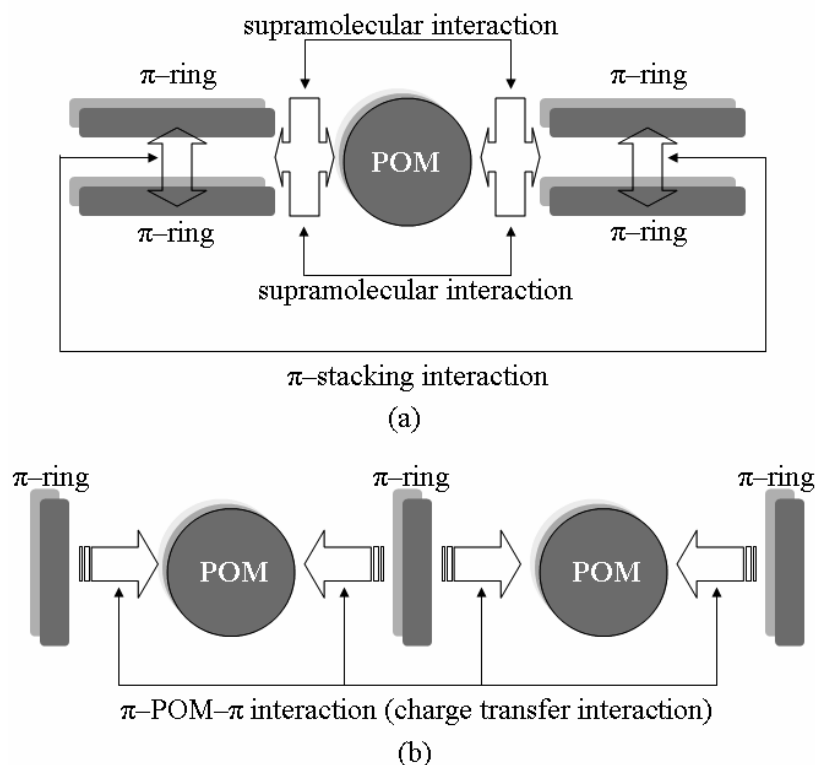
Scheme 3.1 Two possible ways of interactions between flat aromatics and POMs.

been documented in literature that illustrate usage of the POM anions as building blocks in the area of crystal engineering. However, cocrystallization of the POM anions with π–donor flat aromatic coformers is of great crystallographic challenge due to size incompatibility between the respective components. Aromatics containing flat π surfaces (e.g. anthracene, pyrene, etc., see Figure 3.3) can interact with the surface of the POM anions *via* two possible ways as depicted in Scheme 3.1. The planar aromatics mostly

pack with each other through π–staking interactions in their crystals. These π–staked aromatics could further associate with the POM macroanions through C–H⋯O hydrogen bonding interactions as shown in Scheme 3.1a. Thus, in this way of interaction, there are no direct contacts between the π cloud of the aromatics and the POM anions. The other interaction mode, as shown in Scheme 3.1b, demonstrates direct contact between the π surface of the flat aromatics and the electron accepting POM surfaces thereby including possibility of charge transfer interaction between the components that result in partial oxidation and partial reduction of the aromatics and the POM anions respectively.
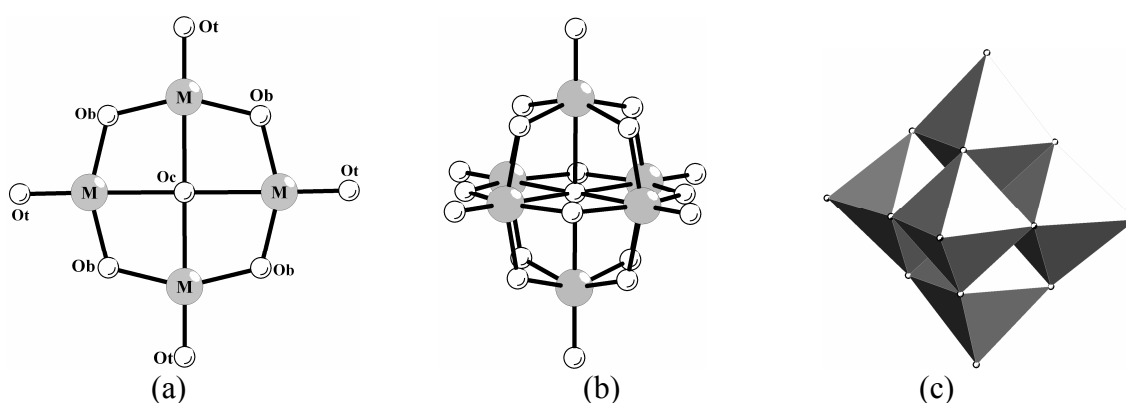
Figure 2.4 (a) Segment of a $[M_6O_{19}]^{2-}$ anion, (b) ball and stick, and (c) polyhedral presentation of $[M_6O_{19}]^{2-}$ anion.

The hexametalate POM cluster anions, also known as Lindqvist type isopolyanions (see Figure 3.4), are simple, symmetrical, almost spherical shaped and one of the most frequent visitor (among the POM anions) to the Cambridge Structural Database (CSD). The concerned polyanions are constructed from six distorted octahedral {MO_6} units through edge sharing and consist three different types of oxygen atoms *viz.* terminal (O_t), bridging (O_b) and central (O_c). These di–anions are octahedral symmetrical (O_h) comprising of an inversion centre (*i*) at the central oxygen atom and these anions can meet hydrogen bond donors through the terminal and bridging oxygen atoms. The spherical shape of these anions clearly manifests size mismatch between them and the flat aromatics. Kochi and coworkers first reported the π⋯POM interactions in a series of cocrystals made up of anthracene or pyrene based coformers.[27] The relevant publication comments that, coulombic interactions between the POM anions and the alkylammonium or pyridinium groups attached to the polyaromatic hydrocarbons (anthracene and pyrene)

via flexible polymethylene chains help the planar surfaces of the aromatics to came closer to the POM surfaces thus involving in the π···POM interactions (see Scheme 3.1 and Figure 3.5). This has led to charge transfer from the π–donors to the POM anions.[27]
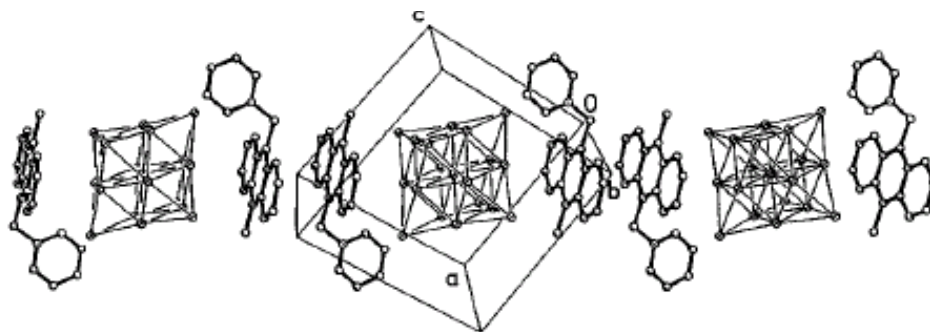
Figure 3.5 Picture displaying the π–POM interactions between the anthracene donors and the hexametalate anions reported by Kochi and coworkers.

In continuation of this work, a series of hexamolybdate and hexatungstate based ion–pair salts containing anthracene–imidazolium or anthracene–benzimidazolium based counter cations have been synthesized and reported in this chapter. The van der Walls thickness of anthracene is ~3.4 Å and the dimensions of anthracene and hexametalates are ~7.4 x 11.6 Å and ~7.5 x 11.1 Å respectively.[27] Spherical and flat shape of the hexametalates and anthracene respectively along with their dimensions clearly indicate size mismatching / structural incompatibility between them. However, Kochi group in their publication[27] commented about stabilization of such cocrystals through coulombic / electrostatic forces. Some of the charge transfer cocrystals reported in the relevant publication incorporate alkylammonium / pyridinium cationic counterparts attached to 9–methylanthracene through a methylene spacer. We wish to analyze the structural and physical properties of the cocrystals constructed from anthracene based counter cations bearing a heavy atom (instead of the methyl group) at the 9th position of anthracene. 9–bromo–10–brmomethyl anthracene is a useful starting precursor in synthesizing many photochemically active compounds and is easily accessible through bromination of 9–anthracene methanol.[28] Surprisingly, crystallographic analyses on the present synthesized solids (**10a–11f**, **12a–13e**) have not revealed any π···POM interaction between anthracene and the POM cluster anions. Coulombic association between the POM surfaces and the imidazolium or benzimidazolium cationic counterparts have been observed whereas, the

anthracene moieties have involved in C–H⋯O, C–H⋯π or π⋯π interactions to optimize the lattice energy. Single crystal as well as powder X–ray diffraction analyses show that both the molybdate and tungstate salts of the same counter cation are isostructural. Varying the alkyl chain length of the imidazolium cation or changing the substituents in benzimidazolium moieties causes slight modification in hydrogen bonding situation, whereas in the all the crystals, the nature of the π⋯π stacking interaction remains invariant. The remaining part of this chapter deals with the detailed structural analysis and solid state absorption spectroscopy of the cocrystals that are electro–neutral in nature.
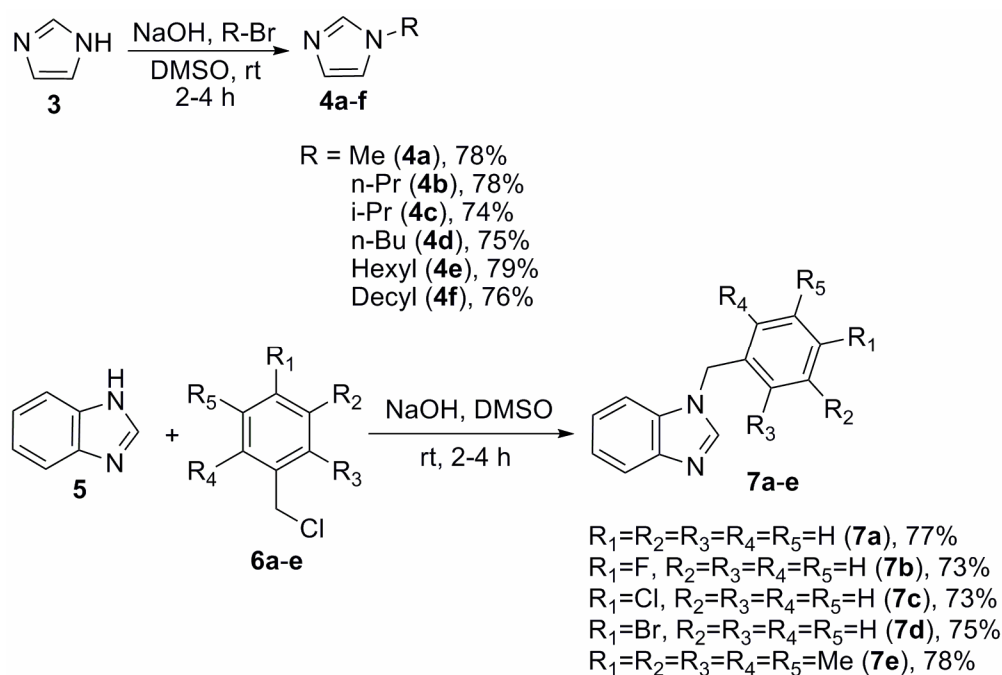
Scheme 3.2 Synthesis of the N–alkyl–imidazoles and N–benzyl–benzimidazoles.

3.2. Results and Discussion

3.2.1. Synthesis and Characterization

9–Anthracene methanol (**1**) has been used as the starting precursor to obtain the anthracene based cations. Treatment of one equivalent triphenyl phosphine with two equivalents of molecular bromine generates the Lewis acid–base adduct $PPh_3 \cdot Br_2$ that brominates the alcohol function of **1** whereas, the remaining free molecular bromine brominates the anthracene ring at the 9th position resulting in the formation of the desired brominated precursor 9–bromo–10–bromomethyl–anthracene (**2**). N–alkyl–imidazoles

(**4a**–**f**) and N–benzyl–benzimidazoles (**7a**–**e**) have been synthesized from imidazole (**3**) and benzimidazole (**5**) respectively, by means of base mediated electrophillic substitution at nitrogen (see Scheme 3.2). All the reactions have been carried out in air in DMSO using NaOH as the base. Choice over the solvent and base is arbitrary in the present study as any other solvents like THF, MeCN, toluene etc. or base like triethylamine, diisopropylamine, sodium hydride etc. can also be conveniently used for these reactions.
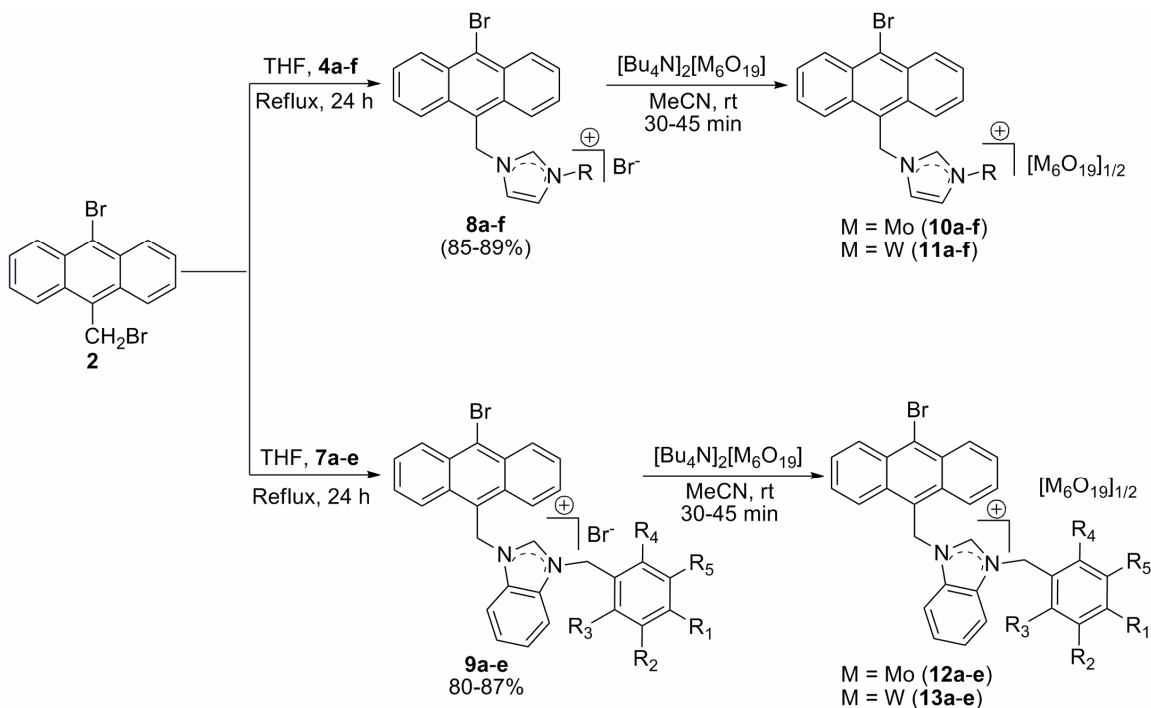
Scheme 3.3. Synthesis of the POM–anthracene ion–pair compounds.

Sometimes, usage of a phase transfer catalyst for example, 18–crown–6, tetrabutylammonium bromide, benzenetriethylammonium chloride etc. helps in smoother progress of such reactions. However, in the present case, no phase transfer catalyst has been used as the monitoring of the reactions by TLC indicates clear progress of the same without any catalyst. Similarly, reaction conditions such as, dry solvent or heat etc. have not explored any considerable improvement of the product yields thereby the reactions having been carried out in air at ambient conditions. Addition of 1.5 equiv. of base in a DMSO solution of **3** or **5**, followed by slow addition of the corresponding electrophiles (alkyl bromides or benzyl chlorides) at 20–25 ºC results in formation of the products (**4a**–**f** and/or **7a**–**3**). They have been isolated in good yields after regular workups followed by

purification through column chromatography (silica gel, 100–200 mesh, MeOH : EtOAc = 5:95 v/v, see experimental). Purification of the N–alkyl imidazoles by distillation method has been avoided because of their high boiling points and chances of product loss due to decomposition at elevated temperature. All the isolated compounds have been characterized by NMR (^{1}H and ^{13}C) spectroscopy, LC–MS and successful elemental analysis.

Reactions between 9–bromo–10–(bromomethyl)anthracene (**2**) and the corresponding N–alkyl imidazoles (**4a–f**) / N–benzyl benzimidazoles (**7a–e**) in THF under refluxing condition have resulted in precipitation of the corresponding bromide salts **8a–f** and **9a–e** respectively (see Scheme 3.3), that have been isolated by filtration. Stoichiometric ion–exchange between these salts with [Bu$_4$N]$_2$[M$_6$O$_{19}$] (2:1) (M = Mo, W) in acetonitrile renders immediate precipitation of the hexamolybdate or hexatungstate salts of the anthracene cations. Molybdate salts (**10a–f**, **12a–e**) are orange in color while tungstates (**11a–f**, **13a–e**) are yellow. Single crystals suitable for X–ray analysis have been grown by diffusion of diethyl ether into DMSO solutions of the POM salts.

3.2.2. Crystallography

It has already been mentioned in the Section 3.1. that, the hexametalate POM cluster anions have isometric (almost spherical) shape and the polyaromatic hydrocarbon anthracene is of highly anisometric (flat) shaped with π–electron clouds above and below the plane of the molecule. Therefore, to cocrystallize these structurally incompatible / mismatched molecular components (hexametalates and anthracene), sufficient energy should be provided to overcome the destabilization that arises due to presence of them in the same cryatal lattice. In this regard, coulombic forces have been shown to play the major role toward stabilization of the cocrystals thus built from the structurally mismatched components.[27] Basically one cationic fragment should be attached with the anthracene ring to associate the cation with the POM surface through electrostatic / coulombic forces and the anthracene ring, if possible, would orient itself to the POM surface. Thus, in the present case, N–alkyl imidazolium or N–benzyl benzimidazolium moieties have been used as the cationic anchors to the anthracene–based cations. The cationic counterparts in all the cases are attached to the anthracene ring *via* a methylene

spacer (–CH$_2$–). Although the solids (**10a**–**13e**), obtained by the ionic metathesis between the POM cluster anions (tetrabutylammonium salt) and anthracene–based cations (bromide), can best be considered as salts or ion–pair solids, we would like to use the phrase 'coulombic cocrystals' to describe them. There is no apparent reason for using such term except the major contribution from the coulombic forces towards stabilization

(10a)

(10d)

(11a)

(11b)

(11c)

(11d)
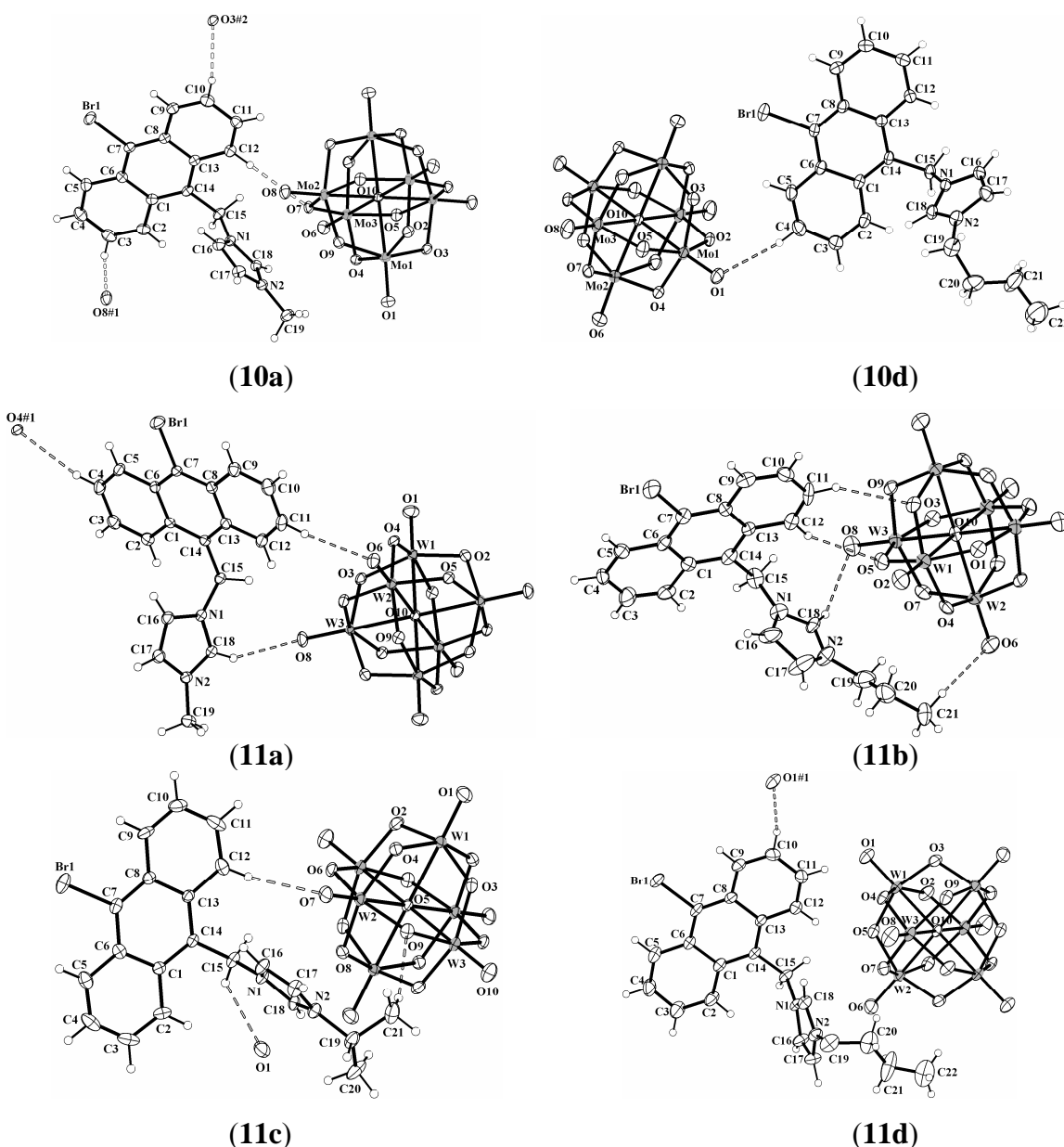
Figure 3.6 Thermal ellipsoidal plot of various coulombic cocrystals (as indicated by the numbers in the parentheses) in 20% probability. Only one cationic unit has been shown for clarity with various hydrogen bonding interactions between the different molecular components. Solvent molecules located in some of the structures have been excluded.

of the isometric : anisometric cocrystals (**10a**–**13e**). X-ray diffraction quality crystals have been grown using ether as the anti-solvent (precipitant) to the DMSO solution of the appropriate solids.
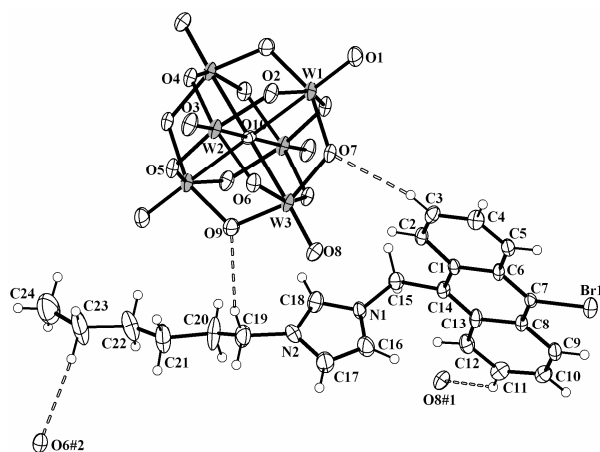
(**11e**)
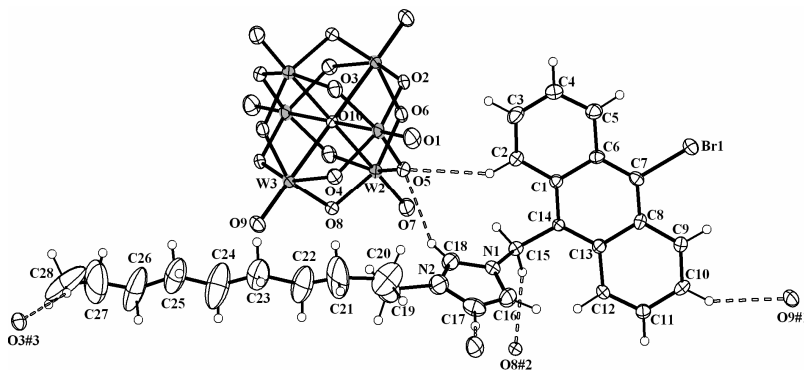
(**11f**)

Figure 3.7 Crystal structures of the compounds **11e**–**f** in 20% thermal probability distributions. Only one cationic unit has been displayed for clarity.

Structures of the crystallographically characterized solids have been presented in Figures 3.6–3.8 and various structure refinement parameters have been summarized in Tables 3.1–3.5. Mainly the tungstate salts have been structurally characterized. For the comparison purpose, two molybdates (**10a** and **10d**) have been crystallographically characterized. Molybdate and tungstate salts of the same counteraction are found to be isostructural. For example, unit cell parameters of the compounds **10a** and **11a** (or **10d** and **11d**) are almost identical (see Table 3.1–3.3) and the molecules in the concerned

solids pack under same space symmetry. Thus, changing the metal centers of the Lindqvist type isopolyanions from molybdenum to tungsten has not induced any significant alteration of the molecular ensemble. This is clearly in accord with the expectation as both the $[Mo_6O_{19}]^{2-}$ and $[W_6O_{19}]^{2-}$ cluster anions have many similar features e.g. almost spherical shape, octahedral symmetrical (O_h) etc. The matter is further evident from the powder x–ray diffraction data that reveal (almost) identical diffraction patters for the molybdates (**10a–f**, **12a–e**) and the corresponding tungstates (**11a–f**, **13a–e**).

Crystal structures of all the solids are characterized by the presence of two cations associated with one POM cluster anion. Some of the crystals have been isolated as DMSO solvates. Structural analysis of the relevant solids reveals some common features, which are summarized below.

(a)   Asymmetric units of all the crystal structures consist of one anthracene–based mono–cation and half of the POM cluster di–anion for electro neutrality. All the molecules are centrosymmetric with respect to the centre of inversion at the central oxygen atom of the POM cluster anions. The full molecules are generated upon operation of the inversion symmetry on the concerned asymmetric units. Therefore, all the solids have maintained 2:1 stoichiometry between the cations and the anions and the respective solids are considered as stoichiometric solids.

(b)   The imidazolium / benzimidazolium cationic counterparts in all the structures have been observed to face toward one of the octrahedral facets of the POM cluster anions due to coulombic association between them.

(c)   The anthracene rings are away of the POM surfaces and pack with each other through π···π stacking interactions. No π···POM interactions are observed in the relevant crystals where the π–stacked anthracenes interact with the POM cluster anions only by C–H···O weak hydrogen bonding interactions. Thus, the solids described in this chapter cannot be considered as donor–acceptor π···POM solids even though they are intensely colored contrast to their starting precursors.

Two different space symmetry *viz. P–1* (triclinic) and *P2_1/c* (monoclinic) have been observed for the crystal packing of the compounds containing anthracene–imidazolium counter cations (**10a–11f**). The crystals containing methyl, i–propyl, hexyl and decyl

Table 3.1 Crystal data and structure refinement parameters for **10a** and **10d**.

	10a	10d
empirical formula	$C_{42}H_{44}Br_2Mo_6N_4O_{21}S_2$	$C_{48}H_{56}Br_2Mo_6N_4O_{21}S_2$
formula weight	1740.39	1824.55
T (K), λ (Å)	298 (2), 0.71073	298 (2), 0.71073
crystal system	triclinic	monoclinic
space group	$P–1$	$P2_1/c$
a (Å)	10.705(5)	11.0467(7)
b (Å)	11.509(5)	12.3811(8)
c (Å)	12.013(6)	22.1829(14)
α (°)	116.856(6)	90.00
β (°)	93.369(7)	99.2150(10)
γ (°)	90.529(7)	90.00
V (Å^3)	1317.1(10)	2994.8(3)
Z, d_{calcd} (g cm^{-3})	1, 2.194	2, 2.023
μ (mm^{-1}), $F(000)$	3.062, 846	2.699, 1788
GooF on F^2	1.059	1.032
R_1/w$R_2[I>2\sigma(I)]$	0.0312/0.0801	0.0458/0.1069
R_1/wR_2 (all data)	0.0384/0.0836	0.0805/ 0.1214
largest diff. peak/hole(e.Å^{-3})	0.657/–0.553	0.772/ –0.434

Table 3.2. Crystal data and structure refinement parameters for **11a–c**.

	11a	11b	11c
empirical formula	$C_{42}H_{44}Br_2N_4$ $O_{21}S_2W_6$	$C_{46}H_{52}Br_2N_4$ $O_{21}S_2W_6$	$C_{46}H_{52}Br_2N_4$ $O_{21}S_2W_6$
formula weight	2267.85	2323.94	2323.96
T (K), λ (Å)	298 (2), 0.71073	298 (2), 0.71073	298 (2), 0.71073
crystal system, space gr.	triclinic, $P–1$	monoclinic, $P2_1/c$	triclinic, $P–1$
a (Å)	10.799(3)	10.371(4)	10.1433(12)
b (Å)	11.533(3)	12.851(5)	11.7753(14)
c (Å)	12.016(3)	21.899(8)	13.1042(16)
α (°)	117.088(4)	90.00	67.945(2)
β (°)	93.323(4)	93.172(7)	87.633(2)
γ (°)	90.887(4)	90.00	86.138(2)
V (Å^3)	1328.6(6)	2914.2(19)	1447.1(3)
Z, d_{calcd} (g cm^{-3})	1, 2.819	2, 2.642	2, 2.585
μ (mm^{-1}), $F(000)$	14.597, 1026	13.313, 2128	13.405, 1070
GooF on F^2	1.060	1.373	1.204
R_1/w$R_2[I>2\sigma(I)]$	0.0203/ 0.0509	0.0932/0.1750	0.0399/0.0847
R_1/wR_2 (all data)	0.0232/ 0.0520	0.1032/0.1792	0.0442/0.0865
largest diff. peak/hole (e.Å^{-3})	0.685/ –0.884	1.852/–1.362	1.241/–1.134

Table 3.3 Crystal data and structure refinement parameters for **11d–f**.

	11d	11e	11f
empirical formula	$C_{48}H_{48}Br_2N_4$ $O_{21}S_2W_6$	$C_{48}H_{52}Br_2$ $N_4O_{19}W_6$	$C_{56}H_{68}Br_2$ $N_4O_{19}W_6$
formula weight	2343.94	2251.86	2364.06
T (K), λ (Å)	298 (2), 0.71073	298 (2), 0.71073	298 (2), 0.71073
crystal system, space gr.	monoclinic, $P2_1/c$	triclinic, $P–1$	triclinic, $P–1$
a (Å)	11.120(3)	9.9087(11)	11.2164(16)
b (Å)	12.375(3)	11.7099(13)	11.9454(17)
c (Å)	22.166(5)	12.4878(13)	12.8091(18)
α (°)	90.00	107.775(2)	76.337(2)
β (°)	99.222(4)	90.262(2)	85.806(2)
γ (°)	90.00	94.106(2)	70.853(2)
V (Å^3)	3010.9(12)	1375.7(3)	1575.4(4)
Z, d_{calcd} (g cm^{-3})	2, 2.585	1, 2.718	1, 2.492
μ (mm^{-1}), F(000)	12.887, 2156	14.020, 1034	12.250, 1098
GooF on F^2	1.022	0.990	1.317
R_1/wR_2[$I>2\sigma(I)$]	0.0316/0.0737	0.0431/0.0822	0.0554/ 0.0909
R_1/wR_2 (all data)	0.0429/0.0787	0.0694/0.0909	0.0633/ 0.0933
largest diff. peak/hole (e.Å^3)	1.470/–1.161	–0.771/0.176	1.073/–1.405

Table 3.4 Crystal data and structure refinement parameters for **13a–c**.

	13a	13b	13c
empirical formula	$C_{58}H_{44}Br_2$ $N_4O_{19}W_6$	$C_{66}H_{66}Br_2F_2$ $N_4O_{23}S_4W_6$	$C_{58}H_{42}Br_2Cl_2$ $N_4O_{19}W_6$
formula weight	2363.89	2712.39	2432.78
T (K), λ (Å)	298 (2), 0.71073	298 (2), 0.71073	298 (2), 0.71073
crystal system, space gr.	triclinic, $P–1$	triclinic, $P–1$	monoclinic, $P2_1/c$
a (Å)	9.4925(12)	11.628(3)	11.8559(12)
b (Å)	10.1101(12)	11.924(3)	12.5348(13)
c (Å)	15.7024(19)	15.585(4)	25.243(3)
α (°)	92.964(2)	92.288(4)	
β (°)	100.955(2)	110.777(3)	97.995(2)
γ (°)	97.339(2)	109.182(3)	
V (Å^3)	1462.9(3)	1878.1(7)	3714.9(7)
Z, d_{calcd} (g cm^{-3})	1, 2.683	1, 2.398	2, 2.175
μ (mm^{-1}), F(000)	13.192, 1086	10.407, 1270	10.463, 2236
GooF on F^2	1.219	1.115	0.987
R_1/wR_2[$I>2\sigma(I)$]	0.0355/0.0772	0.0593/0.1547	0.0403/0.0790
R_1/wR_2 (all data)	0.0377/0.0782	0.0634/0.1575	0.0597/0.0841
largest diff. peak/hole (e.Å^3)	0.670/–1.705	2.439/–3.877	1.196/–0.799

(13a)

(13b)

(13c)

(13d)

(13e)
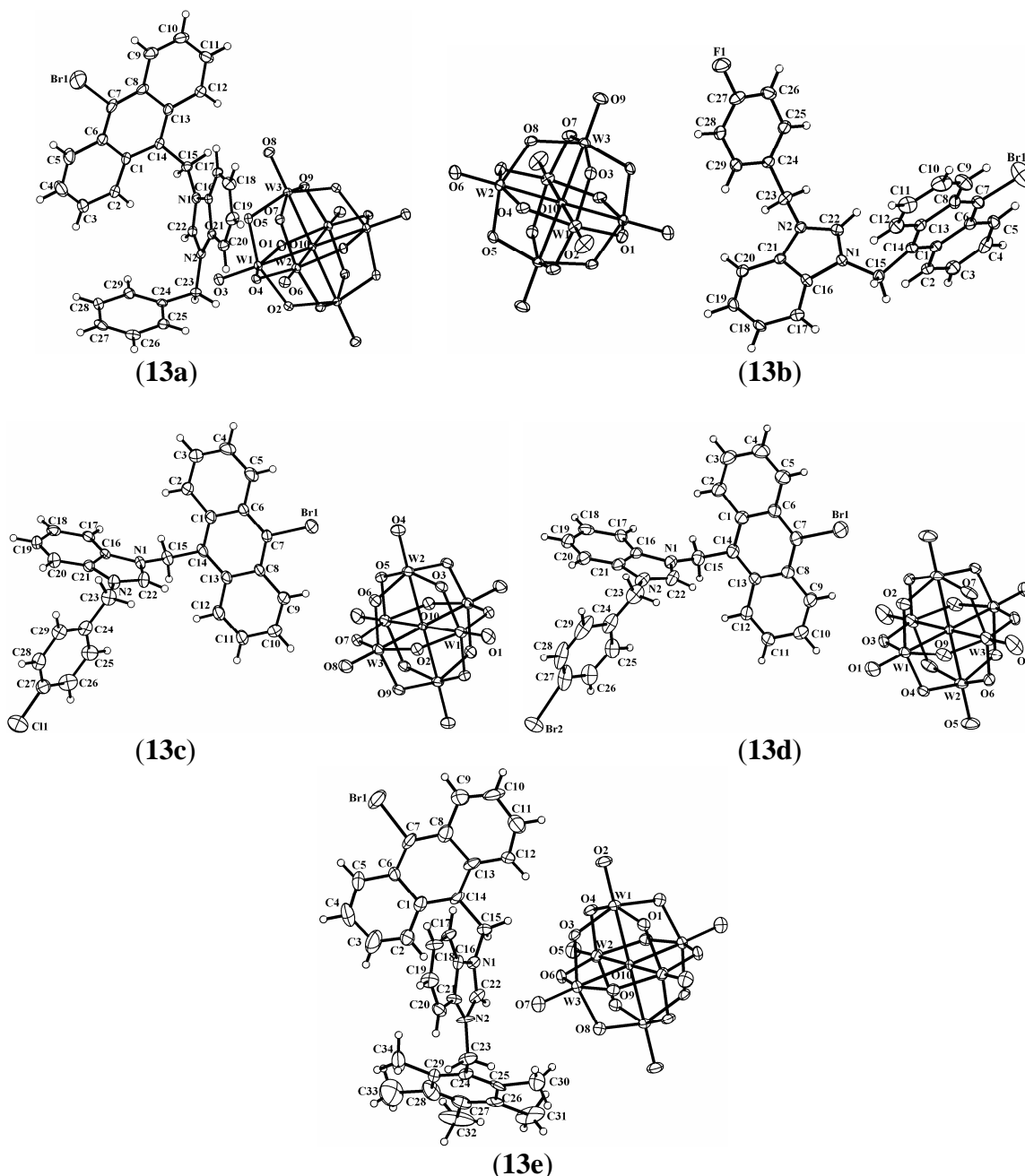
Figure 3.8 ORTEP (20%) diagram of the compounds **13a–e**. Only one cation has been shown for clarity. Br(2) in the crystal structure of compound **13d** is disordered over two positions. However, in the relevant structural representation only one part has been shown.

alkyl chains in the imidazolium cationic counterparts feature packing of the molecules obeying the lower space symmetry (*P–1*). But, in case of the *n*–propyl and butyl alkyl chains, the molecules tend to crystallize under higher special symmetry (*P2₁/c*). This symmetry alteration might be due to variation of the hydrogen boding environments in

the relevant solids. In all the cases, molecules have crystallized with one cation and half of the POM cluster anion in the asymmetric unit ($Z' = \frac{1}{2}$) where the two cations are related to each other by the inversion symmetry with respect to the central oxygen atom of the cluster anion. Although the structural analysis of the solids **11a–f** exhibit many similarities in packing of the molecules, a little change in the intermolecular interactions

Table 3.5 Crystal data and structure refinement parameters for **13d** and **13e**.

	13d	13e
empirical formula	$C_{58}H_{42}Br_4N_4O_{19}W_6$	C68H64Br2N4O19W6
formula weight	2521.70	2504.15
crystal system, space gr.	monoclinic, $P2_1/c$	triclinic, $P–1$
T (K), λ (Å)	298 (2), 0.71073	298 (2), 0.71073
a (Å)	12.1119(15)	11.357(8)
b (Å)	12.3712(15)	12.033(8)
c (Å)	25.455(3)	16.571(11)
α (°)		81.165(11)
β (°)	97.635(2)	84.535(11)
γ (°)		75.025(11)
V (Å^3)	3780.3(8)	2158(3)
Z, d_{calcd} (g cm^{-3})	2, 2.215	1, 1.927
μ (mm^{-1}), $F(000)$	11.268, 2308	8.949, 1166
GooF on F^2	1.067	0.883
R_1/w$R_2[I>2\sigma(I)]$	0.0364/0.0775	0.0597/0.1333
R_1/wR_2 (all data)	0.0497/0.0813	0.1085/0.1483
largest diff. peak/hole(e.Å^{-3})	1.759/–1.673	2.275/–1.441

has been observed with the variation of the alkyl chain lengths in the cations. The imidazolium ring has a rotational freedom around the C(15)–N(1) bond and this rotation determines the dihedral angle between the anthracene and imidazolium planes. Variation of the alkyl chain lengths in the imidazolium cations causes a change in this torsion angle in an irregular manner as summarized in Table 3.6. There is a partial overlapping between the anthracene rings in the relevant crystals as shown in Figure 3.9. Distances for these π···π stacking interactions have been summarized in Table 3.6. Figure 3.9 shows the basic crystal packing natures in the compounds **11a–f**. The complete crystals are built up of the operation of the proper symmetry upon these supramolecular and electrostatic interactions. In the crystal structures of the compounds **10a**, **11c** and **11e**, the

imidazolium and anthracene planes are oriented in such an angular span that interactions between two inversion symmetry related cations result in the formation of a π–stacked dimer. The other crystals exclude such dimer formation due to improper spacial orientation of the imidazole and the anthracene rings, although there is C–H⋯π stacking

Table 3.6 Geometrical parameters for packing of the ANT–IM compounds.

	Sp. Gr.	M[a]	R	<(ANT–IM)[b]	C–H⋯π interaction		d(ANT⋯ANT)[e]
					IM⋯ANT[c]	R⋯ANT[d]	
10a	*P–1*	Mo	methyl	77.15	yes (C17)	no	3.732
10d	*P2₁/c*	Mo	butyl	68.71	no	yes (C20)	3.717
11a	*P–1*	W	methyl	77.03	yes (C17)	no	3.735
11b	*P2₁/c*	W	propyl	88.66	no	yes (C20)	3.876
11c	*P–1*	W	*i*–propyl	89.02	yes (C17)	no	3.751
11d	*P2₁/c*	W	butyl	68.65	no	yes (C20)	3.714
11e	*P–1*	W	hexyl	86.39	yes (C17)	yes (C24)	3.914
11f	*P–1*	W	decyl	71.36	no	yes (C23)	3.828

[a] Metal centre of the POM cluster anion; [b]Angle between anthracene and imidazole rings (°); [c,d]C⋯H–π interactions between imidazole ring or alkyl chain and anthracene, $d(C⋯Cg) \leq 4.00Å$, $< (C–H⋯Cg) \geq 140°$; [e]Distance between centroids of two π⋯π stacked anthracenes (Å) with ±10 esd tollerability.

interactions between the alkyl chain of one cation with the anthracene ring of the other inversion related cation (see Figure 3.9). No direct interaction between the π–cloud of the anthracene ring and the POM surface is noticed in these solids. Thus, the lattice energy of such coulombic cocrystals incorporating both flat and spherical shaped molecular components are minimized by the abundance of coulombic association between the imidazolium cations and POM anions, C–H⋯O weak hydrogen bonding interactions with the POM acceptors, C–H⋯π and π⋯π stacking interactions between the various crystal components. In all the solids, the anthracene cations have packed with each other through π⋯π stacking interactions in a *trans*–fashion as far as orientations of the N–alkyl imidazolium moieties and bromine atoms are concerned. A little change in the distance between centroids of two such stacked anthracene rings has been observed with the variation of the alkyl chain as mentioned in Table 3.6. These π–stacked anthracene rings

have further interacted with the POM anions through C–H⋯O supramolecular interactions in an alike fashion as mentioned in Scheme 3.1a. Matrices for such supramolecular interactions have been summarized in Table 3.7.

Table 3.7 Geometrical parameters for several hydrogen bonding interactions in the crystal structures of the anthracene–imidazolium compounds.

D–H⋯A	d(D–H)	d(H⋯A)	d(D⋯A)	<(DHA)
	Compound–**10a**			
C(3)–H(3)⋯O(8#1)	0.93	2.47	3.366(6)	162
C(10)–H(10)⋯O(3#2)	0.93	2.56	3.482(6)	169
C(12)–H(12)⋯O(7)	0.93	2.67	3.580(5)	168
[#1 1+x,y,z; #2 x,y,1+z]				
	Compound–**10d**			
C(4)–H(4)⋯O(1)	0.93	2.47	3.353(10)	159
	Compound–**11a**			
C(4)–H(4)⋯O(4#1)	0.93	2.61	3.532(10)	170
C(11)–H(11)⋯O(6)	0.93	2.48	3.371(7)	161
C(18)–H(18)⋯O(8)	0.93	2.43	3.200(6)	140
[#1 1–x, 1–y, –z]				
	Compound–**11b**			
C(11)–H(11)⋯O(3)	0.93	2.63	3.49(3)	155
C(12)–H(12)⋯O(5)	0.93	2.62	3.42(4)	145
C(18)–H(18)⋯O(8)	0.93	2.59	3.35(3)	140
C(21)–H(21C)⋯O(6)	0.96	2.54	3.50(4)	173
	Compound–**11c**			
C(12)–H(12)⋯O(7)	0.93	2.58	3.370(12)	143
C(15)–H(15A)⋯O(1#1)	0.97	2.68	3.476(12)	140
C(21)–H(21A)⋯O(9)	0.96	2.49	3.373(13)	153
[#1 –1+x, y, z]				
	Compound–**11d**			
C(10)–H(10)⋯O(1#1)	0.93	2.46	3.352(11)	160
[#1 2–x, 1–y, 1–z]				
	Compound–**11e**			
C(3)–H(3)⋯O(7)	0.93	2.65	3.445(12)	144
C(11)–H(11)⋯O(8#1)	0.93	2.54	3.307(14)	140
C(23)–H(23A)⋯O(6#2)	0.97	2.70	3.65(2)	168
[#1 –1+x, y, z; #2 1–x, 2–y, 1–z]				
	Compound–**11f**			
C(10)–H(10)⋯O(9#1)	0.93	2.48	3.319(15)	151
C(15)–H(15B)⋯O(8#2)	0.97	2.68	3.615(13)	161
C(28)–H(28C)⋯O(3#3)	0.96	2.69	3.52(3)	144
[#1 1+x, y, 1+z; #2 –x, –y, 1–z; #3 1–x, 1–y, –z]				

(**10a**)

(**11b**)

(**11c**)

(**11d**)

(**11e**)

(**11f**)
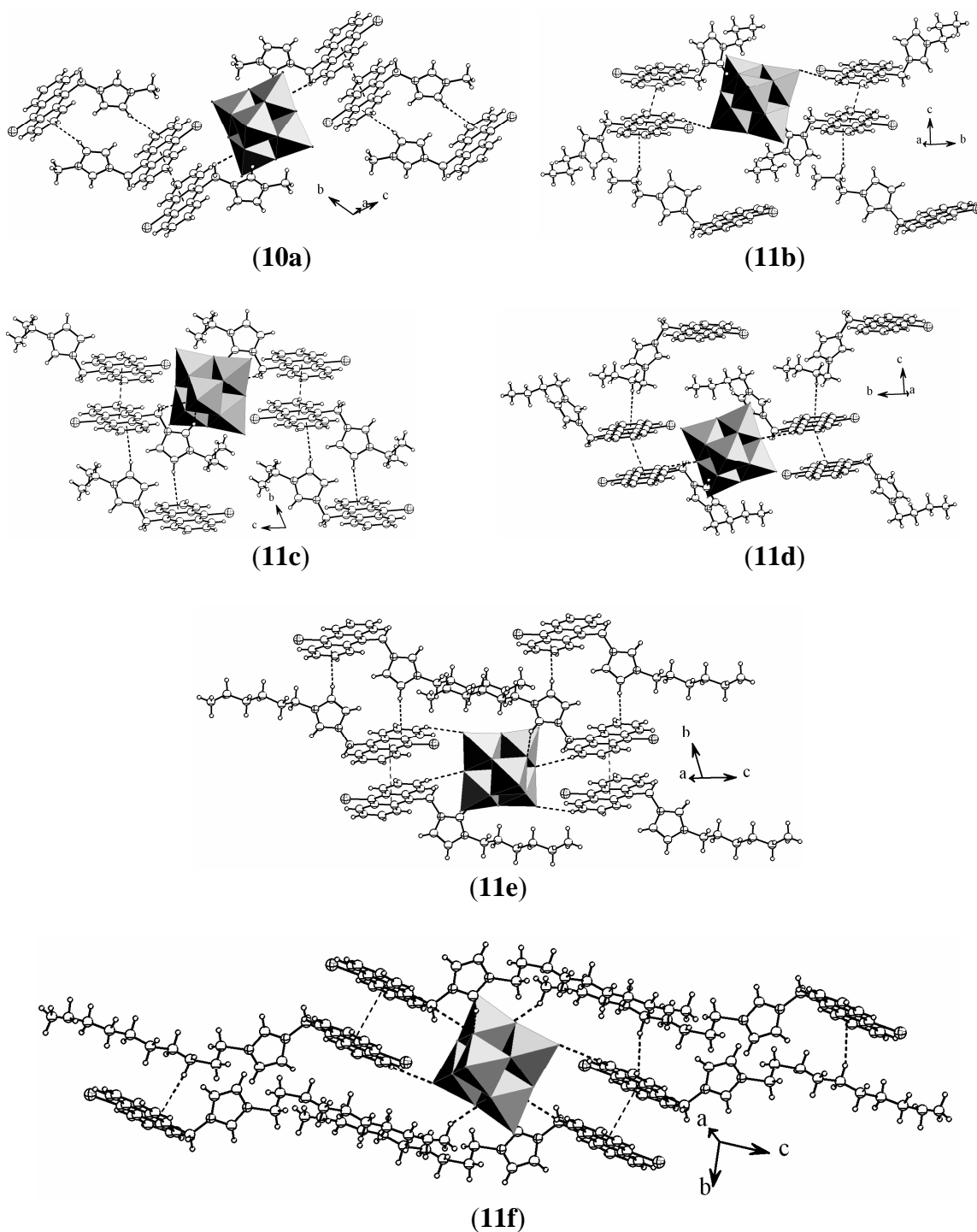
Figure 3.9 Pictures displaying basic intermolecular contacts between the components in the imidazolium cation containing solids.

The crystal structures, discussed so far, contained only one π–ring i.e. the anthracene ring attached to the imidazolium moiety. The situation is bit different in the case of N–benzyl benzimidazolium cations which consists of more number of π–rings. The

imidazolium cations consist only of one π–rings i.e. the anthracene ring. But the benzimidazolium cations comprise of three π–rings *viz.* the anthracene ring, benzimidazole ring and the phenyl ring of the benzyl counterpart. Both the anthracene and the benzene ring of the benzyl fragment have C–C rotational freedom around the benzimidazolium plane. Thus, these cations are more puckared compared to the alkylimidazolium cations. The only structural difference between the benzimidazolium cations is the variation of bulkiness in the benzyl group. As previously stated, PXRD analysis of the molydates and the tungstates have revealed isostructurality between the two, only the tungstates (**13a–e**) have been crystallographically characterized. The solid **12a** and **13a** do not contain any substitution on the benzyl ring whereas, in case of the others bulkiness of the benzyl groups has been increased by attaching F (**12b**, **13b**), Cl (**12c**, **13c**), Br (**12d**, **13d**) and five methyl groups (**12e**, **13e**). Depending upon the spacial

Table 3.8 Rotamers of the benzyl benzimidazolium cations and some geometrical parameters for the intermolecular stacking interactions in the relevant crystals.

eclipsed   gauche   staggered
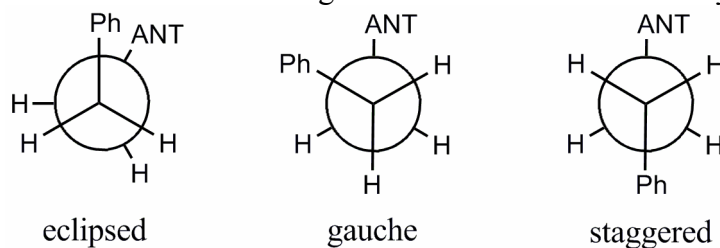
	Sp. Gr.	Geometry[a]	<(BIM–ANT)[b]	<(BIM–Ph)[c]	Torsion[d]
13a	*P–1*	eclipsed	82.48	80.50	19.95
13b	*P–1*	gauche	78.25	61.46	71.85
13c	*P2₁/c*	gauche	78.75	89.14	138.00
13d	*P2₁/c*	gauche	76.23	84.80	142.82
13e	*P–1*	eclipsed	76.55	88.37	106.11

[a] geometry of the benzyl benzimidazolium cations based on the spatial orientation of the phenyl and anthracene rings; [b, c] angle between the benzimidazole and anthracene plane and benzimidazole and phenyl plane respectively (°); C(24)–C(23)–C(15)–C(14) dihedral angles.

spans of the anthracene and the phenyl (benzyl) rings, the cations can be classified into three rotamers i.e. ecclipsed, gauche and staggered. If both of them are projected at the

same side of the benzimidazolium plane, the conformation of the concerned cation is ecclipsed. Similarly, if the relevant C–C rotations make them to flang on opposite direction of the mentioned plane, then the conformation of the cation is staggered. For the gauched conformation, both the rings are on same direction of the benzimidazolium plane but at a certain dihedral angle between 0 and 180º. Crystal structures of the solids **13a–e** have been presented in Figure 3.8 and the concerned crystal data have been summarized
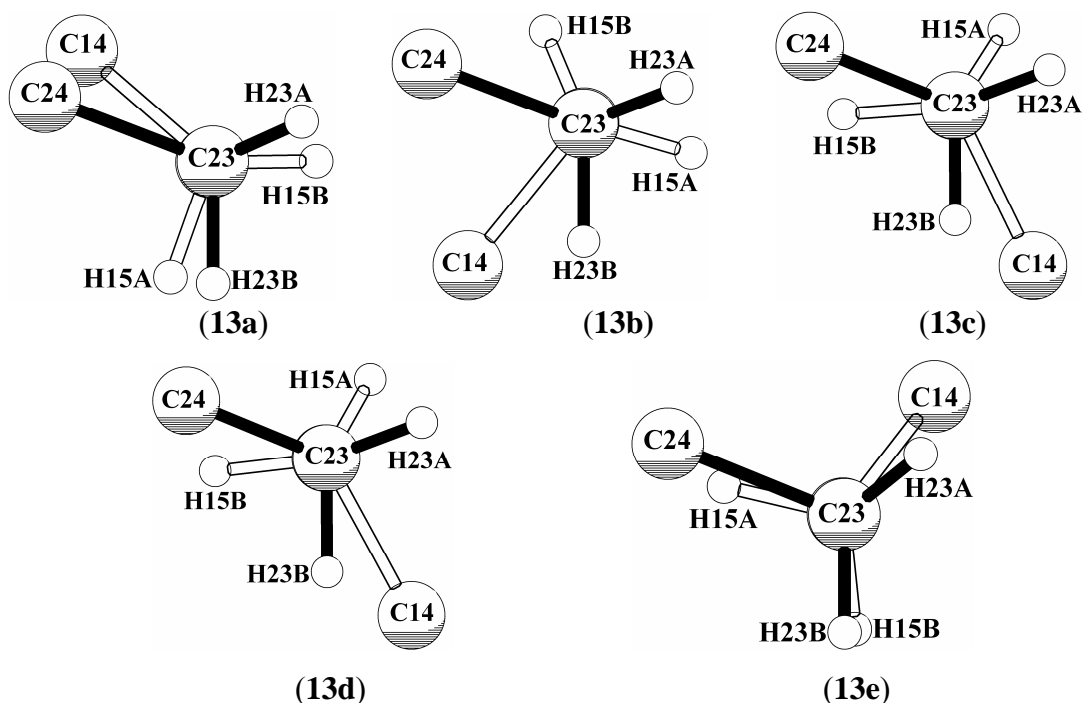
Figure 3.10 Newman projection for different orientations of the anthracene and phenyl rings of the benzimidazolium cations in the crystal structures of the compounds **13a–e** viewed down C(23)–C(15) axis. Solid bonds = atoms in front, hollow bonds = atoms at back.

in Tables 3.4 and 3.5. Structures of all the compounds **13a–e** are characterized by one cation and half of the POM cluster anion in the asymmetric unit (Z' = ½). In the relevant crystals, two different orientations of the anthracene and the phenyl (benzyl) rings have been observed with respect to the benzimidazolium plane. Several observed angular parameters in the concerned crystal structures have been summarized in Table 3.8. Crystallographically observed angular spans of the anthracene and the phenyl ring of the benzyl fragment have been pictorially represented in Figure 3.10 that clearly depicts eclipsed and gauche orientations of the concerned rings in the relevant crystals. However,

alike all the crystals built from N–alkyl imidazolium cations, the present case too demonstrate similar crystal packing features and will not be discussed separately. For example, in all the crystals (**13a–e**), the anthracene rings are stacked with each other *via* π···π stacking interactions, the benzimidazolium cationic counterparts are oriented toward a facet of the POM anions due to coulombic association and the cations are further associated with the POM cluser anions *via* supramolecular C–H···O interactions. Two representative crystal–packing features have been displayed in Figure 3.11. Due to more bulkiness of the benzyl benzimidazolium cations compared to the alkyl imidazolium cations, complete overlap between the π–electron clouds of two anthracene rings have been forbidden and a partial overlapping between the two rings have been observed in the relevant crystals (see Figure 3.11). Thus, changing the cation from alkyl imidazolium to benzyl benzimidazolium has not induced much difference in the packing feature of the molecules in their crystals.

(**13a**)

(**13c**)
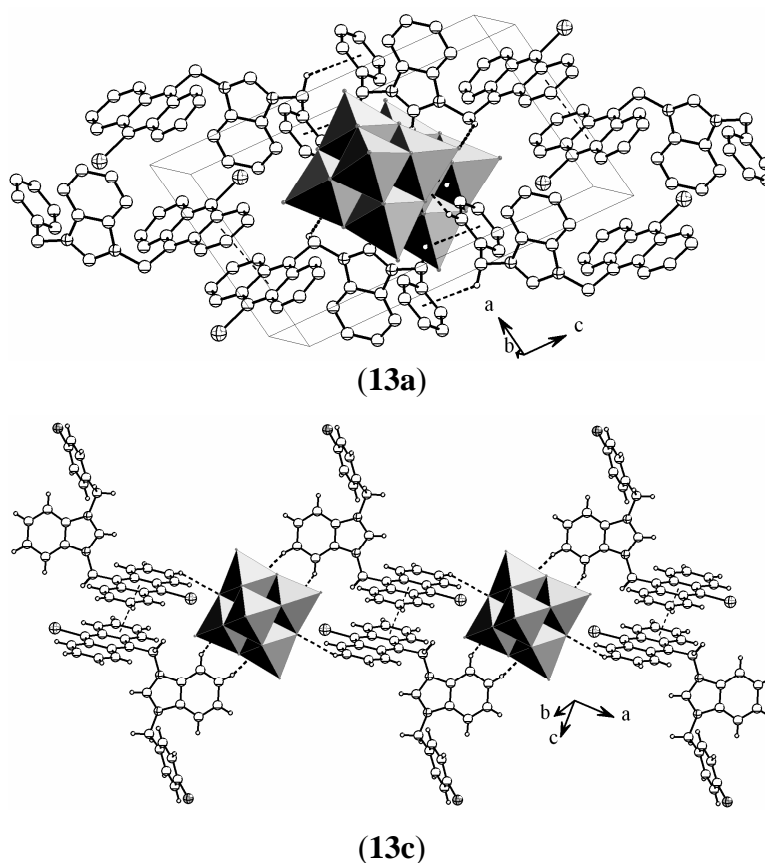
Figure 3.11 Portion of crystal packing in the lattice of the compounds **13a** (*P–1*) and **13a** (*P2$_1$/c*).

3.2.3. Spectroscopy

(a)

(b)
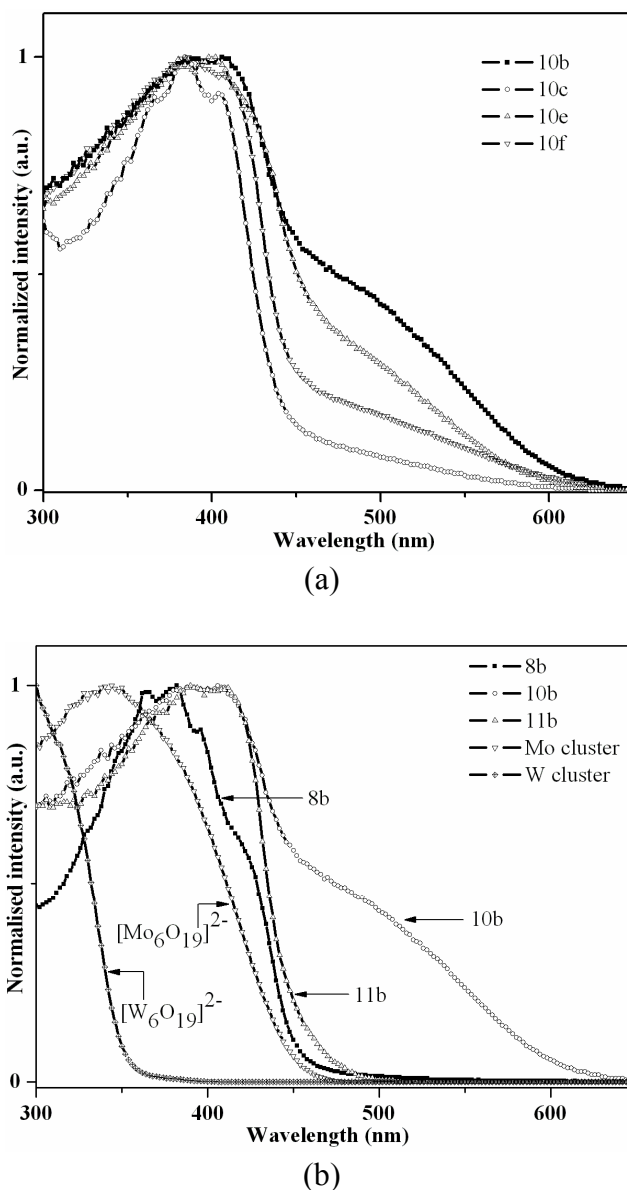
Figure 3.12 Diffuse reflectance spectra (spread over $BaSO_4$) of the (a) various hexamolybdates containing N–alkyl imidazolium counter cations. The same feature has been observed in the benzimidazolium salts and has not shown here. (b) bromide, hexamolybdate and hexatungstate salts of a same counter cation showing difference in spectroscopic behavior with the variation of the anion.

It has already been mentioned that, the hexamolydbate salts are intense orange–red and the tungstate salts are intense yellow in color. Dissolution of the molybdates in DMF or in DMSO (these salts are not soluble in other common organic solvents e.g. MeCN, MeOH etc.) causes disappearance of the orange color and a pale yellow color persists in

the solution. Absorption spectra of the resulting solution are found to be equivalent to that obtained from a 2:1 physical mixture of the anthracene cations and $[Bu_4N]_2[Mo_6O_{19}]$. Even the absorption properties of the solutions remain invariant upon addition of large amount of the ionic counterparts. The corresponding absorption spectra are characterized by discrete and broad absorptions due to the anthracene cations and the hexamolybdate cluster anion in solution. The similar matter is observed for the hexatungstate analogues. Contrast to the solution–state absortion spectra of the concerned solids, the solid–state absorption spectra show remarkable difference. Absorption spectra of the concerned solids have been obtained by the diffused reflectance technique by dispersing the powdery samples in $BaSO_4$. Both the various anthracene cations, $[Bu_4N]_2[Mo_6O_{19}]$ and $[Bu_4N]_2[W_6O_{19}]$ are transparent (solid–state) at wavelengths more than 500 nm. The $[Bu_4N]_2[W_6O_{19}]$ cluster absorb at higher energy ($\lambda_{max} < 300$ nm) that the $[Bu_4N]_2[Mo_6O_{19}]$ cluster ($\lambda_{max} \approx 345$ nm). Both the cluster precursors exhibit structureless absorption patterns. A structured broad absorption band ($\lambda_{max} \approx 380$ nm) features the solid–state absorption spectra of the anthracene cations as shown in Figure 3.12. Also, the 2:1 physical mixtures of the anthracene bromide salts and the POM tetrabutylammonium salts exhibit the similar feature. The concerned ion–exchanged molybdates, described in this chapter, rather feature a modulated absorption spectra i.e. appearance of a new band (or tail) in the visible region of the spectra ($\lambda > 500$ nm). The yellow tungstates exhibit a tail initiating from *ca*. 550 nm. Again, in all the cases, the absorption spectra of the anthracene–POM salts exhibit very distinct features than the same of their ionic parents. For example, the absorption bands due to the hexametalate cluster anions and anthracene remain indistinctive in the absorption spectra of the anthrane–POM solids demonstrated here. Therefore, commencement of the new bands in the visible region is due to some sort of interaction between the molecular components only in the solid sate. In another word, it can be said that, spectroscopic identities of the anthracene and hexametalate counterparts vanish upon their ionic and supramolecular association in the solid state.

3.3. Conclusion

In conclusion, a series of hexametalate cluster based solids comprising of various anthracene-imidazolium and anthracene-benzimidazolium cationic counterparts have

been synthesized and their structures have been determined through crystallography. Both the hexamolybdates and hexatungstates of the same counter cation are isomorphus. All the solids maintain 2:1 stoichiometry between the mono-cations and the di-anions and are centrosymmetric with respect to the central oxygen atom of the octahedral symmetrical POMs. The cationic counterparts (imidazolium and benzimidazolium) in all the solids project toward surface of the POMs due to electrostatic interaction between the oppositely charged species. Apart from coulombic association between the anthracenes and the POM, supramolecular hydrogen bonding interactions are also observed to optimize the lattice destabilization due to coexistence of the structurally mismatched molecular components in the same crystal. Color of the molybdates are observed only in the solid state and probably no adduct formation takes place in the solution state as revealed by the solid state as well as the solution state UV-visible spectroscopy. Variation of the alkyl chain lengths in the imidazolium cationic moiety or alteration of the substituents in the benzimidazolium moiety does not change the intermolecular association of the components to a greater extent. Possibly, due the shorter spacer, the anthracene ring could not interact with the POM surface, which results in charge transfer interaction between the two.

3.4. Experimental section

3.4.1. Materials and Methods

All the materials have been purchased from commercial sources and used as received. The reactions have been performed in air unless mentioned elsewhere. Instrumentation and methods for the spectroscopic and crystallographic characterizations are as described in Chapter 2.

3.4.2. Synthesis

9–bromo–10–(bromomethyl)anthracene (2). Bromine (2 equivalents) was added dropwise to a stirred solution of triphenylphosphine (1 equivalent) in acetonitrile at room temperature and the pale yellow slurry was stirred for 15 mins. Solid 9–anthracene methanol (1 equivalent) was then slowly added and the reactants were allowed to react at room temperature until total consumption of the starting material (TLC) after which, it

was refrigerated overnight. The product, which appeared as yellow precipitate, was isolated by filtration, washed with little cold methanol and then dried under vacuum. It was further re–crystallized twice from chloroform before use. Characterization data completely corroborated with the literature reported data.[28]

General procedure for the synthesis of the N–alkyl imidazoles (4a–f) and N–benzyl benzimidazoles (7a–e). Imidazole (**3**) / benzimidazole (**5**) (10 mmol) was dissolved in 10 ml of DMSO and solid NaOH (15 mmol) was added. The resulting pale yellow suspension was stirred in air at room temperature for 1.5 h, after which, the alkyl bromides or benzyl chlorides (15 mmol) were added and allowed to react until completion (TLC). Water (50 ml) was then added and the products were extracted with ethyl acetate. Combined organic layers were washed several times with water then with brine, dried over Na_2SO_4 and subjected to chromatographic purification over silica (100–200 mesh) using MeOH : EtOAc 5:95 (v/v) as the mobile phase. Compounds **4a–f** were isolated as yellow oils whereas, the compounds **7a–e** were white solid. Spectroscopic data of the N–alkyl imidazoles are in accord with earlier literature and thus haven't shown here.[29]

N–**benzyl–benzimidazole (7a).** White solid; Yield = 77%; ^{1}H NMR (400 MHz, CDCl$_3$, TMS) δ: 7.92 (s, 1H), 7.84 (d, J = 8 Hz, 1H), 7.21–7.37 (m, 6H), 7.15 (d, J = 8 Hz, 2H), 5.29 (s, 2H). ^{13}C NMR (100 MHz, CDCl$_3$, TMS) δ: 143.9, 143.3, 135.5, 133.9, 129.0, 128.3, 127.0, 123.1, 120.4, 110.1, 48.8. LC–MS (positive mode) m/z = 209 (M$^+$+H)$^+$. Anal. Calcd. For. $C_{14}H_{12}N_2$ (208.26): C, 80.74; H, 5.81; N, 13.45. Found: C, 80.72; H, 5.84; N, 13.44.

N–**(4–fluorobenzyl)–benzimidazole (7b).** Off–white solid; Yield = 73%; ^{1}H NMR (400 MHz, CDCl$_3$, TMS) δ: 7.91 (s, 1H), 7.76–7,82 (m, 1H), 6.90–7.33 (m, 7H), 5.26 (s, 2H). ^{13}C NMR (100 MHz, CDCl$_3$, TMS) δ: 163.7, 161.3, 143.9, 143.1, 131.2, 128.9, 123.2, 122.4, 120.4, 116.1, 115.9, 110.0, 48.1. LC–MS (positive mode) m/z = 227 (M$^+$+H)$^+$. Anal. Calcd. For. $C_{14}H_{11}FN_2$ (226.25): C, 74.32; H, 4.90; N, 12.38. Found: C, 74.36; H, 4.87; N, 12.41.

1–(4–chlorobenzyl)–benzimidazole (7c). Off–white solid; Yield = 73%; ^{1}H NMR (400 MHz, CDCl$_3$, TMS) δ: 8.05 (s, 1H), 7.82 (m, 2H), 7.00–7.37 (m, 6H), 5.30 (s, 2H). ^{13}C NMR (100 MHz, CDCl$_3$, TMS) δ: 143.3, 142.9, 134.2, 133.9, 133.5, 129.2, 128.4, 123.4, 122.7, 120.2, 110.1, 48.3. LC–MS (positive mode) m/z = 244 (M$^+$+H)$^+$. Anal. Calcd. For. C$_{14}$H$_{11}$ClN$_2$ (242.70): C, 69.28; H, 4.57; N, 11.54. Found: C, 69.27; H, 4.53; N, 11.57.

N–(4–bromobenzyl)–benzimidazole (7d). Pale–yellow solid; Yield = 75%; ^{1}H NMR (400 MHz, CDCl$_3$, TMS) δ: 7.92 (s, 1H), 7.83 (d, *J* = 8 Hz, 1H), 7.43 (d, *J* = 8 Hz, 2H), 7.23–7.28 (m, 3H), 7.01 (d, *J* = 8 Hz, 2H), 5.26 (s, 2H). ^{13}C NMR (100 MHz, CDCl$_3$, TMS) δ: 143.9, 143.1, 134.5, 133.7, 132.2, 128.7, 123.3, 122.3, 120.5, 109.9, 48.2. LC–MS (positive mode) m/z = 288 (M$^+$+H)$^+$. Anal. Calcd. For. C$_{14}$H$_{11}$BrN$_2$ (287.15): C, 58.56; H, 3.86; N, 9.76. Found: C, 58.55; H, 3.83; N, 9.80.

N–(2,3,4,5,6–pentamethylbenzyl)–benzimidazole (7e). White solid; Yield = 78%; ^{1}H NMR (400 MHz, CDCl$_3$, TMS) δ: 7.87 (s, 1H), 7.20–7.63 (m, 4H), 5.33 (s, 2H), 2.14–2.38 (m, 15H). ^{13}C NMR (100 MHz, CDCl$_3$, TMS) δ: 144.2, 142.0, 136.2, 134.2, 133.5, 127.2, 122.8, 122.3, 120.4, 109.6, 44.4, 17.2, 16.9, 16.6. LC–MS (positive mode) m/z = 279 (M$^+$+H)$^+$. Anal. Calcd. For. C$_{19}$H$_{22}$N$_2$ (278.39): C, 81.97; H, 7.97; N, 10.06. Found: C, 81.93; H, 7.99; N, 10.08.

General procedure for the synthesis of the ANT–Im or ANT–BenzIm bromide salts (8a–f and 9a–e). A mixture of 9–bromo–10–(bromomethyl)anthracene (**2**) (1 mmol) and the relevant N–alkyl imidazoles (**4a–f**) or N–benzyl benzimidazoles (**7a–e**) in THF (15 ml) was refluxed at open condition for 24 h. By this time the products **8a–f** and **9a–e** appeared as yellow precipitates which were isolated by filtration, washed with little THF, then with ether and were air–dried. Yield: 85–89% (imidazolium salts) and 80–87% (benzimidazolium salts).

Bromide 8a. Yellow solid. Anal. Calcd. For. C$_{19}$H$_{16}$Br$_2$N$_2$ (432.25): C, 52.81; H, 3.73; N, 6.48. Found: C, 52.76; H, 3.75; N, 6.51.

Bromide 8b. Yellow solid. Anal. Calcd. For. C$_{21}$H$_{20}$Br$_2$N$_2$ (460.20): C, 54.81; H, 4.38; N, 6.09. Found: C, 54.82; H, 4.36; N, 6.05.

Bromide 8c. Yellow solid Anal. Calcd. For. $C_{21}H_{20}Br_2N_2$ (460.20): C, 54.81; H, 4.38; N, 6.09. Found: C, 54.84; H, 4.37; N, 6.07.

Bromide 8d. Yellow solid. Anal. Calcd. For. $C_{22}H_{22}Br_2N_2$ (474.23): C, 55.72; H, 4.68; N, 5.91. Found: C, 55.74; H, 4.71; N, 5.89.

Bromide 8e. Yellow solid. Anal. Calcd. For. $C_{24}H_{26}Br_2N_2$ (502.28): C, 57.39; H, 5.22; N, 5.58. Found: C, 57.37; H, 5.16; N, 5.60.

Bromide 8f. Yellow solid. Anal. Calcd. For. $C_{28}H_{34}Br_2N_2$ (558.39): C, 60.23; H, 6.14; N, 5.02. Found: C, 60.27; H, 6.11; N, 4.98.

Bromide 9a. Yellow solid. Anal. Calcd. For. $C_{29}H_{22}BrClN_2$ (513.86): C, 67.78; H, 4.32; N, 5.45. Found: C, 67.80; H, 4.27; N, 5.37.

Bromide 9b. Yellow solid. Anal. Calcd. For. $C_{29}H_{21}BrClFN_2$ (531.85): C, 65.49; H, 3.98; N, 5.27. Found: C, 65.51; H, 3.99; N, 5.26.

Bromide 9c. Yellow solid. Anal. Calcd. For. $C_{29}H_{21}BrCl_2N_2$ (548.30): C, 63.53; H, 3.86; N, 5.11. Found: C, 63.56; H, 3.84; N, 5.13.

Bromide 9d. Yellow solid. Anal. Calcd. For. $C_{29}H_{21}Br_2ClN_2$ (592.75): C, 58.76; H, 3.57; N, 4.73. Found: C, 58.79; H, 3.55; N, 4.72.

Bromide 9e. Yellow solid. Anal. Calcd. For. $C_{34}H_{32}BrClN_2$ (583.99): C, 69.93; H, 5.52; N, 4.80. Found: C, 69.96; H, 5.53; N, 4.73.

Hexamolybdate 10a. Orange yellow solid. IR (KBr, cm^{-1}): 3144.25 (C–H), 3097.96 (C–H), 956.78 (Mo=O), 898.91 (Mo–O–Mo). Anal. Calcd. For. $C_{38}H_{32}Br_2N_4Mo_6O_{19}$ (1584.12): C, 28.81; H, 2.04; N, 3.54. Found: C, 28.66; H, 1.99; N, 3.61.

Hexamolybdate 10b. Orange yellow solid. IR (KBr, cm^{-1}): 3152.17 (C–H), 3070.29 (C–H), 954.87 (Mo=O), 895.11 (Mo–O–Mo). Anal. Calcd. For. $C_{42}H_{40}Br_2N_4Mo_6O_{19}$ (1640.23): C, 30.75; H, 2.46; N, 3.42. Found: C, 30.41; H, 2.39; N, 3.53.

Hexamolybdate 10c. Orange yellow solid. IR (KBr, cm^{-1}): 3145.19 (C–H), 3092.58 (C–H), 949.19 (Mo=O), 890.17 (Mo–O–Mo). Anal. Calcd. For. $C_{42}H_{40}Br_2N_4Mo_6O_{19}$ (1640.23): C, 30.75; H, 2.46; N, 3.42. Found: C, 30.57; H, 2.44; N, 3.56.

Hexamolybdate 10d. Orange yellow solid. IR (KBr, cm^{-1}): 3141.15 (C–H), 3089.91 (C–H), 958.78 (Mo=O), 897.41 (Mo–O–Mo). Anal. Calcd. For. $C_{44}H_{44}Br_2N_4Mo_6O_{19}$ (1668.28): C, 31.68; H, 2.66; N, 3.36. Found: C, 31.63; H, 2.63; N, 2.42.

Hexamolybdate 10e. Orange yellow solid. IR (KBr, cm^{-1}): 3157.33 (C–H), 3068.97 (C–H), 941.48 (Mo=O), 891.96 (Mo–O–Mo). Anal. Calcd. For. $C_{48}H_{52}Br_2N_4Mo_6O_{19}$ (1724.39): C, 33.43; H, 3.04; N, 3.25. Found: C, 33.35; H, 3.01; N, 3.30.

Hexamolybdate 10f. Orange yellow solid. IR (KBr, cm^{-1}): 3162.19 (C–H), 3091.17 (C–H), 957.12 (Mo=O), 893.22 (Mo–O–Mo). Anal. Calcd. For. $C_{56}H_{68}Br_2N_4Mo_6O_{19}$ (1836.60): C, 36.62; H, 3.73; N, 3.05. Found: C, 36.53; H, 3.71; N, 3.12.

Hexatungstate 11a. Yellow solid. IR (KBr, cm^{-1}): 3150.04 (C–H), 3092.17 (C–H), 978.00 (W=O), 802.46 (W–O–W). Anal. Calcd. For. $C_{38}H_{32}Br_2N_4W_6O_{19}$ (2111.52): C, 21.62; H, 1.53; N, 2.65. Found: C, 21.59; H, 1.51; N, 2.68.

Hexatungstate 11b. Yellow solid. IR (KBr, cm^{-1}): 3157.12 (C–H), 3076.49 (C–H), 982.54 (W=O), 799.35 (W–O–W). Anal. Calcd. For. $C_{42}H_{40}Br_2N_4W_6O_{19}$ (2167.63): C, 23.27; H, 1.86; N, 2.58. Found: C, 23.22; H, 1.83; N, 2.62.

Hexatungstate 11c. Yellow solid. IR (KBr, cm^{-1}): 3147.97 (C–H), 3096.19 (C–H), 982.88 (W=O), 789.79 (W–O–W). Anal. Calcd. For. $C_{42}H_{40}Br_2N_4W_6O_{19}$ (2167.63): C, 23.27; H, 1.86; N, 2.58. Found: C, 23.24; H, 1.81; N, 2.65.

Hexatungstate 11d. Yellow solid. IR (KBr, cm^{-1}): 3148.83 (C–H), 3043.27 (C–H), 988.72 (W=O), 801.91 (W–O–W). Anal. Calcd. For. $C_{44}H_{44}Br_2N_4W_6O_{19}$ (2195.68): C, 24.07; H, 2.02; N, 2.55. Found: C, 24.03; H, 2.00; N, 2.61.

Hexatungstate 11e. Yellow solid. IR (KBr, cm^{-1}): 3142.26 (C–H), 3045.27 (C–H), 979.89 (W=O), 800.22 (W–O–W). Anal. Calcd. For. $C_{48}H_{52}Br_2N_4W_6O_{19}$ (2251.79): C, 25.60; H, 2.33; N, 2.49. Found: C, 25.51; H, 2.30; N, 2.52.

Hexatungstate 11f. Yellow solid. IR (KBr, cm^{-1}): 3134.19 (C–H), 3042.55 (C–H), 976.17 (W=O), 785.60 (W–O–W). Anal. Calcd. For. $C_{56}H_{68}Br_2N_4W_6O_{19}$ (2364.00): C, 28.45; H, 2.90; N, 2.37. Found: C, 28.41; H, 2.88; N, 2.39.

Hexamolybdate 12a. Orange yellow solid. IR (KBr, cm^{-1}): 3146.83 (C–H), 3109.36 (C–H), 943.21 (Mo=O), 892.37 (Mo–O–Mo). Anal. Calcd. For. $C_{58}H_{44}Br_2N_4Mo_6O_{19}$ (1836.43): C, 37.93; H, 2.41; N, 3.05. Found: C, 37.91; H, 2.37; N, 3.07.

Hexamolybdate 12b. Orange yellow solid. IR (KBr, cm^{-1}): 3159.23 (C–H), 3091.41 (C–H), 955.25 (Mo=O), 889.56 (Mo–O–Mo). Anal. Calcd. For. $C_{58}H_{42}Br_2F_2N_4Mo_6O_{19}$ (1872.41): C, 37.20; H, 2.26; N, 2.99. Found: C, 37.11; H, 2.23; N, 3.04.

Hexamolybdate 12c. Orange yellow solid. IR (KBr, cm^{-1}): 3153.15 (C–H), 3096.18 (C–H), 948.23 (Mo=O), 881.07 (Mo–O–Mo). Anal. Calcd. For. $C_{58}H_{42}Br_2Cl_2N_4Mo_6O_{19}$ (1905.32): C, 36.56; H, 2.22; N, 2.94. Found: C, 36.47; H, 2.19; N, 3.01.

Hexamolybdate 12d. Orange yellow solid. IR (KBr, cm^{-1}): 3158.11 (C–H), 3097.44 (C–H), 941.60 (Mo=O), 892.75 (Mo–O–Mo). Anal. Calcd. For. $C_{58}H_{42}Br_4N_4Mo_6O_{19}$ (1994.23): C, 34.93; H, 2.12; N, 2.81. Found: C, 34.88; H, 2.09; N, 2.84.

Hexamolybdate 12e. Orange yellow solid. IR (KBr, cm^{-1}): 3161.20 (C–H), 3091.28 (C–H), 945.28 (Mo=O), 898.10 (Mo–O–Mo). Anal. Calcd. For. $C_{68}H_{64}Br_2N_4Mo_6O_{19}$ (1976.70): C, 41.32; H, 3.26; N, 2.83. Found: C, 41.25; H, 3.22; N, 2.89.

Hexatungstate 13a. Yellow solid. IR (KBr, cm^{-1}): 3139.85 (C–H), 3048.49 (C–H), 980.56 (W=O), 788.21 (W–O–W). Anal. Calcd. For. $C_{58}H_{44}Br_2N_4W_6O_{19}$ (2363.83): C, 29.47; H, 1.88; N, 2.37. Found: C, 29.39; H, 1.86; N; 2.38.

Hexatungstate 13b. Yellow solid. IR (KBr, cm^{-1}): 3144.18 (C–H), 3040.13 (C–H), 981.67 (W=O), 792.63 (W–O–W). Anal. Calcd. For. $C_{58}H_{42}Br_2F_2N_4W_6O_{19}$ (2399.81): C, 29.03; H, 1.76; N, 2.33. Found: C, 28.95; H, 1.71; N, 2.36.

Hexatungstate 13c. Yellow solid. IR (KBr, cm^{-1}): 3143.59 (C–H), 3049.97 (C–H), 976.23 (W=O), 792.14 (W–O–W). Anal. Calcd. For. $C_{58}H_{42}Br_2Cl_2N_4W_6O_{19}$ (2432.72): C, 28.64; H, 1.74; N, 2.30. Found: C, 28.59; H, 1.72; N, 2.33.

Hexatungstate 13d. Yellow solid. IR (KBr, cm^{-1}): 3141.72 (C–H), 3036.36 (C–H), 979.30 (W=O), 790.85 (W–O–W). Anal. Calcd. For. $C_{58}H_{42}Br_4N_4W_6O_{19}$ (2521.63): C, 27.63; H, 1.68; N, 2.22. Found: C, 27.58; H, 1.66; N, 2.25.

Hexatungstate 13e. Yellow solid. IR (KBr, cm^{-1}): 3137.54 (C–H), 3029.12 (C–H), 978.86 (W=O), 793.45 (W–O–W). Anal. Calcd. For. $C_{68}H_{64}Br_2N_4W_6O_{19}$ (2504.10): C, 32.62; H, 2.58; N, 2.24. Found: C, 32.53; H, 2.55; N, 2.26.

3.5 References

1. (a) G. P. Stahly, *Cryst. Growth Des.*, **2007**, *7*, 1007. (b) J. D. Dunitz, *CrystEngComm*, **2003**, *4*, 506. (c) G. R. Desiraju, *CrystEngComm*, **2003**, *5*, 466. (d) A. D. Bond, *CrystEngComm*, **2007**, *9*, 833.

2. (a) A. I. Kitaigorodsky, *Mixed Crystals*; Springer–Verlag: Berlin, 1984. (b) A. B. Aakeröy, D. J. Salmon, *CrystEngComm*, **2005**, *7*, 439. (c) P. Vishweshwar, J. A. McMahon, M. J. Zaworotko, *J. Pharm. Sci.*, **2006**, *95*, 499. (d) W. Jones, W. D. Motherwell, A. V. Trask, *MRS Bull.*, **2006**, *341*, 875. (e) S. L. Childs, K. I. Hardcastle, C*ryst. Growth Des.*, **2007**, *7*, 1291. (f) A. B. Bond, *CrystEngComm*, **2007**, *9*, 833. (g) B. R. Bhogala, A. Nangia, *New J. Chem.*, **2008**, *32*, 800.

3. G. P. Stahly, *Cryst. Growth Des.*, **2009**, *9*, 4212 and the references therein.

4. F. Wohler, *Annalen Chem. Pharm.*, **1844**, *51*, 145.

5. J. S. Anderson, *Nature* **1937**, *140*, 850.

6. For a review see: N. Schultheiss, A. Newman, *Cryst. Growth. Des.*, **2009**, *9*, 2950 and the references therein.

7.   N. G. Anderson, D. A. Lust, K. A. Colapret, J. H. Simpson, M. F. Malley, J. Z. Gougoutas, *J. Org. Chem.*, **1996**, *61*, 7955.

8.   P. M. Bhatt, N. V. Ravindra, R. Banerjee, G. R. Desiraju, *Chem. Commun.*, **2005**, 1073.

9.   J. M. Lehn, *Supramolecular chemistry: concepts and perspectives*, Wiley–VCH, 1995. (b) J. W. Steed, J. L. Atwood, *Supramolecular Chemistry*, John Wiley and Sons, 2009. (c) J. W. Steed, J. L. Atwood, *Encyclopedia of Supramolecular Chemistry, Vol. 2*, M. Dekker, 2004.

10.   M. M. Olmstead, A. Maitra, K.; A. L. Balch, *Angew. Chem., Int. Ed.*, **1999**, *38*, 231.

11.   (a) J. L. Atwood, L. J. Barbour, C. L. Raston, I. B. N. Sudria, *Angew.Chem., Int. Ed.*, **1998**, *37*, 981. (b) J. L. Atwood, G. A. Koutsantonis, C. L. Raston, *Nature*, **1994**, *368*, 229. (c) D. E. Cliffel, A. J. Bard, S. Shinkai, *Anal. Chem.,* **1998**, *70*, 4146. (d) T. Suzuki, K. Nakashima, S. Shinkai, *Tetrahedron Lett.*, **1995**, *36*, 249. (e) A. Drijaca, C. Kepert, L. Spiccia, C. L. Raston, C. A. Sandoval, T. D. Smith, *Chem. Commun.*, **1997**, 195. (f) T. Haino, M. Yanase, Y. Fukazawa, *Angew. Chem., Int. Ed.*, **1998**, *37*, 997. (g) K. Tsubaki, K. Tanaka, T. Kinoshita, K. Fuji, *Chem. Commun.*, 1998, 895. (h) R. M. Williams, J. M. Zwier, J. W. Verhoeven, *J. Am. Chem. Soc.*, **1994**, *116*, 6965. (i) L. J. Barbour, G. W., J. L. Atwood, *Chem. Commun.*, **1997**, 1439. (j) L. J. Barbour, G. W. Orr, J. L. Atwood, *Chem. Commun.*, **1998**, 1901. (k) P. J. Nichols, C. L. Raston, C. A. Sandoval, D. J. Young, *Chem.Commun.*, **1997**, 1839. (l) T. Haino, M. Yanase, Y. Fukazawa, *Angew. Chem., Int. Ed.*, **1997**, *36*, 259. (m) B. Paci, G. Amoretti, G. Arduini, G. Ruani, S. Shinkai, T. Suzuki, F. Ugozzoli, R. Caciuffo, *Phys. Rev. B*, **1997**, *53*, 5566.

12.   (a) Z. Yoshida, H. Takekuma, S. Takekuma, Y. Matsubara, *Angew.Chem., Int. Ed.*, **1994**, *33*, 1597. (b) T. Andersson, G. Westman, G. Stenhagen, M. Sundahl, O. Wennerström, *Tetrahedron Lett.*, **1995**, *36*, 597.

13.   (a) R. S. Burkhalter, *J. Am. Chem. Soc.*, **1994**, *116*, 10346. (b) J. L. Atwood, M. Barnes, M. G. Gardiner, C. L. Raston, Chem. Commun., **1996**, 1449.

14. P. C. Andrews, J. L. Atwood, L. J. Barbour, P. J. Nichols, C. L. Raston, *Chem. Eur. J.*, **1998**, *4*, 1384.

15. (a) A. Ikeda, A.; C. Fukuhara, S. Shinkai, *Chem. Lett.*, **1997**, 407. (b) T. Drovetskaya, C. A. Reed, P. D. W. Boyd, *Tetrahedron Lett.*, **1995**, *36*, 7971. (c) H. Imahori, K. Hagiwara, T. Akiyama, S. Taniguchi, T. Okada, Y. Sakata, *Chem. Lett.*, **1995**, 265. (d) H. Imahori, Y. Sakata, *Chem. Lett.*, **1996**, 199. (e) T. Akiyama, H. Imahori, A. Ajawakom, Y. Sakata, *Chem. Lett.*, **1996**, 907. (f) P. A. Liddell, D. Kuciauskas, J. P. Sumida, B. Nash, D. Nguyen, A. L. Moore, D. Gust, *J. Am. Chem. Soc.*, **1997**, *119*, 1400. (g) H. Imahori, K. Yamada, M. Hasegawa, S. Taniguchi, T. Okada, Y. Sakata, *Angew.Chem., Int. Ed.*, **1997**, *36*, 2626. (h) H. Imahori, Y. Sakata, *Adv. Mater.*, **1997**, *9*, 537. (i) D. Kuciauskas, S. Lin, G. R. Seely, A. L. Moore, D. Gust, T. Drovetskaya, C. A. Reed, P. D. W. Boyd, *J. Phys. Chem.*, **1996**, *100*, 15926. (j) Y. Sun, T. Drovetskaya, R. D. Bolskar, R. Bau, P. D. W. Boyd, C. A. Reed, *J. Org. Chem.*, **1997**, *62*, 3642. (k) E. Dietel, A. Hirsch, E. Eichhorn, A. Rieker, S. Hackbarth, B. Röder, *Chem. Commun.*, **1998**, 1981.

16. (a) M. M. Olmstead, D. A. Costa, K. Maitra, B. C. Noll, S. L. Phillips, P. M. Van Calcar, A. L. Balch, *J. Am. Chem. Soc.*, **1999,** *121,* 7090. (b) P. D. W. Boyd, M. C. Hodgson, C. E. F. Rickard, A. G. Oliver, L. Chaker, P. J. Brothers, R. Bolskar, F. S. Tham, C. A. Reed, *J. Am. Chem. Soc.*, **1999,** *121,* 10487. (c) T. Ishii, N. Aizawa, M. Yamashita, H. Matsuzaka, T. Kodama, K. Kikuchi, I. Ikemoto, Y. Iwasa, *J. Chem. Soc.*, *Dalton Trans.*, **2000**, 4407.

17. M. T. Pope, *Heteropoly and Isopoly Oxometalates*, Springer–Verlag: Berlin, 1983.

18. (a) A. Müller, E. Beckmann, H. Bögge, M. Schidtmann, A. Dress, *Angew. Chem. Int. Ed.*, **2002**, *41*, 1162. (b) P. J. Kulesza, L. R. Faulkner, *Proc. Electrochem. Soc.*, **1994**, *94*, 20. (c) T. Yamase, *Kikan Kagaku Sosetsu.*, **1993**, *20*, 190. (d) T. Sanac, K. Akira, H. Koichiro, K. Tetsuichi, *Solid State Ionics*, **1994**, *70–71*, 636. (e) K. Nomiya, M. Miwa, *Polyhedron*, **1985**, *4*, 675. (f) K. Nomiya, *Polyhrdron*, **1987**, *6*, 309. (g) K. Nomiya, M. Miwa, *Polyhedron*, **1984**, *3*, 341. (g) A. Müller, S. K. Das, C. Kuhlmann, H. Bögge, M. Schidtmann, E. Diemann, E. Krickmeyer, J. Hormes, H. Modrow, M. Schindler, *Chem. Commun.*, **2001**, 655. (h) A. Müller,

R. Maiti, M. Schidtmann, H. Bögge, S. K. Das, W. Zhang, *Chem. Commun.*, **2001**, 2126. (i) W. Yang, C. Lu, X. Lin, H. Zhuang, *Chem. Commun.*, **2000**, 1623. (j) Z. Han, Y. Zhao, J. Peng, Y. Feng, J. Yin, Q. Liu, *Electroanalysis*, **2005**, *17*, 1097. (k) A. Nicoara, A. Patrut, D. Margineanu, A. Müller, *Electrochemistry Communications*, **2003**, *5*, 511. (l) M. Sadakane, E. Steckhan, *Chem. Rev.*, **1998**, *98*, 219 and the references therein.

19.   (a) S. S. Mal, B. S. Bassil, M. Ibrahim, S. Nellutla, J. van Tol, N. S. Dalal, J. A. Fernández, X. López, J. M. Poblet, R. N. Biboum, B. Keita, U. Kortz, *Inorg. Chem.*, **2009**, *48*, 11636. (b) V. Ball, F. Bernsmann, S. Werner, J.–C. Voegel, L. F. Piedra–Garza, U. Kortz, *Eur. J. Inorg. Chem.*, **2009**, 5115. (c) S. S. Mal, N. H. Nsouli, M. Carraro, A. Sartorel, G. Scorrano, H. Oelrich, L. Walder, M. Bonchio, U. Kortz, *Inorg. Chem.*, **2010**, *49*, 7. (d) Y.–Y. Bao, L.–H. Bi, L.–X. Wu, S. S. Mal, U. Kortz, *Langmuir*, **2009**, *25*, 13000.

20.   A. Müller, E. Krickemeyer, H. Bögge, et al., *Angew. Chem., Int. Ed. Engl.*, **1998**, *37*, 3360.

21.   (a) J. L. Stark, V. G. Jr. Young, E. A. Maatta, *Angew. Chem., Int. Ed.*, **1995**, *34*, 2547. (b) P. Gouzerh, A. Proust, *Chem. Rev.*, **1998**, *98*, 77. (c) I. Bar–nahum, H. Cohen, R. Neumann, *Inorg. Chem.*, **2003**, *42*, 3677. (d) J. B. Strong, G. P. A. Yap, R. Ostrander, L. M. Liable–Sands, E. A. Maatta, *J. Am. Chem. Soc.*, **2000**, *122*, 3275. (e) W. Clegg, R. J. Errington, K. A. Fraser, S. A. Holmes, A. Schäffer, *J. Chem. Soc., Chem. Commun.*, **1995**, 455. (f) J. B. Strong, B. S. Haggerty, A. L. Rheingold, E. A. Maatta, *Chem. Commun.*, **1997**, 1137. (g) J. B. Strong, G. P. A. Yap, R. Ostrander, L. M. Liable–Sands, A. L. Rheingold, R. Thouvenot, P. Gouzerh, E. A. Maatta, *J. Am. Chem. Soc.*, **2000**, *122*, 639. (h) Y. Wei, B. Xu, C. L. Barnes, Z. Peng, *J. Am. Chem. Soc.*, **2001**, *123*, 4083. (i) Y. Wei, M. Lu, C. F.–C. Cheung, C. L. Barnes, Z. Peng, *Inorg. Chem.*, **2001**, *40*, 5489. (j) J. L. Stark, A. L. Rheingold, E. A. Maatta, *J. Chem. Soc., Chem. Commun.*, **1995**, 1165. (k) J. Kang, J. A. Nelson, M. Lu, B. Xie, Z. Peng, D. R. Powell, *Inorg. Chem.*, **2004**, *43*, 6408. (l) J. Kang, B. Xu, Z. Peng, X. Zhu, Y. Wei, D. R. Powell, *Angew. Chem., Int. Ed.*, **2005**, *44*, 6902.

22. (a) M. Dabbabi, M. Boyer, J. P. Launay, Y. Jeannin, *Electroanal. Chem.*, **1977**, *76*, 153. (b) M. T. Pope, J. M. Varga, *Inorg. Chem.*, **1966**, *7*, 1249. (c) Launay. J. P. *J. Inorg. Nucl. Chem.*, **1976**, *18*, 807.

23. For example see: V. Shivaiah, S. K. Das, *Inorg. Chem.*, **2005**, *44*, 8846.

24. (a) T. Chatterjee, M. Sarma, S. K. Das, *Cryst. Growth Des.*, **2010**, *10*, 3149. (b) T. Chatterjee, M. Sarma, S. K. Das, *J. Mol. Struct.*, **2010**, *91*, 34. (c) M. Sarma, T. Chatterjee, S. K. Das, Inorg. Chem. Commun., **2010**, *13*, 1114.

25. See for example: (a) Y. Li, Na Hao, E. Wang, M. Yuan, C. Hu, N. Hu, H. Jia, *Inorg. Chem.*, **2003**, *42*, 2729. (b) W. You, E. Wang, Y. Xu, Y. Li, L. Xu, C. Hu, *Inorg. Chem.*, **2001,** *40,* 5468.

26. (a) J. Thomas, A. Ramanan, *Cryst. Growth Des.*, **2008**, *8*, 3390. (b) K. Pavani, S. E. Lofland, K. V. Ramanujachary, A. Ramanan, *Eur. J. Inorg. Chem.*, **2007**, 568. (c) S. Upreti, A. Ramanan, *Crystal Growth Des.*, **2006**, *6*, 2066. (d) S. Upreti, A. Ramanan, *Crystal Growth Des.*, **2005**, *5*, 1837. (e) K. Pavani, A. Ramanan, *Eur. J. Inorg. Chem.*, **2005**, 3080. (f) M. Asnani, S. Sharma, S. E. Lofland, K. V. Ramanujachary, P. A. Buffat, A. Ramanan, *Eur. J. Inorg. Chem.*, **2005**, 401. (g) S. Chakrabarti, S. Natarajan, *Crystal Growth Des.*, **2002**, *2*, 333.

27. P. Le Maguere`s, S. M. Hubig, S. V. Lindeman, P. Veya, J. K. Kochi**,** *J. Am. Chem. Soc.*, **2000,** *122,* 10073.

28. (a) S. H. Yang, O. J. Shon, K. M. Park, S. S. Lee, H. J. Park, M. J. Kim, J. H. Lee, J. S. Kim, Bull. *Korean Chem. Soc.*, **2002**, *23*, 1585. (b) S. Duan, J. Turk, J. Speigle, J. Corbin, J. Masnovi, R. J. Baker, *J. Org. Chem.*, **2000**, *65*, 3005. (c) M. Michelswirth, M. Rakers, C. Schafer, J. Mattay, M. Neumann, U. Heinzmann, *J. Phys. Chem. B*, **2010**, *114*, 3482. (d) J. H. Clements, S. E. Webber, *J. Phys. Chem. B*, **1999**, *103*, 9366. (e) J. H. Clements, S. E. Webber, *Macromolecules*, **2004**, *37*, 1531.

29. For spectroscopic data of the N–alkylimidazoles see: S. Khabnadideh, Z. Rezaei, A. Khalafi–Nezhad, R. Bahrinajafi, R. Mohamadia, A. A. Farrokhroza, *Bioorg. Med. Chem. Lett.*, **2003**, *13*, 2863.

Concluding remarks and future scopes of the present work

5

5.1. Concluding remarks

Ionic *versus* supramolecular assembly between crown ether inclusion complexes of simple ammonium or organic ammonium ions and polyoxometalate (POM) cluster anions have been demonstrated in the Chapter 2. Although such inclusion complexes of ammonium and crown ether were long known, the same was not known in the polyoxometalate (POM) association. These cluster macroanions are bigger in size and more symmetrical than the other common counter anions e.g. ClO_4^-, BF_4^-, PF_6^- *etc.* Out of the six solids, described in the relevant chapter, five of them are made up of hydrogen bonded complexes of simple ammonium (NH_4^+) ion and various crown ethers. Variation of the size of the crown ether cavity or symmetry of the macrocyclic polyethers causes alteration of the supramolecular contacts between the inclusion complexes and the POMs. The tetrahedral symmetrical (T_d) guest molecular cation NH_4^+ ion usually interacts with the 18–crown–6 and its derivatives through three N–H bonds and the fourth N–H bond is projected outwards the crown ether cavity. Four different crown ethers *viz.*, benzo–18–crown–6 (B18C6), dibenzo–18–crown–6 (DB18C6), dicyclohexyl–18–crown–6 (DC18 C6) and dibenzo–30–crown–10 (DB30C10) and two different POM cluster anions ($[Mo_6 O_{19}]^{2-}$ and $[SiW_{12}O_{40}]^{4-}$) have been used for the present study. The crown ethers are distinct from each other as far as their shape and size are concerned. Similarly, the two POM cluster anions, chosen for the present case, are different from each other with respect to their symmetry. The $[Mo_6O_{19}]^{2-}$ cluster is octahedral symmetrical (O_h) and centrosymmetric whereas, the $[SiW_{12}O_{40}]^{4-}$ cluster is tetrahedral symmetrical and non centrocymmetric cluster anion. But variation of the POM clusters has not induced any change in the space symmetrical arrangement of the molecular components. For example, the $[NH_4^+ \subset B18C6]$ supramolecular complex prefers same spatial symmetry ($P–1$) to pack with both of the two cluster anions. Changing the crown ether from the less symmetrical B18C6 to the more symmetrical one (DB18C6) causes a dramatic change in
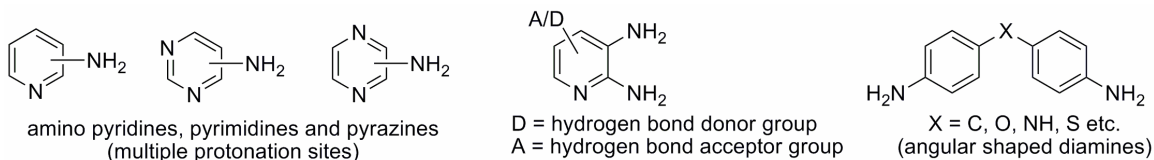
the crystal symmetry. Bowl–type shape of the macrocycle prevents direct contact between the [$NH_4^+ \subset$ DB18C6] inclusion complexes and the POMs. But a more puckered and non–aromatic crown ether DC18C6 restores the N^+–H⋯O interaction between the supramolecular complexes and the POMs. The situation fully diverges in case of the larger sized crown ether DB30C10 which wraps around the guest cation and thus hinders the supramolecular contact (N^+–H⋯O) with the POM. However, in all the cases, C–H⋯O interactions between the crown ethers and the POMs sustain. One important observation is that, in the lattices of the solids formulated as, [NH_4(B18C6)][Bu_4N][Mo_6O_{19}] (**1**), [NH_4(B18C6)]$_4$[$SiW_{12}O_{40}$].2CH_3CN (**2**) and [NH_4(DC18C6)]$_2$[Mo_6O_{19}] (**4**), the POM anions have used the bridging oxygen atoms instead of the terminal oxygen atoms as the N^+–H⋯O hydrogen bonding receptor. The probable reason for this phenomenon can be understood from an imagination of close packing model. As described in the Scheme 2.1, usage of the bridging O atom of the POM anion makes the latter in slightly tilted orientation thereby bringing the terminal O atoms closer to the crown ethers to accept the C–H bond donation. This type of interaction might result in more close packing of the molecules in the crystal compared to the other mode of interaction *i.e.* interaction with the ammonium ion using the terminal O atom. In this mode of interaction, the bridging O atoms of the POM anion are apart from the crown ethers to accept the C–H bond donation from the latter. The sixth compound of the concerned chapter features the supramolecular interactions between the 18–crown–6 inclusion complex of protonated *ortho*–phenylenediamine and hexamolybdate cluster. In addition to the crystallographic analysis, detailed spectroscopic investigations have been accomplished in order to comprehend the adduct formation.

Chapter 3 documents synthesis and crystallographic characterizations of a series of hexametalate cluster–based solids comprising of various anthracene–imidazolium and anthracene–benzimidazolium cationic counterparts. The cationic fragments are attached to the anthracene ring by a methylene spacer. Powder X–ray diffraction analysis exhibits isomorphic character of the hexamolybdate and hexatungstate salts of the same counter cations. All the solids maintain 2:1 stoichiometry between the mono–cations and the di–anions and are centrosymmetric with respect to the central oxygen atom of the octahedral symmetrical POMs. The cationic counterparts (imidazolium and benzimidazolium) in all

the solids project toward surface of the POMs due to electrostatic interaction between the oppositely charged species. Apart from coulombic association between the anthracenes and the POM, supramolecular hydrogen bonding interactions are also observed to optimize the lattice destabilization due to coexistence of the structurally mismatched molecular components in the same crystal. However, no direct contact between the anthracene and the POM surface has been observed in the crystallographically characterized solids described in the concerned chapter. Even though, the ionic precursors of the anthracene–POM salts are light yellow (anthracene bromide salts and the tetrabutylamonium salt of the hexamolybdate cluster anion) or white (tetrabutylammonium salt of the hexatungstate cluster anion) in color, the resulting ion exchanged anthracene–POM salts are intensely colored. Solution state absorption spectroscopy on these salts along with the 1:2 mixture of the ionic precursors exhibit similar aspect which precludes any adduct formation between the anthracenes and the POMs in solution. However, absorption spectroscopy in the solid state reveals dramatic loss of the identity of the parents with concomitant indication for the adduct formations. Thus, these solids have been described as coulombic cocrystals. Variation of the alkyl chain lengths in the imidazolium cationic moiety or alteration of the substituents in the benzimidazolium moiety has not changed the intermolecular association of the components in a greater extent. Possibly due the shorter spacer, the anthracene ring couldn't interact with the POM surface which results charge transfer interaction between the two.

Work, demonstrated in the Chapter 4, incorporates spectroscopy as the major characterization tool. A series of donor–acceptor π–conjugated 2,2'–bipyridine derivatives have been synthesized following standard and well–established organic synthetic methodologies and have been characterized through spectroscopy. Synthetic routes of the present study clearly indicate that, wide range of symmetrically and dissymetrically substituted π–conjugated 2,2'–bipyridine derivatives can be obtained *via* controlled Knoevenagel condensation between the appropriate bipyridine precursors and aldehydes. Variation of the conjugating system causes alteration of the absorption and emission properties of the synthesized compounds. Thus, it can be said that tuning of the optical properties of the bipyridine derivatives can be achieved by modification of the π–

backbones. Molar extinction coefficient of the resulting bipyridine derivatives is also dependent upon the number of donor groups present in the relevant system. For the 4,4'–π–substituted styryl–2,2'–bipyridine series, the bathochromic shift of the absorption maxima is consistent with relative values of the donor strengths in the order dialkylamino > 9–anthryl > naphthyl > ethynyl. Similarly, for the same donor group a bathochromic shift is noticed in the order styryl < bistryl. The emission energy and fluorescence efficiency are also dictated by the nature of the end substituents and π–conjugated systems. Increment of the conjugation length causes a huge enhancement of the photoluminescent quantum yield of the synthesized chromophores. Similarly, the present study indicates that, emission efficiency of a given bipyridine chromophore strongly depends upon the position of the donor groups. The stepwise protonation–deprotonation reactions of the alkylamino substituted bipyridine derivatives reveal the easy optical tunability of these chromophores over a large wavelength range. Thermo-gravimetric studies have been performed which illustrate the thermal robustness of the synthesized chromophores. Chemical stabilities of the synthesized compounds have also been checked by NMR and UV–visible spectroscopy after prolonged storage of the samples under air. Introduction of the hydroxyl functionality does not alter the basic intrinsic properties of the given chromophores in a considerable extent. In–a–word, it can be said that, the concerned chapter demonstrates synthesis and characterization of a series of bipyridine chromophores or fluorophores and easy modulation of their optical properties of by simple protonation–deprotonation reactions.

Chart 5.1

amino pyridines, pyrimidines and pyrazines
(multiple protonation sites)

D = hydrogen bond donor group
A = hydrogen bond acceptor group

X = C, O, NH, S etc.
(angular shaped diamines)

5.2. Future scopes

5.2.1. Polyoxometalates as building blocks in Crystal Engineering

As described in the chapters 2 and 3, the polyoxometalates are good building blocks for the construction of composite and stoichiometric solids. The only limitation in using

such macrocanions in the supramolecular chemistry is the solubility of the resulting solids in common organic solvents which often hinders the crystallographic and / or spectroscopic characterizations. Supramolecular assembly of the crown ether inclusion complexes is still less explored and several new oxide based solids can be obtained from hydrogen bonded complexes of crown ethers with various protonated amines (see Chart 5.1). Work in this direction is in progress.

Chart 5.2

heteroleptic octahedral complexes

square planar complexes

tetrahedral complexes
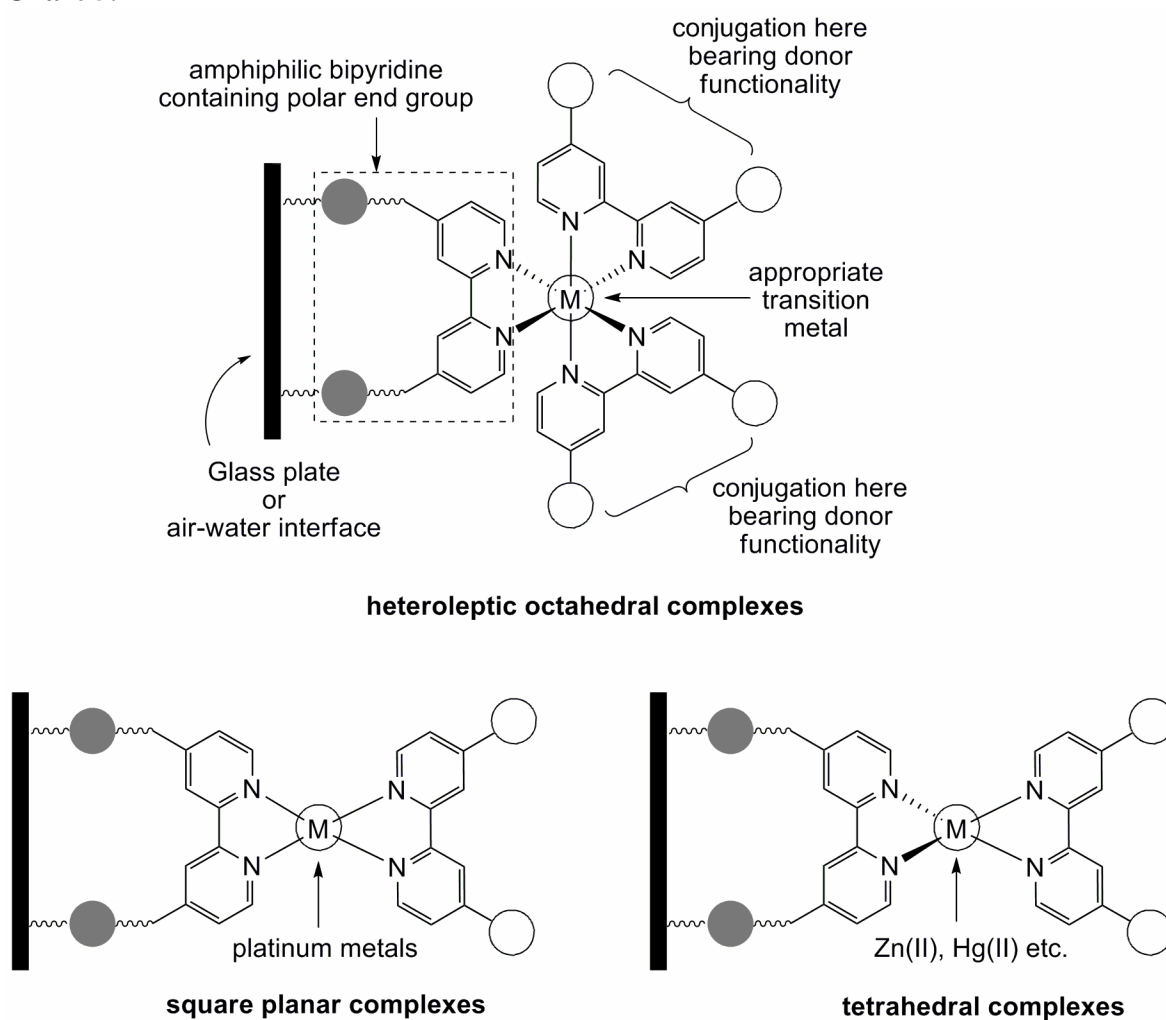
5.2.2. LB films based on coordination complexes of 2,2'–bipyridines

Bypyridines are excellent bidentate chilating ligands for metal ion coordination. Several homoleptic and heteroleptic coordination complexes of octahedral, square planer and tetrahedral complexes are easily obtained upon controlled reaction between metal

salts and bipyridine ligands. Heteroleptic complexes bearing an amphiphilic bipyridine ligand with proper polar end groups can form a monolayer disposition (LB film) on silica glass plate or air water interface as depicted in Chart 5.2. The luminescent properties of thus obtained LB films can easily be tuned through variation of the other coordinating chromophore. This work is under progress.

4,4'–π–Conjugated 2,2′–bipyridine chromophores and fluorophores: Synthesis, linear optical and thermal properties

4

Abstract:– π–conjugated–2,2'–bipyridine chromophores are important class of organic compounds that show potential application in fabricating integrated photonic devices. A series of π–conjugated–2,2'–bipyridines (**TM 1–11**) have been synthesized and their photo–physical properties (absorption and emission) have been investigated. The Horner–Wordsworth–Emmons or Knoevenagel reactions have been used to synthesize the desired π–conjugated bipyridines. The newly synthesized bipyridine compounds comprise different substituents at their π–backbone viz. dialkylamino, methoxy, ethynyl, naphthyl and anthryl. Modification of the electronic backbone of the compounds (for example substituents or conjugation length) has resulted in diversity of their optical properties, which paves the way toward a fine tuning of their optical / photo–physical properties. Thermogravemetric analyses on compounds **TM 1–6** reveal thermal robustness of the synthesized chromophores.

4.1. Preface

The ongoing research with organic molecules can be classified into two broad categories such as: (i) developing new and effective methodologies in synthesizing known or new compounds, and (ii) synthesizing new compounds with materialistic significances adopting / modifying known methodologies. The beauty of organic chemistry in a broader sense, lies in the fact that, larger molecules with practical applications can be synthesized via pre–designed functionalization of smaller molecular fragments.[1]

There is a considerable research interest on the electron donor–acceptor (EDA) molecules because of their widespread applications, especially in the areas of non–linear optics (NLO) and optoelectronics etc. 2,2'–bipyridines are excellent bidentate chelating ligands in forming coordination complexes due to their potential metal ion binding capability.[3] The electronic blending of 2,2'–bipyridine with suitable donor groups attached to the 4– or 4,4'– positions through π–linker (transmitter), results in the construction of 4– or 4,4'–π–conjugated–2,2'–bipyridines, where the electron drifting nature of the pyridine rings makes them archetypal examples of the 'push–pull' or EDA

molecules (see Scheme 4.1). These molecules are synthetically flexible and offer easy optical tuning (absorption, emission etc.) through variation / simple modification of their π–backbones. Two synthetic pathways can be followed for synthesizing such molecular systems: (i) C=C vinyl bond formation at the 4– position of 2–halo–4–picoline, followed

Retro here
1. Witting
2. Horner-Wordsworth-Emmons
3. Heck
5. Knoevenagel etc.

Retro here
1. Suzuki-Miyaura (Pd^0)
2. Stille (Pd^0)
3. Negishi (Pd^0)
4. Ullmann type homo coupling (Ni^0) etc.

(a)

e-pushing moiety

e-pulling moiety

e-pulling moiety

e-pushing moiety

D = donor group

(b)
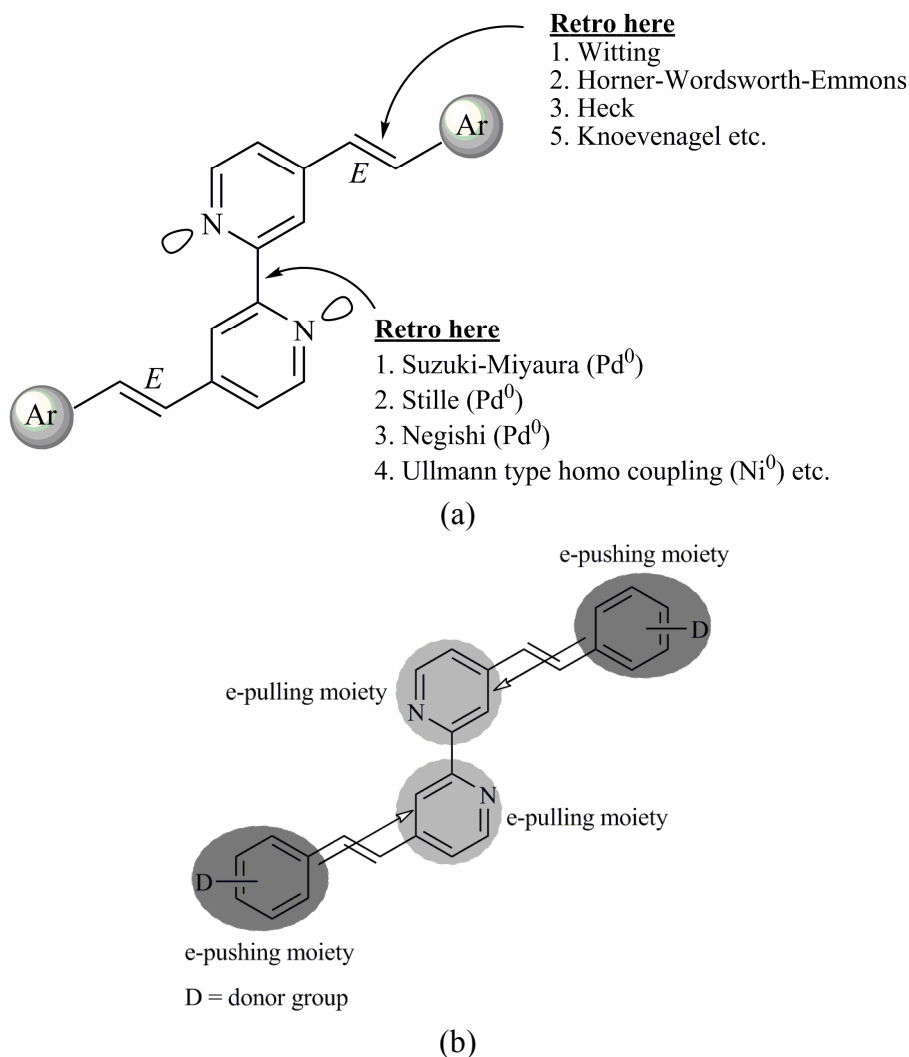
Scheme 4.1 (a) Structural representation of the 4,4'–π–conjugated–2,2'–bipyridines with possible synthetic routes. (b) Representation of π–conjugated 2,2'–bipyridine based 'push–pull' molecule

by, homo–coupling or cross coupling between thus formed 2–halo–4–styryl pyridines to join them at the 2,2′– positions, or (ii) direct usage of an appropriate 2,2'–bipyridine precursor for C=C vinyl bond formations at the 4,4′– positions. The second methodology is more popular due to its involvement of less number of reaction steps and exclusion of

hazardous or expensive chemicals like organo–tins or palladium reagents etc. The resulting 4,4'–π–conjugated–2,2'–bipyridine molecules are symmetrical (centrosymmetric) or unsymmetrical (non–centrosymmetric) depending upon whether the aryl groups attached to the π–backbone of 2,2'–bipyridine are same or different (Scheme 4.1). 4,4′–dimethyl–2,2′–bipyridine is a useful starting material in obtaining such bipyridine compounds. A wide range of symmetrically and dissymetrically substituted 4,4'–π–conjugated–2,2'–bipyridines are accessible via stepwise functionalization of 4,4′–
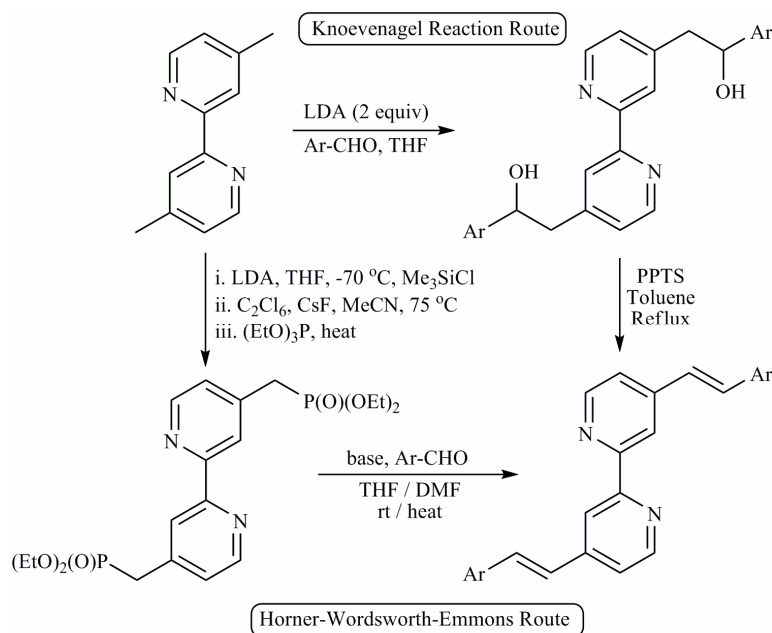
Scheme 4.2 Major synthetic routes to obtain the 4,4'–π–functionalized–2,2'–bipyridines.

dimethyl–2,2′–bipyridine, triggering at the reactivity of 4,4'–methyl protons of the substrate. From the range of methodologies developed, two major synthetic routes involve the reaction between an appropriate bipyridine precursor and an aldehyde either via the classical Knoevenagel type reaction or via the Horner–Wordsworth–Emmons reaction as shown in Scheme 4.2. In the former case, the reactive intermediate involved in the reaction is the carbanion generated in situ during deprotonation of 4,4′–dimethyl–2,2′–bipyridine by a strong base (e.g. LDA, KOBu^t etc.) whereas, the latter deals with the acidity of the α–methylene proton of the appropriate phosphonate ester. The Horner–Wordsworth–Emmons reaction is an effective synthetic route to form C=C bond with predominantly *E*–selectivity.[4]

Electron donor–acceptor or push–pull molecules are dipolar chromophores or fluorophores that incorporate charge dislocation from the donor species (electron pushing group) to the acceptor subunit (electron pulling group) of the molecules through a conjugated backbone. These molecules are of particular interest in contemporary research because of their potential optoelectronic properties and confer widespread applications in materials chemistry especially in non–linear optics (NLO)[5] and electroluminescence[6] etc. Since the past two decades, many research groups have reported several 4,4'–π–conjugated–2,2'–bipyridine chromophores.[7–9] For example various 4,4'–π–conjugated–2,2'–bipyridine compounds featuring styryl, thienylvinyl, phenylimino, azophenyl π–backbone,[7a,b] oligophenylenevinylene (OPV) functionalization,[7c] amino alkyl donor subunit with and without hydroxy functionality,[7d] polyimide backbone,[7e] multidentate coordination ability,[7f,g] star–shaped polymeric structures,[7h] photochromism[7i] etc. have been reported by Bozec and coworkers. Similarly, many other molecular systems comprising modified / modulated π–backbone with optical excellence of both the parent ligands and their transition metal coordination complexes have been reported in literature.[8] Crown macrocycle or ferrocene functionalized symmetrical and unsymmetrical 4,4'–vinyl linked 2,2'–bipyridines along with spectroscopic, electrochemical and cation recognition properties of their transition metal complexes have also been examined by Beer and coworkers in early literature.[9] Langmuir–Blodgett (LB) technique is the most efficient technique in fabricating ultra–thin monolayered deposition of amphiphilic compounds with precise and accurate thickness.[10] LB films formed from transition metal based surfactants are still less explored in contemporary literature. A recent publication by Bolink et al describes dual–emitting nature of LB films built from Ru(II) or Ir(III) complexes of amphiphilic bipyridyl compounds with other co–ligands.[11] Opligophenylenevinylene (OPV) derivatives are highly conjugated organic molecules and potential application of these molecules in constructing electroluminescent devices is worth mentioning.[12] 4,4'–π–conjugated–2,2'–bipyridines can also act as organic light emitting diodes (OLED) if suitable donor groups are attached to specified positions in the 4,4'–π–transmitter of 2,2'–bipyridines.[13] Whereas the amphiphilic nature of the coordinating ligands would serve toward the LB film formation, coordination complexes of the appropriate transition metals bearing both the amphiphilic and OPV coordinating

ligands might build electroluminescent LB film and a research in this direction would be interesting.

Metal ions are excellent three–dimensional templates for macroscopic assemblies of the 2,2'–bipyridine based coordinating ligands. Transition metal coordination complexes of the functionalized bipyridines have been found to have potentiality as NLO–phores[14] and as sensitizers in the photovoltaic devices.[15–17]

In this chapter, synthesis of a series of 2,2'–bipyridine compounds of the type D–π–A (D = donor, A = acceptor) (see Chart 4.1) along with their detailed spectroscopic and thermal properties have been demonstrated. The relevant compounds (**TM 1–11**) consist of different conjugating groups at their π–backbones e.g., alkylamino styryl (**TM 1–3**), methoxy stilbene (**TM 4–6**), ethynyl (**TM 7–8**), napthyl (**TM 9–10**) and 9–anthryl (**TM 11**). Modification of the π–backbones has resulted in diversities of their spectral properties. Thermogravimetric analyses on the compounds **TM 1–6** reveal thermal robustness of the bipyridyl compounds. Solvatochromic behaviour of the compounds **TM 1–6** has also been checked in order to investigate the effect of medium on the electronic properties of the relevant compounds. The end of the chapter descibes, controlled acid–base reactions performed on the amphiphilic chromophores (**TM 1–3**).

4.2. Results and Discussion

4.2.1. Synthesis

All the bipyridyl compounds (**TM 1–11**) (see Chart 4.1) have been obtained in gram quantities (2–3 gm) following standard synthetic methodologies as described in this section. The basic reaction protocols follow condensation between appropriate bipyridine precursors and aldehydes either via modified Witting route (**TM 1–2**, **TM 4–11**) or through classical Knoevenagel condensation route (**TM 3**). As the aldehydes **Ald 1–7** are not commercially available, they have been synthesized in bulk amount (ca 3–15 gm) using standard synthetic procedures. The 4–(N,N–dialkylamino) benzaldehydes **Ald 1–2** bearing long alkyl chains (C_{10} and C_{14} respectively) have been prepared following routine synthetic methodologies that originate from N–alkylation of N–methyl aniline (see Scheme 4.3). As the bipyridine **TM 1** bear hydroxy groups at the distant end of the alkyl chain, the synthetic pathway to obtain the corresponding aldehyde (**Ald 1**) takes care abo-

Chart 4.1

m = n = 8, X = Y = OH (**TM 1**)
m = n = 12, X = Y = H (**TM 2**)

m = 12, X = H (**TM 3**)

TM 4

TM 5

TM 6

TM 7

TM 8

TM 9

TM 10

TM 11
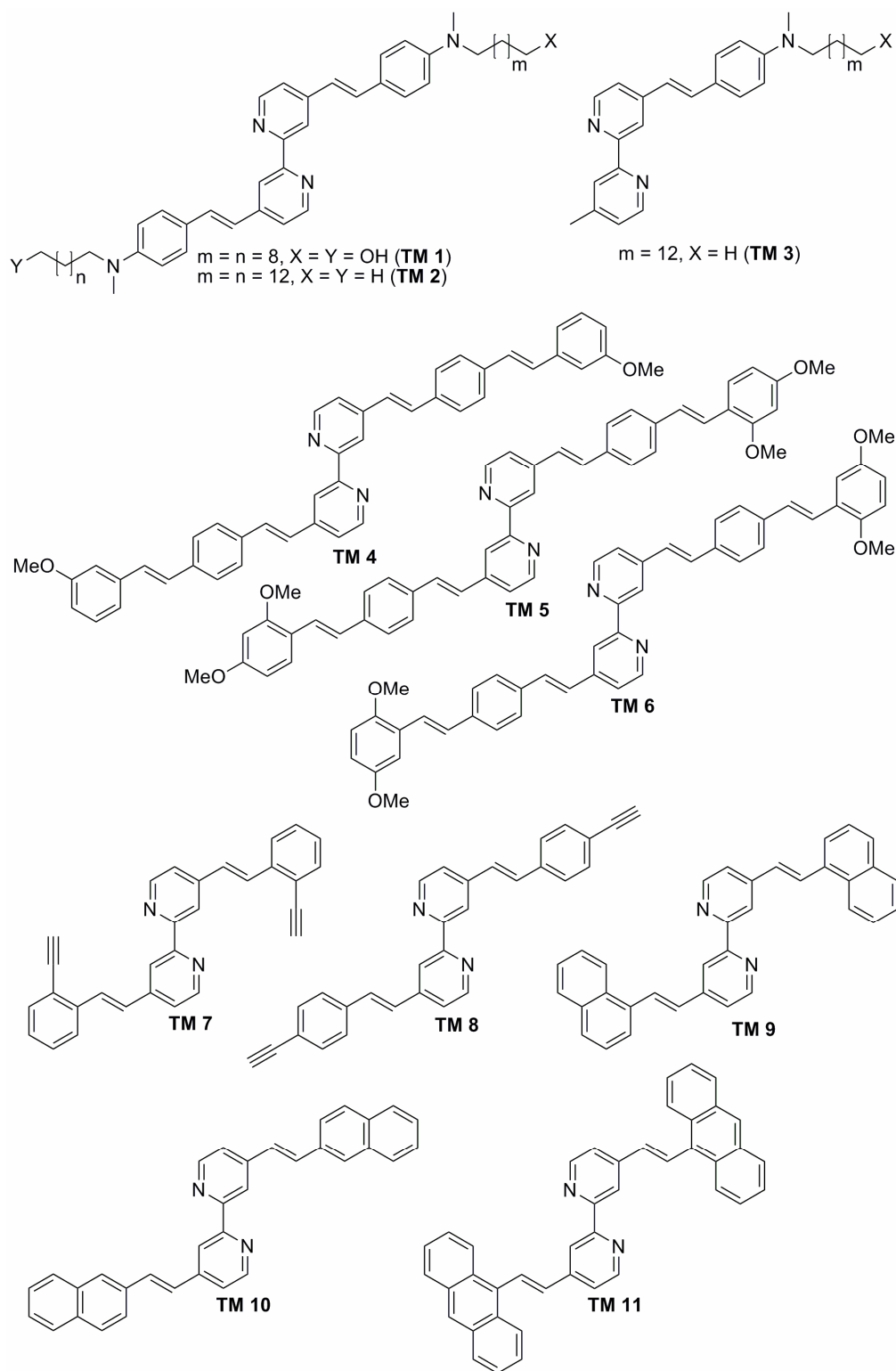
-ut reactivity of the concerned functional group (–OH) during course of the reaction steps which are either basic or acidic. Accordingly, the hydroxy group has been undergone

routine base or acid tolerable protection–deprotection synthetic strategy in order to keep the concerned group intact at the end of the reaction steps. At the first step, the di–ol (**1**) has been undergone a controlled mono–bromination by HBr in refluxing toluene using an analogous procedure reported by Chong et al.[18] The hydroxy group of thus prepared 10–bromodecan–1–ol (**1a**) has then been protected by formation of its tetrahydropyranyl (THP) ether after overnight stirring of a THF solution of **1a** containing 1.5 equivalents of
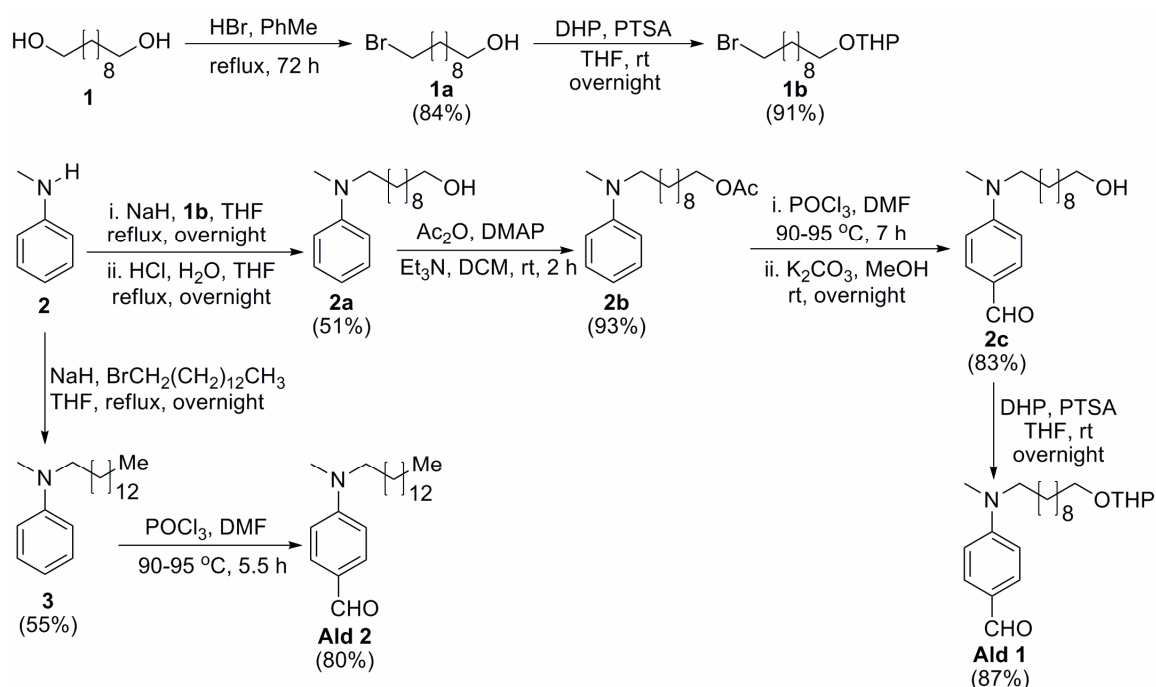
Scheme 4.3 Synthesis of the 4–(N–methyl–N–alkyl)amino benzaldehydes.

3,4–dihydro–2H–pyran (DHP) and 5 mole % of p–toluenesulphonic acid (PTSA) as the catalyst. Successive N–alkylation of N–methyl aniline (**2**) has then been preformed with the THP protected 10–bromodecan–1–ol (**1b**) in refluxing THF in presence of NaH as base. After an acid mediated cleavage of the THP group of the respective product, the hydroxy containing N,N–dialkyl aniline (**2a**) has been obtained in a moderate yield (51%). The hydroxy group has then been almost quantitatively protected by acetyl functionalization in dichloromethane using acetic anhydride in presence of catalytic amount (10% mol) of 4–dimethylamino pyridine (DMAP). The next step involves Vilsmeier–Haack formylation of 10–(methyl(phenyl)amino)decyl acetate (**2b**) followed by cleavage of the acetyl group by K_2CO_3 in MeOH. The aldehyde **2c** has been obtained

in good yield (83%) after chromatographic purification, hydroxy group of which, has then been converted to its THP ether (**Ald 1**). Synthesis of 4–(methyl (tetradecyl)amino)benzaldehyde (**Ald 2**) involves N–alkylation of N–methyl aniline with 1–bromo–tetradecane followed by classical Vilsmeier–Haack formylation of the N,N–dialkyl aniline (**3**) in an analogous synthetic route described for the synthesis of **Ald 1**.

$R^1 = R^3 = R^4 = H, R^2 = OMe$ (**6a**)
$R^1 = R^3 = OMe, R^2 = R^4 = H$ (**6b**)
$R^1 = R^4 = OMe, R^2 = R^3 = H$ (**6c**)

S.N.	Reactant (**5a-c**)	Product (**6a-c**)	Product (**Ald 3-5**)
1	**5a**	**6a** (93%)	**Ald 3** (86%)
2	**5b**	**6b** (92%)	**Ald 4** (65%)
3	**5c**	**6c** (92%)	**Ald 5** (45%)
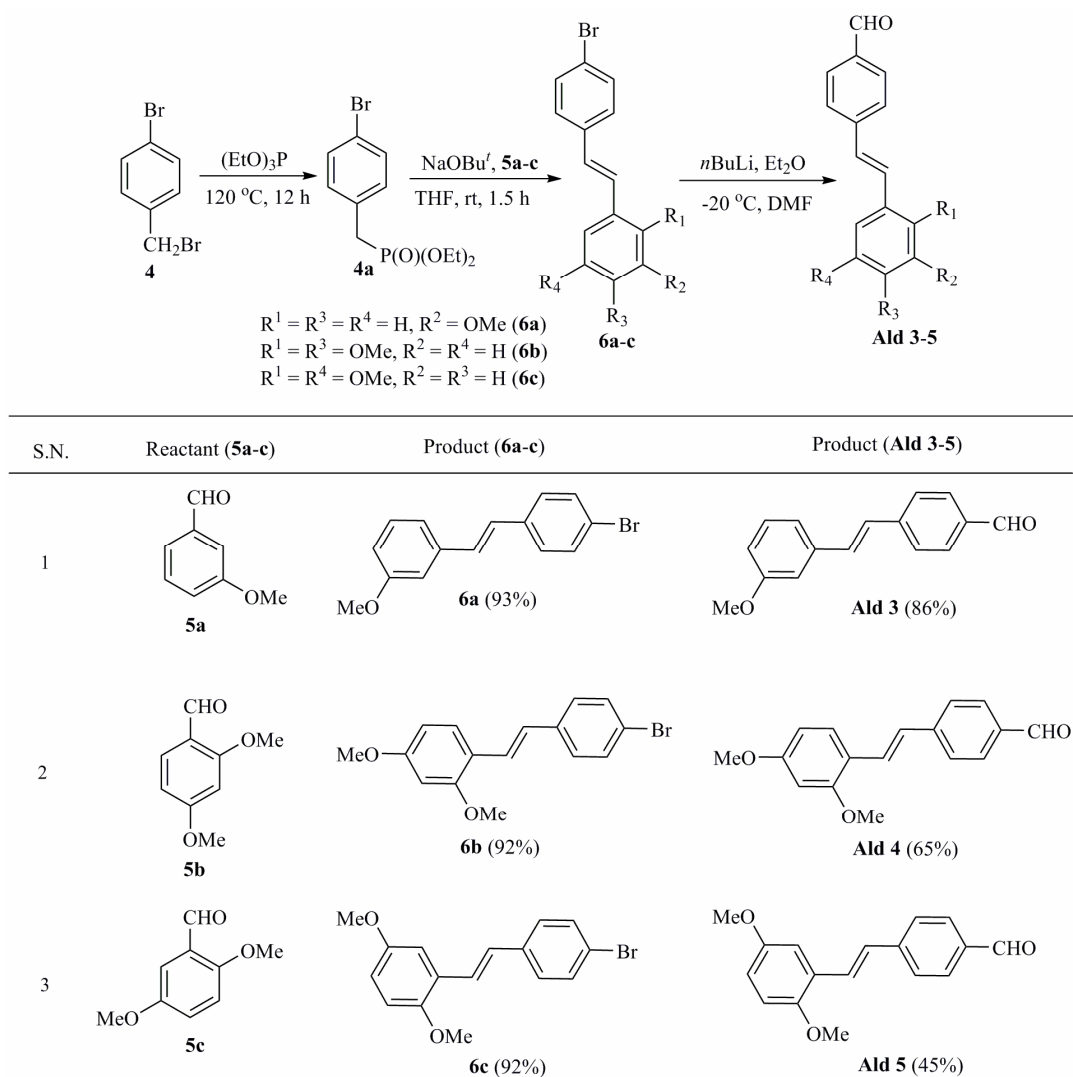
Scheme 4.4 Synthesis of the methoxy substituted 4–styryl benzaldehydes.

The methoxy substituted stilbene aldehydes (**Ald 3**–**5**) have been obtained accounting into a four–step synthesis using 4–bromo benzyl bromide (**4**) as the starting precursor. The corresponding phosphonate (**4a**) have been obtained (95%) by means of an Arbuzov reaction by heating an 1:1 mixture of **4** and triehtylphosphite at 120 °C for 12 h followed

by chromatographic (silica) removal of the untreated amount of **4.** Horner–Wordsworth–Emmons condensations between the phosphonate (**4a**) and appropriate methoxy benzaldehydes (**5a–c**) resulted in isolation of the bromo–stilbenes (**6a–c**) in excellent yields after a regular work–up followed by chromatographic purifications (see Scheme 4.4). Subsequent halogen–lithium exchange reactions of the bromo–stilbenes (**6a–c**) with *n*–BuLi at low temperature, followed by quenching of the lithiated intermediates with dimethylformamide yielded the corresponding benzaldehydes (**Ald 3–5**) in moderate to excellent yields (45–86%). Attempts to formylate the bromobenzenes (**6a–c**) in THF failed. Similarly, all the trials to increase yield of the aldehyde, **Ald 5** have remained ineffective. *E*–geometry of the vinylic bonds of these aldehydes (**Ald 3–5**) have been established on the basis of J_{HH} coupling constant (ca. 16 Hz) between the vinylic protons.
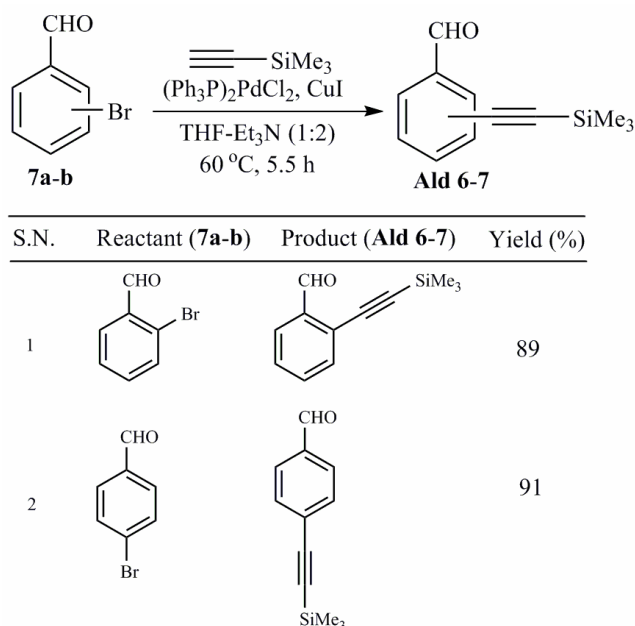
Scheme 4.5 Synthesis of the trimethylsilylethynyl benzaldehydes.

The trimeyhylsilylethynyl benzaldehydes (**Ald 6–7**) have been synthesized by means of Sonogashira coupling between the corresponding bromobenzaldehydes (**7a–b**) with trimethylsilylacetylene. Usage of 1% mol Pd catalyst with 2% mol of CuI in 2:1 mixture of Et$_3$N–THF solvent system resulted in isolation of the desired products (**Ald 6–7**) in excellent yields after heating the reaction mixture in a Schlenk tube at 60 ºC for 5.5 h, followed by chromatographic purifications (see Scheme 4.5).
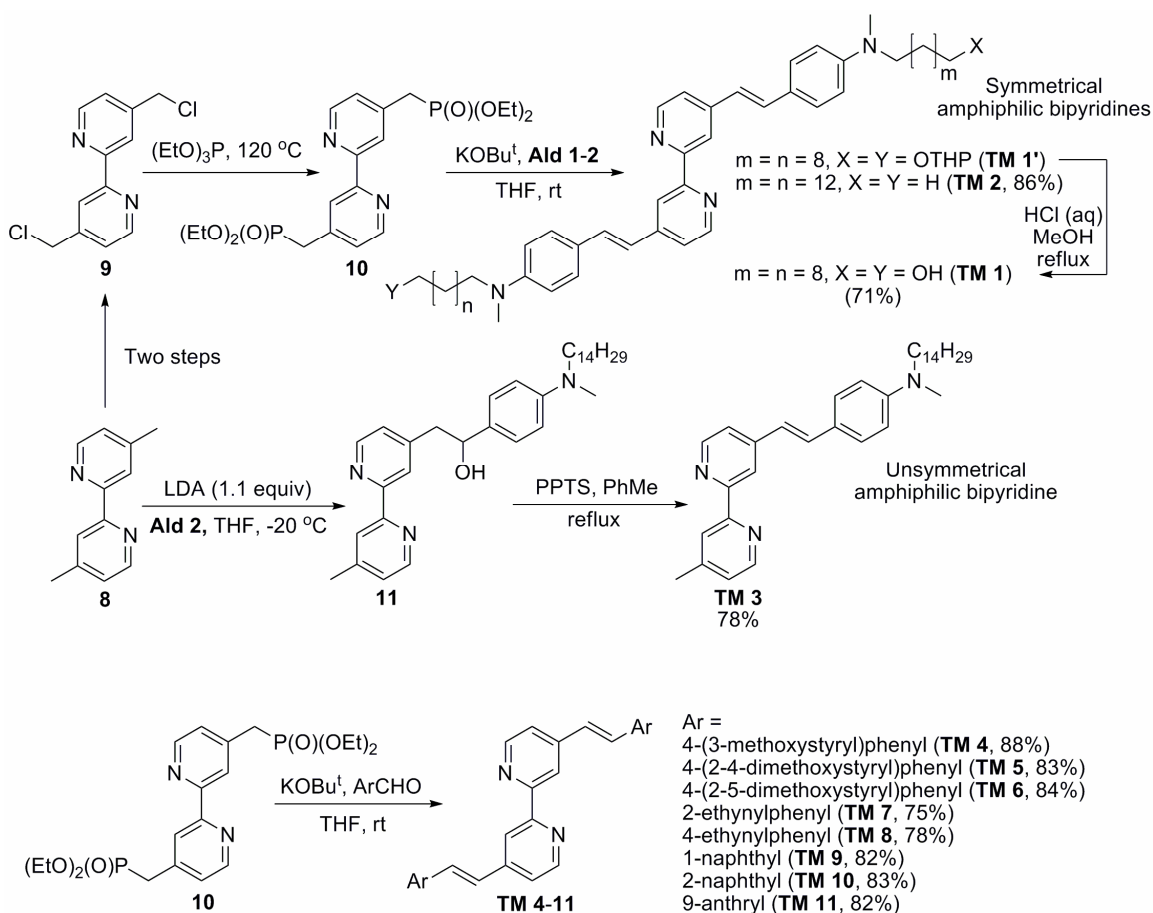
Scheme 4.6 Synthesis of the 4,4'–π–conjugated bipyridine ligands.

The 4,4'–π–functionalized–2,2'–bipyridine compounds (**TM 1–11**) have been synthesized following two different synthetic routes viz. (ii) Knoevenagel condensation between 4,4'–dimethyl–2,2'–bipyridine (**8**) and appropriate aldehydes (**TM 3**), and (ii) Horner–Wordsworth–Emmons (HWE) condensation of the *bis*–phosphonate precursor (**10**) with suitable aldehydes (**TM 1–2**, **TM 4–11**). Depending upon solubility of the resulting π–conjugated bipyridines (**TM 1–11**) in common organic solvents, they have been isolated in pure form either by simple filtration or by regular work–up and purification through column chromatography on silica (see experimental section). The tricky step of the synthesis is the halogenation of 4,4'–dimethyl–2,2'–bipyridine (**8**). Attempt to prepare the brominated precursor 4,4'–*bis*–bromomethyl–2,2'–bipyridine by a radical mechanized bromination of 4,4'–dimethyl–2,2'–bipyridine (**8**) with N–bromosuccinimide (NBS) in refluxing CCl_4 (in presence of radical initiator benzoyl peroxide or AIBN) has resulted in multiple number of products (closely spaced multiple

spots in TLC) from where, chromatographic separation of the desired product (4,4'–bis–bromomethyl–2,2'–bipyridine) could be difficult. This is in accord with some literature reports that also comment about poorer performance of this reaction,[19] although there are some reports that document even selective bromination (mono– or di–) of **8** under similar reaction condition.[20] However, in the present case, the chlorinated precursor, 4,4'–*bis*–chloromethyl–2,2'–bipyridine (**9**) has been used that has been synthesized following an efficient procedure (of preparing 4,4'–*bis*–halomethyl–2,2'–bipyridines) described by Fraser and co–workers.[21] The concerned synthetic strategy involves deprotonation of **8** by lithium diisopropylamide (LDA) followed by trapping of the resulting di–anion with chlorotrimethylsilane and finally chlorination with a commercially cheaper electrophile, hexachloroethane, in presence of a dry fluoride source e.g. CsF. An Arbuzov reaction of 4,4'–*bis*–chloromethyl–2,2'–bipyridine (**9**) with triethylphosphite at elevated temperature converted the former to the corresponding *bis*–phosphonate (**10**) which is the key precursor of the HWE reaction. Finally, the HWE condensation between **10** and appropriate aldehydes in presence of KOBu^t in THF at room temperature has afforded the symmetrical 4,4'–π–conjugated–2,2'–bipyridine compounds (**TM 1–2**, **TM 4–11**) in good yields (see Scheme 4.6). **TM 1** containing hydroxyl functionalization has required an acid–hydrolysis of its corresponding THP ether (**TM 1'**) and has been isolated in 71% overall yield. The unsymmetrical bipyridine chromophore (**TM 3**) has been synthesized via controlled Knoevenagel condensation between **8** and **Ald 2** followed by dehydration of the resulted mono–ol (**11**) in presence of catalytic amount of pyridinium–p–toluene–sulphonate (PPTS) in refluxing toluene (see Scheme 4.6).

4.2.2. Characterizations

All the synthesized compounds have been characterized by IR, NMR (^{1}H, ^{13}C, DEPT–135 etc.) spectroscopy, absorption and emission spectroscopy, LC–MS including successful elemental analysis. Relative low solubility of the compounds **TM 4–6** and **TM 9–11** in common organic solvents has precluded complete solution state spectroscopic characterization (e.g. ^{13}C NMR) of these compounds. Conformation of the vinylic bonds of the synthesized bipyridine compounds **TM 1–11** have unequivocally been designated as *E* on the basis of J_{HH} vinylic coupling constant of ca. 16 Hz (see experimental).

Although resonance due to the –OH group in the bipyridine **TM 1** and the intermediate compounds during protection–deprotection reaction pathway while synthesizing the aldehyde, **Ald 1** has not been detected by the ^{1}H NMR spectroscopy (room temperature), broad absorption due to the O–H stretching vibration (ca. 3400 cm^{-1}) has been observed in the relevant IR spectra. ^{1}H NMR resonances (aromatic zone) of the symmetrically and
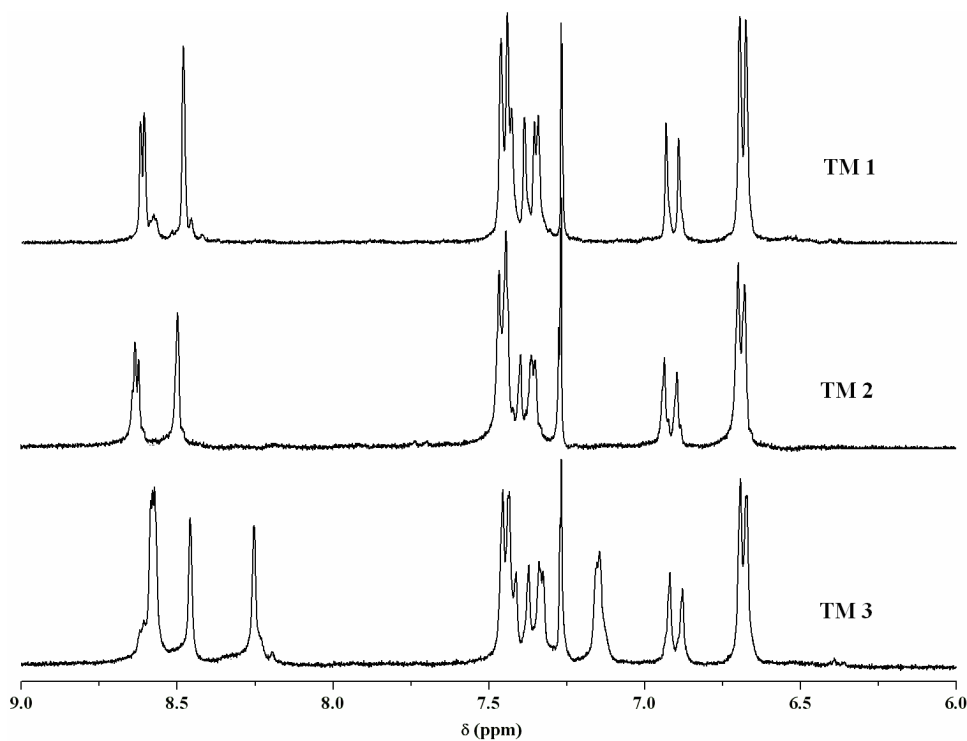
Figure 4.1 ^{1}H NMR chemical shifts of the amphiphilic bipyridines (**TM 1–3**) in the aromatic region.

dissymmetrically substituted amphiphilic bipyridine chromophores (**TM 1–3**) have been shown in Figure 4.1 and a summary of the resonances due to the pyridine ring protons (H^6, H^3, H^5) and the vinylic protons (H^7, H^8) for the compounds (**TM 1–11**) have been tabularized in Table 4.1. The lowest field signal in all the spectra is due to the H^6 proton, which is strongly deshielded by the adjacent nitrogen atom. The compounds **TM 1–2** and **TM 4–11** have exhibited only one set of signal (H^6, H^3, H^5) due to the pyridinic and vinylic protons as expected for their symmetrical substitutions (see Table 4.1). The unsymmetrical compound **TM 3** has rather revealed two different sets of signals (H^6, H$^{3,3'}$, H$^{5,5'}$) for these protons due to breakage of its molecular symmetry (see Figure 4.1). Again, all the spectra exhibit resonances due to the H$^{3,3'}$ protons at relatively down field

than the $H^{5,5'}$ protons as expected for the less–energetic *transoid–* conformation of the free bipyridine ligands.[7a] Similarly, in all the cases resonances due to the vinylic protons

Table 3.1 Pyridine and vinyl group resonances (^{1}H NMR) of the bipyridines (**TM 1–11**)
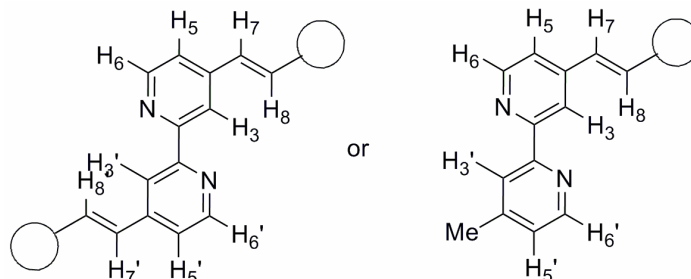
Compound	$H^{6,6'}$	$H^{3,3'}$	$H^{5,5'}$	H^8	H^7	J_{7-8} (Hz)
TM 1[a]	8.62	8.48	7.34	7.37	6.91	16.4
TM 2[a]	8.63	8.49	7.35	7.38	6.91	16.2
TM 3[a]	8.58	8.46	7.16	7.39	6.90	16.0
		8.25	7.34			
TM 4[b]	8.70	8.58	—	—	—	—
TM 5[b]	8.69	8.57	—	7.42	7.13	16.3
TM 6[b]	8.70	8.56	7.25	7.44	7.29	16.4
TM 7[a]	8.70	8.52	7.30	7.95	7.23	16.4
TM 8[b]	8.67	8.54	7.49	7.62	7.44	16.4
TM 9[b]	8.76	8.66	—	8.44	7.48	16.2
TM 10[b]	8.74	8.64	—	—	—	—
TM 11[b]	8.81	8.65	—	8.53	7.17	16.4

[a] recorded in CDCl$_3$, [b] recorded in DMSO–d$_6$

$H^{8,8'}$ have been observed in the relatively down field region of the relevant spectra than that of the $H^{7,7'}$ vinylic proton resonances. ^{1}H NMR spectra of all the amphiphilic bipyridines (**TM 1–3**) have shown a sharp singlet at δ ~3.0 (3H) corresponding to resonance of the N–Me protons. Relevant spectrum of the compound **TM 3** exhibits another strong singlet at δ ~2.45 (3H) due to the resonance of the 4–picolyl protons (see experimental). Similarly, sharp singlets at δ ~3.9 (3H) in the ^{1}H NMR spectra of the oligophenylenevinylene bipyridine compounds (**TM 4–6**) (one for **TM 4** and two for **TM 5** and **6**) are attributed to the resonances of the methoxy protons attached to the π– backbone of these compounds. The ethynyl substituted bipyridines (**TM 7–8**) have been

obtained from the corresponding trimethylsilyl group protected ethynyl benzaldehydes (**Ald 6–7**). However, subsequent ^{1}H NMR spectral analyses on the compounds **TM 7–8** haven't exhibited any resonance due to the trimethylsilyl group, rather a sharp singlet at δ
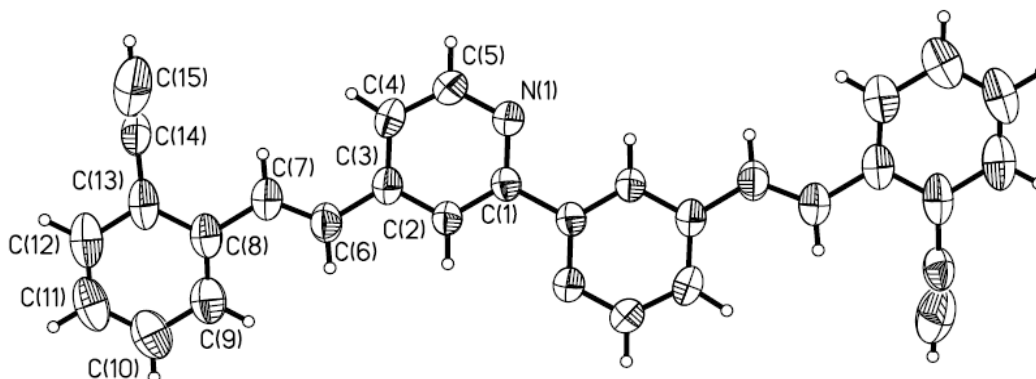

Figure 4.2 ORTEP drawing for the crystal structure of the compound **TM 7** in 50% confidence level. Only the asymmetric unit has been labeled. The various bond lengths are observed as follows: C(Ar)–C(Ar) 1.357–1.411 Å, C(vinyl)–C(vinyl) 1.312(3) Å, C–N 1.334–1.337 Å, C(sp)–C(sp) 1.004(4) Å.

3.46 (1H) for **TM 7** and δ 4.27 (1H) for **TM 8** have been observed that are attributable to the resonances due to the acetylenic ($\equiv$C–H̲) protons. The trimethylsilyl groups have been cleaved in the basic reaction medium while quenching of the respective reactions, which generate OH$^-$ ion due to hydrolysis of KOBu^t. LC–MS analysis on all these compounds have shown appropriate m/z peaks corresponding to the molecular ion peaks (see experimental). Thus, spectroscopic analyses on all these newly synthesized bipyridine compounds (**TM 1–11**) undoubtedly corroborate with their proposed chemical structures as shown in the Chart 4.1. The compound **TM 7** has further been characterized by single crystal X–ray crystallography. Dark brown block shaped crystals suitable for X–ray diffraction have been obtained after a slow evaporation of CHCl$_3$–MeOH solvent mixture. A thermal ellipsoidal plot of the relevant crystal structure has been shown in Figure 4.2. Crystal data for compound **TM 7** has been summarized in Table 4.2. The compound **TM 7** crystallizes in *P2$_1$/n* space group with a center of inversion laying middle of the 2,2' C–C bond. (Figure 4.2). In the relevant crystal structure, the phenyl and pyridyl rings are tilted by an angular span of 12.02(18)°, thus are almost coplaner. The crystal structure clearly shows the *E–* geometry of the vinyl bonds. A view of packing of the molecules in the relevant crystal structure has been shown in Figure 4.3.

Table 4.2 Crystal data and structure refinement parameters for **TM 7**.

Formula	$C_{30}H_{20}N_2$
Formula weight	408.48
T [K]	298(2)
λ [Å]	0.71073
Crystal System	Monoclinic
Space Group	$P2_1/n$ (No. 14)
Unit cell dimensions	
a [Å]	7.4196(6)
b [Å]	13.6299(12)
c [Å]	12.9800(14)
β [º]	98.887(10)
V [Å^3]	1106.60(19)
Z, ρ_{calcd} [gm cm^{-3}]	2, 3.226
μ (mm^{-1})	0.072
$F(000)$	428
Size (mm)	0.70 x 0.20 x 0.10
θ range for data collection (º)	3.41–25.00
Limiting indices	–8<=h<=5,
	–13<=k<=11,
	–15<=l<=14
Reflections collected / unique	4402/1954 [R(int) = 0.0236]
Completeness to theta	99.7 %
Data / restraints / parameters	1954 / 0 / 145
Goodness–of–fit on F^2	0.916
Final R indices [I>2σ(I)]	$R_1 = 0.0481$, w$R_2 = 0.1240$
R indices (all data)	$R_1 = 0.0955$, w$R_2 = 0.1410$
Largest diff. peak / hole (e.Å^{-3})	0.200 / –0.141 e.A^{-3}

4.2.3. Linear optical (absorption and emission) properties of TM 1–11

Electronic absorption and emission properties of the newly synthesized π–conjugated bipyridyl chromophores or fluorophores (**TM 1–11**) have been investigated in dilute dichloromethane at room temperature (298±2 K). Relevant spectra have been shown in Figure 4.4 and the concerned optical data have been summarized in Table 4.3. From the relevant spectral data, it is very clear that, linear optical properties of these compounds are sensitive to the substituents at their π–backbone. Electronic absorption spectra of the amphiphilic bipyridine chromophores (**TM 1–3**) and the OPV functionalized bipyridines (**TM 4–6**) are characterized by a broad structureless absorption band in UV or near–visible region (λ_{max} 365–395 nm) with higher molar absorption coefficient (ε ~ 35000–

60000). These bands are unambiguously assigned to the intra–ligand charge transfer (ICT) bands which are originated due to charge delocalization from the dialkylamino (**TM 1–3**) or methoxy (**TM 4–6**) donor groups to the pyridinic acceptor subunits through the π–transmitters in the 'push–pull' molecules. That these bands appear because of an intra–molecular charge transfer (ICT) is obvious from the following observations: (i) the
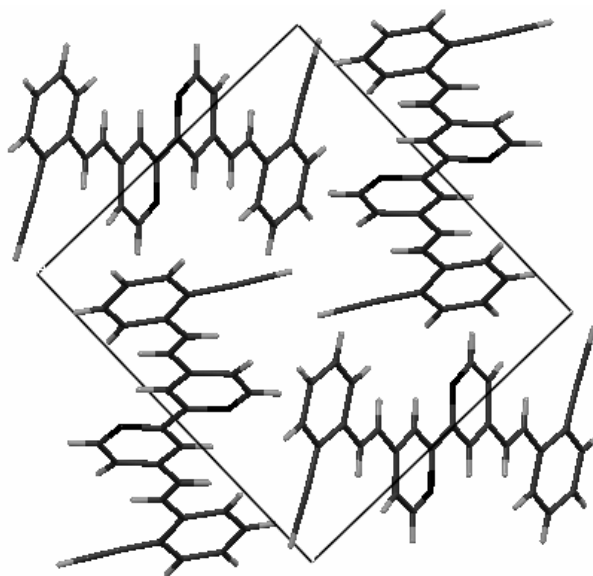
Figure 4.3 Packing of the molecules in the crystal structure of **TM 7** viewed down the crystallographic *a*–axis.

absorptions are fairly broad and intense and (ii) position of the bands is rather sensitive to the polarity of the fluid medium (see Section 4.2.4). From the absorption spectra of the amphiphilic bipyridine chromophores (**TM 1–3**), it is evident that introduction of the hydroxy function into the alkylamino donor subunits has not induced any significant shift in the position of the absorption maxima of the concerned compounds. The lower homologues of **TM 4–6** namely, 4,4'–di(2–(3–methoxyphenyl)ethynyl)–2,2'–bipyridine (**TM 4'**, λ_{max} = 315 nm), 4,4'–di(2–(2,4–dimethoxyphenyl)ethynyl)–2,2'–bipyridine (**TM 5'**, λ_{max} = 347 nm) and 4,4'–di(2–(2,5–dimethoxyphenyl)ethynyl)–2,2'–bipyridine (**TM6'**, λ_{max} = 358 nm)[13] respectively (not included in the thesis) absorb in UV region, position of the absorption maxima being sensitive to position of the substituents / donor groups in the π–backbone. However, a strong bathochromic shift of the absorption maxima (~ 40–80 nm) has been observed upon changing the donor groups from methoxy (**TM 4'–6'**) to dia-

Figure 4.4 Electronic absorption (Left) and corresponding emission (right) spectra of **TM 1–11** (top to bottom). Concentrations of the samples have been adjusted to maintain OD ≈ 0.05. All the excitations have been performed at the lowest energy absorption maxima. The relevant fluorescence spectra have been normalized with respect to their respective emission maxima.
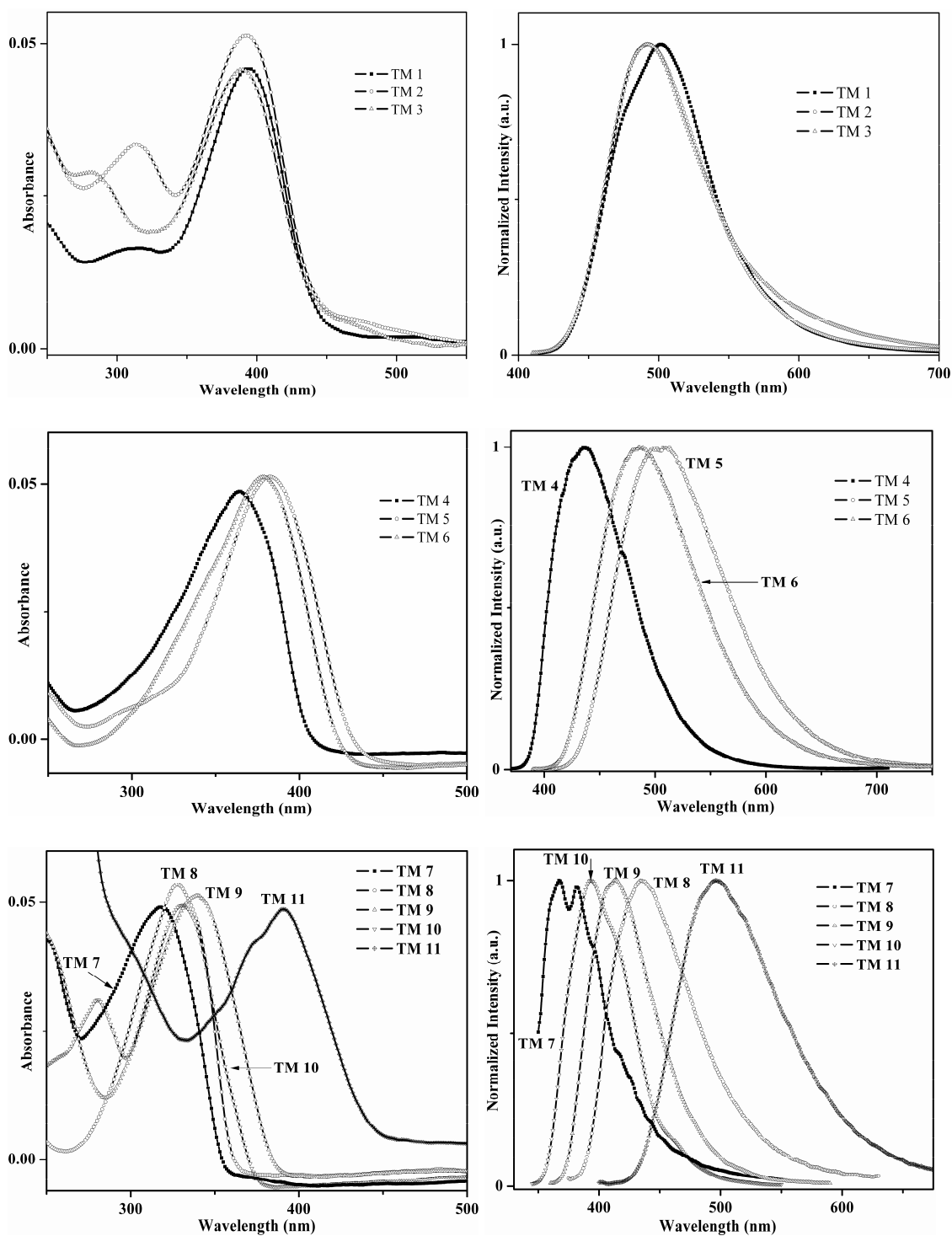
-lkylamino function (**TM 4–6**). Moreover, a bathochromic shift of the absorption maxima by 50 nm, 37 nm and 22 nm respectively have been observed upon increasing the conjugation from styryl (**TM 4'–6'**) to bistyryl (**TM 4–6**). This is undoubtedly in accord with the expectation, as increasing conjugation decreases the energy of the electronic transitions. At this point it is worth mentioning that, although a bathochromic shift of the absorption maxima is generally observed for the first homologation (from styryl to bistyryl), an additional red–shift has not been noticed for the second homologation (bistyryl to tristyryl) in a similar OPV functionalized bipyridine chromophore containing dibutylamino donor groups (λ_{max} = 421 nm).[7c] This has been explained accounting into decrease of charge transfer character upon increasing of the conjugation length and for the electron donor–acceptor OPV molecules containing the dialkylamino chromophoric groups, a saturation in λ_{max} has been observed at ca. 421 nm.[7c] However, as the OPV compounds **TM 4–6**, themselves are sparingly soluble in common organic solvents (e.g. DCM, chloroform, THF etc.) attempt to further increase the conjugation of the compounds to tristyryl homologue has not been made accounting that, the tristyryl homologues can nevertheless have same or enhanced solubility than the bistyryl derivatives. The ethynyl substituted bipyridines (**TM 7–8**), although both of them have exhibited similar absorption patterns (Figure 4.4) , position of the respective absorption maxima and molar absorptivity (ε) of the concerned compounds are found to be affected by the position of the ethynyl groups in the phenyl ring. Changing the position of the acetylene group from *ortho–* (**TM 7**) to *para–* position (**TM 8**) in the styryl backbone has caused a 10 nm red–shift of the absorption maxima and a large enhancement of the molar extinction coefficient. However, both the compounds are found to absorb in the UV region and their respective absorption maxima at 318 nm (**TM 7**) and 328 nm (**TM 8**) represent $\pi–\pi^{*}$ transition of the molecules. The polyaromatic hydrocarbons, naphthalene and anthracene show structured absorption patterns in DCM at λ_{max} = 277 nm and 377 nm respectively (room temperature). However, upon conjugation of the concerned hydrocarbons with the pyridine heterocycle via the vinyl linkages results in significant bathochromic shift of their respective absorption maxima (ca. 50–60 nm for **TM 9–10** and ca. 13 nm for **TM 11**) and the structural feature of the absorption bands disappears. This phenomenon clearly indicates the electronic grouping between the polyaromatic

hydrocarbons (naphthalene and anthracene) with the pyridine electron–pulling units and the corresponding absorptions at 340, 330 and 390 nm for **TM 9–11** respectively might be attributed to the charge–transfer (ICT) band.

Table 4.3 Summary of the linear optical data for the bipyridine compounds (**TM 1–11**).

Compound	λ_{max} (nm)	ε (L.mol^{-1}.cm^{-1})	λ_{em} (nm)	$\Delta\lambda$ (nm)	Φ_{em}
TM 1	395	42274	495	100	0.138
TM 2	393	43585	493	100	0.135
TM 3	390	35114	490	100	0.096
TM 4	365	61736	435	70	0.590
TM 5	384	49257	505	121	0.700
TM 6	380	45855	488	108	0.730
TM 7	318	29034	382	64	0.037
TM 8	328	37125	435	107	0.018
TM 9	340	20145	415	75	0.054
TM 10	330	51200	392	62	0.114
TM 11	390	—	495	105	0.082

Photoluminescence has been observed for all the synthesized bipyridine compounds **TM 1–11** at room temperature. All the solutions have been excited at their respective lowest energy absorption maxima, and in all the cases, origination of the emission bands has been crosschecked by correlating the excitation spectra with the absorption spectra of the respective compounds. Fluorescence spectra of the compounds **TM 1–11** in DCM at room temperature have been shown in Figure 4.4 and subsequent optical data have been summarized in Table 4.3. The fluorescence quantum yields have been measured using quinine sulfate as the reference substance whose luminescence quantum yield in 1N H$_2$SO$_4$, is known to be 0.545.[22] The individual quantum yields of the compounds have been calculated using the equation:

$$\frac{\Phi_{sample}}{\Phi_{standard}} = \frac{A_{sample}}{A_{standard}} \times \frac{OD_{standard}}{OD_{sample}} \times \frac{\eta^2_{sample}}{\eta^2_{standard}}$$

where standard correspond to the reference substance (here quinine sulfate) and sample denotes the substance whose quantum yield has to be measured, A is the integrated emission intensity, OD stands for the optical density at the excited wavelength and η is the refractive index of the medium (for dichloromethane η = 1.424 and for water

solutions η = 1.333). Dilute solutions with OD ≈ 0.05 at the excitation wavelength have been used for the quantum yield measurements. Optically matched solutions of the sample and the reference were measured under same operating condition and instrumental settings.

As revealed by the emission spectra of the amphiphilic (**TM 1–3**) and the OPV functionalized (**TM 4–6**) bipyridine chromophores, these compounds exhibit broad structureless emission bands in visible region when excited at their respective lowest energy absorption maxima. Alike absorption spectra, the emission spectra of the amphiphiles (**TM 1–3**) have not shown any alteration / considerable shift of the emission maxima upon introduction of the hydroxy functionality into the N–alkylamino donor sub–chromophores of the concerned bipyridine compounds. The OPV functionalized bistyryl compounds **TM 4–6** are the most fluorescent among all the compounds demonstrated here (Φ_{em} ≈ 0.60–0.70). The compounds **TM 5–6** bearing two methoxy donor groups emit at longer wavelength than the compound **TM 4** bearing only one donor (methoxy) group (see Figure 4.4). At this point, it is important to mention that, fluorescence quantum yield of the bipyridine chromophores are strongly influenced by the position of the donor groups at the π–backbone of the compounds. It has also been observed that, the 4,4'–*bis*–styryl–2,2'–bipyridines become more fluorescent when the electron donor groups are substituted on phenyl ring at *ortho*– and *meta*– positions.[13] In this regard it is worth mentioning that, the compound 4,4'–di(2–(2,5–dimethoxyphenyl) ethynyl)–2,2'–bipyridine (lower homologue of **TM 6**, commonly known as N965L)[13] which has the methoxy substituents at *ortho*– and *meta*– positions in the phenyl ring (λ_{em} = 450 nm) has a high quantum yield (Φ_{em} = 0.49) compared to its other positional isomers. The compound N965L has been found to show application toward fabricating electroluminescent devices (OLED).[13] The fluorescence properties of the bipyridine chromophores are also dependent upon the conjugation length. For example, the styryl homologues of **TM 4–6** i.e. **TM 4'–6'** have photoluminescent quantum yield of 0.08, 0.01 and 0.49 respectively but, it is amazing to observe a large fluorescence enhancement upon increasing the conjugation from styryl (**TM 4'–6'**) to bistyryl (**TM 4–6**) (Φ_{em} = 0.59, 0.70, 0.73 respectively). Note the 70 times enhancement of quantum yield from **TM 5'** to **TM 5**.

The ethynyl substituted bipyridines (**TM 7**–**8**) exhibit different emissive natures in DCM (see Figure 4.4). The 2–ethynyl substituted bipyridine (**TM 7**) shows some structure in its emission band (λ_{em} = 382 nm) but, broad structureless emission band (λ_{em} = 435 nm) has been observed for the other positional isomer bearing the acetylene function at 4– position of the phenyl ring (**TM 8**). Thus, the emission band of the 4–ethynyl substituted compound (**TM 8**) is 53 nm red–shifted than that of the 2–ethynyl substituted compound (**TM 7**). Again, a two–fold enhancement of the fluorescent quantum yield has been noticed for the 2–ethynyl derivative (**TM 7**) compared to the 4–ethynyl one (**TM 8**).

Although, naphthalene and anthracene both exhibit prominent structural features in their emission spectra (λ_{em} = 336 and λ_{em} = 452 respectively), broad structureless fluorescent bands have been observed upon their electronic association with the pyridine acceptor subunit in the compounds **TM 9**–**11**. The 2–naphthyl vinyl compound **TM 10** shows a 23 nm blue–shifted emission band (λ_{em} = 415 nm) compared to the 1–naphthyl vinyl compound **TM 9** (λ_{em} = 392 nm) and the former one is found to be doubly emissive (Φ_{em} = 0.114) compared to the latter one (Φ_{em} = 0.054). The 9–anthryl vinyl compound **TM 11** exhibits a broad structureless blue luminescence at 495 nm with a photoluminescent quantum yield of 0.082.

Thus, the overall photo–physical investigations on the bipyridine compounds **TM 1**–**11** clearly illustrate that; absorption and emissive properties of the π–conjugate bipyridine compounds are immensely influenced by the nature and/or position of the donor substituents at their π– backbone and the conjugation length. Simple modification of the π– backbone of such chromophores allows tuning of their photo–physical properties.

4.2.4. Solvatochromism of the amphiphilic (TM 1–3) and the OPV bipyridine (TM 5–6) derivatives

The term 'solvatochromism' is defined as the influence of solvent polarity on the electronic properties (absorption, emission etc.) of chromophoric compounds i.e. alteration of band position, shape, intensity etc. with the change of solvent polarity. If the ground electronic state of a chromophoric compound is more stabilized by solvation compared to its first excited electronic state, then more energy is required to excite the

molecules, thereby making the relevant compound to absorb at a higher energy (lower wavelength). Therefore, the corresponding absorption band shifts to lower wavelength (hypsochromic or blue shift) and a negative solvatochromism is observed. The reverse is true for the positive solvatochromism, where a bathochromic or red shifted absorption band is noticed with increasing solvent polarity. The same convention holds for the shifting of emission or fluorescence band positions with solvent polarity.

The effect of medium on the absorption and emission properties of the amphiphilic bipyridine compounds (**TM 1–3**) and dimethoxy–substituted oligophenylenevinylene bipyridine compounds (**TM 5–6**) have been investigated in multiple (non–polar to polar) solvents. It has already been stated in the previous section that, these compounds exhibit broad absorption bands with higher molecular extinction coefficients ($\varepsilon \sim 23000 - 50000$ $L{\cdot}mol^{-1}{\cdot}cm^{-1}$) due to intra–ligand charge transfer (ILCT) from the dialkylamino or methoxy donor groups to the pyridyl acceptor subunits. Absorption due to the charge transfer transition or emission from the corresponding excited state is susceptible to the polarity of the medium and a Stokes shift is expected upon changing the polarity of the fluid in which the compound is dissolved. This phenomenon indeed correctly denotes an absorption in the UV–visible spectrum as ICT band of a 'push–pull' or 'electron donor–acceptor' molecule. On the other hand, the emissive nature of a compound is strongly dependent upon the rate of several competitive nonradiative decay processes of the exited fluorescent state. In general, the change of dipole moment is more prominent in the exited electronic state compared to the ground electronic state of the molecules and so, polarity of the fluid medium will have more profound effect on the emissive property than on the absorption nature of a compound. For example, if the fluid medium allows slow relaxation of the excited fluorescent state, then, a broader emission band is observed in the corresponding fluorescent spectra.

Solvatochromic behavior of the amphiphilic bipyridines (**TM 1–3**) have been examined using eight different solvents. Figure 4.5 depicts the pictorial representation of the phenomenon and Table 4.4 summarizes the corresponding optical data. **TM 1**, bearing two hydroxy groups at the alkylamino functionalities is very poorly soluble in hexane and so, the subsequent absorption spectrum has not shown any significant absorption (OD << 0.01) due to the relevant compound. In all other solvents (except hex-
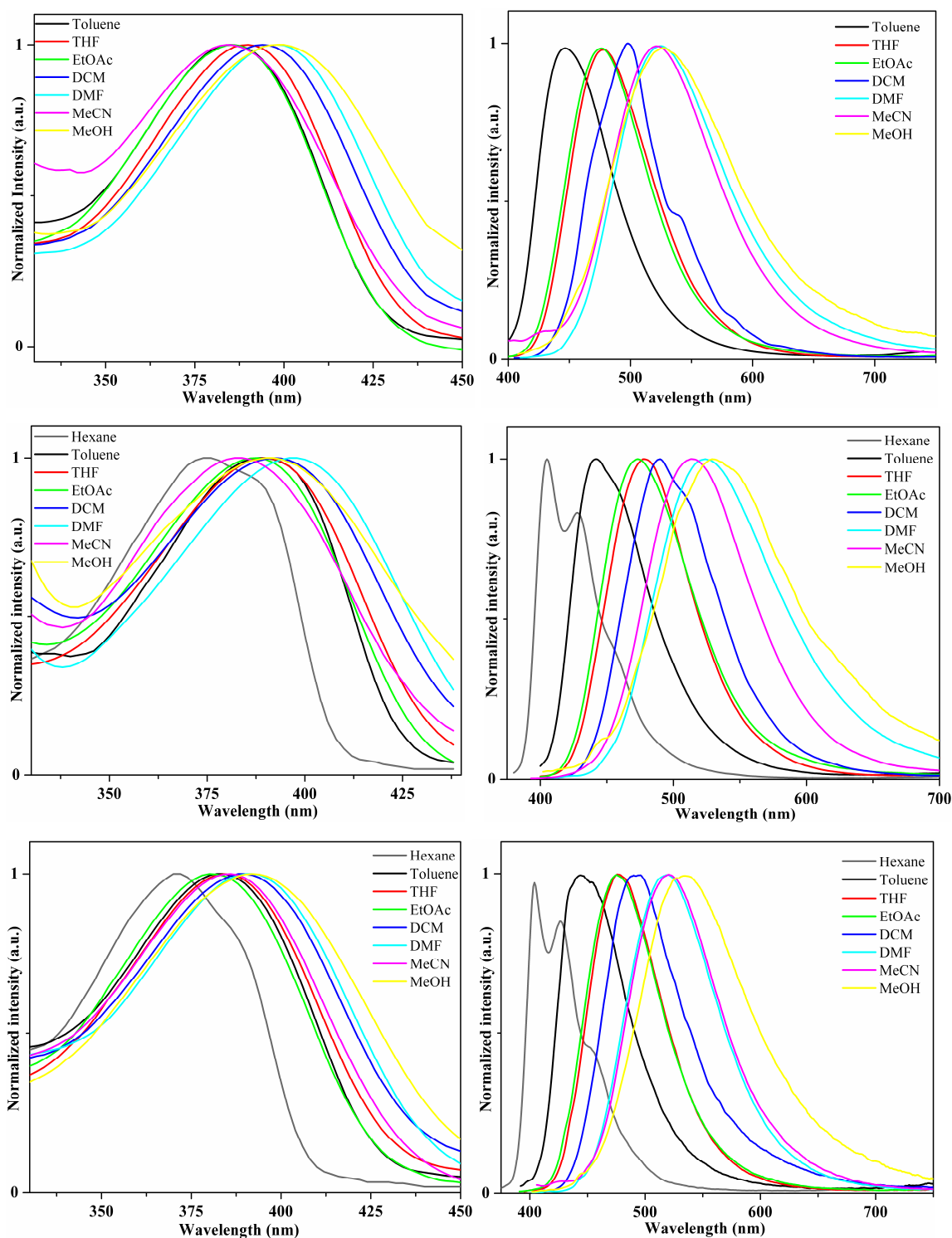
Figure 4.5 Absorption (left) and emission (right) spectra of the amphiphilic bipyridines (**TM 1**–**3**) (Top: **TM 1**, Middle: **TM 2**, Bottom: **TM 3**) in different solvents. Only the lowest energy absorption band has been displayed for clarity. All the excitations have been performed at the relevant lowest energy absorption maxima (OD ≈ 0.05). For a clearer view, all intensities have been normalized at the respective band maxima.

-ane), broad structureless absorption patterns have been observed (see Figure 4.5). However, an irregular trend in the position of the absorption band maxima has been observed in the Reichardt's $E_T(30)$ solvent polarity scale.[23] While changing the solvent from hexane to THF has led to a 10–13 nm bathochromic shift of the respective absorption maxima, usage of more polar solvent ethyl acetate, has resulted in a small hypsochromic shift (1–5 nm), that contradicts the expectation. Although increment of the polarity from ethyl acetate to DMF has shown a further regular bathochromic shift (8–14 nm) of the absorption maxima, acetonitrile [$\{E_T(30)\}_{MeCN} > \{E_T(30)\}_{DMF}$] has induced a

Table 4.4 Summary of the optical data (absorption and emission) for **TM 1–3** in various solvents at room temperature.

Solvent	$E_T(30)$	TM 1			TM 2			TM 3		
		λ_{max}	λ_{em}	$\Delta\lambda$	λ_{max}	λ_{em}	$\Delta\lambda$	λ_{max}	λ_{em}	$\Delta\lambda$
Hexane	32.4	—	—	—	380	428	48	372	426	54
Toluene	33.9	385	445	60	390	440	50	382	445	63
THF	37.4	391	476	85	390	477	87	385	475	90
EtOAc	38.1	386	476	90	389	473	84	381	476	95
DCM	40.7	395	495	100	393	493	100	390	490	100
DMF	43.2	400	524	124	397	524	127	392	518	126
MeCN	45.6	385	521	136	383	515	132	386	521	135
MeOH	55.4	398	530	132	390	535	145	392	533	141

second hypsochromic effect (6–15 nm). It is again surprising to observe that in MeOH, the corresponding ICT bands have appeared in almost the same or higher energy than that in DMF. However, Stokes shift of the absorption maxima demonstrates the polarity–dependent nature of the ground electronic state of the relevant compounds (**TM 1–3**). The molecules in their solution (**TM 1–3**) have been excited at the respective lowest energy absorption maxima and compared to their absorption spectra; the effect of medium on the position and/or shape of the emission bands in the corresponding fluorescent spectra has been found to be profound. The relevant emission spectra consist of one broad structureless band except in hexane (**TM 2–3**) that reveal some structural features (Figure 4.5). The fluorescence bands in methanol have appeared as the broadest bands among all the solvents used in the present study. As shown in Figure 4.5 and Table 4.4, significant

bathochromic Stokes shift of the emission maxima has been observed with increasing polarity in the Reichardt's $E_T(30)$ solvent polarity scale though there is a little irregularity too. The largest separation between the emission and absorption maxima has been observed in acetonitrile ($\Delta\lambda$ = 136 nm) for **TM 1**, whereas, for **TM 2** and **3** this has been observed in methanol ($\Delta\lambda$ = 145 nm for **TM 2** and $\Delta\lambda$ = 141 nm for **TM 3** respectively). In all the cases, excitation spectra have shown good correlation with the absorption spectra. Prominent red–shift of the emission maxima with increasing solvent polarity clearly comments about more polar nature of the excited fluorescent state of the molecules than their ground states. Presence of the hydroxy functionalization has not shown much disparity in solvatochromic behavior of these compounds.

Table 4.5 Collection of linear optical data for **TM 5–6** in different solvents.

Solvent	$E_T(30)$	TM 5				TM 6			
		λ_{max}	λ_{em}	$\Delta\lambda$	Φ_{em}	λ_{max}	λ_{em}	$\Delta\lambda$	Φ_{em}
Toluene	33.9	384	463	79	0.551	381	456	75	0.575
1,4–dioxane	36.0	384	478	94	0.579	381	468	87	0.620
THF	37.4	384	487	103	0.644	380	476	96	0.722
DCM	40.7	384	505	121	0.700	380	488	108	0.730
DMF	43.2	387	530	143	0.429	382	516	134	0.613
DMSO	45.1	388	538	150	0.368	384	528	144	0.484
MeCN	45.6	379	536	157	0.429	375	518	143	0.663

As shown in the previous section (4.2.3), the oligophenylenevinylene bipyridine compounds (**TM 5–6**) show excellent emission at room temperature ($\Phi_{em} \approx 0.60 – 0.73$). The solvatochromic behavior of these compounds has been examined with seven different solvents. The variation of photoluminescent quantum yields has also been checked with solvent polarity. Respective optical data have been composed in Table 4.5 and the solvatochromic behavior has been presented in Figure 4.6. Extreme poorer solubility of these compounds (**TM 5–6**) in protic solvents (e.g. MeOH, EtOH etc.) has precluded spectroscopic measurements of the compounds in these solvents. Both the compounds show broad structureless absorption patterns in all the solvents and their absorption maxima are not found to be shifted to a significant extent with increment of

the solvent polarity. Thus, it can be said that, the ground electronic state of these OPV functionalized chromophores (**TM 5–6**) do not depend upon the polarity of the fluid medium. Such polarity independent nature of the ground electronic state has already been
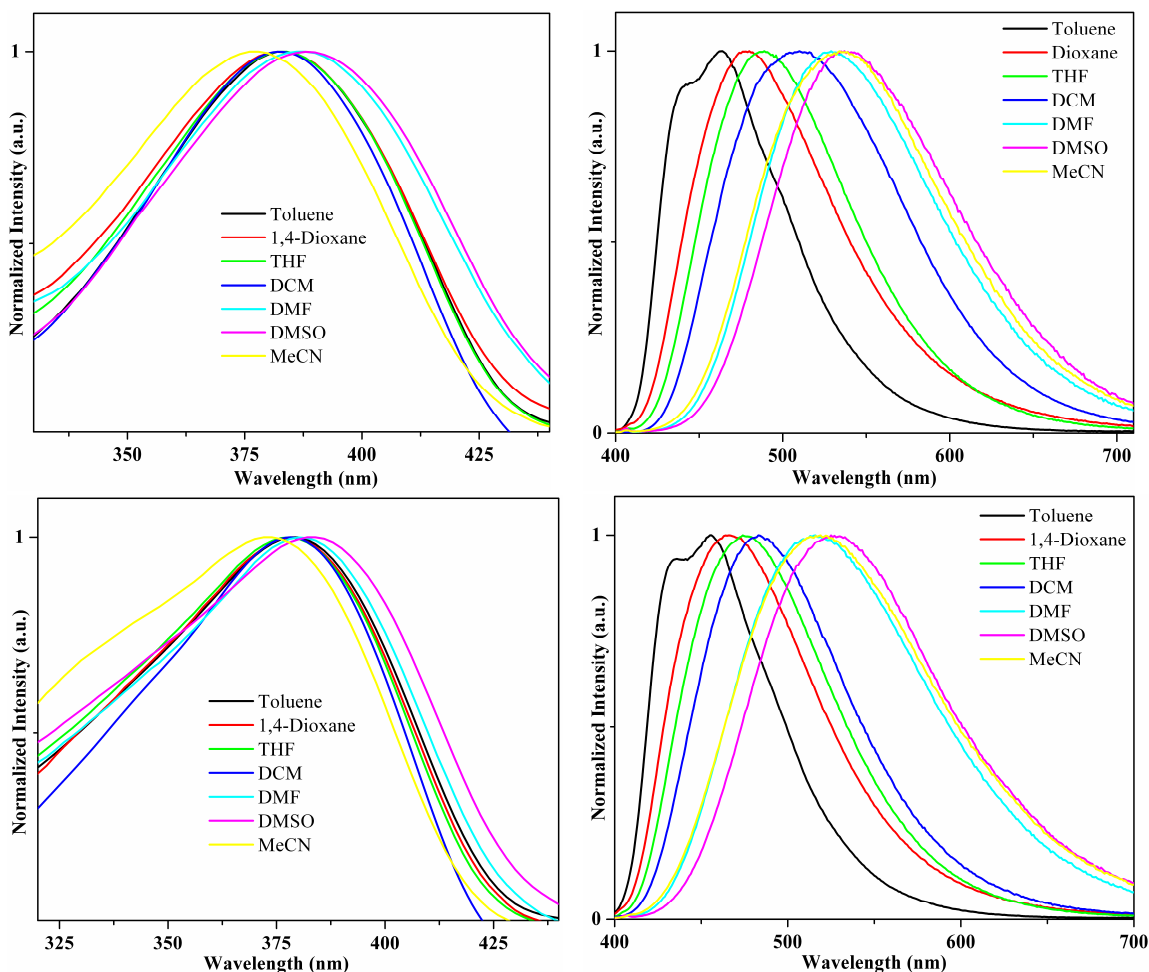

Figure 4.6 Solvatochromic behavior of **TM 5–6** (Top: **TM 5**, Bottom: **TM 6**) in different solvents (Left: absorption, Right: emission). Only the lowest energy absorption band has been displayed for clarity. All the intensities have been normalized with respect to the corresponding band maxima. The solutions have been excited at their respective absorption maxima after maintaining the optical density in a close proximity of 0.05.

noticed for similar OPV functionalized bipyridine chromophores containing dibutylamino donors.[24] In contrast to the absorption nature of the two compounds (**TM 5–6**); significant alteration in their fluorescence property has been observed with the variation of polarity of the medium. Broad, structureless emission bands have been observed in all the solvents except in hexane where, some structure could be observed. In all the

solvents, absorption or emission maxima of the compound, **TM 5** (that contains methoxy substituents at 2– and 4–positions) have appeared in slightly lower energy than that of compound, **TM 6** which contains donor (–OMe) substituents at 2– and 5– positions. It is evident from Table 4.5 and Figure 4.6 that, the magnitude of shift of the fluorescence maxima with increasing solvent polarity is much larger than that of the absorption maxima. For example, while changing the polarity of solvent from toluene to DMSO has led to a Stokes shift of the absorption maxima by only ca. 4 nm, the extent of shift of the relevant emission maxima lies in the range of 72–75 nm. This observation clearly manifests the more polar nature of the fluorescence excited state compared to the ground electronic state of the molecules. Significant change in photoluminescent quantum yields of these compounds has also been observed upon variation of the solvent polarity. It has been observed that a change in solvent polarity from toluene to DCM has resulted in a steady increase of the quantum yields of the compounds, while in more polar solvents; further decrease of the quantum yields has been noticed.

4.2.5 Controlled protonation of the amphiphilic bipyridine chromophores (TM 1–3)

The amphiphilic bipyridine chromophores (**TM 1–3**) have two different types of protonation sites, viz. (i) pyridine rings and (ii) amino groups. As pyridine is more nucleophilic than the amino functions, addition of controlled amount of an acid (≤ 2 equivalents) to a solution containing the bipyrdines (**TM 1–3**), will result in selective protonation of the pyridine nitrogens first instead of the alkyl amino groups (see Scheme 4.7). As pyridinium group is more electron drifting than simple pyridine, the electronic interaction (charge–transfer) between the amino donor sub–chromophore and the pyridinium function would be more facile compared to the same with pyridine. Stepwise protonation reactions of the amphiphilic chromophores (**TM 1–3**) have been performed using p–toluenesulphonic acid (PTSA) in dichloromethane at room temperature. The resulting processes have been followed by absorption and emission spectroscopy. Relevant spectra have been shown in Figure 4.7 and a summary of the subsequent spectral data has been composed in Table 4.6. Addition of one equivalent of acid to the solutions containing the ligands has resulted in deepening of the color of the solutions (yellow to reddish). The corresponding absorption spectra have shown a drastic change.

The free ligands (**TM 1–3**) absorb at 390–395 nm region due to charge transfer (ICT) form dialkyl amino groups to the pyridyl subunits of the ligands (see Figure 4.7). But, in the absorption spectra of the corresponding protonated ligands, almost one half reduction of the absorbance of the ICT bands have been observed, along with appearance of a new
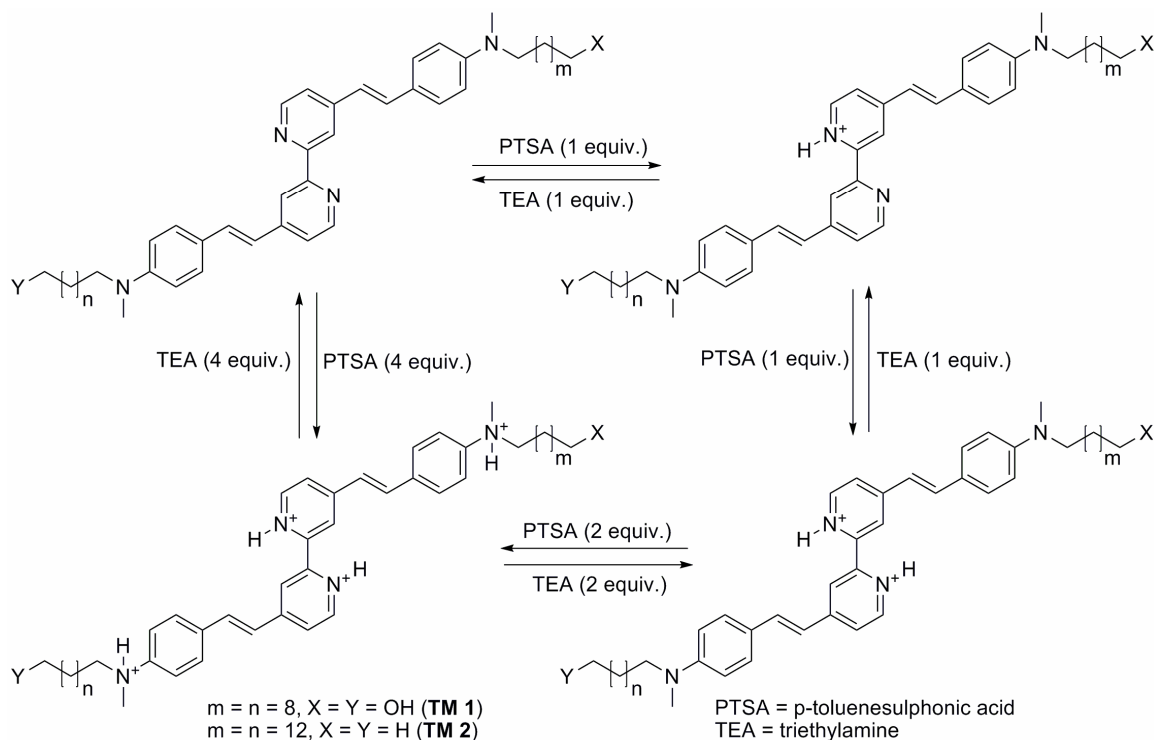
Scheme 4.7 Acid–base reaction of the amphiphilic bipyridine chromophores (**TM 1–2**).

intense band in the visible region (503–501 nm). Addition of one equivalent of acid causes protonation to one pyridine ring of the ligands. Therefore, in the resulting mono–protonated compounds, two different types of charge–transfer interactions exist that involve both the pyridine and pyridinium electron–pulling groups. As charge–transfer involving pyridinium ring is more facile thus of less energy than that involving pyridyl acceptor group, the new band in the visible region of the relevant spectra is unambiguously assigned to the ICT band originated due to charge transfer from the dialkylamino group to the pyridinium group. Moreover, the existence of two ICT bands evidently point up presence of both the charge–transfer interactions as mentioned above thus confirms, mono–protonation of the ligands, the reduction of the absorbance at 390–395 nm being due to involvement of only one pyridine ring compared to two in the free

ligands. Similarly, a change in the emission spectra of the compounds has also been noticed upon acid addition. The free ligands (**TM 1–3**) emit at 495–490 nm region when excited at their corresponding absorption maxima. The emission spectra of the mono–protonated ligands reveal significant decrease in fluorescence intensity of the respective emission band (see Figure 4.7). A concomitant weak red–emission at 617–620 nm is also observed, demonstrating emission from both the excited ICT states (dialkyl amino → pyridinium, dialkyl amino → pyridine). Further addition of one equivalent of acid results in protonation of both the pyridine rings. The corresponding absorption spectra shows disappearance of the ICT band at 390–395 nm (dialkyl amino → pyridine) and only one

Table 4.6 Summary of linear optical data for **TM 1–3** and the protonated intermediates.

Compound	Acid Equiv	λ_{max}(nm)		λ_{ex}(nm)	λ_{em}(nm)	
TM 1	0		395	395		495
	1	503	395	395	617	485
				503	627	
	2	503		395	628	
				503	633	
	4		333			
TM 2	0		393	393		493
	1	501	393	393	620	493
				501	622	
	2	506		393	630	
				506	630	
	4		328			
TM 3	0		390	390		490
	1	503	390	390	620	490
			503		620	
	2	503		390	623	
				503	625	
	3		334			

intense absorption band at 503–506 nm sustains. This clearly illustrates that both the pyridine rings have undergone protonation and only one type of charge transfer transition (dialkyl amino → pyridinium) remains in solution. The emission spectra again corroborate this phenomenon. Excitation at the respective absorption maxima of the free

ligands has shown a feebly intense emission band at 490–495 nm (emission due to the free ligands) whereas; excitation at the lowest energy absorption maxima (503–506 nm)
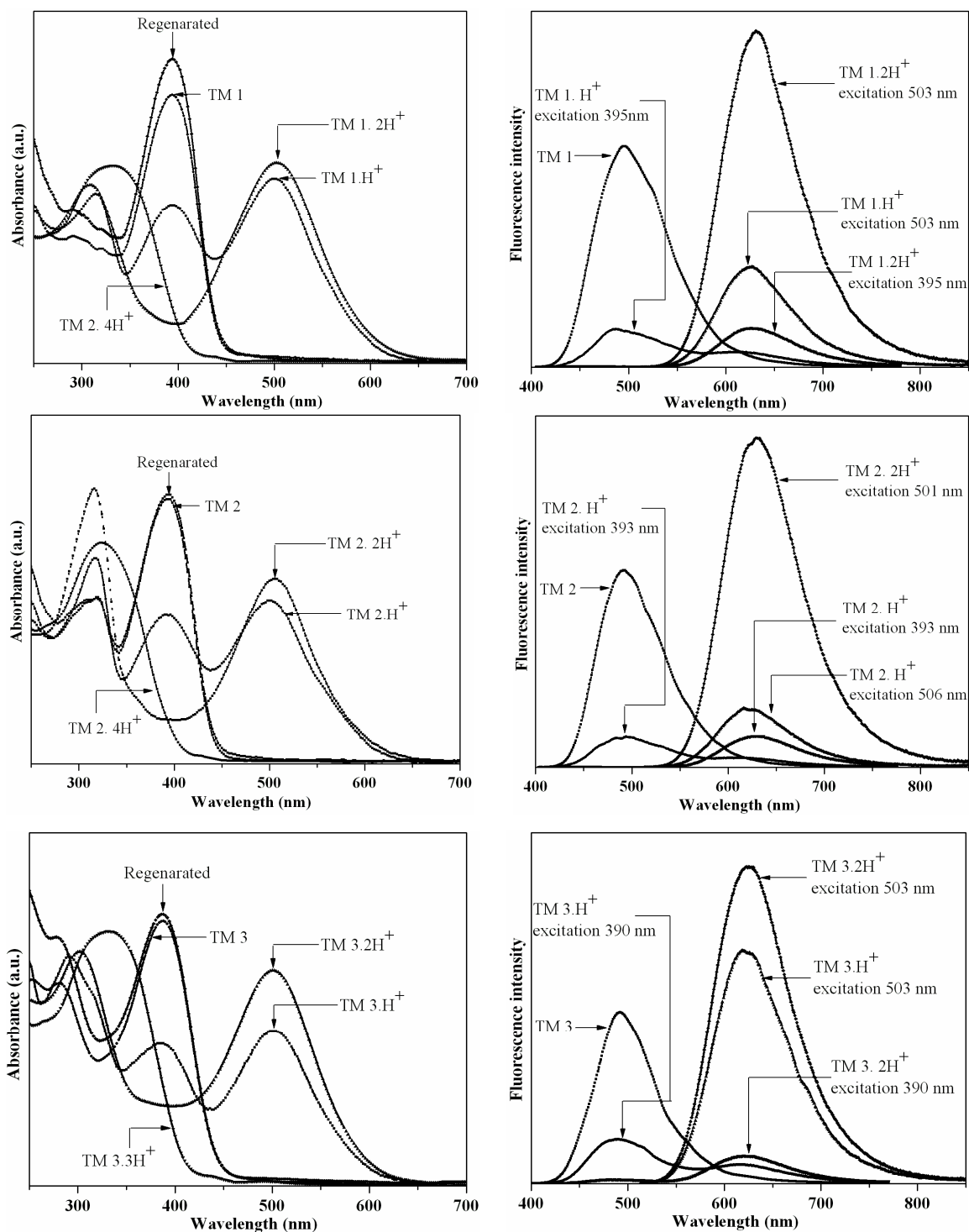

Figure 4.7 Changes of the linear optical properties of **TM 1–3** (top–bottom) upon protonation (left: absorption, right: emission).

exhibits an intense red–emission at 630–625 nm. The large red–shifted emission band ($\Delta\lambda_{em}$ 135–138 nm) of the doubly–protonated ligands compared to emission band of the free ligands is due to more spontaneity in charge delocalization in pyridinium derivatives than pyridine derivatives due to more electro negativity of the former. Addition of four equivalents of acid causes protonation of all the four nitrogen atoms of the ligands, thereby blocking the donor–acceptor interaction inside the push–pull chromophores. A significant visual change is also observed, the solutions have turned colorless. Subsequent absorption spectra have illustrated disappearance of the bands in the visible
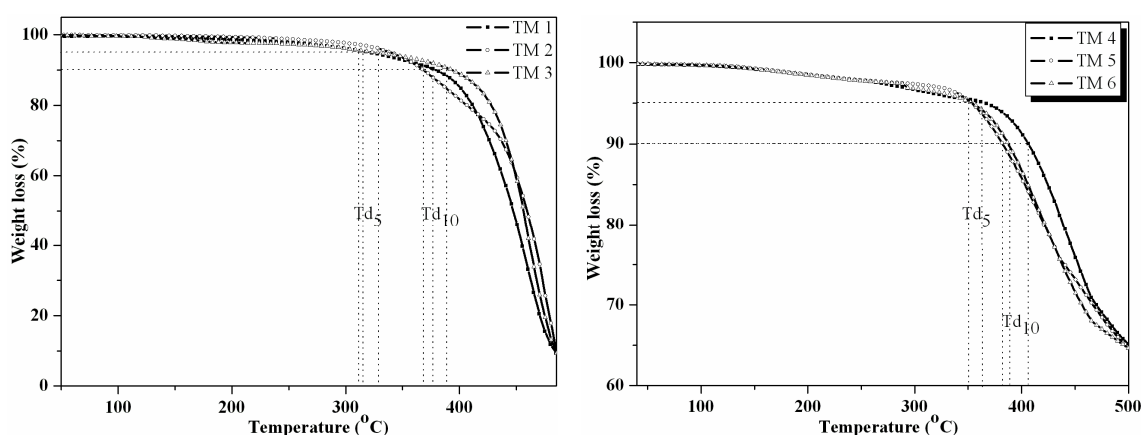

Figure 4.8 Thermogravimetric analysis on **TM 1–6**.

region revealing only one absorption band in the high–energy region (328–334 nm) that might be due to a ligand–centered transition. The emission spectra show a switching–off of the photoluminescence from both the excited ICT states. All these steps are reversible

Table 4.7 Summary of the thermogravimetric analytical data of **TM 1–6**.

Compound	Mp (°)[a]	Td_5 (°)	Td_{10} (°)
TM 1	122	311	377
TM 2	110	328	368
TM 3	124	329	390
TM 4	288	364	406
TM 5	258	351	382
TM 6	250	351	388

[a] determined from DTA

as revealed by regeneration of the protonated intermediates and fluorescence switching–on upon addition of controlled amount of triethylamine (for clarity only the regenerated ligands have been shown in Figure 4.7). All the emissions have been crosschecked with the corresponding excitation spectra that have completely correlated the relevant absorpt--ion spectra. Thus, it can be said that, the linear optical behavior of the push–pull chromophores can be tuned over a large range simply by controlled acid–base reaction as revealed by the present study. The present observations are in complete support with a literature report that demonstrates acid–base titration performed with dibutylaminostyrl–2,2'–bipyridine chromophore.[7b]

4.2.6. Thermal properties

Chemical and thermal stability are the basic and intrinsic requirement for the materialistic applications of the bench–top synthesized compounds. Spectroscopic properties of the synthesized bipyridine compounds **TM 1–11** are found to remain unchanged over long time storage in air as indicated by the NMR and UV–visible spectroscopic studies, indicating chemical inertness of these chromophores or fluorophores toward air or moisture. Similarly, no isomerization / interconversion between the 1–naphthyl (**TM 8**) and 2–naphthyl (**TM 9**) derivatives upon prolonged storage have been observed as indicated by the UV–visible and emission spectroscopy. Thermogravimetric analyses on the compounds **TM 1–6** under nitrogen exhibit high thermal stability of these chromophores (see Figure 4.8 and Table 4.7). Thermal decomposition temperatures of these compounds T_{d5} (5% weight loss) and T_{d10} (10% weight loss) are essentially higher (Table 4.7) which indicate thermal robustness of these chromophores. The melting points of the compounds **TM 1–6** have been determined from the relevant DTA plot and have been reported in Table 4.7.

4.3. Conclusion

In conclusion, a series of 4,4'–π–conjugated–2,2'–bipyridine compounds have been synthesized and characterized through spectroscopy (IR, NMR, LC–MS) including successful elemental analyses. Their photo–physical properties have been explored by electronic absorption and emission spectroscopy. These newly synthesized bipyridine

compounds comprise a variety of modified π–backbone, which has resulted in diversity of their photo–physical properties (absorption and emission maxima, molar absorptivity, photoluminescent quantum yields etc.). Controlled acid–base titrations with the dialkylamino donor substituted bipyridines explore tuning of their absorption and emission properties over a long wavelength range. An increase in conjugation from styryl to bistyryl has caused a drastic enhancement of the fluorescent quantum yields of the 4,4'–π–conjugated–2,2'–bipyridine compounds. Solvatochromic behavior of the bipyridine chromophores **TM 1–6** have also been investigated which illustrate significant polar nature of their fluorescent excited states. Furthermore, thermal analyses performed on compounds **TM 1–6** exhibit excellent thermal stabilities of these compounds up to higher temperature.

4.4. Experimental Section

4.4.1. Materials and methods

All the reactions have been performed under ultra high pure nitrogen or argon atmosphere unless mentioned elsewhere. The following materials have been purchased from commercial sources and have been used without further purification unless noted: 4,4'–dimethyl–2,2'–bipyridine, potassium *t*–butoxide, *n*–butyl lithium (1.6 M and 2.5M in hexane), chlorotrimethylsilane, extra dry DMF, hexacloroethane, acetic anhydride, p–toluenesulphonic acid, potassium carbonate (Acros Organics); *2*– and *4*–bromobenzaldehydes (Alfa–Acer); trimethylsilylacetylene, cesium fluoride, 4–bromobenzylbromide, sodium hydride (60% dispersion in oil), 3–4–dihydro–2H–pyran, phosphorous oxychloride (Avra, India); *bis*–triphenylphosphene palladium(II) dichloride, cuprous iodide, triethylphosphite, 9–anthracene caboxaldehyde, 1– and 2–naphthaldehyde (Aldrich); 1,10–decanediol, sodium *t*–butoxide (Lancaster); 3–methoxy benzaldehyde, 2,4–dimethoxy benzaldehyde, diisopropylamine, triethylamine, 1–bromotetradecane, N–methylaniline (Merck); 2,5–dimethoxy benzaldehyde (Fluka). Triethylphosphite has been distilled prior to use. THF, diethyl ether have been freshly distilled over Na / Benzophenone under nitrogen until a deep purple color persists and used either immediately (THF) or stored over sodium wire in dark (ether). Triethylamine, diisopropylamine have been distilled thrice over calcium hydride under nitrogen and

stored over KOH / NaOH pellets in a CaCl$_2$ desiccators. N–methyl aniline has been distilled over KOH and used immediately. All the deuteriated NMR solvents have been purchased from Acros Organics and have been used as received. Column chromatography have been performed with silica gel (100–200 mesh) (SRL, India) unless mentioned. All the solvents used for the chromatographic purifications have been distilled prior to use.

NMR spectra (^{1}H and ^{13}C) have been recorded by Bruker DRX–400 MHz spectrometer using tetramethylsilane (TMS) as internal standard in case of CDCl$_3$ solvent. Signal multiplicities are reported as follows: s = singles, d = doublet, t = triplet, m = multiplet, br = broad. Elemental analyses have been performed by FLASH EA series 1112 CHNS analyzer. Infrared spectra have been recorded on a JASCO–5300 FT–IR spectrophotometer. Thermogravimetric analyses have been carried out on a STA 409 PC analyzer under the flow of nitrogen. LC–MS have been used to obtain molecular mass of the synthesized compounds. Cary 100 Bio UV–visible spectrophotometer and Shimadzu UV–3600 spectrophotometer have been used to record the electronic absorption spectra. The emission spectra have been recorded on a Fluromax–4 (Jobin Yvon) spectrofluorometer and have been corrected for the instrumental response.

4.4.2. Synthetic procedures and characterization data

2–(10–bromodecyloxy)tetrahydro–2H–pyran (1b). 3,4–dihydro–2H–pyran (16.5 ml, 183 mmol, 1.5 equiv.) was slowly added to a THF solution (100 ml) containing 10–bromodecan–1–ol (**1a**) (29 g, 122 mmol) and p–toluene sulphonic acid (3.57 g, 5% mol) at room temperature and the resulting yellowish reaction mixture was stirred overnight. The reaction was then quenched with saturated NaHCO$_3$ solution and after removal of THF under reduced pressure, the product was extracted with hexane. The combined organic layer was washed with brine, dried (Na$_2$SO$_4$) and chromatographed on basic alumina using hexane as the mobile phase to obtain **1b** as a colorless liquid (35.6 gm, 91%).

IR (Neat, cm^{-1}): 2928.21 (s, br, C–H), 2854.90, 1734.16–723.37 (multiple bands).

^{1}H NMR (400 MHz, CDCl$_3$, TMS) δ: 4.57 (1H), 3.87–3.36 (m, 6H), 3.86–3.29 (m, 23H).

^{13}C NMR (100 MHz, CDCl$_3$, TMS) δ: 98.8, 67.6, 62.3, 34.0, 32.8, 30.8, 29.7, 29.4, 28.7, 28.2, 26.2, 25.5.

LC–MS: only fragmented peaks have been observed.

Anal. Calcd. For. C$_{15}$H$_{29}$BrO$_2$ (323.29): C, 56.07; H, 9.10. Found: C, 56.10; H, 9.04.

3–(methyl(phenyl)amino)decan–1–ol (2a). N–methyl aniline (12.1 ml, 112 mmol) was added drop wise to a 100 ml THF suspension of NaH (9 gm, 224 mmol) at room temperature. The reaction mixture was then refluxed for 30–45 mins before 27.6 gm (86 mmol) of 2–(10–bromodecyloxy)tetrahydro–2H–pyran (**1b**) was injected. The reaction was allowed to continue overnight at this temperature, cooled in an ice bath and carefully quenched with water, followed by an ethereal extraction of the product. After removal of the solvent, the reddish liquid was dissolved in 100 ml of methanol and 30 ml of 1:1 HCl (aq) was added followed by overnight reflux in air. After cooling to room temperature, the reaction mixture was neutralized with saturated Na$_2$CO$_3$ solution (until basic pH), methanol was then removed and the product was extracted with ether. The ether extracts were combined, washed with brine, dried over anhydrous Na$_2$SO$_4$ and evaporated. The crude product was purified by column chromatography on silica gel using dichloromethane as the mobile phase to obtain the product as yellow light sensitive liquid (13.5 gm, 51% based on **2**).

IR (Neat, cm^{-1}): 3350.65 (br, O–H), 2926.28 (s, C–H), 1601.06–692.51 (multiple bands).

^{1}H NMR (400 MHz, CDCl$_3$, TMS) δ: 7.27–7.22 (m, 2H), 6.71 (br, 3H), 3.66–3.63 (t, 2H), 3.32–3.29 (t, 2H), 2.93 (s, 3H), 3.57 (br, 4H), 3.31 (br, 13H).

^{13}C NMR (100 MHz, CDCl$_3$, TMS) δ: 149.3, 129.2, 116.1, 112.4, 63.0, 53.0, 38.5, 32.8, 29.6, 29.5, 27.2, 26.6, 25.8.

LC–MS (positive mode): m/z = 264 (M+H)$^+$.

Anal. Calcd. For. C$_{17}$H$_{29}$NO (263.42): C, 77.51; H, 11.10; N, 5.32. Found: C, 77.55; H, 11.03; N, 5.37.

10–(methyl(phenyl)amino)decyl acetate (2b). Acetic anhydride (6.5 ml, 69 mmol, 3.5 equiv.) was added to a DCM solution (100 ml) containing 3–(methyl(phenyl)amino) propan–1–ol (**2a**) (12 gm, 46 mmol) and 4–dimethylamino pyridine (560 mg, 10% mol) with cooling in an ice bath. The reaction mixture was slowly warmed up to room

temperature and stirred until completion (1.5 – 2 h) after which, it was quenched with water and extracted with dichloromethane. The combined organic layer was washed with brine, dried (Na_2SO_4) and chromatographed on silica gel using EtOAc–Hexane 20:80 (v/v) as the eluant. The product was isolated as a pale yellow liquid (light sensitive). Yield: 13 gm (93%).

IR (Neat, cm^{-1}): 3032.37 (m, C–H), 2928.21 (s, C–H), 2854.90, 1739.95 (C=O), 1601.06–692.51 (multiple bands).

^{1}H NMR (400 MHz, CDCl$_3$, TMS) δ: 7.27–7.21 (m, 2H), 6.71–6.66 (m, 2H), 4.08–4.05 (m, 2H), 3.32–3.29 (m, 2H), 2.93 (s, 3H), 2.06 (s, 3H), 3.63–3.58 (m, 4H), 3.31 (br, 12H).

^{13}C NMR (100 MHz, CDCl$_3$, TMS) δ: 173.3, 149.4, 129.1, 115.8, 112.1, 64.7, 52.8, 38.3, 29.5, 29.2, 28.6, 27.2, 26.7, 25.9, 21.0.

LC–MS (positive mode): m/z = 306 (M+H)$^{+}$.

Anal. Calcd. For. $C_{19}H_{31}NO_2$ (305.45): C, 74.71; H, 10.23; N, 4.59. Found: C, 74.75; H, 10.20; N, 4.63.

4–((10–hydroxydecyl)(methyl)amino)benzaldehyde (2c). POCl$_3$ (5.1 ml, 54 mmol, 3.3 equiv.) was slowly added to 12 ml of ice–cooled DMF (excess). The orange red viscous liquid was then slowly warmed up to room temperature and stirred for 1 h before being re–cooled to 0 °C after which, 12.7 gm (42 mmol) of 10–(methyl(phenyl)amino)decyl acetate (**2b**) was added via a syringe. The red reaction mixture was heated at 90–95 °C for 7 h after which, it was cooled in an ice bath, carefully quenched with water, neutralized with saturated Na$_2$CO$_3$ solution and extracted with ether. The combined organic layer was washed several times with water, then with brine, dried (Na$_2$SO$_4$) followed by removal of the solvent left a red gel. It was then dissolved in 100 ml of methanol. K$_2$CO$_3$ (12 gm, 84 mmol) was added to it and the slurry was stirred overnight at room temperature in air after which, it was filtered, solvent was removed under reduced pressure and the product was extracted with ether. The combined organic layer was washed with water, brine, dried over Na$_2$SO$_4$ and subjected to chromatography on silica gel. The product was isolated as a pale yellow solid (10 gm, 83%) after eluting the column with EtOAc–Hexane 50:50 (v/v) solvent mixture.

IR (KBr, cm^{-1}): 3433.60 (br, O–H), 3053.59 (m, C–H), 2928.21 (s, C–H), 1662.79 (s, C=O), 1597.20–513.18 (multiple bands).

^{1}H NMR (400 MHz, CDCl$_3$, TMS) δ: 9.70 (s, 1H), 7.71 (d, J = 8Hz, 2H), 6.67 (d, J = 8Hz, 2H), 3.64–3.61 (t, 2H), 3.40–3.37 (t, 2H), 3.03 (s, 3H), 3.59–3.54 (m, 5H), 3.29 (unresolved, 13H).

^{13}C NMR (100 MHz, CDCl$_3$, TMS) δ: 190.2, 153.5, 132.2, 124.7, 110.8, 62.8, 52.4, 38.5, 32.7, 29.5, 29.4, 27.0, 26.8, 25.8, 21.0, 14.2.

LC–MS (positive mode): m/z = 292 (M+H)$^{+}$.

Anal. Calcd. For. C$_{18}$H$_{29}$NO$_2$ (293.43): C, 74.18; H, 10.03; N, 4.81. Found. C, 74.20; H, 9.95, N, 4.85.

4–(methyl(10–(tetrahydro–2H–pyran–2–yloxy)decyl)amino)benzaldehyde (Ald 1). This compound was prepared following an analogous procedure as described for **1b**. Orange yellow liquid. Yield: 87%.

IR (Neat, cm^{-1}): 2930.14 (s, C–H), 2858.76, 2729.52, 1682.08 (s, C=O), 1597.20–736.87 (multiple bands).

^{1}H NMR (400 MHz, CDCl$_3$, TMS) δ: 9.72 (s, 1H), 7.72 (d, J = 8 Hz, 2H), 6.68 (d, J = 8Hz, 2H), 4.57 (br, 1H), 3.87 (m, 1H), 3.74 (m, 1H), 3.50 (m, 1H), 3.41–3.48 (t, 2H), 3.05 (s, 3H), 3.72–3.30 (m, 25H).

^{13}C NMR (100 MHz, CDCl$_3$, TMS) δ: 190.1, 153.5, 132.1, 124.9, 110.8, 98.9, 67.7, 62.4, 52.5, 38.5, 30.8, 29.7, 29.5, 29.4, 27.0, 26.9, 26.2, 25.5, 19.7.

LC–MS (positive mode): m/z = 376 (M+H)$^{+}$.

Anal. Calcd. For. C$_{23}$H$_{37}$NO$_3$ (375.28): C, 73.56; H, 9.93; N, 3.73. Found: C, 73.59; H, 9.87; N, 3.75.

N–methyl–N–tetradecylaniline (3). This compound was synthesized using the same synthetic procedure as described for the preparation of **2a** (without addition of HCl). Yellow light sensitive liquid. Yield: 55%. Mobile phase: DCM–Hexane 3:97 (v/v) on silica gel.

IR (Neat, cm^{-1}): 2924.35 (s, CH), 2852.98–690.58 (multiple bands).

^{1}H NMR (400 MHz, CDCl$_3$, TMS) δ: 7.22 (d, J = 8 Hz, 2H), 6.71–6.68 (m, 3H), 3.30 (t, 2H), 2.93 (s, 3H), 3.57 (unresolved, 2H), 3.31–3.19 (unresolved, 22H), 0.89 (t, 3H).

^{13}C NMR (100 MHz, CDCl$_3$, TMS) δ: 149.4, 129.2, 115.8, 112.1, 52.9, 38.3, 32.0, 29.9, 29.7, 29.4, 27.3, 26.7, 22.8, 14.2.

LC–MS (positive mode): m/z = 304 (M+H)$^+$.

Anal. Calcd. For. C$_{21}$H$_{37}$N (303.53): C, 83.10; H, 12.29; N, 4.61. Found: C, 83.07; H, 12.27; N, 4.66.

4–(methyl(tetradecyl)amino)benzaldehyde (Ald 2). Synthetic procedure in obtaining this compound was similar as described for the synthesis of **2c** (without K$_2$CO$_3$ / MeOH step). Yellow liquid that solidified upon cooling and standing. Yield: 80%.

IR (Neat, cm^{-1}): 2918.56 (s, C–H), 2847.19, 1664.72 (C=O), 1595.27–453.31 (multiple bands).

^{1}H NMR (400 MHz, CDCl$_3$, TMS) δ: 9.72 (s, 1H), 7.72 (d, J = 8Hz, 2H), 6.68 (d, J = 8Hz, 2H), 3.40 (t, 2H), 3.05 (s, 3H), 3.64–3.61 (unresolved, 2H), 3.32–3.26 (unresolved, 23H), 0.88 (unresolved, 3H).

^{13}C NMR (100 MHz, CDCl$_3$, TMS) δ: 190.1, 153.5, 132.1, 124.9, 110.8, 52.5, 38.5, 33.9, 29.7, 29.6, 29.5, 29.4, 27.0, 26.9, 22.7, 14.1.

LC–MS (positive mode): m/z = 332 (M+H)$^+$.

Anal. Calcd. For. C$_{22}$H$_{37}$NO (333.29): C, 79.70; H, 13.25; N, 4.22. Found: C, 79.73; H, 13.20; N, 4.26.

General procedure for the synthesis of methoxy substituted 1–Bromo–4–Styryl Benzenes (6a–c). Solid sodium t–butoxide (3.92 g, 20 mmol) was added at a time to a 50 ml THF solution of diethyl 4–bromophenylphosphonate (**4a**) (4 g, 13 mmol) and the corresponding aldehyde (**5a–c**) (10 mmol) at 0 ºC. The resulting slurry was warmed up to room temperature and stirred for 90 mins. The reaction was then quenched with water and extracted with hexane. The combined organic layer was washed with brine, dried over Na$_2$SO$_4$ and evaporated. The crude product was purified through silica gel column using ethyl acetate – hexane = 5:95 (v/v) as the mobile phase.

1–(4–bromostyryl)–3–methoxybenzene (6a). White solid. Yield: 93%. Mp: 73–74 ºC.

^{1}H NMR (400 MHz, CDCl$_3$, TMS) δ: 7.48 (d, J = 8 Hz, 2H), 7.37 (d, J = 8 Hz, 2H), 7.29 (d, J = 8 Hz, 1H) 7.10 (d, J = 8 Hz, 1H), 7.04 (d, J = 8 Hz, 3H), 6.84 (d, J = 8 Hz, 1H) 3.85 (s, 3H).

^{13}C NMR (100 MHz, CDCl$_3$, TMS) δ: 159.95, 138.43, 136.20, 133.82, 129.76, 129.34, 128.06, 127.73, 123.42, 119.33, 113.58, 113.88, 55.29.

LC–MS (positive mode): m/z = 291 (M+2H)$^+$.

Anal. Calcd. For. C$_{15}$H$_{13}$BrO (289.17): C, 62.30; H, 4.53. Found: C, 62.26%; H, 4.58%.

1–(4–bromostyryl)–2,4–dimethoxybenzene (6b). White weightless solid. Yield: 92%. Mp: 78–80 ºC.

^{1}H NMR (400 MHz, CDCl$_3$, TMS) δ: 7.35 – 7.49 (m, 6H), 6.93 (d, J = 16 Hz, 2H), 6.51 (d, J = 8 Hz, 1H), 6.47 (s, 1H), 3.86 (s, 3H), 3.83 (s, 3H).

^{13}C NMR (100 MHz, CDCl$_3$, TMS) δ: 163.56, 158.92, 138.11, 132.42, 128.60, 128.17, 126.43, 124.86, 123.29, 119.92, 105.84, 99.28, 56.31.

LC–MS (positive mode): m/z = 321 (M+2H)$^+$.

Anal. Calcd. For. C$_{16}$H$_{15}$BrO$_2$ (319.19): C, 60.21; H , 4.74. Found: C, 59.98; H, 4.77.

1–(4–bromostyryl)–2,5–dimethoxybenzene (6c). White solid. Yield: 92%. Mp: 68–69 ºC.

^{1}H NMR (400 MHz, CDCl$_3$, TMS) δ: 7.38 – 7.47 (m, 5H), 7.12 (s, 1H), 7.01 (d, 1H, J = 16 Hz), 6.79 – 6.85 (m, 2H), 3.84 (s, 3H), 3.81 (s, 3H).

^{13}C NMR (100 MHz, CDCl$_3$, TMS) δ: 154.54, 152.30, 137.56, 132.50, 133.31, 128.91, 127.60, 124.86, 123.94, 114.80, 113.03, 112.50, 56.99, 56.59.

LC–MS (positive mode): m/z = 321 (M+2H)$^+$.

Anal. Calcd. For. C$_{16}$H$_{15}$BrO$_2$ (319.19): C, 60.21; H, 4.74. Found: C, 60.28; H, 4.79.

General procedure for the synthesis of methoxy substituted 4–Styryl Benzaldehydes (Ald 3–5). *n*–Butyl lithium (2.5 M in hexane) (4 ml, 10 mmol) was added drop wise to a 50 ml ether solution containing appropriate 4–styryl bromobenzene (**6a–c**) (5 mmol) at – 20 ºC. The reaction mixture was stirred at this temperature for 60 mins, after which it was warmed up to 0 ºC before DMF (0.77 ml, 10 mmol) was injected. Reaction was continued at this temperature (0 ºC) until completion (monitored by TLC). It was then quenched with water and the product was extracted with ethyl acetate. The crude product was purified through silica gel column, eluant as mentioned below.

4–(3–methoxystyryl)benzaldehyde (Ald 3). Off–white solid. Mobile phase: EtOAc : Hexane = 10:90 (v/v). Yield: 86%. Mp: 59–60 ºC.

IR (KBr, cm^{-1}): 3022.73–2752.67 (multiple bands), 1693.72 (C=O), 1601.06 – 503.47 (multiple bands).

^{1}H NMR (400 MHz, CDCl$_3$, TMS) δ: 9.99 (s, 1H), 7.87 (d, J = 8 Hz, 2H), 7.65 (d, J = 8 Hz, 2H), 7.28–7.32 (m, 1H), 7.07 – 7.21 (m, 4H), 3.86 (s, 3H).

^{13}C NMR (100 MHz, CDCl$_3$, TMS) δ: 193.66, 159.96, 143.31, 137.98, 135.35, 132.08, 130.25, 129.84, 127.62, 126.96, 119.64, 114.15, 112.17, 55.30.

LC–MS (positive mode): m/z = 239 (M+H)$^+$.

Anal. Calcd. For. C$_{16}$H$_{14}$O$_2$ (238.28): C, 80.65; H, 5.92. Found: C, 80.55; H, 5.94.

4–(2,4–dimethoxystyryl)benzaldehyde (Ald 4). Fluorescent yellow solid. Eluant: EtOAc: Hexane = 20:80 (v/v). Yield: 65%. Mp: 90–92 ºC.

IR (KBr, cm^{-1}): 2935.92 – 2743.02 (multiple bands), 1687.87 (C=O), 1595.27 – 515.04 (multiple bands).

^{1}H NMR (400 MHz, CDCl$_3$, TMS) δ: 9.97 (s, 1H), 7.84 (d, J = 8Hz, 2H), 7.64 (d, J = 8Hz, 2H), 7.52 – 7.58 (m, 2H), 7.05 (d, J = 16Hz, 1H), 6.48 – 6.55 (m, 2H), 3.89 (s, 3H), 3.85 (s, 3H).

^{13}C NMR (100 MHz, CDCl$_3$, TMS) δ: 193.70, 163.31, 158.50, 144.64, 134.76, 130.22, 127.79, 127.01, 126.61, 125.44, 118.73, 105.23, 98.48, 77.43, 77.11, 76.80, 55.56, 55.46.

LC–MS (positive mode): m/z = 269 (M+H)$^+$.

Anal. Calcd. For. C$_{17}$H$_{16}$O$_3$ (268.31): C, 76.10; H, 6.01. Found: C, 76.18; H, 5.97.

4–(2,5–dimethoxystyryl)benzaldehyde (Ald 5). Fluorescent yellow solid. Mobile phase: EtOAc: Hexane = 20:80 (v/v). Yield: 45%. Mp: 52–53 ºC.

IR (KBr, cm^{-1}): 3045.87 – 1819.04 (multiple bands), 1695.58 (C=O), 1599.13 – 505.40 (multiple bands).

^{1}H NMR (400 MHz, CDCl$_3$, TMS) δ: 9.97 (s, 1H), 7.84 (d, J = 8Hz, 2H), 7.58–7.66 (m, 3H), 7.09–7.15 (m, 2H), 6.84 (s, 2H), 3.85 (s, 3H), 3.81 (s, 3H).

^{13}C NMR (100 MHz, CDCl$_3$, TMS) δ: 193.70, 153.75, 153.81, 143.98, 135.19, 130.21, 127.91, 127.00, 126.93, 126.35, 114.76, 112.30, 113.91, 56.20, 55.83.

LC–MS (positive mode): m/z = 269 (M+H)$^+$.

Anal. Calcd. For. $C_{17}H_{16}O_3$ (268.31): C, 76.10; H, 6.01. Found: C, 75.95; H, 6.10.

General procedure for the synthesis of trimethylsilylethynyl benzaldehydes (Ald 6–7). A shlenk tube was charged with the corresponding bromo benzaldehyde (**7a–b**) (5 mmol), (Ph$_3$P)$_2$PdCl$_2$ (70 mg, 1 mol %) and CuI (38.1 mg, 2 mol %). The tube was evacuated and filled up with ultra high pure nitrogen. 15 ml of 2:1 Et$_3$N–THF solvent was injected into the tube, which was then immersed into liquid nitrogen until the reaction mixture solidified. High vacuum was then applied for 10 mins while holding the tube at 100K after which, vacuum was stopped and the solidified reaction mixture was slowly warmed until it melted. This process was repeated thrice. Trimethylsilyl acetylene (3.12 ml, 8 mmol) was injected into the tube. The dark reaction mixture was then heated at 60 ºC for 5.5 h, cooled to room temperature and filtered through a pad of celite to remove the precipitated amine salt and evaporated to dryness. The crude material was finally purified through column chromatography on silica gel using EtOAc–Hexane = 5:95 (v/v) as the mobile phase.

2–trimethylsilylethynyl benzaldehyde (Ald 6). Pale yellow solid. Yield: 89%. Mobile phase: EtOAc: Hexane = 5:95.

IR (KBr, cm^{-1}): 3369.94 – 2150.82 (multiple bands), 1695.58 (C=O), 1593.35 – 443.74 (multiple bands).

^{1}H NMR (400 MHz, CDCl$_3$, TMS) δ: 10.56 (s, 1H); 7.91 (d, J = 8 Hz, 1H), 7.52–7.58 (m, 2H), 7.42–7.45 (m, 1H), 0.28 (s, 9H).

^{13}C NMR (100 MHz, CDCl$_3$, TMS) δ: 192.1, 136.2, 133.7, 133.5, 128.8, 126.9, 102.6, 100.0, –0.2.

LC–MS (positive mode) m/z: 203 (M+H)$^+$.

Anal. Calcd. For. $C_{12}H_{14}OSi$ (202.32): C, 73.24; H, 6.97. Found: C, 73.20; H, 6.99.

4–trimethylsilylethynyl benzaldehyde (Ald 7). Off–white solid. Yield: 91%. Mobile phase: EtOAc: Hexane = 3:97 (v/v).

IR (KBr, cm^{-1}): 2959.07 – 2156.61 (multiple bands), 1703.30 (C=O), 1601.06–536.26 (multiple bands).

^{1}H NMR (400 MHz, CDCl$_3$, TMS) δ: 10.01 (s, 1H), 7.82 (d, J = 8 Hz, 2H), 7.61 (d, J = 8 Hz, 2H), 0.28 (s, 9H).

^{13}C NMR (100 MHz, CDCl$_3$, TMS) δ: 193.4, 135.7, 132.5, 129.3, 103.8, 100.8, 99.1, –0.2.

LC–MS (positive mode) m/z: 203 (M+H)$^+$.

Anal. Calcd. For. C$_{12}$H$_{14}$OSi (202.32): C, 73.24; H, 6.97. Found: C, 73.22; H, 6.91.

General procedure for the synthesis of the symmetrically substituted 4,4'–*bis*–vinyl–2,2'–bipyridines (TM 1–2, TM 4–11)

The bipyridines have been isolated in two different methods depending upon their solubility.

Method 1: To a mixture of 1 equivalent of the *bis*–phosphonate (**10**) and 3 equivalents of the corresponding aldehydes in 20 ml of THF at room temperature, was added solid potassium *t*–butoxide (4 equivalents) at a time. The resulting slurry was then stirred at room temperature until TLC monitoring indicated completion of the reaction (3–4 h). The reaction was subsequently quenched with water (5 ml), evaporated to dryness by means of rotary evaporation and the crude solid was subjected to column chromatography (silica gel) using MeOH–Chloroform–Et$_3$N = 5:95:0.5 (v/v) as the eluant.

Method 2: After the reaction ceased, it was quenched with water and methanol was added resulting in precipitation of the desired compound, which was isolated by filtration, washed thoroughly with methanol, ether and dried under vacuum.

4,4'–*bis*–(4–(methyl)(hydroxydecyl)amino)styryl)–2,2'–bipyridine (TM 1). This compound was obtained as a yellow solid after acid hydrolysis of the chromatographed Horner–Wordsworth–Emmons product (**TM 1'**). Method 1. Yield: 71%. Mp: 122 ºC (DTA).

IR (KBr, cm^{-1}): 3371.87 (O–H), 2922.42–569.05 (multiple bands).

^{1}H NMR (400 MHz, CDCl$_3$, TMS) δ: 8.62 (d,
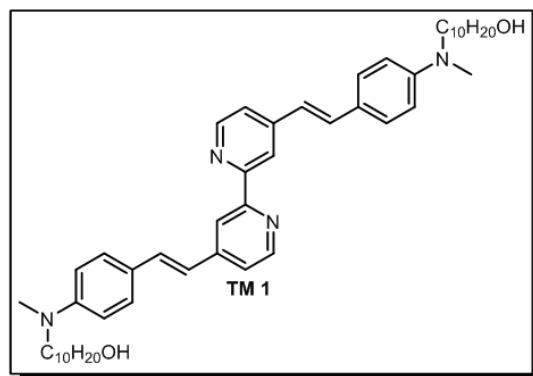
J = 4 Hz, 2H), 8.48 (s, 2H), 7.45 (d, J = 8 Hz, 4H), 7.41 (d, J = 16 Hz, 2H), 7.35 (d, J = 8 Hz, 2H), 6.91 (d, J = 16 Hz, 2H), 6.69 (d, J = 8 Hz, 4H), 3.65 (t, 4H, –C$\underline{H}_2$–OH), 3.35 (t, 4H, –N–C$\underline{H}_2$–), 2.99 (s, 6H, –N–C$\underline{H}_3$), 1.59–1.55 (unresolved, 8H, –N–CH$_2$–C$\underline{H}_2$–, –C$\underline{H}_2$–CH$_2$–OH), 1.30 (unresolved, 28H, –C$\underline{H}_2$–).

^{13}C NMR (100 MHz, CDCl$_3$, TMS) δ: 156.4, 149.6, 149.3, 146.8, 133.6, 128.5, 123.8, 121.0, 120.5, 117.9, 111.8, 63.0, 52.6, 38.3, 32.8, 29.5, 27.1, 26.8, 25.8.

LC–MS (positive mode) m/z: 731 (M+H)$^+$.

Anal. Calcd. For. C$_{48}$H$_{66}$N$_4$O$_2$ (730.52): C, 78.86; H, 9.10; N, 7.66. Found: C, 78.83; H, 9.06; N, 7.71.

UV/Vis (CH$_2$Cl$_2$): λ_{max} (ε) = 250 (20685), 395 nm (42274).

4,4'–*bis*–(4–(methyl)(tetradecyl)amino)styryl)–2,2'–bipyridine (TM 2). Yellow solid.

Method 1. Yield: 86%. Mp: 110 ºC (DTA).

^{1}H NMR (400 MHz, CDCl$_3$, TMS) δ: 8.63 (d, J = 4 Hz, 2H), 8.49 (s, 2H), 7.46–7.35 (m, 10H), 6.91 (d, J = 16 Hz, 2H), 6.69 (d, J = 8 Hz, 4H), 3.35 (t, 4H, –N–C$\underline{H}_2$–), 3.02 (s, 6H, –N–C$\underline{H}_3$), 1.60 (unresolved, 4H, –N–CH$_2$–C$\underline{H}_2$–), 1.32 (unresolved, 48H, –C$\underline{H}_2$–), 0.90–0.87 (unresolved, 6H, –CH$_2$–C$\underline{H}_3$).
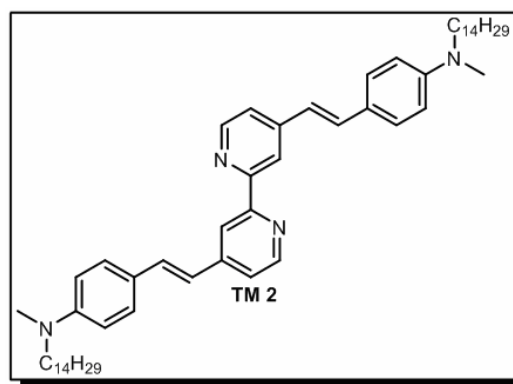
^{13}C NMR (100 MHz, TMS, CDCl$_3$) δ: 156.4, 149.6, 149.3, 146.8, 133.7, 128.5, 123.9, 121.0, 120.5, 117.9, 111.8, 52.6, 38.4, 32.0, 29.6, 29.4, 27.2, 26.8, 22.7, 14.2.

LC–MS (positive mode) m/z: 812 (M+H)$^+$.

Anal. Calcd. For. C$_{56}$H$_{82}$N$_4$ (810.65): C, 82.91; H, 10.19; N, 6.91. Found: C, 82.89; H, 10.16; N, 6.95.

UV/Vis (CH$_2$Cl$_2$): λ_{max} (ε) = 247 (24228), 320 (25142), 393 nm (43585).

4,4'–*bis*–(4–(3–methoxystyryl)styryl)–2,2'–bipyridine (TM 4). Pale yellow solid.
Method 2. Yield: 88%. Mp: 288 °C (DTA).

IR (KBr, cm^{-1}): 3018.87– 2922.42 (multiple bands), 1577.91 (C=C), 1543.19–418.59 (multiple bands).

^{1}H NMR (400 MHz, DMSO–d$_6$) δ: 8.70 (d, J = 4 Hz, 2H), 8.58 (s, 2H), 7.76–7.60 (m, 12H), 7.45 (d, J = 16 Hz, 2H), 7.31–7.19 (m, 10H), 6.86 (d, J = 8 Hz, 2H), 3.80 (s, 6H, –OCH$_3$).
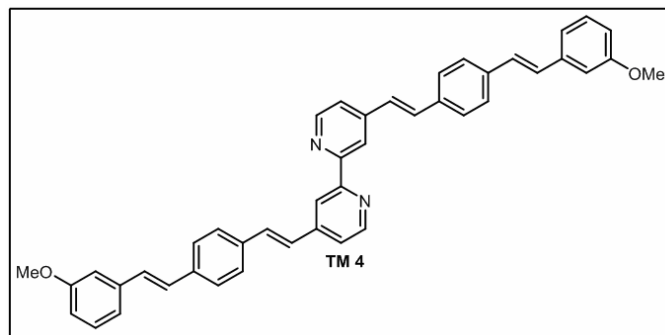
^{13}C NMR: Due to very poor solubility of this compound in common organic solvents, ^{13}C NMR was not possible.

LC–MS (negative mode): m/z = 624 (M–H)$^+$.

Anal. Calcd. For. C$_{44}$H$_{36}$N$_2$O$_2$ (624.77): C, 84.59; H, 5.81; N, 4.48. Found: C, 84.49; H, 5.85; N, 4.56.

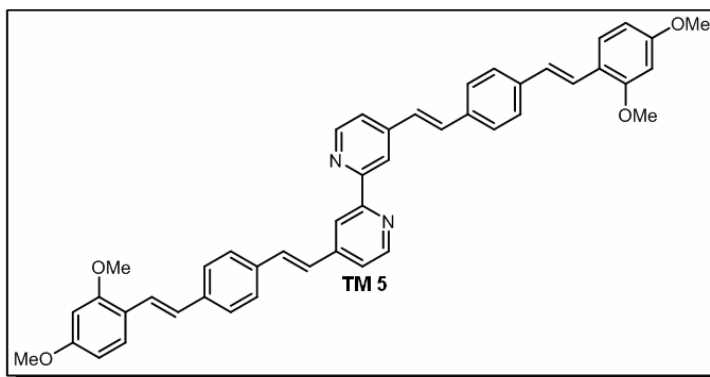UV/Vis (CH$_2$Cl$_2$): λ_{max} (ε) = 365 (61736) nm.

4,4'–bis–(4–(2,4–dimethoxystyryl)styryl)–2,2'–bipyridine (TM 5). Fluorescent yellow solid. Method 2. Yield: 83%. Mp: 258 °C (DTA).

IR (KBr, cm^{-1}): 3024.66–2835.61 (multiple bands), 1606.85 (C=C), 1583.77–570.98 (multiple bands).

^{1}H NMR (400 MHz, DMSO–d$_6$) δ: 8.68 (d, J = 4 Hz, 2H), 8.57 (s, 2H), 7.56–7.72 (m, 12H), 7.37–7.42 (m, 4H), 7.13 (d, J = 16 Hz, 2H), 6.58 (d, J = 16 Hz, 4H), 3.86 (s, 6H, –OCH$_3$), 3.79 (s, 6H).

^{13}C NMR: Due to very poor solubility of this compound in common organic solvents, ^{13}C NMR was not possible.

LC–MS (positive mode): m/z = 686 (M+H)$^+$.

Anal. Calcd. For. C$_{46}$H$_{40}$N$_2$O$_4$ (684.82): C, 80.68; H, 5.89; N, 4.09. Found: C, 80.58; H, 5.81; N, 4.15.

UV/Vis (CH$_2$Cl$_2$): λ_{max} (ε) = 384 (49257) nm.

4,4'–_bis_–(4–(2,5–dimethoxystyryl)styryl)–2,2'–bipyridine (TM 6). Orange yellow solid. Method 2. Yield: 84%. Mp: 250 °C (DTA).

IR (KBr, cm^{-1}): 3026.58 – 2825.97 (multiple bands), 1583.70 (C=C), 1543.26 – 509.25 (multiple bands).
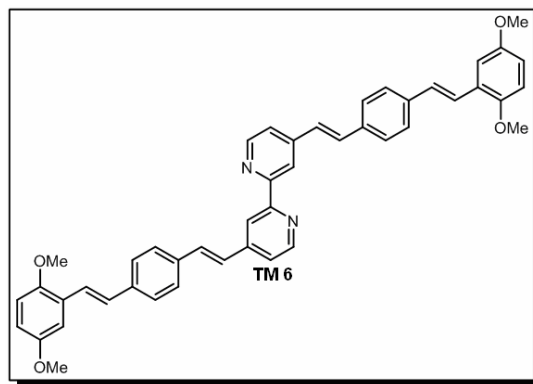

^{1}H NMR (400 MHz, DMSO–d$_6$) δ: 8.69 (d, J = 4.6 Hz, 2H), 8.58 (s, 2H), 7.63–7.65 (m, 12H), 7.42–7.48 (m, 4H), 2.26–2.32 (m, 4H), 6.98 (d, J = 8 Hz, 2H), 6.86 (d, J = 8 Hz, 2H), 3.81 (s, 6H, –OC$\underline{H}_3$), 3.76 (s, 6H, –OC$\underline{H}_3$).

^{13}C NMR: Due to very poor solubility of this compound in common organic solvents, ^{13}C NMR was not possible.

LC–MS (positive mode): m/z = 686 (M+H)$^+$.

Anal. Calcd. For. C$_{46}$H$_{40}$N$_2$O$_4$ (684.82): C, 80.68; H, 5.89; N, 4.09. Found: C, 80.72; H, 5.93; N, 4.12.

UV/Vis (CH$_2$Cl$_2$): λ_{max} (ε) = 380 (45855) nm.

4,4'–_bis_–(2–ethynylstyryl)–2,2'–bipyridine (TM 7). Dark brown solid. Method 1. Yield: 75%. Mp: not measured.

IR (KBr, cm^{-1}): 3294.71 (C–H), 3202.12, 1587.56 (C=C), 1543.19–540.12 (multiple bands).

^{1}H NMR (400 MHz, CDCl$_3$, TMS) δ: 8.69 (d, J = 4 Hz, 2H), 8.52 (s, 2H), 7.95 (d, J = 16 Hz, 2H), 7.73 (d, J = 8 Hz, 2H), 7.56 (d, J = 8 Hz, 2H), 7.51 (d, J = 4 Hz, 2H), 7.38–7.42 (m, 2H), 7.30 (d, J = 8 Hz, 2H), 7.23 (d, J = 16 Hz, 2H), 3.46 (s, 2H, ≡C–$\underline{H}$).

^{13}C NMR (100 MHz, CDCl$_3$, TMS) δ: 156.6, 149.5, 145.6, 138.3, 133.5, 131.0, 129.2, 128.3, 125.2, 123.7, 120.7, 119.3, 82.9, 83.8.

LC–MS (positive mode) m/z: 409 (M+H)$^+$.

Anal. Calcd. for C$_{30}$H$_{20}$N$_2$ (408.49): C, 88.21; H, 4.93; N, 6.86. Found: C, 88.25; H, 4.85; N, 6.90.
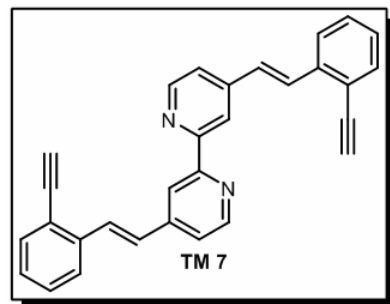
UV/Vis (CH$_2$Cl$_2$): λ$_{max}$ (ε) = 318 (29034) nm.

4,4'–*bis*–(4–ethynylstyryl)–2,2'–bipyridine (TM 8). Yellow powder. Method 2. Yield: 78%. Mp: not measured.

IR (KBr, cm^{-1}): 2926.28, 1628.07, 1585.63 (C=C), 1543.26–569.05 (multiple bands).
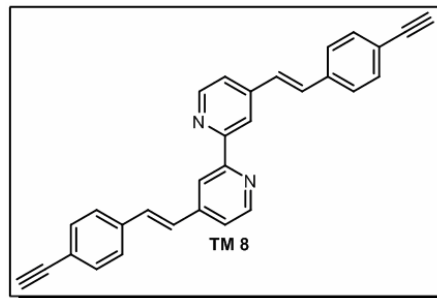

^{1}H NMR (400 MHz, DMSO–d$_6$) δ: 8.67 (d, J = 4 Hz, 2H), 8.54 (s, 2H), 7.71 (d, J = 8 Hz, 4H), 7.65–7.59 (m, 4H), 7.49 (d, J = 8 Hz, 4H), 7.44 (d, J = 16 Hz, 2H), 4.27 (s, 2H, ≡C–H̲).

^{13}C NMR (100 MHz, DMSO–d$_6$) δ: 156.3, 150.18, 145.7, 137.3, 132.7, 128.0, 122.1, 123.8, 118.4, 84.0, 82.5.

LC–MS (positive mode) m/z: 409 (M+H)$^+$.

Anal. Calcd. for C$_{30}$H$_{20}$N$_2$ (408.49): C, 88.21; H, 4.93; N, 6.86. Found: C, 88.23; H, 4.96; N, 6.81.

UV/Vis (CH$_2$Cl$_2$): λ$_{max}$ (ε) = 328 (37125) nm.

4,4'–*bis*–((naphthalen–1–yl)vinyl)–2,2'–bipyridine (TM 9). Off–white solid. Method 2. Yield: 82%. Mp: more than 200 ºC.

IR (KBr, cm^{-1}): 3045.87, 3003.44, 1695.58, 1587.56 (C=C), 1543.26–646.21 (multiple bands).
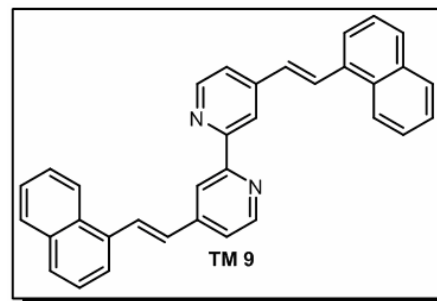

^{1}H NMR (400 MHz, DMSO–d$_6$) δ: 8.76 (d, J = 4 Hz, 2H), 8.66 (s, 2H), 8.49 (d, J = 8 Hz, 2H), 8.44 (d, J = 16 Hz, 2H), 8.02-7.95 (m, 8H), 7.64-7.59 (m, 6H), 7.48 (d, J = 16 Hz, 2H).

^{13}C NMR: Due to very poor solubility of this compound in common organic solvents, ^{13}C NMR was not possible.

LC–MS (positive mode) m/z: 461 (M+H)$^+$.

Anal. Calcd. for C$_{34}$H$_{24}$N$_2$ (460.57): C, 88.67; H, 5.25; N, 6.08. Found: C, 88.69; H, 5.20; N, 6.11.

UV/Vis (CH$_2$Cl$_2$): λ$_{max}$ (ε) = 340 (20145) nm.

4,4'–*bis*–((naphthalen–2–yl)vinyl)–2,2'–bipyridine (TM 10). Off–white solid. Method

2. Yield = 83%. Mp: not measured.

IR (KBr, cm^{-1}): 3047.80–1628.07 (multiple
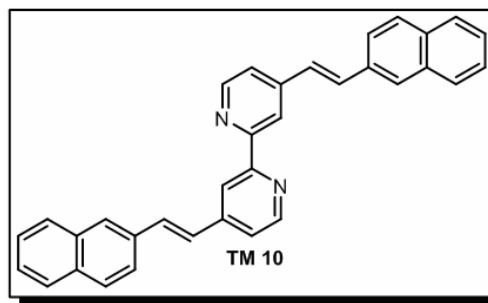
bands), 1583.70 (C=C), 1537.40–470.67

(multiple bands).

^{1}H NMR (400 MHz, DMSO–d$_6$) δ: 8.74 (d, J =

4 Hz, 2H), 8.64 (s, 2H), 7.98-7.92 (m, 8H), 7.82

(d, J = 16 Hz, 2H), 7.74-7.70 (m, 4H), 7.56-7.53 (m, 6H).

^{13}C NMR: Due to very poor solubility of this compound in common organic solvents, ^{13}C

NMR was not possible.

LC–MS (positive mode) m/z: 461 (M+H)$^+$.

Anal. Calcd. for C$_{34}$H$_{24}$N$_2$ (460.57): C, 88.67; H, 5.25; N, 6.08. Found: C, 88.61; H, 5.23;

N, 6.16.

UV/Vis (CH$_2$Cl$_2$): λ_{max} (ε) = 330 (51200) nm.

4,4'–*bis*–((anthracen–9–yl)vinyl)–2,2'–bipyridine (TM 11). Yellow powder. Method 2.

Yield = 82%. Mp: more than 200 ºC.

IR (KBr, cm^{-1}): 3439.39–1628.07 (multiple bands);

1583.70 (C=C), 1496.90–823.75 (multiple bands).

^{1}H NMR (400 MHz, DMSO–d$_6$) δ: 8.81 (d, J = 4Hz, 2H),

8.75 (s, 2H), 8.65 (s, 2H), 8.53 (d, J = 16 Hz, 2H), 8.15–

8.10 (m, 8H), 7.59–7.48 (m, 8H), 7.17 (d, J = 16 Hz, 2H).

^{13}C NMR: We could not record the same because of the

less solubility of the compound in common organic solvents.

LC–MS (negative mode) m/z: 560 (M–H)$^+$.

Anal. Calcd. for C$_{42}$H$_{28}$N$_2$ (560.69): C, 89.97; H, 5.03; N, 5.00. Found: C, 89.95; H, 4.99;

N, 5.06.

UV/Vis (CH$_2$Cl$_2$): λ_{max} = 390 nm.
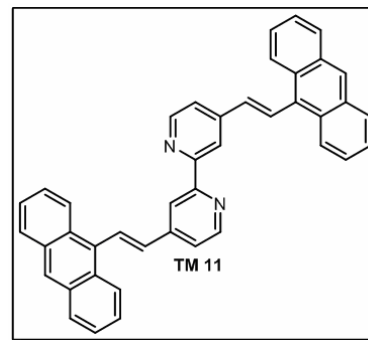
**Synthesis of the unsymmetrically substituted compound 4–(4–(methyl)(tetradecyl)
amino)styryl)–4'–methyl–2,2'–bipyridine (TM 3)**. This compound was obtained

following a controlled Knoevenagel reaction between 4,4'–dimethyl–2,2'–bipyridine (**8**)

with **Ald 2** using LDA as the base (freshly prepared by adding n–BuLi to a THF solution of diisopropylamine at –20 ℃ followed by stirring the mixture at this temperature for 30 min). In a typical procedure, freshly prepared LDA (11 mmol, 1.1 equiv.) was added dropwise over 15 min period via cannula to a 50 ml THF solution of **8** (1.84 gm, 10 mmol) at –20 ℃. The dark reaction mixture was stirred at this temperature for one hour, **Ald 2** (4.1 gm, 11 mmol) dissolved in 20 ml of THF was then added via a dropping funnel and the reaction was allowed to continue at this temperature until completion (monitored by TLC). The reaction was subsequently quenched with saturated NH_4Cl solution (aq) and extracted with DCM. The combined organic layer was washed with brine, dried over anhydrous Na_2SO_4 and evaporated. The crude product was purified through column chromatography on silica gel using MeOH : $CHCl_3$: Et_3N = 5 : 95 : 0.5 (v/v) as the mobile phase. The pure mono–ol thus obtained (**11**) was then dissolved in toluene (ca 30 ml) and refluxed overnight under a Dean–Stark trap in presence of catalytic amount of pyridinium–p–toluene–sulphonate (PPTS). After cooling the red–orange solution to room temperature, it was washed with saturated $NaHCO_3$ solution, water then with brine and evaporated to obtain the compound **TM 3** as a thick yellow gum that solidified upon prolonged standing (yield = 78%). Mp: 124 ℃ (DTA).

^{1}H NMR (400 MHz, $CDCl_3$, TMS): δ = 8.58 (d, J = 4 Hz, 2 H), 8.46 (s, 1 H), 8.25 (s, 1 H), 7.45 (d, J = 8 Hz, 2 H), 7.39 (d, J = 16 Hz, 1 H), 7.34 (d, J = 4 Hz, 1 H), 7.15 (d, J = 4 Hz, 1 H), 6.90 (d, J = 16 Hz, 1 H), 6.68 (d, J = 8 Hz, 2 H), 3.35 (t, 2 H, –N–C$\underline{H}_2$–), 2.98 (s, 3 H, –N–C$\underline{H}_3$), 2.45 (s, 3 H, 4–py–C$\underline{H}_3$), 1.59 (unresolved, 2 H, –N–CH$_2$–C$\underline{H}_2$–), 1.27 (unresolved, 22 H, –C$\underline{H}_2$–), 0.88 (t, 3 H, –CH$_2$–C$\underline{H}_3$).

TM 3

^{13}C NMR (100 MHz, $CDCl_3$, TMS) δ: 156.4, 156.2, 149.6, 149.3, 148.9, 148.1, 146.8, 133.6, 128.5, 124.7, 123.8, 122.1, 121.0, 120.5, 117.8, 111.8, 52.6, 38.3, 32.0, 29.7, 29.4, 27.2, 26.8, 22.7, 21.2, 14.2.

LC–MS (positive mode) m/z: 498 (M+H)$^+$.
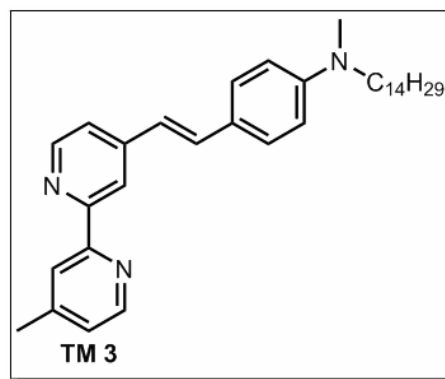
Anal. Calcd. For $C_{34}H_{47}N_3$ (497.38): C, 82.04; H, 9.52; N, 8.44. Found: C, 82.00; H, 9.50; N, 8.50.

UV/Vis (CH_2Cl_2): λ_{max} (ε) = 246 nm (26257), 285 nm (23742), 390 nm (35114).
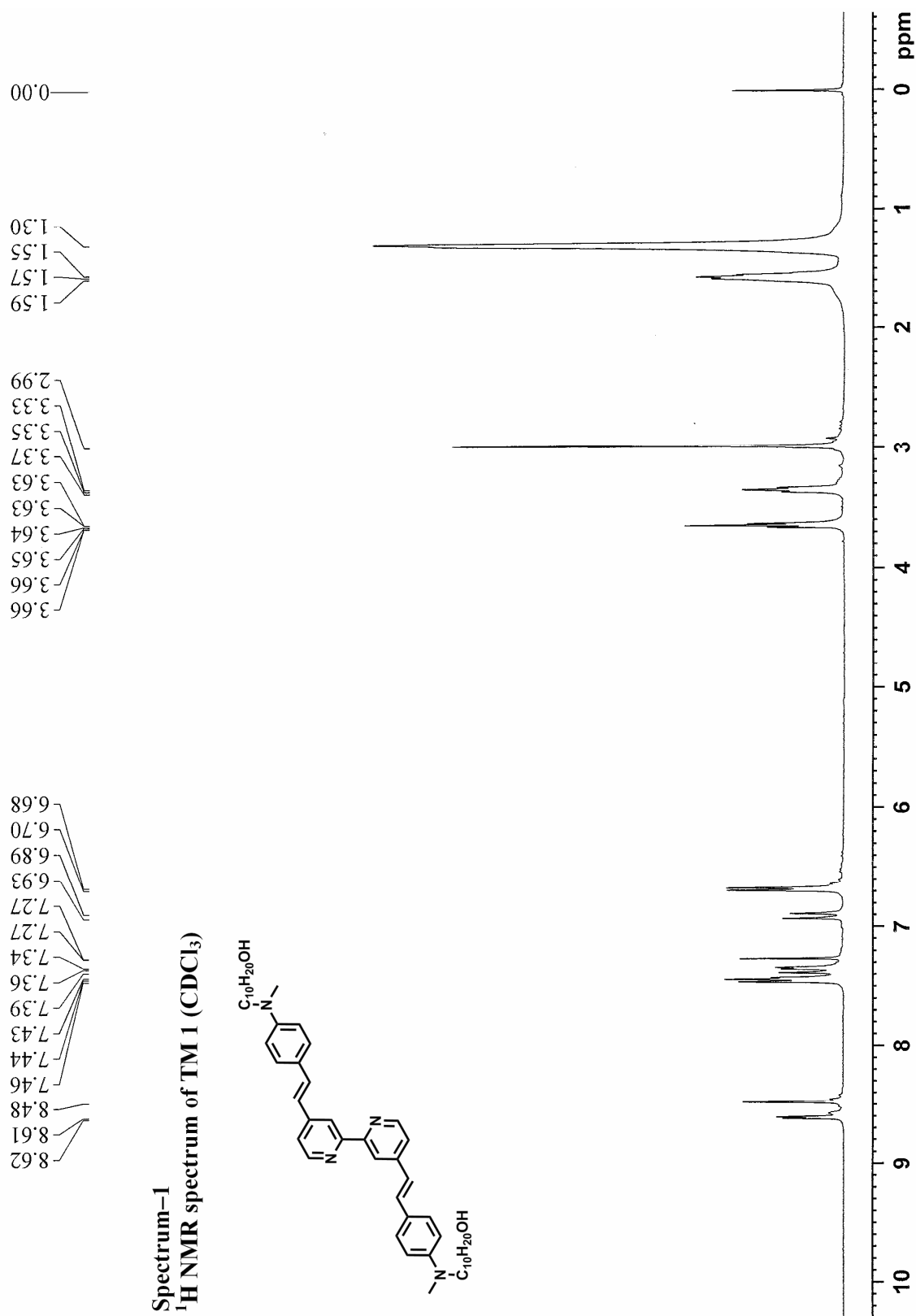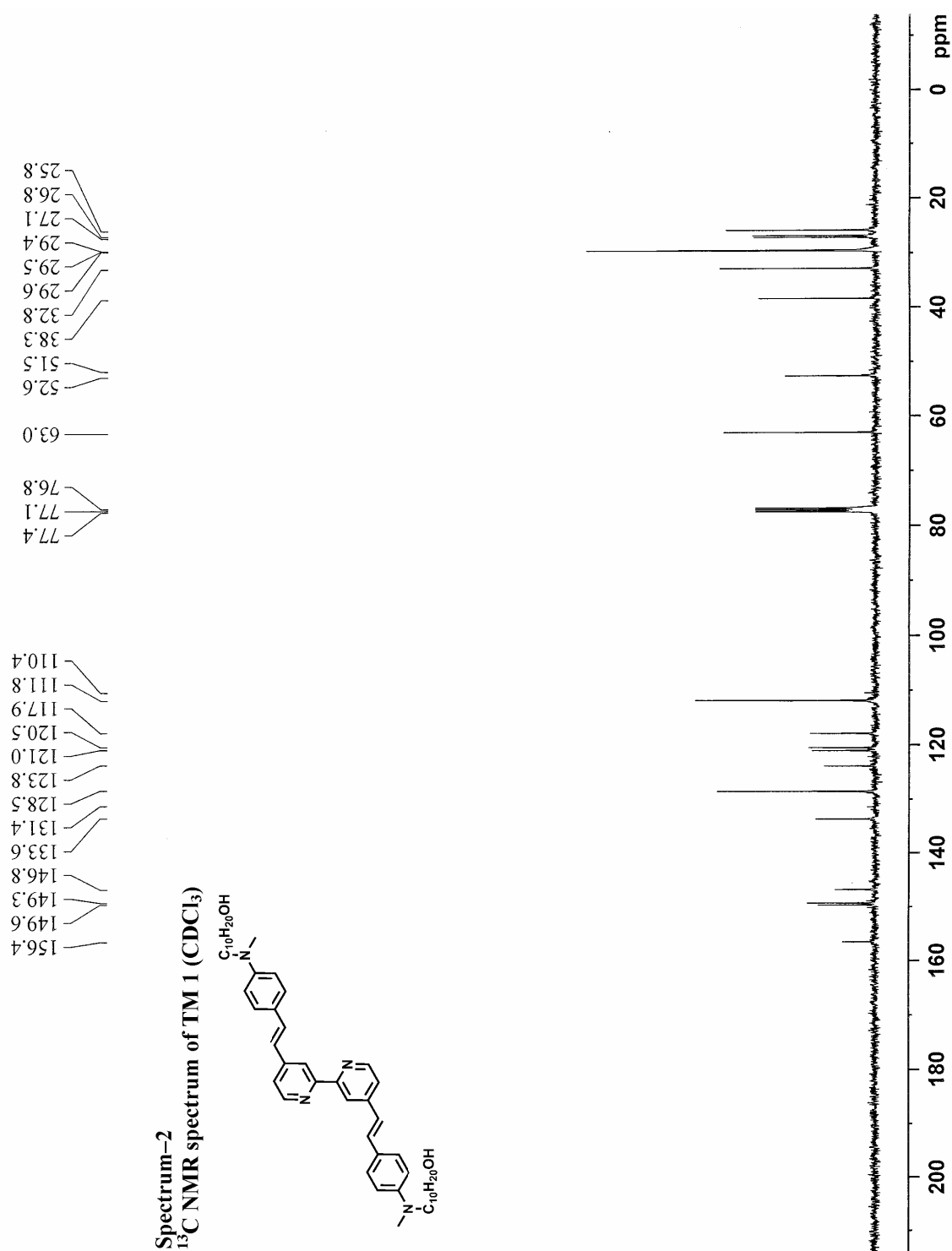
4.5. References

1. S. Warren in *Organic Synthesis: The Disconnection Approach*; John Wiley and Sons, 2007.

2. (a) C. Kaes, A. Katz, M. W. Hosseini, *Chem. Rev.*, **2000**, *100*, 3553–3590 and the references therein. (b) U. S. Schubert, C. Eschbaumer, *Angew. Chem. Int. Ed.*, **2002**, *41*, 2892–2926 and the references therein.

3. A. P. Smith, C. L. Fraser in *Comprehensive Coordination Chemistry II*, Elsevier, 2003, Vol. 1, 1–23 and the references therein.

4. Carry, F. A.; Sundberg, Richerd J. *Advanced Organic Chemistry: Part B, 5th Ed*, 2007, 164.

5. For example see: (a) F. Rizzo, M. Cavazzini, S. Righetto, F. De Angelis, S. Fantacci, S. Quici, *Eur. J. Org. Chem.*, **2010**, 4004–4016. (b) C. Barsu, R. Cheaib, S. Chambert, Y. Queneau, O. Maury, D. Cottet, H. Wege, J. Douady, Y. Bretonnière, C. Andraud, *Org. Bimol. Chem.*, **2010**, *8*, 142–150. (c) C.–G. Liu, W. Guan, P. Song, L.–K. Yan, Z.–M. Su, *Inorg. Chem.*, **2009**, *48*, 6548–6554.

6. For example see: (a) Y. Tao, Q. Wang, L. Ao, C. Zhong, C. Yang, J. Qin, D. Ma, *J. Phys. Chem. C*, **2010**, *114*, 601–609. (b) *Organic Light–Emitting Devices. Synthesis Properties and Electronic Applications*; K. Müllen, U. Scherf, Eds.; Wiley–VCH, Weinheim, **2006**. (c) *Organic Electroluminescence*; Kafafi, Z. H., Ed.; Taylor and Francis: Boca Raton, FL, **2005**; Optical Engineering Vol. 94.

7. (a) M. Bourgault, T. Renouard, B. Lognoné, C. Mountassir, H. Le. Bozec, *Can. J. Chem.*, **1997**, *75*, 318–325. (b) O. Maury, J.–P. Guégan, T. Renouard, A. Hilton, P. Dupau, N. Sandon, L. Toupet, H. Le Bozec, *New J. Chem.*, **2001**, *25*, 1553–1566. (c) L. Viau, O. Maury, H. Le Bozec, *Tetrahedron Lett.*, **2004**, *45*, 125–128. (d) T. Le Bouder, L. Viau, J.–P. Gue´gan, Olivier Maury, H. Le Bozec, *Eur. J. Org. Chem.*, **2002**, 3024–3033. (e) T. Le Bouder, O. Maury, H. Le Bozec, I. Ledoux, J. Zyss, *Chem. Commun.*, **2001**, 2430–2431. (f) H. Le Bozec, T. Le
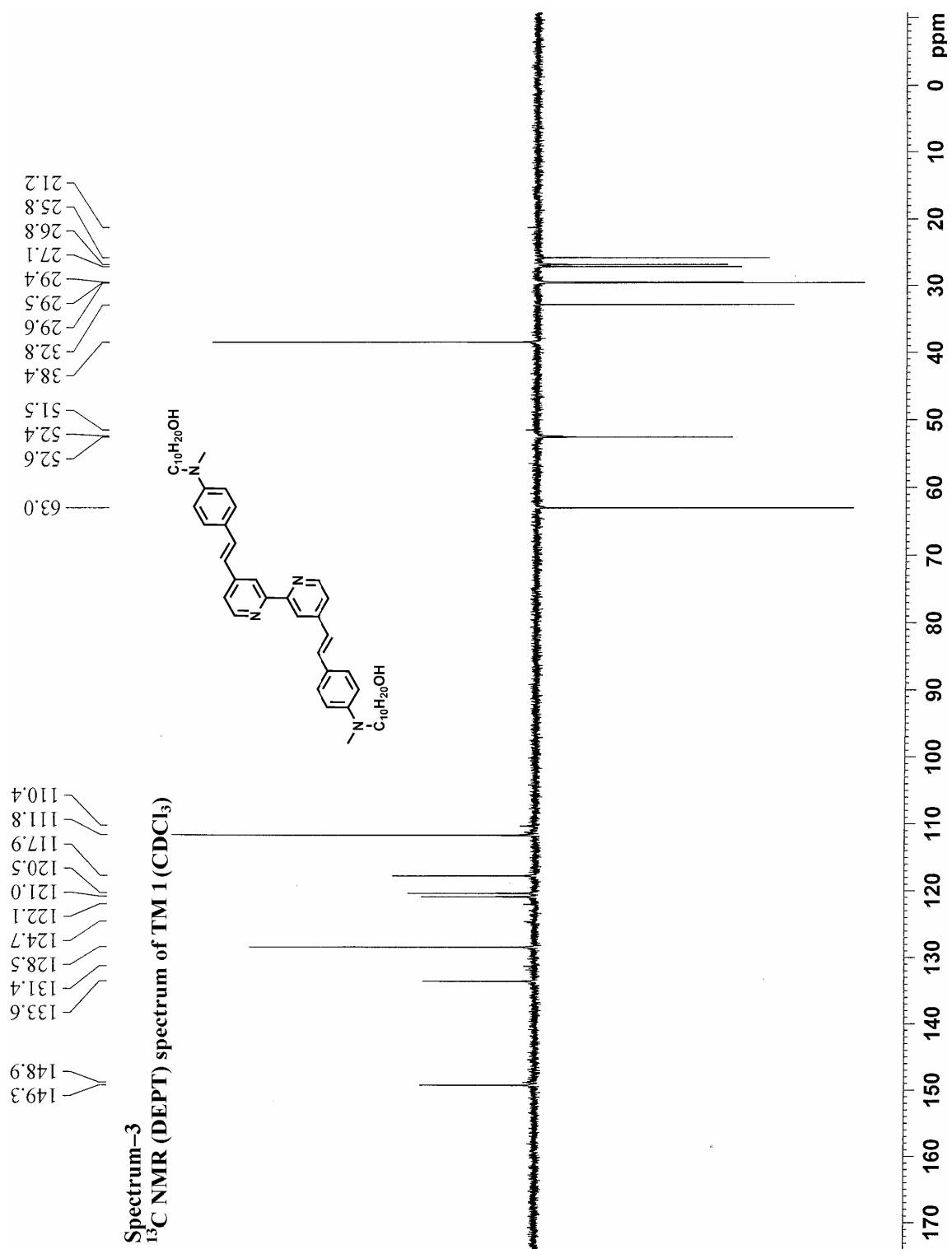
Bouder, O. Maury, A. Bondon, I. Ledoux, S. Deveau, J. Zyss, *Adv. Mater.*, **2001**, *13*, 1677–1681. (g) T. Le Bouder, O. Maury, A. Bondon, K. Costuas, E. Amouyal, I. Ledoux, J. Zyss, H. Le Bozec, *J. Am. Chem. Soc.*, **2003**, *125*, 12284–1299. (h) L. Viau, M. Even, O. Maury, D. M. Haddleton, H. Le Bozec, *Macromol. Rapid Comm.*, **2003**, *24*, 630–635. (i) V. Aubert, E. Ishow, F. Ibersiene, A. Boucekkine, J. A. G. Williams, L. Toupet, R. Me´tivier, K. Nakatani, V. Guerchais, H. Le Bozec, *New. J. chem.*, **2009**, *33*, 1320–1323.

8.   (a) J. C. Araya, J. Gajardo, S. A. Moya, P. Aguirre, L. Toupet, J. A. G. Williams, M. Escadeillas, H. Le Bozec, V. Guerchais, *New. J. Chem.*, **2010**, *34*, 21–24. (b) K. Willinger, K. Fischer, R. Kisselev, M. Thelakkat, *J. Mater. Chem.*, **2009**, *19*, 5364–5376. (c) A. Abbotto, L. Bellotto, F. De Angelis, N. Manfredi, C. Marinzi, *Eur. J. Org. Chem.*, **2008**, 5047–5054. (d) B.–K. An, P. L. Burn, P. Meredith, *Chem. Mater.*, **2009**, *21*, 3315–3324. (e) O. A. Fedorova, E. N. Andryukhina, M. M. Mashura, S. P. Gromov, *ARKIVOC, (Gainesville, FL, United States)* **2005**, *15*, 12–24. (f) T. Chatterjee, M. Sarma, S. K. Das, *Tetrahedron Lett.*, **2010**, *51*, 1985–1988. (g) A. Grabulosa, D. Martineau, M. Beley, P. C. Gros, S. Cazzanti, S. Caramori, C. A. Bignozzi, *Dalton Trans.*, **2009**, 63–70. (h) M. C. Haberecht, J. M. Schnorr, E. V. Andreitchenko, C. G. Clark, Jr., M. Wagner, Klaus Müllen, *Angew. Chem. Int. Ed.*, **2008**, *47*, 1662–1667.

9.   (a) O. Kocian, R. J. Mortimer, P. D. Beer, *J. Chem. Soc., Perkin Trans. 1*, **1990**, 3203. (b) A. A. Abdel–Shafi, P. D. Beer, R. J. Mortimer, F. Wilkinson, *J. Phys. Chem. A*, **2000**, *104*, 192–202. (c) P. D. Beer, O. Kocian, R. J. Mortimer, C. Ridgway, *J. Chem. Soc., Dalton Trans.*, **1993**, 2629–2638. (d) P. D. Beer, O. Kocian, R. J. Mortimer, C. Ridgway, *J. Chem. Soc., Faraday Trans.*, **1993**, *89*, 333–338. (e) P. D. Beer, O. Kocian, R. J. Mortimer, C. Ridgway, *Analyst*, **1992**, *117*, 1247–1249. (f) P. D. Beer, O. Kocian, R. J. Mortimer, C. Ridgway, *J. Chem. Soc., Chem. Commun.*, **1991**, 1460–1463.

10.   (a) A. Ulman, *An Introduction to Ultrathin Organic Films from Langmuir–Blodgett to Self–Assembly*; Academic Press: San Diego, 1991. (b) D. R. Talham, *Chem. Rev.*, **2004**, *104*, 5479.
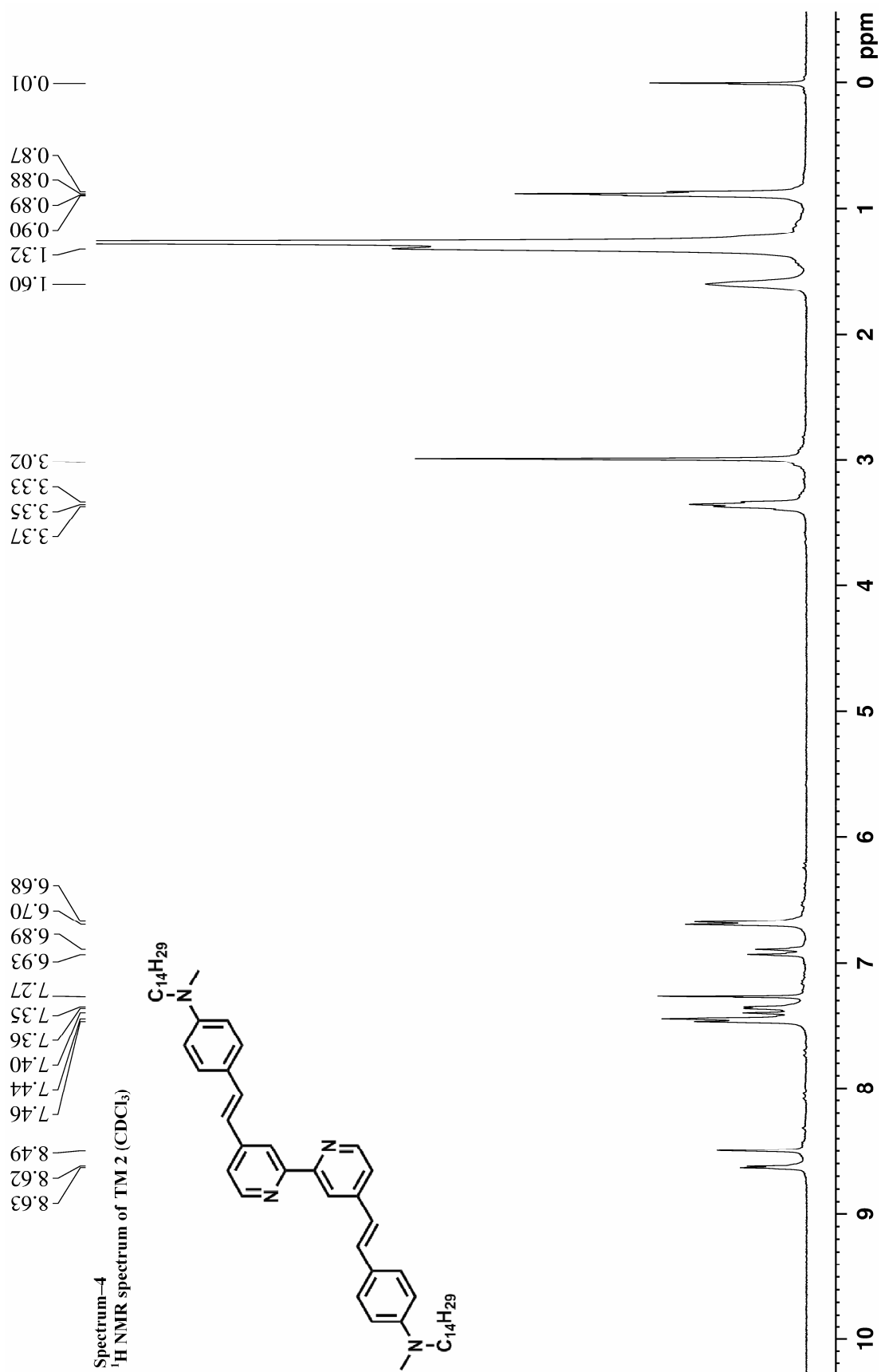
11. H. J. Bolink, E. Baranoff, M. Clemente–León, E. Coronado, N. Lardiés, A. López Muñoz, D. Repetto, M. K. Nazeeruddin, *Langmuir*, **2010**, *26*, 11461–11468.

12. *Organic Electroluminescence*; Kafafi, Z. H., Ed.; Taylor and Francis: Boca Raton, FL, **2005**; Optical Engineering Vol. 94.

13. D. Berner, C. Klein, M. K. Nazeeruddin, F. De Angelis, M. Castellani, Ph. Bugnon, R. Scopelliti, L. Zuppirolid, M. Graetzel, *J. Mater. Chem.*, **2006**, *16*, 4468–4474.

14. (a) H. Le Bozec, T. Renouard, *Eur. J. Inorg. Chem.*, **2000**, 229–239. (b) K. Sénéchal, O. Maury, H. Le Bozec, I. Ledoux, J. Zyss, *J. Am. Chem. Soc.*, **2002**, *124*, 4560–4561. (c) O. Maury, H. Le Bozec, *Acc. Chem. Res.*, **2005**, *38*, 691–704. (d) O. Maury, L. Viau, K. Sénéchal, B. Corre, J.–P. Guégan, T. Renouard, I. Ledoux, J. Zyss, H. Le Bozec, *Chem. Eur. J.*, **2004**, *10*, 4454 – 4466. (e) V. Aubert, V. Guerchais, E. Ishow, K. Hoang–Thi, I. Ledoux, K. Nakatani, H. Le Bozec, *Angew. Chem. Int. Ed.*, **2008**, *47*, 577–580.

15. (a) K. J. Jiang, N. Masaki, J. B. Xia, S. Noda, S. Yanagida, *Chem. Commun.*, **2006**, 2460–2462. (b) C. Klein, M. K. Nazeeruddin, P. Liska, D. Di Censo, N. Hirata, E. Palomares, J. R. Durrant, M. Grätzel, *Inorg. Chem.*, **2005**, *44*, 178–180. (c) P. Wang, C. Klein, R. Humphry–Baker, S. M. Zakeeruddin, M. Grätzel, *J. Am. Chem. Soc.*, **2005**, *127*, 808–809. (d) D. Kuang, C. Klein, S. Ito, J. E. Moser, R. Humphry–Baker, N. Evans, F. Duriaux, C. Grätzel, S. M. Zakeeruddin, M. Grätzel, *Adv. Mater.*, **2007**, *19*, 1133–1137. (e) M. K. Nazeeruddin, T. Bessho, L. Ceveya, S. Ito, C. Klein, F. De Angelis, S. Fantacci, P. Comtea, P. Liska, H. Imai, M. Grätzel, *J. Photochem. Photobiol. A*, **2007**, *185*, 331–337.

16. (a) C. Y. Chen, S. J. Wu, C. G. Wu, J. G. Chen, K. C. Ho, *Angew. Chem., Int. Ed.*, **2006**, *45*, 5822–5825. (b) N. Hirata, J. J. Lagref, E. J. Palomares, J. R. Durrant, M. K. Nazeeruddin, M. Grätzel, D. Di Censo, *Chem. Eur. J.*, **2004**, *10*, 595–602.

17. (a) B. O'Regan, M. Grätzel, *Nature*, **1991**, *353*, 737–740. (b) W. M. Campbell, A. K. Burrell, D. L. Officer, K. W. Jolley, *Coord. Chem. Rev.*, **2004**, *248*, 1363–1379. (c) R. Amadelli, R. Argazzi, C. A. Bignozzi, F. Scandola, *J. Am. Chem. Soc.*, **1990**, *112*, 7099–7103. (d) S. R. Jang, R. Vittal, J. H. Lee, N. Jeong K. J. Kim, *Chem. Commun.*, **2006**, 103–105.
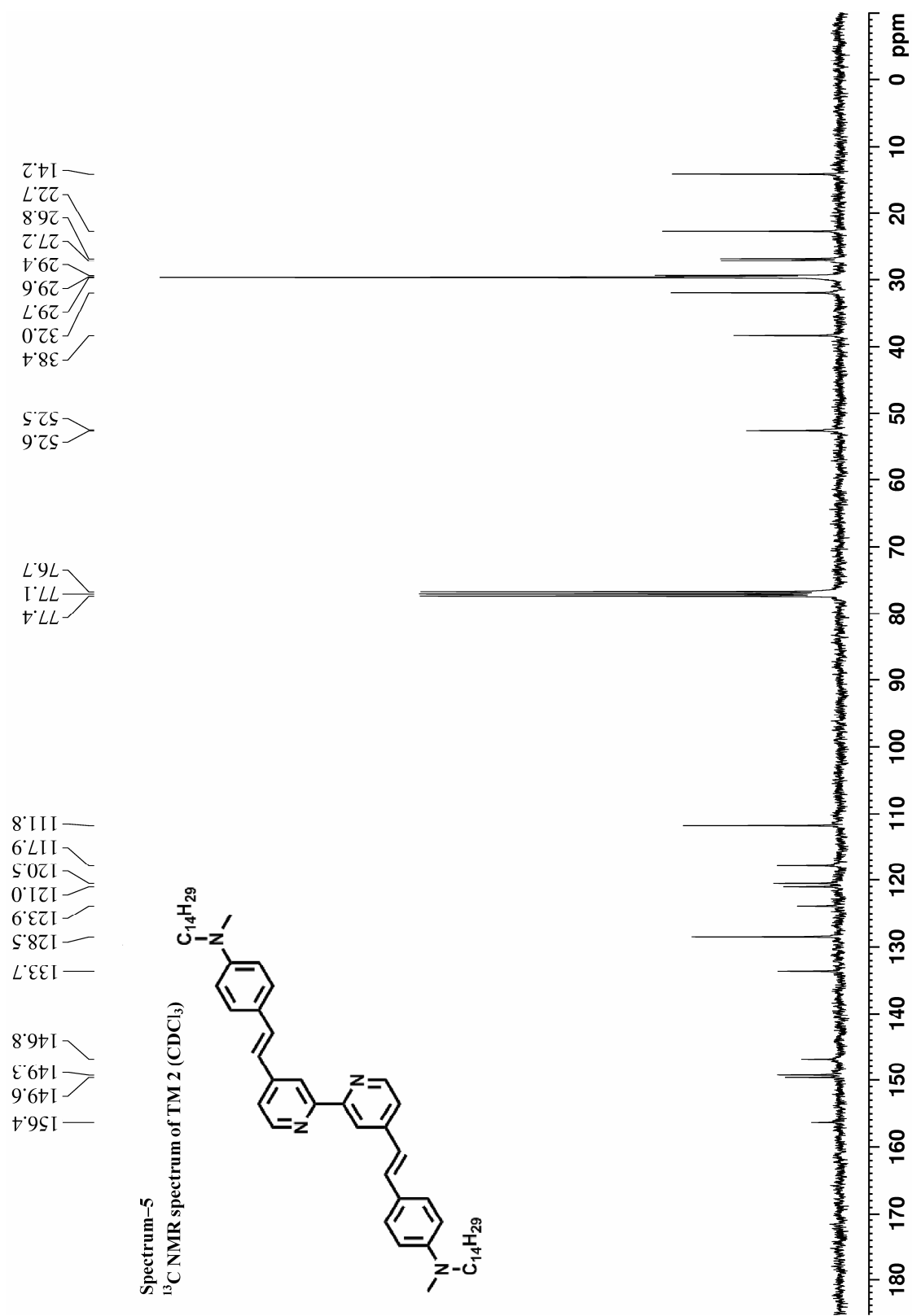
18.   J. M. Chong, M. A. Heuft, P. Rabbat, *J. Org. Chem.*, **2000,** *65,* 5837–5838

19.   (a) D. Chen, R. De, D. L. Mohler, *Synthesis*, **2009**, 211–216. (b) R. S. Ward, D. Branciard, R. A. Dignan, M. C. Pritchard, *Heterocycles*, **2002**, *56*, 157–170.

20.   (a) S. Gould, G. F. Strouse, T. J. Meyer, B. P. Sullivan, *Inorg. Chem.*, 1991, 30, 2942–2949. (b) S.–R. Jang, C. Lee, H. Choi, J. J. Ko, J. Lee, R. Vittal, K.–J. Kim, *Chem. Mater.*, **2006**, *18*, 5604–5608.

21.   (a) A. P. Smith, J. J. S. Lamba, C. L. Fraser, *Org. Syn.*, **2004**, *10*, 107 – 112. (b) C. L. Fraser, N. R. Anastasi, J. J. S. Lamba, *J. Org. Chem.*, **1997,** *62*, 9314–9317.

22.   T. Kartens, K. Kobs, *J. Phys. Chem.*, **1980**, *84*, 1871.

23.   C. Reichardt, *Chem. Rev.* **1994,** *94,* 2319–2358.

24.   C. Toro, L. De Boni, S. Yao, K. D. Belfield, F. E. Hernández, *J. Phys. Chem. B* **2008**, *112,* 12185–12190.

25.   (a) V. E. Lippert, *Z. Elektrochem.* **1957**, *61*, 962. (b) N. Mataga, Y. Kaifu, M. Koizumi, *Bull. Chem. Soc. Jpn.* **1956**, *29*, 465. (c) N. Mataga, *Bull. Chem. Soc. Jpn.* **1963**, *36*, 654.

26.   A. Samanta, S. Saha, *J. Phys. Chem. A* **2002**, *106*, 4763–4771.

Spectrum–1
¹H NMR spectrum of TM 1 (CDCl₃)

Spectrum–2
^{13}C NMR spectrum of TM 1 (CDCl$_3$)

25.8
26.8
27.1
29.4
29.5
29.6
32.8
38.3
51.5
52.6
63.0
76.8
77.1
77.4
110.4
111.8
117.9
120.5
121.0
123.8
128.5
131.4
133.6
146.8
149.3
149.6
156.4

Spectrum–3
^{13}C NMR (DEPT) spectrum of TM 1 (CDCl$_3$)

21.2
25.8
26.8
27.1
29.4
29.5
29.6
32.8
38.4

51.5
52.4
52.6

63.0

110.4
111.8
117.9
120.5
121.0
122.1
124.7
128.5
131.4
133.6

148.9
149.3

Spectrum−4
^{1}H NMR spectrum of TM 2 (CDCl$_3$)

0.01

0.87
0.88
0.89
0.90
1.32
1.60

3.02
3.33
3.35
3.37

6.68
6.70
6.89
6.93
7.27
7.35
7.36
7.40
7.44
7.46
8.49
8.62
8.63

Spectrum–5
^{13}C NMR spectrum of TM 2 (CDCl$_3$)

Spectrum–6

^{13}C NMR (DEPT) Spectrum of TM 2 (CDCl$_3$)

0 ppm

0.01

0.87
0.88
0.90
1.27
1.30
1.59

2.45

2.98
3.33
3.35
3.36

6.67
6.69
6.88
6.92
7.14
7.27
7.33
7.34
7.37
7.41
7.43
7.45
8.25
8.46
8.57
8.58

Spectrum—7
¹H NMR spectrum of TM 3 (CDCl₃)

Spectrum–8
^{13}C NMR spectrum of TM 3 (CDCl$_3$)

14.2
21.2
22.7
26.8
27.2
29.4
29.7
32.0
38.3

52.6

76.8
77.1
77.4

111.8
117.8
120.5
121.0
122.0
123.8
124.7
128.5
133.6
146.8
148.1
148.9
149.3
149.6
156.2
156.4

14.2
21.2
22.7
26.8
27.2
29.4
29.6
29.7
32.0
38.3

52.6

111.8
117.8
120.5
121.0
122.0
124.7
128.5
133.6

148.9
149.3

Spectrum–9
^{13}C NMR (DEPT) spectrum of TM 3 (CDCl$_3$)

Spectrum-10
^{1}H NMR spectrum of TM 4 (DMSO-d$_6$)

2.49
2.49

3.31
3.32
3.53
3.59
3.80

6.85
6.87
7.19
7.28
7.31
7.43
7.47
7.63
7.68
7.74
7.76
8.58
8.69
8.70

Spectrum-11
^{1}H NMR spectrum of TM 5 (DMSO-d$_6$)

2.42
2.49
2.49
2.53

3.30
3.32
3.57

3.79
3.86

6.57
6.60
7.10
7.15
7.37
7.39
7.42
7.44
7.56
7.58
7.61
7.65
7.67
7.68
7.70
7.72
8.57
8.68
8.69

Spectrum-12
^{1}H NMR spectrum of TM 6 (DMSO-d$_6$)

6.85
6.87
6.97
6.99
7.26
7.27
7.32
7.44
7.46
7.48
7.62
7.63
7.67
7.68
7.69
7.73
7.75
8.58
8.69
8.70

2.50

3.31

3.76
3.81

0 ppm

Spectrum-13
^{1}H NMR spectrum of TM 7 (CDCl$_3$)

7.21
7.25
7.27
7.29
7.31
7.38
7.40
7.42
7.47
7.50
7.51
7.55
7.57
7.72
7.74
7.93
7.97
8.52
8.69
8.70

3.46

0.00

CDCl$_3$

Spectrum-14
^{13}C NMR spectrum of TM 7 (CDCl₃)

76.7
77.1
77.4
81.8
82.9

119.3
120.7
121.7
125.2
128.2
128.3
129.2
131.0
133.5
138.3
145.6
149.5
156.6

Spectrum-15
^{1}H NMR spectrum of TM 8 (DMSO-d$_6$)

2.39
2.46
2.47
2.50

3.28
3.30

4.27

7.42
7.46
7.48
7.50
7.59
7.64
7.65
7.70
7.72
8.54
8.66
8.67

ppm
0
1
2
3
4
5
6
7
8
9
10

Spectrum-16
^{13}C NMR spectrum of TM 8 (DMSO-d$_6$)

156.3
150.2
145.7
137.2
132.7
132.6
128.0
127.8
122.1
121.6
118.4

84.0
82.5

40.9
40.7
40.6
40.5
40.4
40.2
40.2
40.0
39.8
39.6
39.4

ppm

Spectrum-17
^{1}H NMR spectrum of TM 9 (DMSO-d$_6$)

7.46
7.50
7.59
7.60
7.60
7.62
7.64
7.95
7.98
8.00
8.02
8.42
8.46
8.48
8.50
8.66
8.75
8.76

2.49
3.31

Spectrum-18
^{1}H NMR spectrum of TM 10 (DMSO-d$_6$)

7.53
7.54
7.55
7.56
7.70
7.72
7.73
7.74
7.80
7.81
7.84
7.93
7.98
8.64
8.73

2.49
2.49
2.49
2.56
2.59
2.66
3.26
3.31
3.36
3.38
3.41
3.44

Spectrum-19
^{1}H NMR spectrum of TM 11 DMSO (d^6)

7.15
7.19
7.48
7.51
7.53
7.54
7.58
7.59
8.10
8.12
8.15
8.51
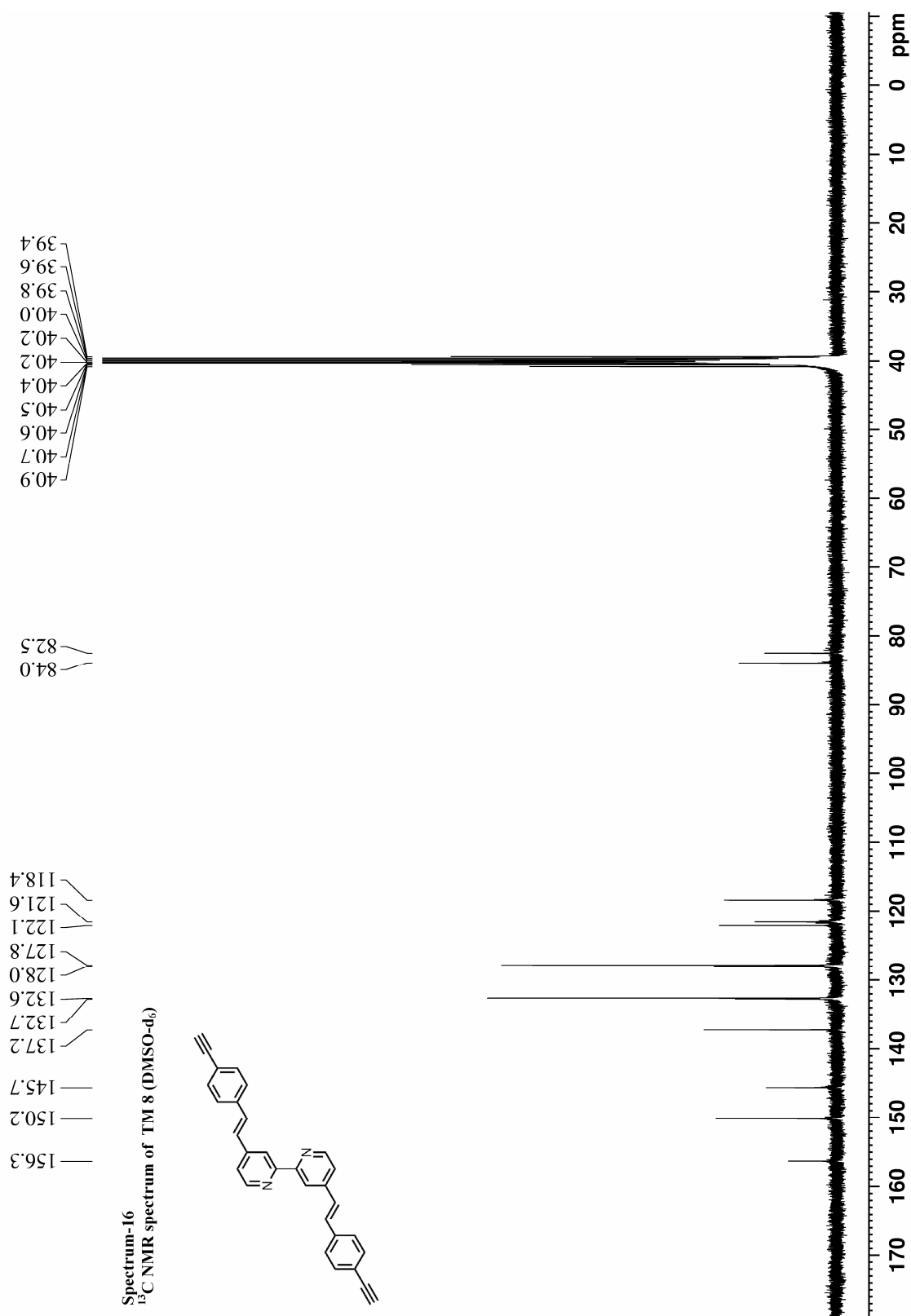8.55
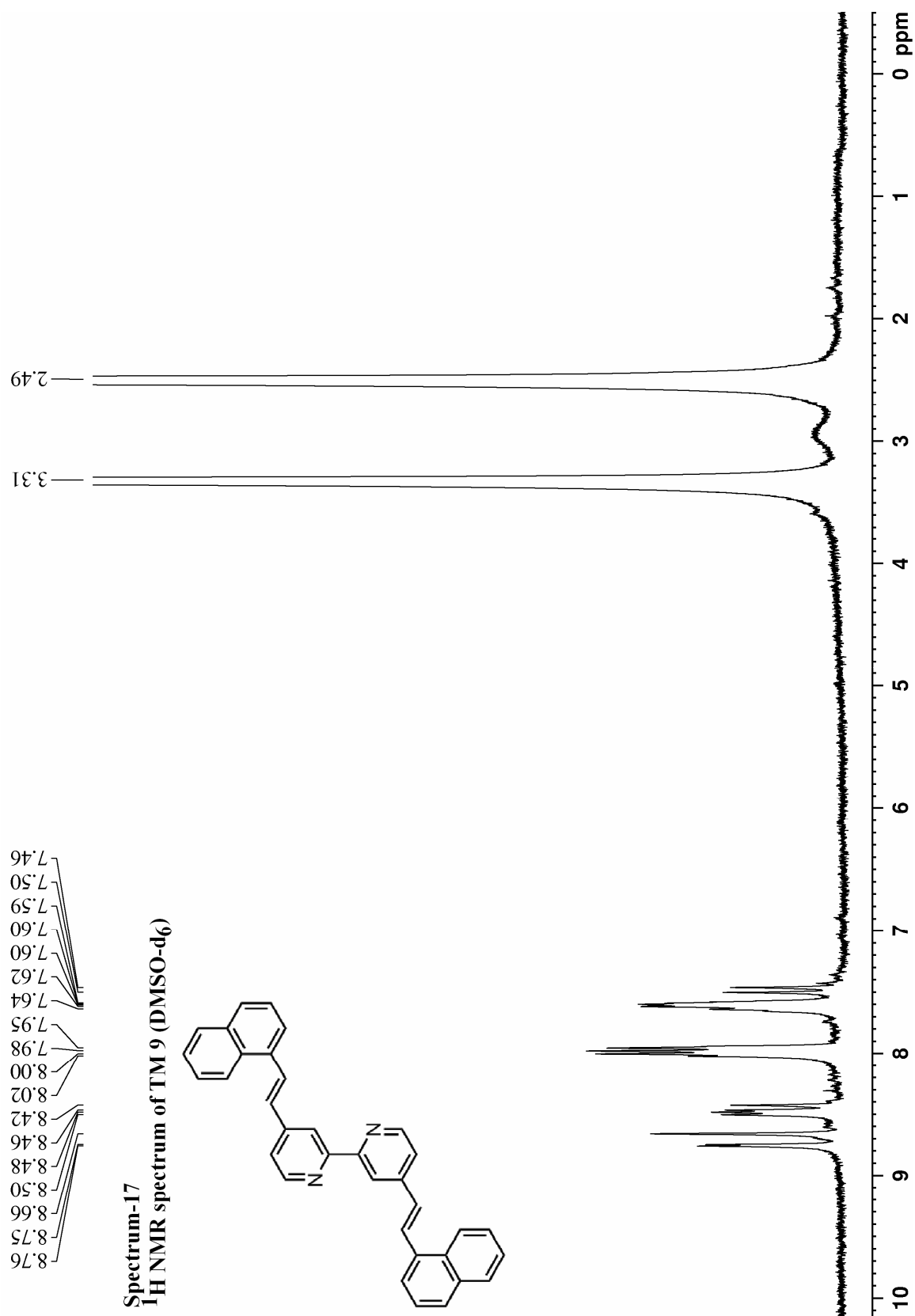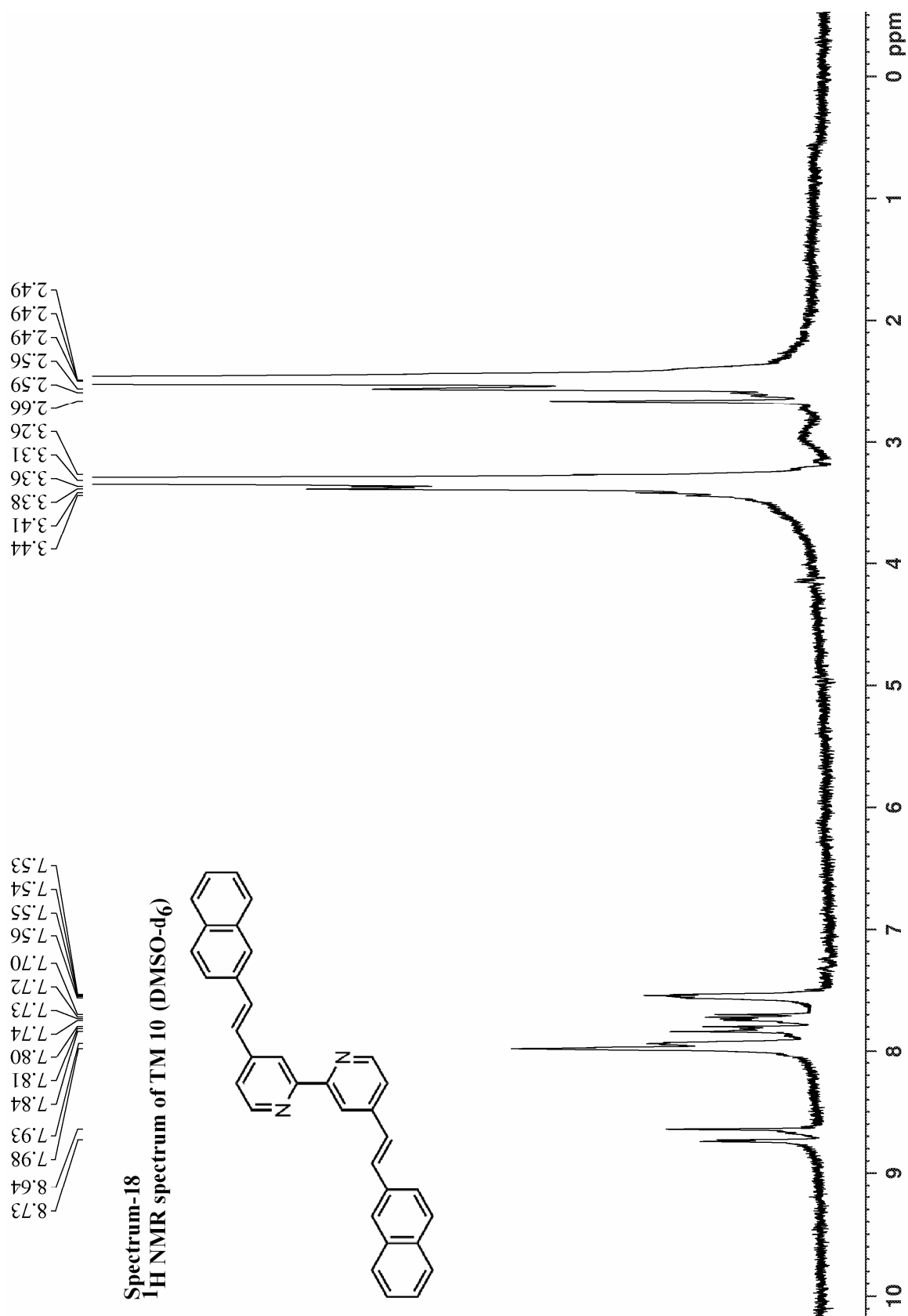8.65
8.66
8.75
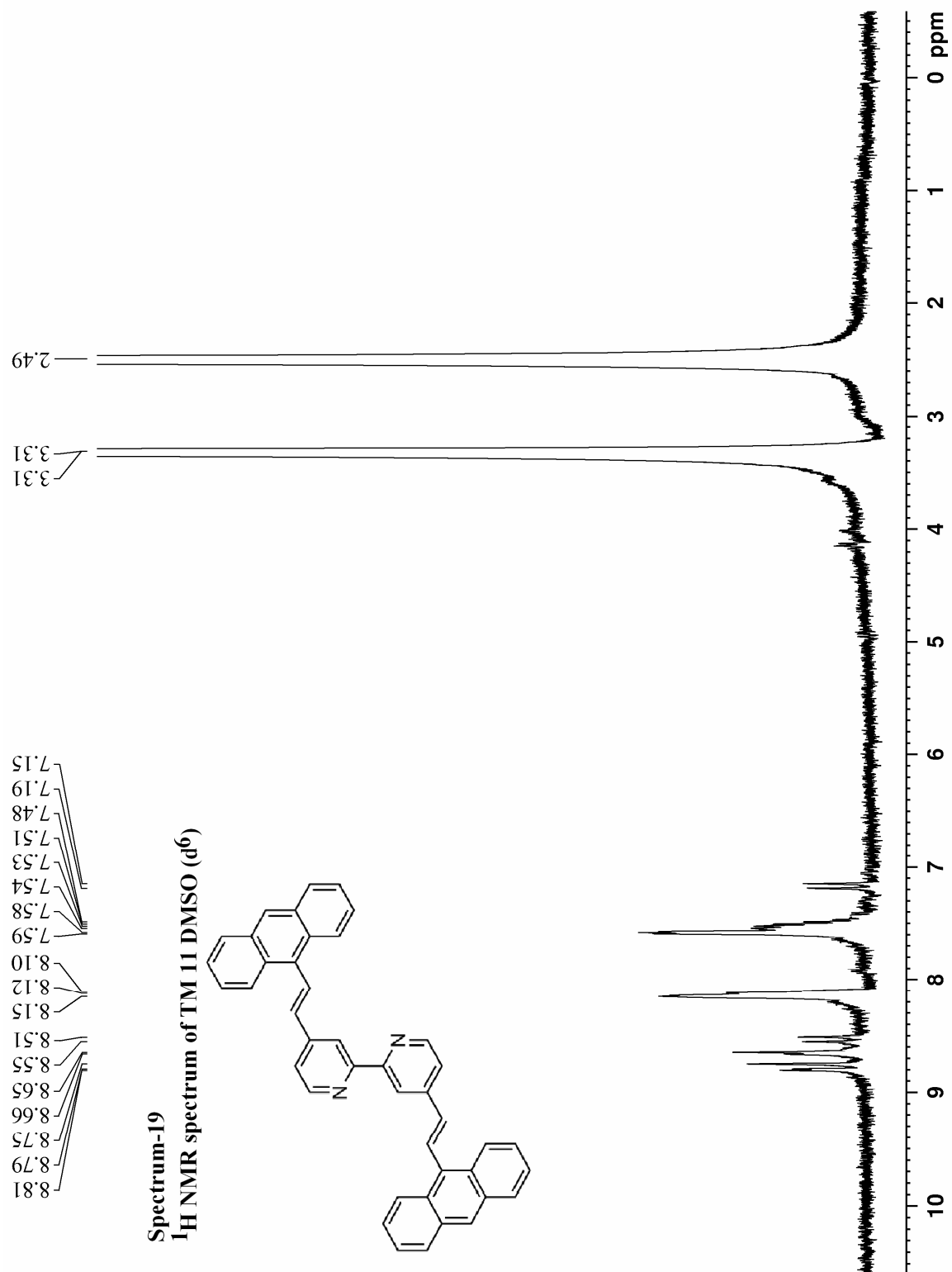8.79
8.81

2.49

3.31
3.31

List of publications

1. Supramolecular architectures from ammonium–crown ether inclusion complexes in polyoxometalate association: Synthesis, structure, and spectroscopy

    <u>Tanmay Chatterjee</u>, Monima Sarma, Samar K. Das[*] *Cryst. Growth Des.* **2010**, *10*, 3149–3163 (article).

2. Polyoxometalate associated ion–pair solid based on a crown ether inclusion complex: Synthesis, structure and spectroscopy

    <u>Tanmay Chatterjee</u>, Monima Sarma, Samar K. Das[*] *J. Mol. Struct.* **2010**, *981*, 34–39 (article).

3. Synthesis and photo–physical properties of methoxy–substituted π–conjugated–2,2'–bipyridines

    <u>Tanmay Chatterjee</u>, Monima Sarma, Samar K. Das[*] *Tetrahedron Lett.* **2010**, *51*, 1985–1988 (letter).

4. Donor–acceptor amphiphilic 2,2'–bipyridine chromophores: Synthesis, linear optical and thermal properties

    <u>Tanmay Chatterjee</u>, Monima Sarma, Samar K. Das* *Tetrahedron Lett.* **2010**, In press (letter).

5. A copper–cyclen coordination complex associated with a polyoxometalate anion: Synthesis, crystal structure and electrochemistry of $[Cu(cyclen)(MeCN)][W_6O_{19}]$

    Monima Sarma, <u>Tanmay Chatterjee</u>, Samar K. Das[*] *Inorg. Chem. Commun.* **2010**, *13*, 1114–1117 (letter).

6. Bringing an important macrocycle into polyoxometalate–matrix: Synthesis, crystal Structure, spectroscopy and electrochemistry of $[Co^{III}(transdiene)(Cl)_2]_2$ $[Mo_6O_{19}]$, $[Ni^{II}(transdiene)][W_6O_{19}]\cdot DMSO\cdot DCM$ and $[Zn^{II}(transdiene)(Cl)]_2$ $[W_6O_{19}]$

    Monima Sarma, <u>Tanmay Chatterjee</u>, Samar K. Das[*] **2010**, *communicated*.

7.   Synthesis, structure, spectroscopic properties and cytotoxic effect of some thiosemicarbazone complexes of palladium

      Sarmistha Halder, Shie–Ming Peng, Gene–Hsiang Lee, <u>Tanmay Chatterjee</u>, Asama Mukherjee, Sushanta Dutta, Utpal Sanyal, Samaresh Bhattacharya[*] *New J. Chem*. **2008**, *32*, 105–114 (article).

8.   Stabilization of a new type of water octamer in the crystalline hydrate of an inorganic–organic hybrid material: Synthesis and characterization of $[\{Cu(phen)(H_2O)_2\}_2(Mo_8O_{26})].8H_2O$

      Vaddypally Shivaiah, <u>Tanmay Chatterjee</u>, Samar K. Das[*] *Synthesis and Reactivity in Inorganic, Metal–Organic, and Nano–Metal Chemistry* **2008**, *38*, 12–17 (article).

9.   A water pipe held up by a polyoxometalate supported transition metal complex: Synthesis and characterization of $[Cu_2(phen)_2(CH_3COO)(CH_3COOH)(H_2O)_2]$ $[Al(OH)_6Mo_6O_{18}]\cdot 28H_2O$

      Vaddypally Shivaiah, <u>Tanmay Chatterjee</u>, Khandregula Srinivasu, Samar K. Das[*] *Eur. J. Inorg. Chem.* **2007**, 231–234 (letter).